

**FLUIDELASTIC STABILITY OF A
ROTATED SQUARE ARRAY WITH
MULTIPLE FLEXIBLE CYLINDERS
SUBJECT TO CROSS-FLOW**

Sermet Kuran

Department of Mechanical Engineering

McGill University

Montréal

A thesis submitted to the Faculty of Graduate Studies and Research

in partial fulfillment of the requirements for the degree of

Doctor of Philosophy.

To: G. Mergen-Kuran

Abstract

Over the past decade, theoretical investigations have revealed the possible existence of two distinct mechanisms, a fluid-damping controlled one requiring only a single degree-of-freedom system and a fluid-stiffness controlled one requiring two or more degree-of-freedom system, instrumental in causing fluidelastic instability of cylinder arrays subjected to fluid cross-flow. As yet, the existence of these mechanisms has not been verified experimentally, and some researchers tend to neglect one or the other of these mechanisms in their theoretical studies.

In this thesis, with the objective of obtaining further insight into the nature of fluidelastic instability mechanisms, experimental and theoretical studies have been performed on a rotated square array with $P/d = 2.12$. Previous theoretical and experimental studies on this array have established the fact that a single flexible cylinder, in an otherwise rigid array, is fluidelastically stable. However, multiple flexible cylinder dynamic (vibration) experiments undertaken in this study show that fluidelastic instability develops when the array incorporates three or more flexible cylinders. This result verifies the duality of the instability mechanisms and suggests that the cylinder motion in the present array is dominated by the fluid-stiffness controlled mechanism, rather than the fluid-damping controlled mechanism.

Involved dynamic (vibration) experiments have been undertaken to elucidate the effect of various parameters such as, number of cylinders, cylinder position, cylinder mass, frequency detuning and fluidelastic coupling on the instability threshold of this array, in which the fluid-stiffness controlled mechanism prevails. It has been determined that varying mechanical damping has a small effect on the critical velocity,

whereas, varying cylinder mass generates, relatively, large changes in the critical velocity. A "Connors type" instability equation, or versions of it, are shown not to be applicable in this array, mainly due to the strong dependence of the mass exponent on the actual value of the non-dimensional mass.

Frequency detuning of adjacent cylinders is also shown to have a significant effect on the critical velocity. Further dynamic (vibration) experiments revealed the co-existence of dynamic and static instabilities within close proximity to each other. It was possible to switch from one type of instability to the other, by varying one, or more, of the mechanical properties of the flexible cylinders.

Next, the time averaged fluid forces acting on static cylinders were measured as a function of monitored, and surrounding, cylinder displacements at different Reynold numbers, to attain a physical understanding of the flow pattern in the array. The results complemented and verified the various dynamic and static instability findings of the vibration (dynamic) experiments.

Finally, the fluid forces were incorporated in a quasi-steady, multiple degree-of-freedom model for comparison with experimental results.

SOMMAIRE

Durant la dernière décennie, des études théoriques ont démontré l'éventuelle existence de deux mécanismes distincts donnant naissance à des instabilités fluidélastiques dans le cas de faisceaux de tubes soumis à un écoulement transversal: un mécanisme relié à l'amortissement introduit par le fluide qui n'exige qu'un système à un degré de liberté et un mécanisme relié à la raideur introduite par le fluide, exigeant un système à deux ou plusieurs degrés de liberté. Jusqu'à présent, l'existence de ces mécanismes n'a pas encore été vérifiée expérimentalement, et certains chercheurs tendent à négliger l'un ou l'autre de ces mécanismes dans leurs études théoriques.

Dans cette thèse, dans le but d'obtenir un aperçu plus profond de la nature des mécanismes des instabilités fluidélastiques, des études théoriques et expérimentales ont été effectuées sur un faisceau à géométrie carrée pivotée ("rotated square array") avec un espacement $P/d = 2.12$. Des études théoriques et expérimentales antérieures sur ce faisceau ont montré qu'un tube flexible, dans un faisceau par ailleurs maintenu fixe, est stable de manière fluidélastique. Cependant, les expériences dynamiques (de vibration) avec plusieurs tubes flexibles entreprises dans la présente étude montre qu'une instabilité fluidélastique se développe lorsque le faisceau contient trois cylindres flexibles ou plus. Ce résultat vérifie la dualité des mécanismes d'instabilité et suggère que le mouvement du tube dans ce faisceau est dominé par un mécanisme de raideur, plutôt qu'un mécanisme d'amortissement du fluide.

Des expériences dynamiques (vibration) complètes ont été entreprises afin d'élucider l'effet de différents paramètres comme le nombre de cylindres, la position du cylindre, la masse du cylindre, la fréquence et le couplage fluidélastique sur le seuil d'instabilité

de ce faisceau, pour lequel le mécanisme contrôlé par la raideur du fluide prévaut. On a pu vérifier que l'amortissement mécanique a peu d'effet sur la vitesse critique alors que les variations de masse du tube génèrent des changements relativement importants.

De plus, on montre que l'équation d'instabilité de type "Connors", ou des versions similaires, ne sont pas applicables pour ce faisceau, principalement à cause de la forte dépendance de l'exposant lié à la masse sur la valeur réelle de la masse adimensionnelle.

On montre aussi que la fréquence des tubes adjacents a un effet considérable sur la vitesse critique. Les expériences révèlent la coexistence d'instabilités dynamiques et statiques lorsque les fréquences sont proches. Il a été possible de sauter d'un type d'instabilité à l'autre en variant une, ou plusieurs, propriétés mécaniques des tubes flexibles.

Ensuite, dans le but d'obtenir une compréhension physique de l'écoulement dans le faisceau, les forces hydrodynamiques moyennes agissant sur les cylindres statiques ont été mesurées en fonction du déplacement contrôlé des cylindres adjacents à différents nombres de Reynolds.

Les résultats ont complété et vérifié les conclusions des expériences en vibration (dynamique) sur les découvertes des instabilités dynamiques et statiques.

Finalement, les forces hydrodynamiques ont été incorporées dans un modèle quasi-statique, à plusieurs degrés de liberté, dans le but de comparer avec les résultats expérimentaux.

Acknowledgements

Over the last few years many people, in many different ways, have helped me to pursue my studies.

I owe gratitude to all, but to none more than Professor S.J. Price, my thesis supervisor, whose capable guidance, knowledge and encouragement have been of the greatest value to me.

I would like to thank my friend and colleague Bill Mark for his valuable help during various stages of this study and for the use of his unique data analysis code, NEWED.

I would also like to thank Steve Markhauser for his assistance in the construction of the test rig and for his very practical outlook to production challenges.

A very special thank you goes to Norma Procyshyn, a friend during difficult times, for her struggle with my handwriting and for turning it into the present manuscript.

I also acknowledge, with gratitude, the financial support of the Department of Mechanical Engineering (McGill), Faculty of Graduate Studies and Research (McGill), Natural Science and Engineering Research Council of Canada and Le Fonds pour la Formation de Chercheurs et l'Aide à la Recherche (FCAR).

NOTE ON CONTRIBUTIONS TO ORIGINAL KNOWLEDGE

The following findings of this study can be considered as contributions to original knowledge.

1. For the first time, conclusive experimental evidence has been furnished for the existence of a multiple-flexible-cylinder, stiffness-controlled fluidelastic instability mechanism requiring coupled motion between adjacent cylinders.
2. It is shown that for this array the resulting flow-induced vibrations are dominated by the stiffness-controlled instability mechanism, requiring multiple flexible cylinders, as opposed to the damping controlled instability mechanism, requiring only a single flexible cylinder. Furthermore, it is shown that the critical flow velocity is considerably less sensitive to structural damping than other results available in the literature. Conversely, the critical flow velocity is considerably more sensitive to dimensionless mass than other results indicate. These results rule out the applicability of a Connor's type equation to predict fluidelastic instability for this array.
3. The effect of frequency detuning upon the instability threshold has been studied in detail to reveal a substantial understanding of the underlying physics of the instability mechanism.

4. The very practical and dangerous scenario of both static and dynamic instability limits co-existing with close proximity to each other in the same array has been detected for the first time. Furthermore, it has been possible to interchange from one type of instability to the other by varying one, or more of the mechanical properties of the flexible cylinders.

Contents

ABSTRACT	ii
SOMMAIRE	iv
ACKNOWLEDGEMENTS	vi
NOTE ON CONTRIBUTIONS TO ORIGINAL KNOWLEDGE	vii
NOMENCLATURE	xxxiii
1 INTRODUCTION	1
1.1 General Introduction	1
1.2 Turbulent Buffeting	2
1.3 Flow-Periodicity-Induced-Resonance	5
1.4 Fluidelastic Instability	7
1.5 Mathematical Models	11
1.5.1 Models Requiring No Experimental Data	11
1.5.2 Models Based on Unsteady Flow Theory Requiring Extensive Experimental Data and the Dynamic Instability Mechanisms .	12
1.5.3 Quasi-Steady Models Requiring Limited Experimental Data .	15
1.5.4 Non-Linear Models	16
1.6 Motivation for the Present Work	17
1.7 Objectives of the Study	19

2	A GENERAL OVERVIEW OF THE WIND TUNNEL AND THE ARRAY	20
2.1	The Wind Tunnel	20
2.2	The Cylinder Array	21
3	VIBRATION MEASUREMENT APPARATUS	23
3.1	The Vibration Measurement Insert	23
3.2	Vibration Measurement Instrumentation	24
3.3	Vibration Measurement Procedure	26
4	DYNAMIC RESULTS	28
4.1	An Overview of the Dynamic Results	28
4.2	Multiple-flexible Cylinder Fluidelastic Instability	29
4.2.1	A Single Flexible Cylinder	29
4.2.2	Two Flexible Cylinders and the Existence of Coupled Motion .	30
4.2.3	Four Flexible Cylinders and the Multiple-Flexible Cylinder, Stiffness Controlled Instability	33
4.2.4	Effect of Number of Flexible Cylinders on Dynamic Instability	36
4.2.5	Effect of Flexible Cylinder Position	37
4.2.6	Effect of Dimensionless Cylinder Mass	39
4.2.7	Effect of Cylinder Damping	41
4.3	The Effect of Frequency Detuning	42
4.3.1	Introduction	42
4.3.2	The Effect of Inter-Cylinder Frequency Variation	43
4.3.3	Further Effects of Frequency Detuning	49
4.4	Static Displacement and Instability	50
4.4.1	Two Flexible Cylinders	50
4.4.2	Three Flexible Cylinders	53
5	FORCE MEASUREMENT APPARATUS	56

5.1	The Force Measurement Insert, the Force Balance and the Associated Instrumentation	56
5.2	The Force Measurement Procedure	57
6	FORCE MEASUREMENTS	60
6.1	Variation of The Drag Coefficient, C_D , with Reynolds Number	60
6.1.1	Variation of The Drag Coefficient, C_D , with Reynolds Number for a Single Cylinder	60
6.1.2	Variation of the Drag Coefficient, C_D , with Reynolds Number for Cylinders in Different Rows of the Array	60
6.2	Lift and Drag Maps	62
6.2.1	Lift and Drag Maps for a Third Row Cylinder	62
6.2.2	Lift and Drag Maps for a Second Row Cylinder	66
6.2.3	Lift and Drag Maps for a First Row Cylinder	67
6.2.4	Lift and Drag Maps for Fourth, Fifth and Seventh Row Cylinders	67
6.3	Effect of the Surrounding Cylinders' Motion	68
6.3.1	The Effect of Surrounding Cylinder Motion Upon a First Row Cylinder	68
6.3.2	The Effect of Surrounding Cylinder Motion Upon a Second Row Cylinder	69
6.3.3	The Effect of Surrounding Cylinder Motion Upon a Third Row Cylinder	70
6.3.4	The Effect of Surrounding Cylinder Motion Upon Fourth, Fifth and Seventh Row Cylinders	72
7	THEORETICAL MODEL	74
7.1	Introduction	74
7.2	Equations of Motion	75
7.3	Fluid Forces	76
7.4	Time Delays and Apparent Displacements	78

8 THEORETICAL RESULTS	85
8.1 Multiple-Flexible Cylinder Fluidelastic Instability	85
8.1.1 Four Flexible Cylinders and The Instability Threshold	85
8.1.2 Sensitivity of Four Flexible Cylinder Motion to "Unsteady Ef- fects"	87
8.1.3 Sensitivity of Four Flexible Cylinder Motion to Fluid Force Co- efficients	88
8.1.4 Multiple Instability Boundaries	89
8.1.5 Three Flexible Cylinders and The Instability Threshold	90
8.2 The Effect of Frequency detuning Upon the Instability Threshold . .	90
8.2.1 The Effect of the Mass-Damping Parameter	90
8.2.2 The Effect of Cylinder Damping	90
8.2.3 The Effect of Dimensionless-Cylinder Mass	92
8.2.4 The Effect of Flexible Cylinder Position	92
9 A GENERAL DISCUSSION & CONCLUSIONS	94
9.1 Single and Two Flexible Cylinders	94
9.2 Three and Four Flexible Cylinders	95
9.3 Applicability of a "Connors' type" Instability Criterion	98
9.4 Frequency Detuning	99
9.5 Static Displacement and Instability.	101
BIBLIOGRAPHY	103
TABLES	115
FIGURES	128
APPENDIX 1	298
APPENDIX 2	301

APPENDIX 3	303
APPENDIX 4	305
APPENDIX 5	308
APPENDIX 6	311

List of Figures

2.1	Schematic of the wind tunnel	129
2.2	The rigid portion of the array (the upper plate is removed for a better view)	130
2.3	Distance From the Leading Edge of the Array (\diamond high velocity, \square low velocity).	131
3.1	The vibration insert (The rigid portion of the array has been removed in this instance for a better view)	132
3.2	Upper portion of the vibration insert.	133
3.3	Lower portion of the vibration insert.	134
3.4	The lower platform with sliders.	135
3.5	Platform holding oil pots.	136
3.6	A typical flexible cylinder and its mounting system (reproduced from ref. [6])	137
3.7	The velocity pick-up.	138
3.8	Comparison of accelerometer (black) and velocity pick-up (red) signals (differentiated).	139
4.1	Schematic drawing of the middle portion of the cylinder array.	140

- 4.2 Typical vibrational acceleration power spectra for a single flexible cylinder in the fourth row of the array 141
- 4.3 Variation of the in-flow (a) and cross-flow (b) vibrational power spectra with flow velocity, $(U_\infty/f_n d)$ (single-flexible-cylinder in the fourth row $\bar{m} = 280, f_3 = 10$ Hz and $\delta = 0.014$). 142
- 4.4 Rms vibrational acceleration of cylinder 4 as a function of the non-dimensional flow velocity, $U/f_n d$ (single flexible cylinder in the fourth row, $\bar{m} = 280, f_3 = 10$ Hz and $\delta = 0.014$). 143
- 4.5 Variation of the fluidelastic frequencies of cylinder 4 with the non-dimensional flow velocity, $U/f_n d$ (single flexible cylinder in the fourth row, $\bar{m} = 280, f_3 = 10$ Hz and $\delta = 0.014$). 144
- 4.6 Variation of the in-flow vibrational power spectra with flow velocity for cylinder 1 (two-flexible cylinders - 1 and 3 -, $\bar{m} = 280, f_1 = f_3 = 10$ Hz and $\delta = 0.014$). 145
- 4.7 Variation of the in-flow (a) and cross-flow (b) vibration power spectra with flow velocity for cylinder 3 (two-flexible cylinders - 1 and 3 -, $\bar{m} = 280, f_1 = f_3 = 10$ Hz and $\delta = 0.014$). 146
- 4.8 Variation of the major fluidelastic frequencies of cylinders 1 and 3 with non-dimensional flow velocity (two-flexible cylinders -1 and 3 -, $\bar{m} = 280, f_1 = f_3 = 10$ Hz and $\delta = 0.014$). 147
- 4.9 Rms acceleration of cylinders 1 and 3 at major fluidelastic frequencies as a function of the non-dimensional flow velocity. (Two-flexible cylinders - 1 and 3 -, $\bar{m} = 280, f_1 = f_3 = 10$ Hz and $\delta = 0.014$.) . . . 148
- 4.10 In-flow vibrational acceleration power spectra of cylinders 1 and 3 at $U_\infty = 7.8$ m/s (two-flexible cylinders -1 and 3 -, $\bar{m} = 280, f_1 = f_3 = 10$ Hz and $\delta = 0.014$). 149

4.11	In-flow acceleration cross-spectra of cylinders 1 and 3 at $U_\infty = 7.8$ m/s (two-flexible cylinders -1 and 3 -, $\bar{m} = 280$, $f_1 = f_3 = 10$ Hz and $\delta = 0.014$).	150
4.12	Coherence between the in-flow signals of cylinders 1 and 3 at $U_\infty = 7.8$ m/s (two-flexible-cylinders - 1 and 3 -, $\bar{m} = 280$, $f_1 = f_3 = 10$ Hz and $\delta = 0.014$).	151
4.13	Coherence between the in-flow vibration signals of cylinders 1 and 3 at different flow velocities (two-flexible cylinders - 1 and 3 -, $m = 280$, $f_1 = f_3 = 10$ Hz and $\delta = 0.014$).	152
4.14	Coherence between the in-flow signal of cylinder 1 and the cross-flow signal of cylinder 3 at different flow velocities (two-flexible-cylinders 1 and 3 -, $\bar{m} = 280$, $f_1 = f_3 = 10$ Hz and $\delta = 0.014$).	153
4.15	A two-flexible cylinder configuration with flexible cylinders in the second and third rows of the array.	154
4.16	Variation of the in-flow (a) and cross-flow (b) vibration power spectra with flow velocity for cylinder 2 (two-flexible cylinders -2 and 3 -, $\bar{m} = 280$, $f_2 = f_3 = 10$ Hz and $\delta = 0.014$).	155
4.17	Variation of the in-flow (a) and cross-flow (b) vibration power spectra with flow velocity for cylinder 3 (two-flexible cylinders - 2 and 3 -, $\bar{m} = 280$, $f_2 = f_3 = 10$ Hz and $\delta = 0.014$).	156
4.18	Coherence between the cross-flow vibration signals of cylinders 2 and 3 at different flow velocities (two-flexible cylinders - 2 and 3 -, $\bar{m} = 280$, $f_2 = f_3 = 10$ Hz and $\delta = 0.014$).	157
4.19	Variation of the in-flow (a) and cross-flow (b) vibration power spectra with flow velocity for cylinder 4 (two-flexible cylinders 4 and 6 -, $\bar{m} = 280$, $f_4 = f_6 = 10$ Hz and $\delta = 0.014$).	158
4.20	Variation of the in-flow (a) and cross-flow vibration power spectra with flow velocity for cylinder 6 (two-flexible cylinders - 4 and 6 -, $\bar{m} = 280$, $f_4 = f_6 = 10$ Hz and $\delta = 0.014$).	159

- 4.21 A four-flexible cylinder configuration in the upstream rows of the array 160
- 4.22 In-flow directional rms acceleration of cylinders 1, 2R, 2L and 3 at their major fluidelastic frequencies as a function of the non-dimensional flow velocity (four-flexible cylinders - 1, 2R, 2L and 3 -, $\bar{m} = 280, f_1 = f_{2R} = f_{2L} = f_3 = 10$ Hz and $\delta = 0.014$). 161
- 4.23 Cross-flow directional rms acceleration of cylinders 1, 2R, 2L and 3 at their major fluidelastic frequencies as a function of the non-dimensional flow velocity (four-flexible cylinders - 1, 2R, 2L and 3 -, $\bar{m} = 280, f_1 = f_{2R} = f_{2L} = f_3 = 10$ Hz and $\delta = 0.014$). 162
- 4.24 Variation of the major fluidelastic frequencies of cylinders 1, 2R, 2L and 3 with non-dimensional flow velocity (four-flexible cylinders - 1, 2R, 2L and 3 -, $\bar{m} = 280, f_1 = f_{2R} = f_{2L} = f_3 = 10$ Hz and $\delta = 0.014$). 163
- 4.25 Coherence between the motion of flexible cylinders at different non-dimensional flow velocities (four-flexible cylinders - 1, 2R, 2L and 3 -, $\bar{m} = 280, f_1 = f_{2R} = f_{2L} = f_3 = 10$ Hz and $\delta = 0.014$). 164
- 4.26 Acceleration power spectra of cylinders 1, 2R, 2L and 3 in the in- and cross-flow directions at $U/f_n d \approx 57.5$ (four-flexible cylinders - 1, 2R, 2L and 3 -, $\bar{m} = 280, f_1 = f_{2R} = f_{2L} = f_3 = 10$ Hz and $\delta = 0.014$). . . . 165
- 4.27 Coherence between the cross-flow signals of cylinders 3 and 2L (a) and between in-flow signals of cylinders 3 and 1 at $U/f_n d \approx 57.5$ (four-flexible cylinders - 1, 2R, 2L and 3 -, $\bar{m} = 280, f_1 = f_{2R} = f_{2L} = f_3 = 10$ Hz and $\delta = 0.014$). 166
- 4.28 Cross-spectra between the cross-flow signals of cylinders 3 and 2L (a) and between the in-flow signals of cylinders 3 and 1 at $U/f_n d \approx 57.5$ four-flexible cylinders - 1, 2R, 2L and 3 -, $\bar{m} = 280, f_1 = f_{2R} = f_{2L} = f_3 = 10$ Hz and $\delta = 0.014$). 167
- 4.29 Variation of the in-flow (a) and cross-flow (b) power spectra with flow velocity for cylinder 3 (four-flexible cylinders - 1, 2R, 2L and 3 -, $\bar{m} = 280, f_1 = f_{2R} = f_{2L} = f_3 = 10$ Hz and $\delta = 0.014$). 168

- 4.30 Rms acceleration of cylinder 3 at its major fluidelastic frequencies as a function of the non-dimensional flow velocity (four-flexible cylinders 1, 2R, 2L and 3 -, $\bar{m} = 280, f_1 = f_{2R} = f_{2L} = f_3 = 10$ Hz and $\delta = 0.014$). 169
- 4.31 Variation of the major fluidelastic frequencies of cylinder 3 with non-dimensional flow velocity (four-flexible cylinders - 1, 2R, 2L and 3 -, $\bar{m} = 280, f_1 = f_{2R} = f_{2L} = f_3 = 10$ Hz and $\delta = 0.014$). 170
- 4.32 In- and cross-flow directional rms acceleration of cylinders 2R, 2L and 3 at their major fluidelastic frequencies as a function of the non-dimensional flow velocity (three-flexible cylinders - 2R, 2L and 3 -, $\bar{m} = 280, f_{2R} = f_{2L} = f_3 = 7$ Hz and $\delta = 0.014$). 171
- 4.33 Variation of the major fluidelastic frequencies of cylinders 2R, 2L and 3 with non-dimensional flow velocity (three-flexible cylinders - 2R, 2L and 3 -, $\bar{m} = 280, f_{2R} = f_{2L} = f_3 = 7$ Hz and $\delta = 0.014$). 172
- 4.34 In-flow directional rms acceleration of cylinders 2, 3R, 3L and 4 at their major fluidelastic frequencies as a function of the non-dimensional flow velocity (four-flexible cylinders - 2, 3R, 3L and 4 -, $\bar{m} = 280, f_2 = f_{3R} = f_{3L} = f_4 = 10$ Hz and $\delta = 0.014$). 173
- 4.35 Cross-flow directional rms acceleration of cylinders 2, 3R, 3L and 4 at their major fluidelastic frequencies as a function of the non-dimensional flow velocity (four flexible cylinders - 2, 3R, 3L and 4 -, $\bar{m} = 280, f_2 = f_{3R} = f_{3L} = f_4 = 10$ Hz and $\delta = 0.014$). 174
- 4.36 Variation of the in-flow (a) and cross-flow (b) vibration power spectra with flow velocity for cylinder 3 (four-flexible cylinders - 3, 4R, 4L and 5 -, $\bar{m} = 280, f_3 = f_{4R} = f_{4L} = f_5 = 10$ Hz and $\delta = 0.014$). 175
- 4.37 Variation of the in-flow (a) and cross-flow (b) vibration power spectra with the flow velocity for cylinder 4R (four-flexible cylinders - 3, 4R, 4L and 5 -, $\bar{m} = 280, f_3 = f_{4R} = f_{4L} = f_5 = 10$ Hz and $\delta = 0.014$). . . 176

4.38 Variation of the in-flow (a) and cross-flow (b) vibration power spectra with the flow velocity for cylinder 4L (four-flexible cylinders - 3, 4R, 4L and 5 -, $\bar{m} = 280, f_3 = f_{4R} = f_{4L} = f_5 = 10$ Hz and $\delta = 0.014$). . . 177

4.39 Variation of the in-flow (a) and cross-flow (b) vibration power spectra with the flow velocity for cylinder 5 (four-flexible cylinders - 3, 4R, 4L and 5 -, $\bar{m} = 280, f_3 = f_{4R} = f_{4L} = f_5 = 10$ Hz and $\delta = 0.014$). 178

4.40 In-flow directional rms acceleration of cylinders 3, 4R 4L and 5 at their major fluidelastic frequencies as a function of the non-dimensional flow velocity (four flexible cylinders - 3, 4R, 4L and 5 -, $\bar{m} = 280, f_3 = f_{4R} = f_{4L} = f_5 = 7$ Hz and $\delta = 0.014$). 179

4.41 Variation of the in-flow (a) and cross-flow (b) vibration power spectra with the flow velocity for cylinder 4 (four-flexible cylinders - 4, 5R, 5L and 6 -, $\bar{m} = 280, f_4 = f_{5R} = f_{5L} = f_6 = 7$ Hz and $\delta = 0.014$). 180

4.42 Variation of the in-flow (a) and cross-flow (b) vibration power spectra with the flow velocity for cylinder 5R (four flexible cylinders - 4, 5R, 5L and 6 -, $\bar{m} = 280, f_4 = f_{5R} = f_{5L} = f_6 = 7$ Hz and $\delta = 0.014$). . . 181

4.43 Variation of the in-flow (a) and cross-flow (b) vibration power spectra with the flow velocity for cylinder 5L (four flexible cylinders - 4, 5R, 5L and 6 -, $\bar{m} = 280, f_4 = f_{5R} = f_{5L} = f_6 = 7$ Hz and $\delta = 0.014$). . . 182

4.44 Variation of the in-flow (a) and cross-flow (b) vibration power spectra with the flow velocity for cylinder 6 (four flexible cylinders - 4, 5R, 5L and 6 -, $\bar{m} = 280, f_4 = f_{5R} = f_{5L} = f_6 = 7$ Hz and $\delta = 0.014$). 183

4.45 Variation of non-dimensional critical velocity with flexible cylinder position in the array (four-flexible cylinders, $\bar{m} = 280, \delta = 0.014, \bigcirc =$ unstable, and $\bullet =$ unstable). 184

4.46 Variation of non-dimensional critical velocity with dimensionless cylinder mass for four flexible cylinders (cylinders 1, 2R, 2L and 3 and $\delta = 0.014$). 185

- 4.47 Variation of non-dimensional critical velocity with cylinder damping for four flexible cylinders (cylinders 1, 2R, 2L and 3, $m = 280$ and 490) 186
- 4.48 Acceleration power spectra of cylinders 1, 2R, 2L and 3 in the in- and cross-flow directions at $U/f_n d \approx 18$ (four-flexible cylinders - 1, 2R, 2L and 3 -, $\bar{m} = 280, f_1 = f_{2R} = f_{2L} = 6.375$ Hz, $f_3 = 10$ Hz and $\delta = 0.014$) 187
- 4.49 Acceleration power spectra of cylinders 1, 2R, 2L and 3 in the in- and cross-flow directions at $U/f_n d \approx 39$ (four-flexible cylinders - 1, 2R, 2L and 3 -, $\bar{m} = 280, f_1 = f_{2R} = f_{2L} = 6.375$ Hz, $f_3 = 10$ Hz and $\delta = 0.014$) 188
- 4.50 Variation of the major fluidelastic frequencies of cylinders 1, 2R, 2L and 3 with non-dimensional flow velocity (four-flexible cylinders - 1, 2R, 2L and 3 -, $\bar{m} = 280, f_1 = f_{2R} = f_{2L} = 6.375$ Hz, $f_3 = f_n = 10$ Hz and $\delta = 0.014$). 189
- 4.51 In-flow directional rms acceleration of cylinders 1, 2R, 2L and 3 at their major fluidelastic frequencies as a function of the non-dimensional flow velocity (four-flexible cylinders - 1, 2R, 2L and 3 -, $\bar{m} = 280, f_1 = f_{2R} = f_{2L} = 6.375$ Hz, $f_3 = f_n = 10$ Hz and $\delta = 0.014$). 190
- 4.52 Cross-flow directional rms acceleration of cylinders 1, 2R, 2L and 3 at their major fluidelastic frequencies as a function of the non-dimensional flow velocity (four-flexible cylinders - 1, 2R, 2L and 3 -, $\bar{m} = 280, f_1 = f_{2R} = f_{2L} = 6.375$ Hz, $f_3 = f_n = 10$ Hz and $\delta = 0.014$). 191
- 4.53 Rms acceleration of cylinder 3 at its major fluidelastic frequencies as a function of the non-dimensional flow velocity (four-flexible cylinders - 1, 2R, 2L and 3 -, $\bar{m} = 280, f_1 = f_{2R} = f_{2L} = 6.5$ Hz, $f_3 = 10$ Hz and $\delta = 0.014$). 192
- 4.54 Acceleration power spectra of cylinders 1, 2R, 2L and 3 in the in- and cross-flow directions at $U/f_n d \approx 33$ (four-flexible cylinders - 1, 2R, 2L and 3 -, $\bar{m} = 280, f_1 = f_{2R} = f_{2L} = 13.5$ Hz, $f_3 = 10$ Hz and $\delta = 0.014$). 193

- 4.55 Acceleration power spectra of cylinders 1, 2R, 2L and 3 in the in- and cross-flow directions at $U/f_n d = 65$ (four-flexible cylinders - 1, 2R, 2L and 3 -, $\bar{m} = 280$, $f_1 = f_{2R} = f_{2L} = 13.5$ Hz, $f_3 = 10$ Hz and $\delta = 0.014$). 194
- 4.56 Variation of the major fluidelastic frequencies of cylinders 1, 2R, 2L and 3 with non-dimensional flow velocity (four-flexible cylinders - 1, 2R, 2L and 3 -, $\bar{m} = 280$, $f_1 = f_{2R} = f_{2L} = 13.5$ Hz, $f_3 = f_n = 10$ Hz and $\delta = 0.014$). 195
- 4.57 Rms acceleration of cylinder 3 at its major fluidelastic frequencies as a function of the non-dimensional flow velocity (four-flexible cylinders - 1, 2R, 2L and 3 -, $\bar{m} = 280$, $f_1 = f_{2R} = f_{2L} = 13.5$ Hz, $f_3 = f_n = 10$ Hz and $\delta = 0.014$). 196
- 4.58 Effect of frequency detuning between adjacent cylinders on non-dimensional critical flow velocity (four-flexible cylinders - 1, 2R, 2L and 3 -, $\bar{m} = 280$, $f_1 = f_{2R} = f_{2L} = 13.5$ Hz, $f_3 = 10$ Hz and $\delta = 0.014$). 197
- 4.59 Effect of frequency detuning on $U_c/f_{n1}d$ (four-flexible cylinders - 1, 2R, 2L and 3 -, $\bar{m} = 280$, $[f_1 = f_3] \neq [f_{2R} = f_{2L}]$, and $\delta = 0.014$). 198
- 4.60 Effect of frequency detuning on $U_c/f_{n2}d$ (four-flexible cylinders - 1, 2R, 2L and 3 -, $\bar{m} = 280$, $[f_1 = f_3] \neq [f_{2R} = f_{2L}]$, and $\delta = 0.014$). 199
- 4.61 Effect of frequency detuning on $U_c/(f_{n1}f_{n2})^{0.5}d$ (four-flexible cylinders - 1, 2R, 2L and 3 -, $\bar{m} = 280$, $[f_1 = f_3] \neq [f_{2R} = f_{2L}]$, and $\delta = 0.014$). 200
- 4.62 A two-flexible cylinder configuration in the second row of the array. 201
- 4.63 Variation of the in-flow (a) and cross-flow (b) vibration power spectra with the flow velocity for cylinder 2R (two-flexible cylinders - 2R, and 2L -, $m = 280$, $f_{2R} = f_{2L} = 7$ Hz and $\delta = 0.014$). 202
- 4.64 Variation of the in-flow (a) and cross-flow (b) vibration power spectra with the flow velocity for cylinder 2L (two-flexible cylinders - 2R, and 2L -, $\bar{m} = 280$, $f_{2R} = f_{2L} = 7$ Hz and $\delta = 0.014$). 203

4.65	Variation of the major cross-flow fluidelastic frequencies of cylinders 2R and 2L with non-dimensional flow velocity (two-flexible cylinders 2R, and 2L -, $\bar{m} = 280, f_{2R} = f_{2L} = 7$ Hz and $\delta = 0.014$).	204
4.66	Rms acceleration of cylinders 2R and 2L at their major cross-flow frequencies as a function of the non-dimensional flow velocity (two-flexible cylinders - 2R, and 2L -, $\bar{m} = 280, f_{2R} = f_{2L} = 7$ Hz and $\delta = 0.014$).	205
4.67	Variation of the cylinder cross-flow displacement with non-dimensional flow velocity (two flexible cylinders - 2R, and 2L -, $\bar{m} = 280, f_{2R} = f_{2L} = 7$ Hz and $\delta = 0.014$).	206
4.68	Vibrational power spectra of cylinder 2L at $U_\infty \approx 15.3$ m/s. (two-flexible cylinders - 2R, and 2L -, $\bar{m} = 280, f_{2R} = f_{2L} = 7$ Hz and $\delta = 0.014$).	207
4.69	Variation of the in-flow (a) and cross-flow (b) vibration power spectra with the flow velocity for cylinder 2L (three-flexible cylinders 2R, 2L and 3 -, $\bar{m} = 280, f_{2R} = f_{2L} = f_3 = 7$ Hz and $\delta = 0.014$).	208
4.70	Variation of the in-flow (a) and cross-flow (b) vibration power spectra with the flow velocity for cylinder 2L (three-flexible cylinders - 2R, 2L and 3 -, $\bar{m} = 280, f_{2R} = f_{2L} = f_3 = 7$ Hz and $\delta = 0.20$).	209
4.71	Variation of the major cross-flow fluidelastic frequency of cylinder 2L with non-dimensional flow velocity (three-flexible cylinders 2R, 2L and 3 -, $\bar{m} = 280, f_{2R} = f_{2L} = f_3 = 7$ Hz and $\delta = 0.20$).	210
4.72	Rms acceleration of cylinder 2L at its major cross-flow frequency as a function of non-dimensional flow velocity (three-flexible cylinders - 2R, 2L and 3 -, $\bar{m} = 280, f_{2R} = f_{2L} = f_3 = 7$ Hz and $\delta = 0.20$).	211
4.73	In- and Cross-flow vibrational power spectra of cylinder 2L at $U_\infty = 16.9$ m/s (three-flexible cylinders - 2R, 2L and 3 -, $\bar{m} = 280, f_{2R} = f_{2L} = f_3 = 7$ Hz and $\delta = 0.20$).	212

4.74	Variation of the cylinder cross-flow displacement with non-dimensional flow velocity (three-flexible cylinders - 2R, 2L and 3 -, $\bar{m} = 280$, $f_{2L} = f_{2R}f_3 = 7$ Hz and $\delta = 0.20$).	213
4.75	Variation of the in-flow (a) and cross-flow (b) vibration power spectra with flow velocity for cylinder 2L (three-flexible cylinders - 2R, 2L and 3 -, $\bar{m} = 280$, $f_{2R} = f_{2L} = 7$ Hz, $f_3 = 13.5$ Hz and $\delta = 0.14$).	214
4.76	Rms acceleration of cylinder 2L at its major cross-flow frequency as a function of non-dimensional flow velocity (three-flexible cylinders - 2R, 2L and 3 -, $\bar{m} = 280$, $f_{2L} = f_{2R} = 7$ Hz, $f_3 = 13.5$ Hz and $\delta = 0.14$).	215
4.77	Variation of the major cross-flow fluidelastic frequency of cylinder 2L with non-dimensional flow velocity (three-flexible cylinders - 2R, 2L and 3 -, $m = 280$, $f_{2R} = f_{2L} = 7$ Hz, $f_3 = 13.5$ Hz and $\delta = 0.14$).	216
4.78	In- and cross-flow vibrational power spectra of cylinder 2L at $U_\infty = 16.1$ m/s (three-flexible cylinders - 2R, 2L and 3 -, $\bar{m} = 280$, $f_{2R} = f_{2L} = 7$ Hz, $f_3 = 13.5$ Hz and $\delta = 0.14$).	217
4.79	Variation of the cylinder cross-flow displacement with non-dimensional flow velocity (three-flexible cylinders - 2R, 2L and 3 -, $\bar{m} = 280$, $f_{2L} = f_{2R} = 7$ Hz, $f_3 = 13.5$ Hz and $\delta = 0.14$).	218
5.1	The force measurement insert.	219
5.2	The gear arrangement.	221
5.3	The force balance and the instrumented cylinder.	222
5.4	Calibration curve for the force transducers.	223
6.1	Variation of the steady drag coefficient of a single cylinder in cross-flow with Reynolds number. The original figure from reference 4. Note: drag coefficient values determined in this study are shown by full triangles.	224

6.2	Variation of the drag coefficient with Reynolds number, for a cylinder in the first row of the array ($\bar{x} = 0, \bar{y} = 0$)	225
6.3	Variation of the drag coefficient with Reynolds number for cylinders in the second (\blacklozenge), third (\blacklozenge) and fourth (\blacktriangledown) rows of the array ($\bar{x} = 0, \bar{y} = 0$)	226
6.4	Variation of the drag coefficient with Reynolds number for cylinders in the fifth (\blacksquare) and seventh (\blacklozenge) rows of the array ($\bar{x} = 0, \bar{y} = 0$).	227
6.5	Variation of the drag coefficient with position in the array at a flow velocity of 16.6 m/s ($\bar{x} = 0, \bar{y} = 0$).	228
6.6	Variation of the drag coefficient with Reynolds number for cylinders in the first (\blacklozenge), seventh (\blacksquare) and rows of the array ($\bar{x} = 0, \bar{y} = 0$).	229
6.7	Variation of the drag coefficient with Reynolds number for cylinders in the second (\blacksquare), third (\blacklozenge), fourth (\blacktriangle) and fifth (\blacklozenge) rows of the array ($\bar{x} = 0, \bar{y} = 0$).	230
6.8	Variation of the drag coefficient with cylinder displacement (third row cylinder, $U_\infty = 8.3$ m/s).	231
6.9	Variation of the drag coefficient with cylinder displacement (third row cylinder, $U_\infty = 16.6$ m/s).	232
6.10	Variation of drag the coefficient with cylinder displacement (third row cylinder, $U_\infty = 21.4$ m/s).	233
6.11	Variation of the lift coefficient with cylinder displacement (third row cylinder, $U_\infty = 8.3$ m/s).	234
6.12	Variation of the lift coefficient with cylinder displacement (third row cylinder, $U_\infty = 16.6$ m/s).	235
6.13	Variation of the lift coefficient with cylinder displacement (third row cylinder, $U_\infty = 21.4$ m/s).	236
6.14	Variation of the force coefficient with cylinder displacement (third row cylinder, $U_\infty = 8.3$ m/s).	237
6.15	Variation of the force coefficient with cylinder displacement (third row cylinder, $U_\infty = 16.6$ m/s).	238

6.16	Variation of the force coefficient vector with cylinder displacement (third row cylinder, $U_\infty = 21.4$ m/s).	239
6.17	Comparison between the force coefficient vectors at $U_\infty = 8.3$ m/s (blue arrows) and the "normalised" force coefficient vectors at $U_\infty = 21.4$ m/s (red arrows).	240
6.18	Variation of the lift coefficient with \bar{y} at $\bar{x} = 0$ (third row cylinder, $U_\infty = 8.3$ m/s).	241
6.19	Variation of the lift coefficient with \bar{y} at $\bar{x} = 0$ (third row cylinder, $U_\infty = 16.6$ m/s).	242
6.20	Variation of the lift coefficient with \bar{y} at $\bar{x} = 0$ (third row cylinder, $U_\infty = 21.4$ m/s).	243
6.21	Variation of the frequency ratio, w^2/w_0^2 , with non-dimensional flow velocity and cross flow displacement (third row cylinder, $\bar{m} = 280$).	244
6.22	Variation of the drag coefficient with cylinder displacement (second row cylinder, $U_\infty = 16.6$ m/s).	245
6.23	Variation of the lift coefficient with cylinder displacement (second row cylinder, $U_\infty = 16.6$ m/s).	246
6.24	Variation of the force coefficient vector with cylinder displacement (sec- ond row cylinder, $U_\infty = 16.6$ m/s).	247
6.25	Variation of the lift coefficient with \bar{y} at $\bar{x} = 0$ (second row cylinder, $U_\infty = 16.6$ m/s).	248
6.26	The experimental (\blacklozenge) and theoretical (\diamond) variation of cross-flow flui- delastic frequency of a second row flexible cylinder with non-dimensional flow velocity ($\bar{m} = 280$, $f_n = 7$ Hz and $\delta = 0.014$).	249
6.27	Variation of the lift coefficient with cylinder displacement (first row cylinder, $U_\infty = 16.6$ m/s).	250
6.28	Variation of the drag coefficient with cylinder displacement (first row cylinder, $U_\infty = 16.6$ m/s).	251

6.29	Variation of the force coefficient vector with cylinder displacement (first row cylinder, $U_\infty = 16.6$ m/s).	252
6.30	Variation of the lift coefficient with cylinder displacement (fourth row cylinder, $U_\infty = 16.6$ m/s).	253
6.31	Variation of the lift coefficient with cylinder displacement (fifth row cylinder, $U_\infty = 16.6$ m/s).	254
6.32	Variation of the lift coefficient with cylinder displacement (seventh row cylinder, $U_\infty = 16.6$ m/s).	255
6.33	Variation of the drag coefficient with cylinder displacement (fourth row cylinder, $U_\infty = 16.6$ m/s).	256
6.34	Variation of the drag coefficient with cylinder displacement (fifth row cylinder, $U_\infty = 16.6$ m/s).	257
6.35	Variation of the drag coefficient with cylinder displacement (seventh row cylinder, $U_\infty = 16.6$ m/s).	258
6.36	Variation of the force coefficient vector with cylinder displacement (fourth row cylinder, $U_\infty = 16.6$ m/s).	259
6.37	Variation of the force coefficient vector with cylinder displacement (fifth row cylinder, $U_\infty = 16.6$ m/s).	260
6.38	Variation of the force coefficient vector with cylinder displacement (seventh row cylinder, $U_\infty = 16.6$ m/s).	261
6.39	Changes in the fluid force coefficients of a first row cylinder due to the displacement of cylinder 1R.	262
6.40	Changes in the fluid force coefficients of a first row cylinder due to the displacement of cylinder 1L.	263
6.41	Changes in the fluid force coefficients of a first row cylinder due to the displacement of cylinder 2R.	264
6.42	Changes in the fluid force coefficients of a first row cylinder due to the displacement of cylinder 3.	265

6.43	Changes in the fluid force coefficients of a second row cylinder due to the displacement of cylinder 1R and 1L.	266
6.44	Changes in the fluid force coefficients of a second row cylinder due to the displacement of cylinders 3R, 3L and 4.	267
6.45	Changes in the fluid force coefficients of a third row cylinder due to the cross-flow displacement of cylinder 1 ($\Delta : U_\infty = 8.3$ m/s, $\square : U_\infty = 16.6$ m/s and $\diamond : U_\infty = 8.3$ m/s normalised).	268
6.46	Changes in the fluid force coefficients of a third row cylinder due to the displacement of cylinder 2R ($\Delta : U_\infty = 8.3$ m/s, $\square : U_\infty = 16.6$ m/s and $\diamond : U_\infty = 8.3$ m/s normalised).	269
6.47	Changes in the fluid force coefficients of a third row cylinder due to the displacement of cylinder 2L ($\Delta : U_\infty = 8.3$ m/s, $\square : U_\infty = 16.6$ m/s and $\diamond : U_\infty = 8.3$ m/s normalised).	270
6.48	Changes in the fluid force coefficients of a third row cylinder due to the displacement of cylinder 4R ($\Delta : U_\infty = 8.3$ m/s, $\square : U_\infty = 16.6$ m/s and $\diamond : U_\infty = 8.3$ m/s normalised).	271
6.49	Changes in the fluid force coefficients of a third row cylinder due to the displacement of cylinder 4L ($\Delta : U_\infty = 8.3$ m/s, $\square : U_\infty = 16.6$ m/s and $\diamond : U_\infty = 8.3$ m/s normalised).	272
6.50	Changes in the fluid force coefficients of a third row cylinder due to the displacement of cylinder 5 ($\Delta : U_\infty = 8.3$ m/s, $\square : U_\infty = 16.6$ m/s and $\diamond : U_\infty = 8.3$ m/s normalised).	273
6.51	Changes in the fluid force coefficients of fourth (\square), fifth (Δ) and seventh (\diamond) row cylinders due to the displacement of an upstream cylinder at $U_\infty = 16.6$ m/s.	274
6.52	Changes in the fluid force coefficients of fourth (\square), fifth (Δ) and seventh (\diamond) row cylinders due to the displacement of an upstream cylinder at $U_\infty = 16.6$ m/s.	275

6.53	Changes in the fluid force coefficients of fourth (\square), fifth (Δ) and seventh (\diamond) row cylinders due to the displacement of a downstream cylinder at $U_\infty = 16.6$ m/s.	276
6.54	The effect induced by the displacement of surrounding cylinders upon the fluid force coefficients of a third (\square) and fifth (\diamond) row cylinder at $U_\infty = 16.6$ m/s.	277
6.55	The effect induced by the displacement of surrounding cylinders upon the fluid force coefficients of a third (\square) and fifth (\diamond) row cylinder at $U_\infty = 16.6$ m/s.	278
6.56	The effect induced by the displacement of surrounding cylinders upon the fluid force coefficients of a third (\square) and fifth (\diamond) row cylinder at $U_\infty = 16.6$ m/s.	279
7.1	(a) Schematic of four flexible cylinders; (b) the resultant velocity vector for cylinder i	280
7.2	The apparent displacements	281
8.1	Variation of the non-dimensional critical flow velocity with dimensionless mass for a four-flexible cylinder configuration in different positions of the array.	282
8.2	Variation of non-dimensional critical flow velocity with damping for a four-flexible cylinder configuration.	283
8.3	The experimental and theoretical variation of the non-dimensional critical velocity with position in the array.	284
8.4	Effect of the time delay factor, μ , on the non-dimensional critical flow velocity	285
8.5	A "numerical search" for multiple instability bands.	286
8.6	Comparison of the non-dimensional critical flow velocity for three- and four-flexible cylinder configurations.	287

8.7	Variation of the non-dimensional critical flow velocity with dimensionless mass for a three flexible cylinder configuration in different positions of the array.	288
8.8	Effect of the mass-damping parameter upon the non-dimensional critical velocity of a detuned, four flexible cylinder configuration.	289
8.9	Effect of the mass-damping parameter upon the non-dimensional critical velocity of a detuned, four flexible cylinder configuration.	290
8.10	Comparison of experimental and theoretical detuning results.	291
8.11	Effect of damping upon the non-dimensional critical velocity of a detuned, four flexible cylinder configuration.	292
8.12	Effect of damping upon the non-dimensional critical velocity of a detuned, four flexible cylinder configuration.	293
8.13	Effect of dimensionless mass upon the non-dimensional critical velocity of a detuned, four flexible cylinder configuration.	294
8.14	Effect of dimensionless mass upon the non-dimensional critical velocity of a detuned, four flexible cylinder configuration.	295
8.15	Effect of dimensionless-mass upon the non-dimensional critical velocity of a detuned, four flexible cylinder configuration.	296
8.16	Effect of detuning at different locales in the array.	297

List of Tables

1.1	Empirical Values of the Constants in Equation (1.3)	116
1.2	Empirical Values of the Constants in Equation (1.5)	116
3.1	Certain Characteristics of Flexible Cylinders Used.	117
3.2	Characteristics of Accelerometers Used.	117
4.1	Summary of the Dynamic Response of a Single Flexible Cylinder in Different Rows of the Array	118
4.2	Summary of the Dynamic Response of Two Flexible Cylinders for Dif- ferent Positions in the Array. Notes: (1) This arrangement is stable in terms of dynamic instability, but unstable in terms of static instability. (2) An extra row of cylinders was added to the array in this experiment	118
4.3	Major Peaks in The In- and Cross-flow Acceleration Power Spectra of Four Flexible Cylinders Located in the Three Upstream Rows for $U_c/f_n d \approx 57.5$. Note: (1) This peak, observed in all cylinders, is a periodicity corresponding to $Su = 0.022$	119
4.4	Summary of the Dynamic Response of Three Flexible Cylinders Posi- tioned in the Second and the Third Rows. Note: (1) A static instability possibly occurred in this experiment.	120
4.5	Summary of the Dynamic Response of Four Flexible Cylinders Posi- tioned In Different Rows of the Array [$\bar{m} = 280, \delta = 0.014$] Notes: (1) cylinders 4L and 5 did not go unstable. (2) An extra row of cylinders was added to the array to eliminate downstream effects.	120

4.6	The Effect of Dimensionless Cylinder Mass on the Dynamic Response of Four Flexible Cylinders	121
4.7	The Effect of Initial Cylinder Damping on Dynamic Response	121
4.8	Major Peaks in the In- and Cross-Flow Acceleration Power Spectra of a -36% Detuned Four Flexible Cylinder Configuration Located in The Three Upstream Rows, $\bar{m} = 280, \delta = 0.014, f_1 = f_{2R} = f_{2L} = 6.375$ Hz and $f_3 = 10$ Hz.	122
4.9	Major Peaks in the In- and Cross-Flow Acceleration Power Spectra of a +35% Detuned Four Flexible Cylinder Configuration Located in The Three Upstream Rows, $\bar{m} = 280, \delta = 0.014, f_1 = f_{2R} = f_{2L} = 13.5$ Hz and $f_3 = 10$ Hz.	123
4.10	Initial Natural Frequency (f_i), Natural Frequency Ratio (f_1/f_3), Critical Velocity (U_{ic}) and Non-dimensional Critical Velocity of Cylinder 3 $\frac{U_{3c(det)}}{U_{3c}}$ for Various Detuning Experiments with Four Flexible Cylinders Located in The Three Upstream Rows of the Array (1, 2L, 2R and 3), $\bar{m} = 280, \delta = 0.014$. Note: (1) n.a. = not available (not measured).	124
4.11	Initial Natural Frequency (f_i) and Critical Flow Velocity (U_i) for Various Detuning Experiments With Four Flexible Cylinders Located in the Three Upstream Rows of the Array (1, 2L, 2R and 3), $\bar{m} = 280, \delta = 0.014$	124
4.12	Further Detuning Experiments With Four Flexible Cylinders ($\bar{m} = 280 \quad \delta = 0.014$)	125
6.1	The Values of Constants in the Equation $C_D = \alpha Re^\beta$ for a Cylinder Located in the Different Rows of the Array	126
6.2	Variation of the Lift and Drag Coefficients With Displacement at a Flow Velocity of 16.63 m/s.	126

- 8.1 The Effect of Varying the fluid Force Coefficients on the Non-dimensional Critical Velocity of the Array. Case A is for the Coefficients Given in Appendix 1. Case B is for the Same Coefficients Increased by 50% and Case C is for the Same Coefficients Decreased by 50% ($\delta = 0.014$). . . 127
- 8.2 The Effect of Varying the Fluid Force Coefficients on the Non-dimensional Critical Velocity of the Array. Case A is for the Coefficients Given in Appendix 1. Case B is for the Same Coefficients Increased by 50% and Case C is for the Same Coefficients Decreased by 50% ($m = 7500$). . . 127

Nomenclature

- [*B*] Fluid damping matrix (eq. (7.28))
- [*C*] Mechanical damping matrix (eq. (7.1))
- C_D* Drag coefficient ($F/\frac{1}{2}\rho U_\infty^2 \ell d$)
- C_L* Lift coefficient ($F/\frac{1}{2}\rho U_\infty^2 \ell d$)
- C_p* Random excitation coefficient (eq. (1.1))
- C_R* Random excitation coefficient (eq. (1.2))
- \bar{C}_D Drag coefficient non-dimensionalised with respect to the local approach velocity (eq. (7.5))
- \bar{C}_L Lift coefficient non-dimensionalised with respect to the local approach velocity (eq. (7.5))
- D, d* Cylinder diameter
- [*E*] Mechanical stiffness matrix (eq. (7.1))
- F* Fluid force(s) acting on a cylinder
- F** Fluid force vector (eq. (7.1))
- f* Natural frequency
- f_n* Natural frequency of oscillation for cylinders in still air (eq. (1.3))

f_x/f_y	Frequency ratio
g	Gravitational acceleration (9.8 m/s ²)
g_t	Time delay factor ($\exp(-\tau_t \lambda)$)
\bar{g}	Time delay factor ($\exp(-\Delta t \lambda)$)
k	Stiffness
$[K]$	Fluid stiffness matrix (eq. (7.28))
k_f	Total fluid stiffness (Appendix 2)
k_s	Structural restoring stiffness (Appendix 2)
k_T	Overall in-flow fluidelastic stiffness (Appendix 2)
L	Equilibrium separation between cylinders in the in-flow direction
ℓ	Cylinder length
L/d	Non-dimensional equilibrium separation between cylinders in the in-flow direction
m	Mass per unit length of the cylinder (eq. (1.3))
\bar{m}	Dimensionless mass ($m/\rho d^2$)
m_T	Mass of the cylinder (Appendix 2)
P	Pitch between cylinders ($((L^2 + T^2)^{1/2})$)
P/d	Non-dimensional value of P
R	Cylinder radius (eq. (7.17))
Re	Reynolds number $\rho U_\infty d/\mu$
S_i	Distance between cylinder centers (eq. (7.11))

Su	Strouhal number ($f_n d/U_\infty$)
T	Equilibrium separation between cylinders in the cross-flow direction
T/d	Non-dimensional value of T
T_i	Turbulence intensity
U_a	Approach velocity ($U(1 - R^2/x^2)$), (eq. (7.17))
U_c	Critical value of U_∞ for oscillatory instability (eq. (1.3))
U_{cp}	Critical value of U_p for oscillatory instability
U_{cr}	Critical value of U_∞ for static instability (Appendix 2)
U_G	Reference gap velocity ($U_\infty T/(T - 0.5d)$)
U_p	Pitch velocity ($U_\infty P/P - d$)
U_r	Resultant velocity vector (eq. (7.3))
U_∞	Free stream velocity
\bar{U}	Non-dimensional velocity ($U_\infty/f_n d$)
\bar{U}_c	Critical value of \bar{U} for oscillatory instability
x, \dot{x}, \ddot{x}	Cylinder displacement, velocity and acceleration in the in-flow direction
x, \dot{x}, \ddot{x}	\dot{x}, \ddot{x} and \ddot{x} normalised with respect to d
y, \dot{y}, \ddot{y}	Cylinder displacement, velocity and acceleration in the cross-flow direction
y, \dot{y}, \ddot{y}	\dot{y}, \ddot{y} and \ddot{y} normalised with respect to d
Y_{rms}	Rms displacement amplitude (eq. (1.1))
z	Distance

- Z Displacement vector
- α_i Angle of induced incidence (eq. (7.2))
- γ Size of turbulent structure
- δ Logarithmic decrement of mechanical dumping in still air (eq. (4.1))
- η_k Apparent displacement normal to the realigned gap velocity (eq. (7.8))
- λ Eigenvalue of the final solution
- μ Time delay factor
- μ Fluid viscosity
- ξ Damping ratio (eq. (1.1))
- ρ Density of fluid
- ξ_k Apparent displacement parallel to the realigned gap velocity (eq. (7.8))
- τ_i Time delay (S_i/U_G) (eq. (7.11))
- ϕ_n Eigenfunction (eq. (1.2))
- ω "In-flow" cyclical frequency of cylinder oscillation (eq. (6.2))
- ω_o Cyclical natural frequency of oscillation in still air (eq. (4.3)).

Chapter 1

INTRODUCTION

1.1 General Introduction

In tube-and-shell type heat exchangers tube vibration can be induced, and sustained, through energy supplied by the fluid flow(s) in the medium. Internal flow in the tubes, external axial flow along the tubes and external cross-flow over the tubes concurrently, or separately, can be the cause of such vibrations. Experience, accumulated the hard and expensive way, indicates that a major portion of tube failures both in the short and long run is caused by external cross-flow over the tubes. Paidoussis [1, 2, 3], Chen [4] documented a rich spectra of cross-flow induced tube failures resulting in costs that can peak to millions of dollars in terms of repair, replacement components and loss of operational revenue. The problem is compounded by the fact that, the ever-endless quest to minimise capital investment costs, as well as to reduce production costs per unit of energy generated, imposes additional constraints on the designers. The usual outcome is more compact components with smaller pitch to diameter ratios, higher flow velocities, elevated temperature differences, smaller and thinner tubes, all to increase convective and conductive heat transfer and minimise heavy water inventory in nuclear power plants. Unfortunately all the above trends tend to increase the occurrence of vibration and associated possibility of tube failure.

It is generally agreed that tube bundles subject to cross-flow experience vibration

due to one or an association of the following excitation mechanisms, namely; a) turbulent buffeting, b) flow periodicity, and c) fluidelastic instability.

In the following sections the important characteristics and some recent developments on these mechanisms will be discussed.

1.2 Turbulent Buffeting

The velocity fluctuations in the fluid cross-flow (normal to the tubes axes) result in random, broadband fluctuating pressures acting on the surface of the tubes. At all cross-flow velocities these fluctuating pressures transfer energy to the tubes. In turn, the tubes act as filters, extracting energy in the frequency bands around their natural frequencies, in particular their fundamental frequencies.

The tube vibrational response to fluctuating pressures is generally of low amplitude and the associated fretting wear at tube supports is a slow process, harmful only in the long run. Thus, for design purposes it is usually necessary to perform hundreds of hours of laboratory tests to determine the reliability of components in terms of turbulent buffeting.

Even though the associated fluid mechanics in a tube array is highly complicated a good understanding of certain turbulent buffeting problems has been obtained experimentally and theoretically.

Fitzpatrick and Donaldson [5], for a 10 row in line tube array with $L/d = 1.97$ and $T/d = 1.75$ in a Reynolds number, Re , range of 5.6×10^3 to 9×10^3 , determined that the turbulence intensity, T_1 , 0.5% in the free-stream, steadily increases from row to row as the flow traverses into the array. In the vicinity of row 5 a maximum turbulence intensity of 14% is attained and it remains constant beyond this row. In a similar Reynolds number range, but for a 7 row rotated square array with $P/d = 2.12$, Price *et al.* [6] found a sharp increase in turbulence intensity up to row 4 and a region of "invariance" deeper in the array for air- and to a reasonable extent for water-flow.

Sandifer and Bailey [7], in a 6 row, $P/d = 1.5$, rotated triangle array using a

noninvasive measurement technique (LDV), obtained results quite similar to those mentioned above. These studies lead to the conclusion that turbulence in the array is induced by the array itself and its intensity is a function of position in the array.

Another issue of practical interest is the effect of upstream turbulence characteristics on cylinder response. Gorman [8, 9], for various arrays, showed that upstream turbulators with characteristic dimension comparable to the diameter of the cylinders in the array can reduce the buffeting response of the cylinders considerably. On the other hand, screen turbulators with much smaller characteristic dimension had a limited effect on vibration response. This is in agreement with results of Price *et al.* [6] who later, in a detailed experimental study, showed that fine upstream grids do not alter the turbulence intensity inside the array relative to the no-grid case. It is likely that the effect of large and small scale upstream obstacles will be understood better through the measurement of turbulence scale, and its decay, before the eddies reach the first row of the cylinder array in future studies.

The relationship between buffeting response and cross-flow velocity has recently received considerable attention. Pettigrew and Gorman [10], for a normal triangular array with a pitch-to-diameter ratio range of 1.23 to 1.54, and later Sandifer and Bailey [7], for a rotated triangular array with a pitch-to-diameter ratio of 1.5, found the cylinder displacement in the buffeting region to be proportional to cross-flow velocity squared. Price and Paidoussis [11], for a square array with a pitch-to-diameter ratio of 1.5, found the buffeting induced displacement to be proportional to $U_\infty^{1.3}$ in the second row and $U_\infty^{2.2}$ in the fifth row. In a further study [6], this time for a rotated square array, the same authors determined the displacement to be proportional to $U_\infty^{1.1}$. These studies suggest that the relationship between buffeting induced cylinder displacement and cross-flow velocity is dependent on array geometry, pitch-to-diameter ratio and position in the array.

Two models, based on random vibration theory have been suggested by Pettigrew *et al.* [10, 12] and Blevins *et al.* [13] to predict cylinder response to turbulent buffeting. The only empirical input into these models is the power spectral density of

the buffeting force per unit length, which has been successfully normalised by Blevins *et al.* [13], Taylor *et al.* [14] and Chen and Jendrzejczyk [15]. With the following simplifying assumptions:

- a) random forces fully correlated along the length of the tube,
- b) no significant power at any frequency other than the fluidelastic natural frequency,
- c) power spectral density of the buffeting force per unit length is proportional to flow velocity squared,

a random excitation coefficient, which is a function of frequency, is obtained from the normalised power spectral density. Pettigrew and Gorman [10] provided a simple equation determining the mid-span r.m.s. vibration amplitude,

$$Y_{rms}(\frac{1}{2}L) = \left[\frac{1}{2} \rho d U^2 C_R \right] / \left[4\pi^5 f_1^3 m^2 \xi_1 \right]^{\frac{1}{2}}, \quad (1.1)$$

where Y_{rms} = mid-span rms displacement amplitude, ρ = flow density, U = flow velocity, C_R = random excitation coefficient, f = fundamental frequency, d = cylinder diameter, ξ = damping ratio.

Blevin's expression for the mid-span rms displacement amplitude is equally simple

$$Y_{rms}(\frac{1}{2}L) = \left[\frac{1}{2} \rho d^{3/2} U_{\infty}^{3/2} J \phi_n(\frac{1}{2}L) \right] / \left[64\pi^3 f_n^3 m^2 \xi_n \right]^{\frac{1}{2}}, \quad (1.2)$$

where J = joint acceptance, $\phi_n(\frac{1}{2}L)$ = eigenfunction at mid-span, the other variables are the same as above.¹

Paidoussis [3], and later Weaver and Fitzpatrick [16] found numerical calculations from both models to be in limited agreement with each other, and attributed the variations that did exist to different empirical random excitation coefficients.

¹In Blevins' model Φ_n , eigenfunction at mid-span, is a function of non-dimensional velocity, Reynolds number, array geometry and position of the tube in the array.

1.3 Flow-Periodicity-Induced-Resonance

For a single cylinder subject to cross-flow it is well known that the vortex shedding process periodically changes the structure of the wake and induces a periodicity on the associated forces acting upon the cylinder. The ratio of the vortex shedding frequency to the cross-flow velocity is a constant and by introducing a characteristic length can be non-dimensionalised. The outcoming value, called the Strouhal number, is equal to 0.20 ± 0.05 in a Reynolds number range of 2×10^2 to 2×10^5 .

For an array of cylinders, depending upon various factors such as; the geometry, the pitch to diameter ratio, position in the array, Reynolds number and turbulence intensity, flow periodicity may or may not be observed. In cases when a flow periodicity is observed, multiple flow periodicities are not uncommon.

A physical understanding of the mechanism inducing flow periodicities in a cylinder array is, as yet, unavailable. Vortex shedding, wake motions, periodic reorganisation of the main flow, shear layer instability, effect of a dominant frequency in the broadband turbulent energy spectrum and slightly varying forms of the above have been proposed as the cause of flow periodicity in cylinder arrays [16-20, 5]. However, even in an environment of such conflicting ideas, some recent works have revealed valuable information on the specific aspects of the problem.

- Axisa *et al.* [21] and Pettigrew *et al.* [22] conclusively showed that flow periodicity for practical purposes occurs only in single phase flows
- Gorman [8] and Savkar *et al.* [23, 24] determined that turbulence induced by upstream obstacles of characteristic dimension comparable to the array cylinder diameter suppressed or eliminated flow periodicity induced resonance. Whereas results of Price *et al.* [6] and Gorman [8], with small scale upstream obstacles, had no sensible effect on the magnitude of flow periodicity induced resonance
- cumulative efforts of Fitzpatrick and co-workers [5, 25], Price *et al.* [6] and Weaver with Fitzpatrick [16], for different geometries and pitch-to-diameter

ratios, determined Strouhal peaks to be a function of Reynolds number and position in the array.

- Weaver and Abd Rabbo [26, 27], Mureithi [28] and Oengoren *et al.* [29], in square and rotated square arrays for low Reynolds numbers, detected explicit vortex shedding through flow visualisation techniques. In a recent and continuing combined flow visualisation and vibration study by McGill researchers [30] it has been conclusively determined that, at least one of the Strouhal peaks detected in the cylinder vibration spectra is induced by vortex shedding.

For a designer of heat exchange equipment it is essential to be aware of the flow induced Strouhal numbers. Only then can flow periodicity, cylinder natural frequency and acoustic resonance be mismatched in order to prevent possible structural damage. Fitz-Hugh [31] and Chen [32], using data from cylinder vibrations, turbulence spectra, pressure spectra on tube surfaces and acoustic resonance, formed Strouhal maps as a function of lateral and transverse spacing of the cylinder arrays. Later Murray *et al.* [33, 34] improved these highly criticized maps into a more useful form by ignoring acoustic resonance data.

A second useful design tool to detect flow-periodicity, is based on a suggestion of Owens [20] in the form; "*the dominant frequency of the vibration ... is equal to the interstitial gap velocity divided by twice the distance between successive rows*". Recently, Weaver *et al.* [35], by observing their own and other published data for the four different cylinder geometries, introduced "calibration constants" into "Owen's rule" to have the best fitting curve for the data displayed as Strouhal number versus the pitch-to-diameter ratio. Zukauskas and Katinas [36], considering a rather limited data basis, have developed an exponential relationship between Strouhal number and pitch-to-diameter ratio to predict the flow-periodicity.

Both approaches mentioned above display a reasonably good fit to the data presented.

1.4 Fluidelastic Instability

As discussed in previous subsections, turbulent buffeting and flow periodicity exist at all cross-flow velocities and interaction between cylinder motion and the surrounding flow is *not* a necessary condition for their existence. On the other hand, at sufficiently high cross-flow velocities, the fluid forces can induce high amplitude cylinder vibrations, which in turn can modify the direction and magnitude of the local fluid forces. Such fluid structure interaction, and the resulting coupled vibrational motion, may amplify rapidly with increasing flow velocity, to cause catastrophic damage in heat exchange equipment. The possibility of such a mechanism, termed as the *fluidelastic instability*, was uncovered by Roberts [37] in a largely ignored pioneering study. Later, Connors [38], using a semi-empirical analytical model, detected that relative displacement of cylinders in a row can alter the surrounding flow field in such a manner that sufficient energy can be transferred to the cylinder in order to overcome its total damping to sustain a limit cycle motion. He proposed an equation, later named after him, to detect the instability threshold velocity, U_c in form of:

$$\frac{U_c}{f_n d} = K(m\delta/\rho d^2)^\beta, \quad (1.3)$$

where f_n = cylinder natural frequency, m = mass per unit length of cylinder, ρ = cross-flow density, d = cylinder diameter, δ = logarithmic decrement of mechanical damping, K and β = empirical constants (9.9 and 0.5 in Connors' case).

The decade following Connors, saw a massive effort to determine the effect of various design parameters, like cylinder mass, structural damping, cylinder natural frequency, array geometry, pitch to diameter ratio, Reynolds number, cylinder span length and number, turbulence characteristics and void fraction upon critical velocity. The developments in that era, reviewed by Paidoussis [3], furnished an extensive data base for those attempting to find a designwise acceptable "K" for Connors' equation. Pettigrew *et al.* [10], by compiling the data for all four standard geometries, in liquid,

air and two-phase flows plotted critical cross-flow pitch velocity², $U_{c,p}$, against mass damping parameter to find a best fit value of 3.3 for K . Later Chen [39, 4], with an expanded data basis, formed the same plot individually for each type of geometry by defining a new reduced velocity³ incorporating the effect of tube spacing. It should be noted here that dividing the stability diagram according to array geometry, and incorporating an effect of pitch-to-diameter ratio, could be quite risky while trying to form design guide lines for actual heat exchangers where the cross-flow angle of attack exhibits a substantial variation from location to location. The natural consequence of this is a relative change in array geometry and pitch-to-diameter ratio within the same heat exchanger which could be under or overdesigned when based on such specialised stability diagrams. Therefore, in the short run, until experimental and theoretical studies reveal a more fundamental understanding of fluidelastic instability, stability diagrams similar to those of references [4, 16 and 39], the only reasonable design tools, should be used with caution.

Paidoussis [3], very correctly recognised that "... *all fluid-mechanical aspects of the instability are hidden within K* ". In fact equation (1.3) for cylinder i can be rewritten in a more general form as;

$$\bar{U}_{c,i} = \frac{U_{c,i}}{f_n d} = F \left\{ \frac{m}{\rho d^2}, \delta, \frac{L}{d}, \frac{T}{d}, \frac{\ell}{d}, \text{Re}, T_i, \frac{\gamma}{d}, \text{no. of flexible cylinders, array geometry,} \right\}, \quad (1.4)$$

where $L/d, T/d =$ longitudinal and transverse separation to diameter ratio,

$\ell/d =$ cylinder length to diameter ratio,

Re = Reynolds number,

$T_i =$ Turbulence intensity,

$\gamma/d =$ Turbulence scale.

² $U_p = U_\infty P/(P - d)$ where $P =$ pitch and $d =$ cylinder diameter

³For each geometry a correction factor which is a function of the transverse cylinder spacing is introduced

When equations (1.3) and (1.4) are compared, $m/\rho d^2$ and δ are the only common terms. The rest of the terms in equation (1.4), some of which can have a substantial effect on the critical velocity, are all lumped into the constant K in Connors' equation. By the mid 70's serious doubts started to develop on the applicability of Connors' equation to individual arrays. When specific arrays were analysed by Blevins *et al.* [13], Gibert *et al.* [40], Heilker and Vincent [41], Chen and Jendrzejczyk [42], Soper [43], Grover and Weaver [44], Tanaka and Takahara [45], they determined a range of 1.25-7.1 for K and a range of 0.2-1.08 for the exponent of the mass-damping parameter in equation (1.3) see Table 1.1.

Another issue of interest is that the mass-damping parameter in Connors' equation is in fact a product of two dimensionless variables, the non-dimensional mass and the logarithmic decrement of damping. Based on insight and dimensional analysis, Grover and Weaver [44] proposed the possibility of non-equal, separate exponents for the mass and logarithmic decrement. Price and Paidoussis [11], Weaver and El-Kashlan [46] and others, see Table 1.2, verified this proposal experimentally at least for some arrays, and obtained an expression for the critical velocity of the form,

$$\frac{U_c}{f_n d} = K \left(\frac{m}{\rho d^2} \right)^{\alpha_1} \delta^{\alpha_2}, \quad (1.5)$$

where K , α_1 and α_2 are empirical constants. The above developments brought into discussion the issue, on how many constants should there be and what their values should be?

Other researchers, including Connors [47] himself and Savkar [48] tried to improve equation (1.3) by including the effect of the distance between the cylinders. Later drawing on this Chen [39, 4] introduced the effect of distance between cylinders into the instability charts

In further studies Y.N. Chen [49] introduced the effect of the Reynolds number into Connors' equation whereas Chen and Jendrzejczyk [42], Price, Mark and Paidoussis [11, 50] investigated the effect of position in the array and upstream turbulence

characteristics on critical velocity.

Another major contribution to improving Connors' equation is from the stability maps of Chen [39, 4] and later Weaver and Fitzpatrick [16], discussed previously in a different context. These log-log plots of non-dimensional critical velocity versus the mass-damping parameter clearly show two distinct regions. In region 1, above a mass-damping parameter of ≈ 0.4 , all available data can be enveloped by a straight line of slope 0.3-0.5 depending on the geometry of the cylinder array. Whereas in region 2, below a mass-damping parameter of ≈ 0.4 , the non-dimensional critical velocity is independent of changes in mass-damping parameter, which implies that β in equation 1.3 and α_1, α_2 in equation (1.5) approaches zero. This is in contrast to Connors' and other researchers who deemed β, α_1 and α_2 to be constant throughout the whole mass-damping parameter range.

While a major portion of the above mentioned studies, directly or indirectly, contributed to developing Connors' equation, a considerable amount of other experimental studies have focused upon a better understanding of the physical mechanisms underlying dynamic instability. To name a few of the many;

- Zdravkovich and co-workers [51-54] using force and pressure distribution measurements, in both cylinder arrays and tandem cylinder arrangements brought a substantial understanding to the flow structure and possible types of interaction between cylinders.
- Chen and Jendrzejczyk [55] found that fluid components of damping in the lift direction can be negative at sufficiently high flow velocities; Weaver and El-Kashlan [46] found substantially the same at 45° to the lift direction. These studies showed that the fluid damping component can be sufficiently negative to overcome structural damping to induce dynamic instability, as predicted by various theoretical models.
- AECL researchers and co-workers [56, 57, 58] analysed several energy dissipation mechanisms contributing to tube damping in actual heat exchangers with an

emphasis on the effect of support parameters.

- McGill University [28, 30] and McMaster University [26, 27] researchers undertook flow visualisation studies probing wake structure, its interaction with surrounding flow and downstream cylinders as well as flow structure variations from row to row.

Andjelic and Popp [59] in an excellent study, experimentally proved the existence of multiple instability bands at low value of the mass-damping parameter, a phenomenon that had been previously proposed to exist via the theoretical models of various researchers.

- Paidoussis *et al.* [60] experimentally detected and studied static instability in a rotated-square array, another destructive instability mechanism which has to be considered in heat exchanger design process.

1.5 Mathematical Models

During the course of the last 20 years various researchers have developed mathematical models of varying complexity to determine the critical flow velocity for fluidelastic instability. None of these models are yet of any reliable deterministic nature for design purposes, but some of them have aided substantially to the understanding of the physical mechanisms underlying fluidelastic instability. In the following section some of these models, catagorised according to their empirical data requirements, will be discussed.

1.5.1 Models Requiring No Experimental Data

Paidoussis, Mavriplis and Price [61], observing small wake structures behind the cylinders in certain arrays, developed a model based on potential flow theory. The model, in its initial form, considers velocity dependent fluid-damping terms to determine the instability threshold for a single degree-of-freedom system. The only empirical

input is a delay term accounting for the lag between fluid forces and the response of the cylinder to these forces. Later [62] at the expense of increasing empirical input, the authors incorporated fluid-stiffness terms, to establish a better agreement with experimental results. Naturally this is a deviation from the original aim of this work to predict fluidelastic instability with minimum empirical input.

Another model, not requiring any empirical fluid force coefficients has been developed by Lever and Weaver [63, 64, 65]. Assuming the vibration of a single cylinder in a flow channel to be representative of a fully flexible array, the authors use the unsteady Bernoulli equation with a phase lag to model the fluid mechanics. This single degree-of-freedom model, considering only fluid-damping forces, is capable of predicting fluidelastic instability with reasonable accuracy only in the cross-flow direction. Even though the lack of fluid-stiffness forces and the concept of the "unit cell" seriously limit the fluid mechanics of the model for any practical application, Weaver and Lever were the first to detect multiple instability bands at low mass-damping parameters through a numerical study. This phenomenon has only been recently proven to exist experimentally [59].

1.5.2 Models Based on Unsteady Flow Theory Requiring Extensive Experimental Data and the Dynamic Instability Mechanisms

At the other end of the spectrum are the models requiring extensive experimental input in form of cylinder motion and flow velocity dependent fluid forces accounting for added mass, fluid-damping and fluid-stiffness effects. Such models, furnishing results in excellent agreement with instability velocities obtained from vibration experiments, are hindered by the fact that input data requirement is exhaustively large and in most cases unavailable. But, so far, the greatest understanding of the fluidelastic instability mechanisms has been attained from such models.

Tanaka and Takahara [66, 67, 68], drawing upon their extensive unsteady fluid-force measurements, developed a fully unsteady flow formulation giving numerical

results in excellent agreement with vibration experiments. They determined that the number of flexible cylinders considered in the analysis can have a significant effect on the stability threshold, depending upon the mass-damping parameter and pitch-to-diameter ratio. In addition, initial frequency differences between cylinders, quite common in heat exchangers, were found to have stabilising and in some cases destabilising effects depending upon the pattern of frequency detuning.

Chen [69, 70], utilising Tanaka and Takahara's fluid-force data, developed a fully unsteady second order model. This approach helped to distinguish, at least in the numerical arena, that fluidelastic instability is in fact composed of two distinct mechanisms. The first instability mechanism proposed by Chen requires a single degree of freedom system (less formally a single flexible cylinder) in which work done by fluid forces proportional to, and in phase with, the velocity of a vibrating cylinder is sufficient to reduce the total modal damping to zero. This mechanism, named as the *velocity or fluid damping-controlled mechanism*, is usually dominant at low mass-damping parameter values, i.e. for high density fluids. The second mechanism proposed requires two or more degrees-of-freedom (multi-flexible cylinder array) with coupled motion. Instability occurs when the total modal damping becomes zero but in this instance due to work done by fluid-forces proportional and in phase with the displacement of the cylinder. Generally, named as the *displacement or fluid stiffness-controlled mechanism*, this type of instability is dominant at high mass damping parameter value, i.e. for low density gas flows.

A better understanding of the duality of the dynamic instability mechanisms can be obtained by analysing an approach taken by Collar and Simpson [87]. The fluid forces acting on the cylinders of an array, with the exception of those due to the added fluid mass, can be written as

$$\mathbf{F} = \mathbf{Kz} + \mathbf{B}\dot{\mathbf{z}}, \quad (1.6)$$

where \mathbf{K} = the fluid stiffness matrix, \mathbf{B} = the fluid-damping matrix and \mathbf{z} = the

displacement vector. If the motion is assumed to be harmonic, the displacement vector, \mathbf{z} , can then be expressed as

$$\mathbf{z} = \mathbf{a} \sin \omega t + \mathbf{b} \cos \omega t, \quad (1.7)$$

where \mathbf{a} and \mathbf{b} are the oscillation amplitudes and ω is the cyclical frequency

By definition, the work done by the fluid forces per cycle of oscillation, W , can be written as

$$W = \int_0^{2\pi/\omega} \dot{\mathbf{z}}^T \mathbf{F} dt. \quad (1.8)$$

Combining equations (1.6) to (1.8) and rearranging yields

$$\begin{aligned} W &= \int_0^{2\pi} (\mathbf{a}^T \mathbf{c} - \mathbf{b}^T \mathbf{s}) [\mathbf{K}(\mathbf{a}\mathbf{s} + \mathbf{b}\mathbf{c}) + \omega \mathbf{B}(\mathbf{a}\mathbf{c} - \mathbf{b}\mathbf{s})] d(\omega t), \\ &= \pi (\mathbf{a}^T \mathbf{K} \mathbf{b} - \mathbf{b}^T \mathbf{K} \mathbf{a} + \omega (\mathbf{a}^T \mathbf{B} \mathbf{a} + \mathbf{b}^T \mathbf{B} \mathbf{b})), \end{aligned} \quad (1.9)$$

where $c = \cos \omega t$ and $s = \sin \omega t$. Equation (1.9) can be transformed into a more useful format as

$$W = \pi [2\mathbf{a}^T \mathbf{K}_2 \mathbf{b} + \omega (\mathbf{a}^T \mathbf{B}_1 \mathbf{a} + \mathbf{b}^T \mathbf{B}_1 \mathbf{b})], \quad (1.10)$$

when the fluid-stiffness matrix, \mathbf{K} , (and the fluid-damping matrix \mathbf{B}) are expressed as the sum of their symmetric and skew-symmetric components - $\mathbf{K} = \mathbf{K}_1 + \mathbf{K}_2$ where $\mathbf{K}_1 = (\mathbf{K} + \mathbf{K}^T)/2 = \mathbf{K}_1^T$ and $\mathbf{K}_2 = (\mathbf{K} - \mathbf{K}^T)/2 = -\mathbf{K}_2^T$ (similarly for \mathbf{B})

Inspection of equation (1.10) reveals the possibility of two distinct mechanisms that can lead to W being negative and hence enabling the cylinders to extract energy from the surrounding flow to become dynamically unstable. The first mechanism requires the system to have a sufficiently negative $\mathbf{a}^T \mathbf{B}_1 \mathbf{a} + \mathbf{b}^T \mathbf{B}_1 \mathbf{b}$ term for exhibiting dynamic instability. This fluid-damping controlled mechanism can generate dynamic instability even in a single degree-of-freedom systems when \mathbf{B}_1 is negative

The existence of a second dynamic instability mechanism can also be deduced from equation (1.10). If $\mathbf{a}^T \mathbf{K}_2 \mathbf{b} < 0$ and $|\mathbf{a}^T \mathbf{K}_2 \mathbf{b}| > \omega (\mathbf{a}^T \mathbf{B}_1 \mathbf{a} + \mathbf{b}^T \mathbf{B}_1 \mathbf{b})$, then $W < 0$ and dynamic instability is initiated. This fluid-stiffness controlled instability

is quite similar to aircraft wing flutter and requires at least two degrees-of-freedom, as the scalar form of \mathbf{K}_2 is equal to zero [87]. It should be stressed that, there is as yet, no experimental evidence proving or disproving the existence of these proposed mechanisms. Also, a significant portion of theoretical studies acknowledge only one or the other of these mechanism.

1.5.3 Quasi-Steady Models Requiring Limited Experimental Data

The limited prediction capability of models requiring no experimental data [61, 63, 64, 65] and the vast magnitude of experimental effort necessary for models based on unsteady flow theory [66-70] has forced a significant portion of researchers to a more optimal path of quasi-steady formulations. In such models, it is assumed that as the tube oscillates, the instantaneous fluid forces acting on it at a given position, can be approximated by the forces acting on the static tube when displaced to the same position. This assumption sharply reduces the experimental input required and the magnitude of the numerical formulation to a manageable level.

Connors [38], and later Blevins [71, 72] developed linearised, quasi-steady models showing good agreement with experimental data at high mass-damping values. Through this quasi-steady model, Blevins was the first to analyse the effect of frequency detuning between adjacent cylinders and between the in- and cross-flow directions of the same cylinder. Whiston and Thomas [73] extended Blevins' model to incorporate the effect of mechanical coupling between cylinders as well as the addition of a limited fluid-damping controlled mechanism. In general, all the above models give poor agreement with experiments at low mass-damping values as fluid forces considered are only displacement dependent.

Price and Paidoussis [74-80] overcame a major limitation of quasi-steady models by introducing a frequency dependent term into their models to produce destabilising fluid-damping forces. In the case of a single degree-of-freedom system [74, 75] they successfully tested their modified quasi-static (quasi-steady) model by obtaining a

dynamic instability due to the fluid-damping controlled mechanism. Various single and multi degree-of-freedom theoretical studies of these authors obtained the following conclusions:

- There are definitely two different dynamic instability mechanisms operative in most arrays,
- both mechanisms can separately cause instability,
- the effect (contribution) of each mechanism is dependent on array geometry, pitch-to-diameter ratio and mass- damping parameter value,
- the exponent of mass-damping parameter in a stability boundary equation is different for each mechanism,
- detuning between cylinders and between the two directions of a single cylinder can significantly effect the instability threshold,
- at low mass-damping parameter values multi-instability bands exist.

With a better estimation, or empirical determination, of the frequency dependent terms for specific arrays and by incorporating the effect of Reynolds number on force coefficients this type of a model promises a good future.

1.5.4 Non-Linear Models

The aforementioned theoretical models are all based on linearised theory. Recently Price and Valerio [81], for a single degree of freedom system, developed an analysis incorporating non-linear quasi-steady forces. Encouraged by this pioneering results further investigations are being pursued at McGill University.

Analyses considering structural non-linearities, i.e. impacting between cylinders and their supports have been performed by Axisa and co-workers [82, 83] and Fricker [84]. Non-linear models are presently at their infancy and important developments are to be expected in the near future.

1.6 Motivation for the Present Work

As discussed in the above subsections, a significant portion of the recent developments on the cross-flow induced vibrations of heat exchanger tubes is from numerical studies (e.g. existence of two different dynamic instability mechanisms, effect of detuning, multiple instability regions at low mass-damping parameter values etc.) But it is rather strange that, at the time this study was undertaken, most of these findings have not been fully verified experimentally. In addition to this lack of experimental data, even in the theoretical arena there is a substantial amount of difference and in some cases controversy between various schools of researchers. To exemplify a few;

- Even though for some arrays Southworth and Zdrovkovich [51], Soper [43], Abd Robbo and Weaver [27] have observed a change in critical velocity with increasing number of flexible cylinders, there is as yet, no clear experimental study proving or disproving the existence of a multiple-flexible cylinder type dynamic instability mechanism. On the other hand some of the theoretical models [63-65] are still based on the assumption that a single flexible cylinder is sufficient to analyse dynamic instability in cylinder arrays. Such an approach rules out the possibility of a multiple-flexible cylinder type dynamic instability mechanism from the very beginning.
- Lever and Weaver [63], Chen and Jendizejczyk [42], Soper [43] Weaver and Koroyannakis [85] have experimentally studied the effect of frequency detuning between the cylinders of an array. These results have indicated little effect of frequency detuning in higher density fluids; otherwise, few conclusions have been obtained. Similarly, results obtained from various numerical studies by Blevins [72], Tanaka and Takahara [66-68], Price and Paidoussis [77] are not in total agreement on the effect of frequency detuning between either adjacent cylinders or the in- and cross-flow directions of the same cylinder.

- Recent experimental results shed doubt on the global nature of a "Connors' type" equation. At least for some arrays it has been determined that the non-dimensional mass and damping cannot be lumped together under the same exponent, see Table 1.2. In fact, as seen in equation (1.4) the non-dimensional mass and damping are separate non-dimensional variables and there is no physical justification of any sort for lumping them together.
- Similarly, for an array where multiple-flexible cylinder, fluid-stiffness type instability mechanism is the main contributor to instability it is not known if a "Connors' type" equation is applicable.
- Also, in cases where the multiple-flexible cylinder, fluid-stiffness type instability is important, the effect of detuning is not clearly understood. Price and Paidoussis [77, 79] and Chen [69, 70] in their theoretical studies, suggest an important effect which experimentally, is as yet unproven.

A series of experimental and theoretical studies performed at McGill University [6, 75, 80] on a seven row rotated square array, with $P/d = 2.12$, have revealed interesting results that can form a basis for future research. A single flexible cylinder placed at various rows of this array has experienced no fluidelastic instability during experimental studies ($\bar{m} = 280$, $\delta = 0.014$, $U/f_n d$ up to 125). Similarly, both linear and non-linear models developed by the same authors determined no fluidelastic instability for a single cylinder in the same array.

All of the above results conclusively show that a single degree-of-freedom, fluid-damping controlled instability mechanism by itself is insufficient to induce fluidelastic instability in a rotated square array with $P/d = 2.12$.

But in a further theoretical study [78] Price and Paidoussis found that with multiple flexible cylinders in this array, fluidelastic instability can occur. If this is demonstrated to be so experimentally then this will be the first, and conclusive proof, for the existence of a multiple-cylinder, stiffness controlled fluidelastic instability mechanism.

1.7 Objectives of the Study

- A. This study undertakes to experimentally prove the existence of a multiple-flexible cylinder type fluidelastic instability mechanism in an array where a single flexible cylinder is known to be stable.
- B. If such an instability is proven to exist, at the next stage the effect of various parameters such as number of cylinders, cylinder position, cylinder mass, cylinder damping, coupled motion between cylinders and frequency detuning on this instability mechanism will be investigated.
- C. The applicability of Connors' type design equations to arrays where the multiple-flexible cylinder type fluidelastic instability mechanism is dominant will be researched.
- D. The time averaged forces acting on static cylinders as a function of the displacement of instrumented and the surrounding cylinders will be determined at different Reynold numbers to gain a physical understanding of the flow pattern in the array.
- E. Finally, the above forces will be incorporated into a quasi-steady multiple degree of freedom numerical model for comparison with experimental results.

Chapter 2

A GENERAL OVERVIEW OF THE WIND TUNNEL AND THE ARRAY

2.1 The Wind Tunnel

The experiments to be discussed in the following chapters have all been performed in a blow-down, subsonic wind tunnel schematically shown in Figure 2.1. The tunnel consists of:

- a) A *fan section* housing a 1220 mm (4-ft.) impeller centrifugal fan driven by a 40 hp d.c. electric motor. The fan shaft speed is regulated by a control system that varies the voltage across the d.c. motor.
- b) A *settling and straightening section* with a honeycomb to destroy large scale flow irregularities and a series of meshwire screens to reduce turbulence-intensity and scale.
- c) A *contracting section* with an exit to inlet flow area ratio of 1.6
- d) A 1829 mm (6-ft.) long *test section* with cross-sectional dimensions of 610 mm (2-ft.) by 914 mm (3-ft.).

A steady volumetric flow rate of 1-24 m³/s which corresponds to a maximum air flow velocity of 43 m/s, can be obtained in an empty test section. A pilot-static tube,

connected to an inclinable manometer, measures the dynamic pressure from which the upstream flow velocity can be calculated by using Bernoulli's equation for inviscid and incompressible flow. Outside the boundary layer, the velocity profile across the tunnel cross-section deviates by less than 1% for an empty test section. In earlier studies [86] the turbulence intensity in the empty test section was shown to be less than 1%.

2.2 The Cylinder Array

To simulate cross-flow over the tubes of a shell-and-tube heat exchanger, a rotated square array with a pitch-to-diameter ratio of 2.12 has been designed and constructed. The array consists of a portion of rigid cylinders, which will be discussed here, and two interchangeable inserts one of which is designed for vibration experiments and the other for force measurements, these will be discussed later in Chapters 3 and 5.

The rigid portion of the array consists of ninety two 591 mm (23.25 in.) long, 25.4 mm (1 in) diameter solid aluminum rods sandwiched between 10 mm (0.39 in) thick aluminum plates as shown in Figure 2.2. These are arranged to form rows of a $P/d = 2.12$ rotated square array. The hole at the center of the aluminum plates, with slight modifications, is capable of housing both the vibration and force measurement inserts.

The array which spans the entire width of the test section was eight rows deep for most of the experiments, except cases where up to three extra rows of cylinders were added to prevent downstream effects occurring during vibration experiments performed on the latter rows of the array.

Prior to any vibration or force measurements the variation of the upstream (approach) velocity with distance from the leading (uppermost) row of the array was measured, as shown in Figure 2.3. For upstream velocities of $U_\infty = 4.52$ m/s and $U_\infty = 20.22$ m/s, corresponding to the minimum and maximum velocities of the experiments, it is seen that 600 mm or further from the leading cylinder of the array,

I there is very limited change in the magnitude of the velocity vector (less than 1%). Based on this preliminary observation, the upstream velocities (U_∞) for the tests reported in this study were measured via a pilot-static probe with its tip at 600 mm upstream of the leading row of the array.

Chapter 3

VIBRATION MEASUREMENT APPARATUS

3.1 The Vibration Measurement Insert

The *vibration insert*, briefly mentioned in section 2.2, is shown in Figure 3.1. This insert has been designed to facilitate the investigation of the flow-induced vibrational response of as many as four flexible cylinders. It consists of:

- a) four, 25.4 mm (1 in.) diameter, 1500 mm (59 in.) long vertical steel posts attached to the plates housing the rigid portion of the array through the arrangement shown in Figures 3.2 and 3.3.
- b) Two 19.1 mm (3/4 in.) thick horizontal steel slabs, as shown in Figures 3.2, 3.3 and 3.4, bolted to the four steel posts to form the lower and the upper platforms for stringing the flexible cylinders.
- c) A sliding platform holding four oil pots, which forms part of the viscous damping system as shown in Figures 3.3 and 3.5.

The insert houses the flexible cylinders, which are in fact rigid cylinders flexibly mounted via piano wires. A schematic of a typical flexible cylinder and its mounting

system is given in Figure 3.6. All the flexible cylinders have a diameter of 25.4 mm (1 in) and a length of 600 mm (23.6 in.).

A carriage located at the center of each cylinder accommodates two miniature accelerometers orthogonal to each other. The accelerometers are aligned in the in and cross-flow directions. 0.76 mm (0.030-in.) piano wires attached to both sides of the carriage are attached to brass sliders on the lower and upper platforms fixed to the top and bottom of the wind tunnel. These sliders, as shown in Figure 3.4 can be moved in the in-flow direction to correct for the blow-back caused by the static drag force acting on the cylinder. Thus, at all flow velocities, it is possible to keep the array geometry sensibly the same. A further function of the upper slider is to vary the tension, via a small mechanism in the wires. This mechanism allows the natural frequency of a cylinder to be set at any desired value with less than 0.5% error within a frequency range of 3.5 to 17 Hz.

A perforated damping bell is located on the lower wire of each cylinder. When this bell is lowered into the previously mentioned oil pot, a viscous damping system is formed. The resulting logarithmic decrement of a cylinder can be varied between 0.014 and 0.3 by:

- a) using different viscosity oils,
- b) varying the depth of the bell in the oil,
- c) varying the distance of both the bell and the pot from the cylinder

Table 3.1 summarises the characteristics of various flexible cylinders used during the experiments.

3.2 Vibration Measurement Instrumentation

In most experiments the vibrational motion of all the flexible cylinders was monitored in both the in-flow (drag) and the cross-flow (lift) directions. This monitoring was realised through two different measurement devices, namely;

- a) miniature piezoelectric accelerometers,
- b) velocity pick-ups consisting of a coil and a horse-shoe magnet.

The above hybrid arrangement was necessitated by the lack of eight miniature piezoelectric accelerometers capable of fitting inside the flexible cylinders.

Up to a maximum of six Endevco *miniature piezoelectric accelerometers* with transverse sensitivities less than 1.5% and a typical frequency response of ± 0.45 dB from 2 Hz to 8 kHz were used. Table 3.2 lists the accelerometer models and charge sensitivities (PC/g) as well as the charge amplifier models and voltage-to-acceleration (mV/g) ratios

The *velocity pick-up*, consisting of a coil and a horse-shoe magnet, was developed at McGill by Mark [88] and used with success in previous experimental studies. The system consists of a coil of wire attached to the upper piano wire which is positioned inside the magnetic field of a horse-shoe magnet as shown in Figure 3.7. The motion of the piano wire, and thus that of the coil, induces a current proportional to the vibrational velocity of the cylinder. The magnitude of this signal can be increased to a satisfactory level, not requiring any amplification, by increasing the magnet strength or by increasing the number of windings in the coil. When electronically differentiated and calibrated against an accelerometer the vibration power spectra obtained from the coils were virtually identical to those obtained via an accelerometer, at least in the frequency range of interest - 2 Hz to 30 Hz - as shown in Figure 3.8. Thus, throughout this study vibration pick-ups with the plane of the coil either parallel or perpendicular to the upstream flow direction were used with confidence to monitor the in- and cross-flow vibrational motion of cylinders

The output signals, from accelerometer charge amplifiers and the vibration pick-ups, were analysed via a Hewlett-Packard 3562A two channel dynamic signal analyser coupled to a Hewlett-Packard 9000 310 microcomputer.

3.3 Vibration Measurement Procedure

In all of the experiments the initial step consisted of choosing the number, position and mass of the flexible cylinders and placing them in the array. Next, the cylinders were tuned to the desired natural frequency and structural damping. This was accomplished by lightly impacting the cylinders to obtain a decaying acceleration signal. The natural frequency of the cylinder, f_n , corresponding to the frequency with the largest amplitude in the power spectra was obtained from this acceleration signal. In all experiments the flexible cylinders was tuned to the previously determined natural frequencies with a maximum deviation of $\pm 0.5\%$.

The logarithmic decrement of damping was obtained directly from the decaying acceleration versus time trace. In some experiments, high structural damping values were required. Such a requirement was realised by dipping the bell into the oil pot. In this type of experiment it was possible to keep the maximum difference between the logarithmic decrement of different cylinders below 7%. But in most experiments the cylinders were only damped by air, and ensuring that the cylinders had equal structural damping was more difficult. Still in all cases the maximum difference in the logarithmic decrement was less than 12%.

Once the natural frequencies and the logarithmic decrement of damping was set to the predetermined values, experiments to measure the flow-induced vibrational behaviour of the cylinders at incrementally increasing flow velocities were performed. At each flow velocity, the cylinder blow-back due to static drag was adjusted. Then according to the requirements of the specific experiment a combination of the measurements listed below were performed.

- The in- and the cross-flow acceleration power spectra of each cylinder.
- The coherence between the vibrational acceleration of different cylinders.
- The cross-spectra between the vibrational acceleration of different cylinders
- Orbits of the oscillation obtained where the in-flow vibration was plotted versus

the cross-flow vibration.

Generally, depending upon the test performed, 50-100 samples were found to be sufficient to reach steady state in all frequency domain measurements.

The test was terminated either at the instability threshold or at the maximum wind tunnel velocity of ≈ 22 m/s if the array was stable.

Finally, the cylinder natural frequencies and the logarithmic decrements were measured again to check for any major variation that may have occurred during the experiment.

Data analysis was done using a Hewlett-Packard 9000 310 computer system utilising the software NEWED, developed by Mark [89], at McGill University.

Chapter 4

DYNAMIC RESULTS

4.1 An Overview of the Dynamic Results

The dynamic (vibration) experiments performed in this study can be categorized into three major groups.

- A Those aimed at determining the possible existence of a multiple-flexible cylinder, fluid-stiffness controlled instability mechanism and factors affecting such a mechanism.
- B Those elucidating the effect of natural frequency variations between adjacent flexible cylinders (detuning) upon the threshold of fluidelastic instability
- C Those investigating flow induced static cylinder displacement and associated instability.

As emphasized above and in previous sections, the major subject of study in this thesis is the instability mechanisms. Turbulent buffeting and flow periodicity induced resonance, even though closely monitored, will only be a marginal issue of interest.

Prior to any detailed discussions, the flexible cylinder numbering system used will be introduced. A flexible cylinder will be named after the row it is positioned in, e.g.: a cylinder in row 3 will be referred to as cylinder 3. Similarly when there are two

flexible cylinders in the same row, such cylinders will be distinguished to be the left and the right cylinders of that row and will be referred to as cylinder (X)L and (X)R. A typical example for second row flexible cylinders ($X = 2$), is as shown in Figure 11

4.2 Multiple-flexible Cylinder Fluidelastic Instability

4.2.1 A Single Flexible Cylinder

In an excellent experimental study at McGill, Mark [86] in air-flow and Macdonald [90] in water flow conclusively determined that a single flexible cylinder positioned in any row of a rotated square array with $P/d = 2.12$ does not become fluidelastically unstable. For the sake of completeness, and to form a basis for comparison with the multiple flexible experiments, a limited number of single flexible cylinder experiments have been repeated in this study.

Figure 4.2 shows a typical vibrational acceleration power spectra for a single flexible cylinder in the array. The main response of the cylinder to fluid forcing as would be expected, is at its first fluidelastic natural frequency. When the in- and cross-flow vibrational acceleration power spectra, for a fourth row flexible cylinder, are measured at many upstream flow velocities, they can be compiled into a three-dimensional format as shown in Figure 4.3. Based on such a display, the variation of vibrational acceleration amplitude and frequency of any mode can be plotted as a function of the non-dimensional velocity, $U/f_n d$, as shown in Figure 4.4 and Figure 4.5. Figure 4.5 reveals a substantial increase in the in-flow directional frequency and a considerable decrease in the cross-flow directional frequency as flow velocity is increased. This divergence of major in- and cross-flow frequencies is typical of all single/multiple flexible cylinder experiments performed in this array and will be encountered often. In a previous study [86] the increase of in-flow stiffness had been attributed to increase of steady drag with flow velocity. Whereas the static force measurements that

will be discussed in Chapter 6 have revealed that the loss of rigidity in the cross-flow direction is purely induced by the aerodynamic force field.

Single flexible cylinder experiments of this study are summarised in Table 4.1. In all cases stable cylinder behaviour prevailed throughout the whole non-dimensional velocity range.

4.2.2 Two Flexible Cylinders and the Existence of Coupled Motion

Once the stable behaviour of a single flexible cylinder had been verified, experiments with two flexible cylinders were initiated. The results, summarised in Table 4.2, show that under no circumstances could instability be obtained with two flexible cylinders. Still, one of these experiments, with a tandem arrangement of flexible cylinders in the first and third rows - $\bar{m} = 280$, $f_n = 10$ Hz, $\delta = 0.014$ - revealed an interesting phenomenon. In Figure 4.6, for the in-flow direction of cylinder 1, and in Figure 4.7, for both the in- and cross-flow directions of cylinder 3, the three-dimensional acceleration power spectra are presented (the cross-flow direction for cylinder 1 was not measured in this experiment). When the major oscillation frequencies (peaks) are extracted from each spectra and plotted as a function of non-dimensional velocity, as shown in Figure 4.8, it is observed that some frequencies are common to both cylinders. At these coinciding frequencies a high magnitude peak is measured in the cross-spectra. Also these coinciding frequencies, from different cylinders, have high coherence levels well in excess of 75%, indicating an input/output type of relationship between the oscillation of the two cylinders. As an example of highly correlated motion Figures 4.10, 4.11 and 4.12, respectively, show the power spectra of cylinders 1 and 3, the cross-spectra of cylinders 1 and 3, coherence between cylinders 1 and 3 at a velocity of 7.8 m/s. Such an intimate relationship between the vibrational modes of both cylinders can also be seen at all the other flow velocities. Figure 4.13 shows the

coherence between the in-flow vibration signals of cylinders 1 and 3 at different flow velocities in a three-dimensional format. A similar result, this time between the in-flow signal of cylinder 1 and the cross-flow signal of cylinder 3 is given in Figure 4.14. Both figures clearly show high levels of coherence at common frequencies, even at fairly low flow velocities. It has also been established that there is no mechanical coupling between the cylinders, and common frequencies are not induced by any known flow-periodicity. This leads to the conclusion that in this array, the vibrational motion of one cylinder can effect and synchronise the motion of the others through fluidelastic coupling. Such a conclusion is important in the sense that, fluidelastic coupling between cylinders has been proposed to be a necessary condition for the existence of multiple cylinder type instability by Price and Paidoussis as well as Chen in their various theoretical models. Thus, it is quite likely that coupled motion between *more numerous* flexible cylinders could induce a fluidelastic instability, even though this arrangement of two flexible cylinders is stable across the non-dimensional velocity range tested, as shown by the acceleration versus non-dimensional velocity plot of Figure 4.9.

Further experiments, two of which will be discussed in detail below, were done to determine some of the variables affecting the fluidelastic coupling between two flexible cylinders. To observe the effect of relative cylinder position with respect to each other, two cylinders, with exactly the same properties, $\bar{m} = 280$, $f_n = 10$ Hz, $\delta = 0.014$ -, were placed in the second and the third rows as shown in Figure 4.15. The major difference between this experiment and the one discussed above is that the downstream (row 3) cylinder is not directly in the wake of the upstream (row 2) cylinder. Thus, intuitively one would expect less interaction between the dynamic behaviour of each flexible cylinder. Figures 4.16 to 4.17 show the stable in- and cross-flow vibrational behaviour of both flexible cylinders for an upstream flow velocities less than ≈ 19.5 m/s ($U_c/f_n d = 77$). As can be seen, both cylinders are stable for the complete velocity range. There are far less peaks common to both cylinders, compared to the previous case, and those that do exist are generally in

the cross-flow direction. In the major portion of the velocity range the coherence between the motion of both cylinders is negligible, signifying an uncoupled motion. In fact, as shown in Figure 4.18 the vibrational motion of both cylinders becomes coherent only for velocities greater than 15 m/s ($U/f_n d = 59$) and then the coherence is only between the cross-flow directional motion of cylinder 2 and 3. When this, and previous experiments are compared, it is observed that changes in the relative position of two flexible cylinders has a major effect on the strength of the fluidelastic coupling between cylinders.

In the experiments discussed next, two flexible cylinders, again with the same initial properties, $\bar{m} = 280$, $f_n = 10$ Hz, $\delta = 0.014$, are located in rows 4 and 6. This experiment is identical to the tandem arrangement previously discussed with flexible cylinders in rows 1 and 3, except that in this case the same arrangement is placed deeper inside the array to determine if position changes in the array have any effect on the fluidelastic coupling between flexible cylinders. Figures 4.19 to 4.20 show the vibrational behaviour of cylinder 4 and cylinder 6 in the in- and cross flow directions. Two important results can be extracted from these figures.

- The maximum rms vibration of both cylinders is less than 0.07g, which is four times smaller than that experienced by the same arrangement in the upstream rows (see Figure 4.9).
- In this position (rows 4 and 6) the motion of either one of the cylinders is totally independent of the other. No significant level of coherence was measured between the vibrational acceleration signals of each cylinder to warrant the possibility of fluidelastically coupled motion.

Therefore, the two-flexible cylinder experiments discussed in this section suggest that the vibrational motion of the cylinders can be fluidelastically coupled to achieve over all synchronisation. The strength of this coupling, which can be measured by the magnitude of common power and coherence¹ at coinciding modes, is a function of the

¹The cross (power) spectra is a measure of the common power between two signals in the frequency

cylinder arrangement with respect to each other and the position of the arrangement in the array. Another interesting result occurring with two flexible cylinders, static displacement and instability, will be discussed in section 4.4.

4.2.3 Four Flexible Cylinders and the Multiple-Flexible Cylinder, Stiffness Controlled Instability

Once fluidelastically coupled motion had been observed to exist between two flexible cylinders, experiments with more flexible cylinders were initiated. Figure 4.21 schematically shows four flexible cylinders, one each in rows 1 and 3 (cylinder 1 and 3), and two in row 2 (cylinder 2R and 2L), all with the properties of $\bar{m} = 280$, $f_n = 10$ Hz and $\delta = 0.011$. It should be noted that these properties, (cylinder mass, damping and natural frequency) are the same as those for the two flexible cylinder experiments presented in subsection 4.2.2 (Figures 4.6 to 4.14); the only difference being the number of flexible cylinders.

The in- and cross-flow rms acceleration of each cylinder, at the major frequency of vibration, are given in Figures 4.22 and 4.23, respectively. At a threshold non-dimensional velocity of ≈ 62 the motion of all the cylinder becomes *fluidelastically unstable*. Instability, which initiates from cylinder 3 at a slightly lower non-dimensional velocity of ≈ 59 , effects all other cylinders through strong fluidelastic coupling, to result in rms vibration acceleration magnitudes as high as 3 g. In such cases, the unstable motion of the cylinders is so violent that, to avoid the destruction of the cylinders and the associated instrumentation, detailed experiments could not be performed beyond the instability threshold in the unstable region.

The above result has great significance in the sense *that arrays stable when hous-*

range of interest. By definition it is the product of the Fourier transform of the two signals and contains both magnitude and phase information. It is an extremely powerful tool to detect portions of the signals common to both measured events. When both signals are high the common power will be high and when they are both low the common power will be low.

The coherence function in the general sense is a measure of causality between two signals. It is the ratio of the cross-spectra squared to auto spectrum squared. This function delivers only a normalised magnitude and lacks the phase information. In fact, it does not have the double information advantage of the cross-spectra. In this study it has been used as an additional mean of data analysis.

ing a single flexible cylinder can become fluidelastically unstable with multiple flexible cylinders. For the first time this furnishes conclusive experimental evidence for the existence of a stiffness-controlled (displacement type) fluidelastic instability mechanism requiring coupled motion between multiple-flexible cylinders.

The in- and cross-flow major fluidelastic frequency variation of each cylinder with non-dimensional flow velocity, Figure 4.24, supplied further interesting results. All four cylinders, initially tuned to the same natural frequency under no flow conditions, exhibit a diverging trend in their individual fluidelastic frequencies with increasing flow velocity. In general, the in-flow frequencies increase and cross-flow frequencies decrease. Just before instability these frequencies start to converge back to each other, and cumulate around two specific frequencies. One of these frequencies ≈ 11.3 Hz, can be detected in the vibration spectra of all four flexible cylinders. In the following sections it will be seen that for most cases of instability, all cylinders oscillate at a single dominant frequency. This frequency *synchronization* of overall cylinder motion is a good indicator of strong fluidelastic coupling between flexible cylinders at the instability threshold. In fact, coupling between different flexible cylinders can also be observed at relatively low non-dimensional flow velocities. As an illustrative example to this argument, in Figure 4.24 the major frequencies common to at least two cylinders are numbered from 1 to 6. Coherence measurements between the cylinders at these frequencies are given in Figure 4.25 as a function of non-dimensional velocity. The general trend, as would be expected, is an increase in the coherence with increasing flow velocity.

It should be stressed that the above mentioned frequencies are those of the peaks with the largest amplitude in the power spectra of each flexible cylinder. In addition to these peaks, all the cylinders exhibit dynamic response at various other frequencies. The complicated nature of the fluidelastic vibration experienced by the cylinders can clearly be seen in Figure 4.26 which presents the acceleration power spectra of each cylinder in the in- and cross-flow directions at a non-dimensional velocity of ≈ 57.5 . Of the numerous peaks in each spectrum, many are common to more than

one cylinder. This can be seen more easily in Table 4.3 which tabulates some of the important frequencies extracted from each power spectra shown in Figure 4.26. One of these frequencies, 12.6 Hz, is due to a flow-periodicity of $Su = 0.022$. All the other common peaks at 9.3, 11.5, 12.3 and 15.6 Hz are due to fluidelastic coupling between cylinders². One can easily see the strength of fluidelastic coupling between cylinders by inspecting Figure 4.27 which shows the coherence between the cross-flow signals of cylinders 3 and 2L as well as between the in-flow signals of cylinders 3 and 1. At the above mentioned common peaks of 9.3 Hz and 12.3 Hz high coherence values of 0.86 and 0.93 are measured. The strong coupling at these peaks is further demonstrated by the high common power in the cross-spectra for the same directions, as shown in Figure 4.28. To further demonstrate the extremely coupled nature of the motion between the flexible cylinders, it should be mentioned that in some experiments as many as *seven* frequencies common to at least two cylinders were monitored.

In all experimental studies, repeatability is a very legitimate issue of concern. Generically in experiments such as these, involving multiple degree-of-freedom coupled motion as well as a considerable amount of initial settings, one would expect a substantial variation between the results of repeat experiments. Surprisingly this has not been the case for the present experiments. In nearly all the repeated cases, the difference in critical velocity between experiments was less than 10%. Figures 4.29 to 4.31, showing the oscillatory behaviour of cylinder 3, in a repeat experiment, for the case discussed above, - four flexible cylinders in the three upstream rows, $\bar{m} = 280$, $f_n = 10$ Hz and $\delta = 0.014$ -, is a good example for this argument. In this repeat experiment, cylinder 3 becomes unstable at a critical non-dimensional velocity of ≈ 58 which compares very well with the previously reported critical non-dimensional velocity of ≈ 59 for the same initial conditions.

Up to this stage of the thesis it has been established that the vibrational response of a combination of two flexible cylinders, located anywhere in the array, is stable,

²During all the experiments the vibrational behaviour of the tunnel has been continuously monitored, sometimes in three different locations, to detect mechanical coupling. In all the experiments the stability of the array has been found to be *unaffected* by a mechanical coupling

while a four flexible-cylinder-combination located in the upstream rows (cylinders 1, 2L, 2R and 3) is unstable. In the next section the dynamic behaviour of three flexible cylinders will be discussed to determine the effect of the number of flexible cylinders on the threshold of multiple-flexible cylinder, stiffness-controlled instability.

4.2.4 Effect of Number of Flexible Cylinders on Dynamic Instability

In³ various single and multiple cylinder experiments the instability threshold was determined to be the lowest for second and third row cylinders.⁴ Based on this observation, a combination of three flexible cylinders (2L, 2R and 3) was placed in the second and third rows of the array, where they have the highest possibility of experiencing instability. Table 4.4 summarises the three flexible cylinder experiments performed at this location. For most cases the three flexible cylinders were fluidelastically stable up to the limiting velocity of the wind tunnel. However, upon reducing the cylinder mass, frequency and damping to the lowest values possible - $m = 280$, $f_n = 7$ Hz and $\delta = 0.014$ - instability was obtained. As seen in Figures 4.32 and 4.33, cylinder 3 initially becomes unstable at a non-dimensional velocity of ≈ 97 followed by cylinders 2R and 2L at a higher non-dimensional velocity of 105.

This result shows that, all other parameters being equal, (cylinder mass, damping and position in the array) the non-dimensional critical velocity is lower for four flexible cylinders ($U_c/f_n d = 62$) than for three $U_c/f_n d = 105$. Even though experimental limitations have prevented tests with more than four flexible cylinders, the present trend strongly suggests a general decrease in the critical velocity with increasing number of flexible cylinders in the array. Naturally when the number of flexible cylinders in the array is large after a substantial amount, the addition of one more flexible cylinder would only have a marginal effect on the critical velocity. Eventually

³In some three-flexible cylinder experiments static deflection and static instability has been observed. This phenomenon will be discussed in section 4.4

⁴Time averaged fluid forces acting on second and third row cylinders as well as the results of the theoretical model reveals the same result. This will be discussed in the forthcoming sections

an asymptotic value independent of the number of cylinders is to be expected. In fact, the theoretical analysis of Price and Paidoussis [76] suggests this trend. It should be emphasised that the reduction of the instability threshold with number of cylinders is only applicable in cases where the instability is mainly induced by the stiffness-controlled mechanism requiring multiple degree-of-freedom coupled motion. The critical velocity of the arrays, in which instability is mainly due to damping-controlled effects, should be insensitive to the number of flexible cylinders.

4.2.5 Effect of Flexible Cylinder Position

In Section 4.2.2 it was shown that there is much less fluidelastic coupling between two flexible cylinders when such a combination of flexible cylinders is placed deep inside the array, instead of in the upstream rows. As coupled motion is one of the main requirements of multiple-flexible cylinder type instability, it is to be expected that its deficit would certainly increase the threshold for fluidelastic instability. To establish the validity of such an argument a series of experiments summarised in Table 4.5 were performed. In these experiments a four-flexible cylinder configuration with properties $m = 280$ and $\delta = 0.011$ was located in different rows of the array. The case in which the leading cylinder of the configuration was in the first row was discussed in Section 4.2.3. Now, the same four-flexible-cylinder configuration is considered with its leading cylinder in the second row (cylinder 2, 3R, 3L and 4). Figures 4.34 and 4.35 show the variation of the in- and cross-flow directional cylinder rms acceleration magnitude with non-dimensional flow velocity. It is interesting to note that cylinder 2 (upstream cylinder) displays a substantially higher response relative to the other cylinders in the buffeting region. At a non-dimensional velocity of ≈ 52 , all the cylinders exhibit unstable vibrational behaviour. The critical velocity for this position is $\approx 20\%$ lower than that for exactly the same arrangement (number of cylinders, cylinder mass and damping) with the leading cylinder in the first row. This shows that, *ceteris paribus*, change in position has a substantial effect on the critical velocity of arrays, at least when multiple-flexible cylinder type instability is dominant. In fact, the importance

of position in the array upon fluidelastic instability becomes more apparent when the same configuration is tested with its leading flexible cylinder in the third row. For the cylinder parameter, of $\bar{m} = 280$, $\delta = 0.014$ and $f_n = 10$ Hz the cylinders display a stable vibrational response up to the limiting velocity of the wind tunnel, as shown by the three-dimensional acceleration power spectra in Figures 4.36 to 4.39. Only when the frequency of all the cylinders was reduced to 7 Hz did instability occur for the four flexible cylinder configuration in this locale (Table 4.5). As shown in Figure 4.40, each cylinder becomes unstable at a different non-dimensional flow velocity. Instability initiates from cylinder 3 at $U/f_n d \approx 67$, then appears for cylinders 4R and 4L at $U/f_n d \approx 70 - 77$ and finally envelopes cylinder 5. This behaviour is quite different to the behaviour of the same configuration with the leading cylinder in the first or second rows - where all cylinders became unstable sensibly at the same flow velocity.

To observe further changes in the instability threshold the same four flexible cylinder arrangement was placed further in the array with its upstream cylinder in row 4⁵ (cylinders 4, 5R, 5L and 6). Even with the lowest possible cylinder natural frequency and damping ($f_n = 7$ Hz, $\delta = 0.014$) the vibrational response of these four flexible cylinders was stable up to the limiting flow velocity attainable from the wind tunnel. Figures 4.41 to 4.44 summarises the vibrational behaviour of the four flexible cylinders in this location. Only a few frequencies are common to two or more cylinders, and at such frequencies the common power or coherence is very low (less than 0.4). This is in strong contrast to what has been observed for flexible cylinders in the entrance rows, where cylinders, undergo highly coupled, or even synchronised motion

An overview of the experiments shows that once past the entrance rows of the array the fluidelastic interaction between the flexible cylinders reduce sharply. Eventually, each flexible cylinder, due to the changing nature of the fluid forces from row to row, starts to act more like a single flexible cylinder with little or no effect from

⁵An extra row of cylinders was added to the array to eliminate end (exit) effects

the other flexible cylinders.⁶ Thus, inside the array, the multiple-flexible cylinder stiffness-controlled instability mechanism, requiring coupled motion between multiple degrees-of-freedom, is *no longer* operative. Once this mechanism is ruled out, the only remaining instability mechanism is the single degree-of-freedom, damping controlled one. In this, and previous studies, it is firmly proved that this mechanism is unable to induce instability in this array solely by itself. *Therefore fluidelastic instability in a rotated square array with a $P/d = 2.12$ is mainly due to the multiple-flexible cylinder, stiffness-controlled mechanism and is confined to the first few entrance rows* Figure 4.45, based on the experiments discussed in this section, illustrates the above conclusion by showing the variation of non-dimensional critical velocity with flexible cylinder position in the array ($\bar{m} = 280, \delta = 0.014$). A practical observation that can be derived from this figure is that; if the instability threshold for the first few entrance rows is substantially lower than that inside the array, then lacing these entrance rows together⁷ can allow higher operational flow velocities – allowing higher heat transfer rates in heat exchangers of a rotated square geometry. Previous research at McGill by Paidoussis *et al.* [60], detecting the critical nature of the entrance rows for a $P/d = 1.5$ rotated square array, lends further support to this practical solution⁸.

4.2.6 Effect of Dimensionless Cylinder Mass

In the previous sections, the effect of the number of flexible cylinders, their position with respect to each other, and the position of the flexible cylinders in the array

⁶In section 6.3 it is shown that the motion of the surrounding cylinders has a major effect on the direction and the magnitude of the fluid forces acting on cylinders located in rows 1, 2 and 3. Once past the third row, the motion of the surrounding cylinders has little or no effect on the fluid forces acting on the cylinders in rows 4, 5, 6 and 7.

⁷Such an action will induce a difference in the fluidelastic natural frequencies of neighbouring cylinders. The in depth consequences of such a scenario, which is termed as “frequency detuning” in this thesis, will be discussed in section 4.3.

⁸Naturally in regions of the heat exchangers where the direction of the flow velocity is ill-defined or exhibits a large variation this observation may have only a limited benefit. It should be appreciated that the P/d ratio and the geometry of the array is defined relative to the upstream flow velocity direction. Thus any major change in the velocity vector can alter the geometry of the array into a format (in-line, etc.) for which this solution may not be applicable.

have been discussed in detail. The effect of the dimensional mass on the instability threshold will be considered in this section. The experiments summarised in Table 4.6 were all performed with four flexible cylinders positioned in the three upstream rows, at a damping value of $\delta = 0.014$. The only variable of these tests is the dimensionless cylinder mass⁹. Four different sets of cylinders with dimensionless masses of 195, 280, 490 and 980 were employed in the tests. Table 4.6 summarises the results. Based on these experiments the variation of the non-dimensional critical velocity¹⁰ with dimensionless cylinder mass is shown in Figure 4.46. It is customary to express this variation in the form

$$U_c / f_n d \propto (m / \rho d^2)^\beta \dots \delta = \text{constant} , \quad (4.1)$$

where β is taken as a constant in the literature. In this array β has two rather unusual properties:

- β itself is a function of the dimensionless cylinder mass, as seen in Figure 4.46
- The value of β at $\bar{m} = 195$ is 0.38 and at $\bar{m} = 980$ is 1.55¹¹. The dimensionless cylinder mass has only been varied in a relatively narrow range ($m = 190$ to 980) due to experimental limitations. But, even in such a limited range β exhibits a large variation as a function of the dimensionless cylinder mass. In fact the data leads to the conclusions that, at the least for this array,¹² a relationship

⁹The effect of different initial natural frequencies is incorporated into the non-dimensional critical velocity

¹⁰From Table 4.6 it is observed that there can be a difference in critical velocity from cylinder to cylinder. In this figure, with an exception at $\bar{m} = 980$, the critical velocity is defined as the velocity at which all the cylinders becomes unstable

¹¹For this high cylinder mass, it was not clear if *all* the cylinders were unstable at this non-dimensional velocity. Cylinder 3 exhibits a sudden increase in its vibrational acceleration magnitude ($\approx 0.7g$) and its major in- and cross-flow frequencies "converge", all pointing to unstable behaviour. The other cylinders were still stable. However, this is not unusual as third row cylinders always become unstable marginally before the others. But as $U_c / f_n d = 236$ corresponds to the limiting flow velocity in this case it cannot be solidly determined if cylinders 1, 2L and 2R will become unstable as expected. If this is not the case, then the value of β will be greater than 1.55 for the dimensionless mass of 980

¹²For design purposes, a modified form of the "Connors equation", is still the only tool, if used with caution

of the "Connors type" between the non-dimensional critical velocity and the dimensionless cylinder mass is *not* applicable.

The β value of 1.55 is the highest exponent of dimensionless cylinder mass reported in the literature so far¹³. There is a likelihood that such a strong dependence of critical velocity upon cylinder mass is a generic property of arrays for which fluidelastic instability is induced by the multiple-flexible cylinder, stiffness-controlled mechanism. However, further research on other arrays is required before this statement can be conclusively stated.

4.2.7 Effect of Cylinder Damping

Table 4.7 summarises the experiments undertaken to elucidate the effect of cylinder damping upon the instability threshold. The stability of the array, with four flexible cylinders in the three upstream rows, has been investigated for different values of cylinder damping at $m = 280$ and 490 . Drawing from these experiments the variation of non-dimensional critical velocity with cylinder damping is given in Figure 4.47 for two different cylinder mass values. This figure shows a relationship between the non-dimensional critical velocity, $U_c/f_n d$, and the logarithmic decrement of damping, δ , of the form

$$U_c/f_n d \propto \delta^\alpha \dots \bar{m} = \text{constant}, \quad (4.2)$$

where $\alpha = 0.06$ and 0.07 , respectively for $\bar{m} = 280$ and 490 . This result, in association with the effect of cylinder mass, discussed in subsection 4.2.6, reveals a series of important points.

The instability threshold of a flexible cylinder configuration in this array, is only *marginally* affected by changes in the mechanical damping of the cylinders ($280 \leq m \leq 490$).

¹³Chen and Jendrzejczyk [42] reported the second highest value for β as 1.08

- Changes in cylinder mass have little or no effect on the relationship between non-dimensional critical velocity and cylinder damping ($280 \leq m \leq 190$).
- For this array, it is impossible to combine the dimensionless mass and the damping together under the same exponent in a Connors type equation. Even if both the dimensionless mass and damping are grouped separately, it is still not possible to form a generalised version of the Connors' type equation in the form

$$U_c/f_n d = K(m/\rho d^2)^{\alpha_1} \delta^{\alpha_2}$$

as α_1 is strongly dependent on the value of $m/\rho d^2$. It is, as yet, not known if this important result is valid only for this array, or if it can be generalised for other arrays in which the dominant instability inducing mechanism is multiple flexible cylinder, stiffness controlled.

4.3 The Effect of Frequency Detuning

4.3.1 Introduction

Variations between the natural frequencies of heat exchanger tubes is an unavoidable and frequently encountered phenomenon. In contrast to its practical importance this issue, termed *frequency detuning*, or simply *detuning* has received rather limited attention. Whatever information is available in the literature is inconclusive and in some cases contradictory. Probably the only common denominator of all such studies, both experimental and numerical, is that frequency detuning will have a more important effect in arrays where strongly coupled cylinder motion exists. In previous subsections of this study, (subsections 4.2.2, and 4.2.3) on various occasions the strongly coupled motion between flexible cylinders has been discussed. It has been strongly emphasized that through fluidelastic coupling, flexible cylinders impose

different vibrational modes on each other and affect/alter each others vibrational motion. Therefore, this array offers an excellent platform to analyse the effect of frequency detuning on fluidelastic instability limits.

4.3.2 The Effect of Inter-Cylinder Frequency Variation

In subsection 4.2.3 the vibrational response of a four-flexible cylinder configuration, located in the three upstream rows (cylinders 1, 2L, 2R and 3), with $\bar{m} = 280$, $f_n = 10$ Hz and $\delta = 0.014$ was discussed in detail. In the first detuning experiment the initial natural frequency of the three upstream flexible cylinders (cylinders 1, 2L and 2R) was reduced to 6.375 Hz, whereas the third row cylinder (cylinder 3) was retained at 10 Hz; all four cylinders had $\bar{m} = 280$ and $\delta = 0.014$ ¹⁴. In the terminology of this subsection such a configuration is termed to be - (minus) 36% detuned¹⁵.

Table 4.8 is a tabulation of the major frequencies extracted from the power spectra of each cylinder at the non-dimensional flow velocities of 18 and 39. In this subsection natural frequency of cylinder 3 is used for non-dimensionalisation. At the non-dimensional flow velocity of 18, which is a relatively low velocity falling in the buffeting region, the three upstream cylinders (1, 2L and 2R) vibrate in the vicinity of their initial natural frequencies¹⁶ as shown in Figure 4.48. Two peaks of 6.44 and 6.87 Hz are common to all three flexible cylinders and inter-cylinder motion at these frequencies is strongly coupled. The response of the downstream cylinder, cylinder 3, is of greater interest. It oscillates in the vicinity of its initial natural frequency¹⁷ at 9.31 and 9.56 Hz *as well as* at two other low magnitude modes of 6.87 and 6.44

¹⁴In detuning experiments all the flexible cylinders are kept at the same cylinder mass and damping. The *only* difference between the flexible cylinders is the initial natural frequency.

¹⁵For the experiments to be presented in this subsection, the frequency of the third row cylinder is always at 10 Hz, unless otherwise stated. So this cylinder will be taken as the reference one in non-dimensionalisation. *Detuning ratio* or simply *detuning* is defined as the ratio of the natural frequency of cylinders 1, 2L, and 2R to the cylinder 3 natural frequency minus one $[(f_{c1} = f_{c2L} = f_{c2R})/f_{c3} - 1]$. For example, when the upstream cylinders are at frequency of 8 Hz, the detuning ratio is $[8/10 - 1] = -0.20 = -20\%$. Such a case is termed as *negatively detuned*. Similarly when the upstream cylinders are at a higher frequency than that of cylinder 3, the system will be termed to be *positively detuned*.

¹⁶6.375 Hz

¹⁷10.0 Hz

Hz. When the cross spectra of the signal from cylinder 3 and the upstream cylinders is examined high level of coherence and common power are detected around 6.87 and 6.44 Hz, signifying strong fluidelastic coupling between all the cylinders. So the low frequency upstream flexible cylinders are capable of imposing an *additional*, lower mode of vibration upon the downstream third row cylinder through fluid coupling. At this velocity, the interaction between the cylinders is still of low magnitude.

At $U/f_n d = 39$, as shown in Figure 4.49, the flexible cylinders become unstable and vibrational acceleration magnitudes close to 2 g are recorded. As seen in Table 4.8, all the cylinders oscillate at a frequency of 11.8 Hz. A lower and a higher harmonic, namely $f/2 = 5.9$ Hz and $3f/2 = 17.7$ Hz is also observed in cylinders 2R and 3¹⁸. It is quite interesting that at this flow velocity cylinders 1, 2L and (if the harmonics are not considered) 2R, have completely "lost" their original natural frequency of 6.375 Hz. Their motion is completely synchronised with that of cylinder 3. Thus, flexible cylinders with different initial frequencies are capable (through fluidelastic coupling) of affecting and synchronising each others motion. Figure 4.50, showing the variation of the major in- and cross-flow fluidelastic natural frequencies of each cylinder with non-dimensional velocity, illustrates this point. Initially, the natural frequency of cylinders 1, 2L and 2R are quite distinct from that of cylinder 3; however, as the velocity is increased the frequencies gradually affect each other and synchronise at a non-dimensional velocity of 39¹⁹. Figures 4.51 and 4.52 show the in- and cross-flow vibrational acceleration of all the cylinders becoming unstable at $U_c/f_n d \approx 35$. Focusing on cylinder 3, it is seen that this cylinder becomes unstable at a non-dimensional velocity $\approx 40\%$ less than when all the flexible cylinders are at the same initial natural frequency²⁰. Therefore, interaction between cylinders results, as discussed above, in a *reduction* of the instability threshold for a downstream cylinder

¹⁸Emergence of harmonics at instability is observed in most experiments. Generally, this can be taken as an indicator of non-linearities in the cylinder vibration which are important at the instability limit.

¹⁹Coherence between cylinders greater than 90%

²⁰Subsection 4.2.3, same conditions but all cylinders at 10 Hz - a critical non-dimensional velocity of ≈ 59 .

in the presence of upstream cylinders with lower frequencies (negative detuning).

The above behaviour is repeatable. Figure 4.53 shows the vibrational response of the third row cylinder in a similar experiment, but with the upstream cylinders (1, 2L and 2R) at a slightly different frequency of 6.5 Hz. The critical non-dimensional velocity for cylinder 3 is ≈ 39 , in agreement with the above experiment.

The next question to be addressed, which is the reverse of the above, is the effect that upstream cylinders with higher frequencies (positively detuned) will have on the third row cylinder. With all other conditions the same, cylinders 1, 2L and 2R were tuned to an initial natural frequency of 13.5 Hz, while cylinder 3 was retained at 10 Hz. Table 4.9, based on the acceleration power spectra of Figures 4.54 and 4.55, summarises the major vibrational modes of the four flexible cylinder configuration at non-dimensional flow velocities of 33 and 65. For $U/f_n d = 33$ all the flexible cylinders, low and high frequency ones, oscillate independently of each other. No trace of coupled motion is detectable²¹. The higher stiffness of the upstream flexible cylinders impedes any interaction with either the surrounding fluid and/or with each other. At $U/f_n d = 65$, corresponding to $\approx 90\%$ of the critical non-dimensional velocity, substantial fluidelastic coupling between the flexible cylinders exists. Cylinders 1, 2L and 2R are affected little by the motion of cylinder 3. But in contrast, cylinder 3 is strongly affected by the motion of the upstream cylinders. Cylinder 2L at 11.6 Hz, cylinder 1 at 12.8 Hz and cylinders 2L and 2R at 13.0 Hz induce high magnitude vibrations of cylinder 3 by fluidelastic coupling. Such an effect delays the instability of cylinder 3 to a non-dimensional velocity of ≈ 69.5 , as seen in Figures 4.56 and 4.57. Thus, the presence of higher frequency cylinders (positive detuning) upstream of the third row cylinder delays the onset of instability by 18% relative to the case where all cylinders have the same initial natural frequency.

Therefore, a third row cylinder located behind three cylinders with *lower* natural frequencies exhibits instability at a *lower* non-dimensional velocity *relative* to

²¹When the upstream cylinders were negatively detuned by 36%, strong fluidelastic coupling between flexible cylinders was measured

a configuration with all cylinders at the same natural frequency. Whereas, a third row cylinder located behind three cylinders with *higher* natural frequencies exhibits instability at a *higher* non-dimensional velocity relative to a configuration with all cylinders at the same natural frequency.

To fortify this observation a series of experiments with four flexible cylinders located in the three upstream rows (cylinders 1, 2L, 2R and 3) was done. All the flexible cylinders had $\bar{n} = 280$ and $\delta = 0.014$. Cylinder 3 was always kept with an initial natural frequency of 10 Hz, while the initial natural frequency of the upstream cylinders (1, 2L and 2R) was varied from experiment to experiment. Table 4.10 summarises some of the important initial properties and results. Based on the data from this table, the effect of frequency detuning on the non-dimensional critical velocity of cylinder 3 is plotted in Figure 4.58. When all the cylinders have the same frequency, cylinder 3 becomes unstable at a non-dimensional velocity of 59. When the initial natural frequency of the upstream cylinders (1, 2L and 2R) is increased to 12.37 Hz the third row cylinder experiences instability at a non-dimensional velocity of 66.5, 13% higher than the non-detuned case. A further increase in the frequency of the upstream cylinders to 13.5 Hz, impedes the instability of cylinder 3 to a non-dimensional velocity of ≈ 70 . At least in this range, the relationship between frequency increase (positive detuning) and non-dimensional critical velocity is reasonably linear.

On the other hand, when the initial natural frequency of the upstream cylinders (1, 2L and 2R) is lower than that of cylinder 3, the instability threshold is lower relative to the non-detuned case. For example, with the upstream cylinders at 9 Hz, cylinder 3 becomes unstable at a non-dimensional velocity of 48.5, 18% less than for the non-detuned case.

The above effects of negative and positive detuning on the instability velocity of cylinder 3 are in agreement with previous detailed discussions. Higher-frequency upstream cylinders are capable, through fluidelastic coupling, of *increasing the effective fluidelastic natural frequency* of the third row cylinder relative to the case when all the cylinders are at the same frequency. The result of such a coupled interaction is, in

a sense, the same as having cylinder 3 tuned to a *higher initial natural frequency* than it actually is. Such a *fluidelastic increase of stiffness* delays the unstable behaviour of cylinder 3 to higher flow velocities. When non-dimensionalised with respect to the *still-air initial natural frequency* of the third row cylinder²², the resulting non-dimensional critical velocity is also higher relative to the case of equal frequencies. Due to set-up limitations the frequency ratio $[(f_1 = f_{2L} = f_{2R})/f_3]$ could not be increased beyond 1.35, but it is likely that a further increase in this ratio would tend to increase the effective stiffness of cylinder 3, resulting in higher critical velocities. Eventually with increasing frequency ratio, cylinders 1, 2L and 2R would be rigid enough not to affect the motion of cylinder 3, which in turn will act as a single flexible cylinder in the array. At this point there will be no fluidelastic instability - a single flexible cylinder does not become unstable in this array [6].

On the other hand, in case of negative detuning, upstream cylinders with lower natural frequencies can attain considerable vibrational displacement at low flow velocities. Such motions perturb the surrounding fluid sufficiently to couple with other low-frequency flexible cylinders. Then, the combined contribution of these low-frequency flexible cylinders, fluidelastically affect the third row high-frequency cylinder at a frequency lower than its own. So cylinder 3, with increasing flow velocity, undergoes vibrational motion both at high frequencies related to its own initial natural frequency and at low frequencies because of coupling with the upstream flexible cylinders. The result of such coupled motion is to reduce the *effective fluidelastic natural frequency* of the third row cylinder relative to the case when all cylinders are at the same frequency. This, in a sense, is equivalent to having cylinder 3 tuned to an *incrementally lower initial natural frequency* than it actually is. Such a *fluidelastic decrease of stiffness* advances the unstable behaviour of cylinder 3 to lower flow velocities, as seen in

²²For detuned arrays it is quite difficult to decide upon the frequency to be used in non-dimensionalisation. In fact as discussed above, the major effect of detuning is to alter the fluidelastic frequency of the other flexible cylinders. The ideally correct frequency of choice should be a *natural frequency* also comprising the effects of detuning that will be induced by the surrounding cylinders during flow conditions. Naturally this is out of the question. So the initial natural frequency of the "non-detuned" cylinder will be used for non-dimensionalisation.

Figure 4.58.

Up to this point, the effect of frequency detuning upon critical velocity has been analysed from the perspective of the third row flexible cylinder of a four-flexible cylinder configuration only. The question of how the upstream cylinders of the configuration (cylinders 1, 2L and 2R) respond to detuning will be addressed next.

Table 4.5 shows the results from four flexible-cylinders in the three upstream rows (1, 2L, 2R and 3), all the flexible cylinders having $\bar{m} = 280$, $\delta = 0.014$ and $f_n = 13.5$ Hz. This non-detuned configuration does not become unstable up to the limit of the wind tunnel, which is $U/f_n d \approx 57$ for this case.

Table 4.10 summarises the results of another experiment, with all conditions the same as the above, except that cylinder 3 has an initial natural frequency of 10 Hz ($\bar{m} = 280$, $\delta = 0.014$, $f_1 = f_{2L} = f_{2R} = 13.5$ Hz and $f_3 = 10$ Hz). This configuration, which has been discussed previously, becomes unstable at a flow velocity of 17.80 m/s, corresponding to $U/f_n d = 52$. Thus the existence of a single lower-frequency cylinder in a *downstream* row (row 3), affects the higher-frequency *upstream* cylinders such that instability is induced in an otherwise stable array. This result leads to some important conclusions;

- in the presence of strong fluidelastic coupling, detuning effects can dissipate from upstream to downstream flexible cylinders as well as from downstream to upstream flexible cylinders.
- in a detuned array the exchange of frequencies between cylinders of different frequencies is *reciprocal*. While higher-frequency cylinders impose greater rigidity on lower-frequency cylinders through fluidelastic coupling, the lower frequency cylinders in return, inflict lower frequencies on higher-frequency cylinders

This mutual exchange of frequencies strongly alters the *fluidelastic natural frequency* of all the cylinders. *Higher-frequency* cylinders becomes unstable at a flow velocity *lower* than the case when all the cylinders have the same frequency, while *lower-frequency* cylinders becomes unstable at a flow velocity *higher* than the case when all

the cylinders have the same frequency. This conclusion will be expanded on in the next subsection.

4.3.3 Further Effects of Frequency Detuning

In this subsection, a configuration of four flexible cylinders²³ is once again located in the three upstream rows. This time, cylinders 1 and 3 are tuned to the same frequency while cylinders 2L and 2R are tuned to a different one. The results obtained in various experiments are summarised in Table 4.11. To illustrate the effect of frequency detuning on *different* cylinders, two figures based on the data of Table 4.11 will be presented.

In Figures 4.59 and 4.60 the non-dimensional critical velocity of each flexible cylinder is plotted against the frequency ratio $[(f_1 = f_3)/(f_{2L} = f_{2R})]$. In Figure 4.59 the non-dimensionalisation is with respect to f_1 (or f_3) and in Figure 4.60 the non-dimensionalisation is with respect to f_{2L} (or f_{2R}). When $[(f_1 = f_3)/(f_{2L} = f_{2R})]$ is *less* than unity, cylinders 1 and 3 are at a lower frequency than cylinders 2L and 2R. The high-frequency, more rigid cylinders (2L and 2R), transfer higher frequency vibrations to cylinders 1 and 3 through fluidelastic coupling and delay instability to a higher flow velocity. When this flow velocity is non-dimensionalised with respect to the initial natural frequency of cylinders 1 or 3 the result is a higher non-dimensional critical velocity compared to the case of no detuning, $[(f_1 = f_3)/(f_{2L} = f_{2R})] = 1$, as seen in Figure 4.59. For example, at $[(f_1 = f_3)/(f_{2L} = f_{2R})] = 0.64$ the average non-dimensional velocity is ≈ 80 , 29% higher than the average value of 62 for the non-detuned case.

Again, in the *same* region, $[(f_1 = f_3)/(f_{2L} = f_{2R})] < 1$, the events can be analysed from the perspective of the higher frequency second row cylinders as shown in Figure 4.60. These cylinders, while affecting the low-frequency cylinders (1 and 3) are in turn *themselves* affected by the low frequency cylinders. Through fluidelastic coupling,

²³All cylinders with $\bar{m} = 280$ and $\delta = 0.014$.

cylinders 2L and 2R, receive lower frequencies from cylinders 1 and 3. This reduces the *effective fluidelastic natural frequency* of cylinders 2L and 2R and results in a lower critical velocity. When this flow velocity is non-dimensionalised with respect to the initial natural frequency of cylinders 2L or 2R, the result is a lower non-dimensional critical velocity, compared to the case of non-detuning. An example of these is when $[(f_1 = f_3)/(f_{2L} = f_{2R})] \approx 0.61$, where the average non-dimensional velocity is about 52, 16% lower than the average value of 62 for the non-detuned case.

Such an exchange of frequencies between the flexible cylinders affecting each others instability limit is also applicable in the region where $[(f_1 = f_2)/(f_{2L} = f_{2R})] > 1$. In a detuned array, the higher frequency cylinders become unstable at a *lower* non dimensional velocity when non-dimensionalised with respect to their initial natural frequency, as shown in Figure 4.59. Similarly, the lower frequency cylinders become unstable at a *higher* non-dimensional velocity when non-dimensionalised with respect to their initial natural frequency, as shown in Figure 4.60.

Exchange of frequencies between detuned cylinders discussed above, can be illustrated further through Figure 4.61. When the critical velocity is non-dimensionalised with respect to the square root of the lower and higher natural frequencies, i.e. $U_c/(f_1 f_{2L})^{0.5} d$ instead of f_1 or f_{2L} , then the average of the non dimensional critical velocities of each frequency ratio change little with frequency ratio. This suggests that the affect of low- and high-frequency cylinders on each other is of relatively equal importance.

Table 4.12 summarises some other frequency detuning experiments, showing trends in agreement with previously presented observations.

4.4 Static Displacement and Instability

4.4.1 Two Flexible Cylinders

In some theoretical studies [79, 69, 65] it has been proposed that if the total stiffness of a cylinder vanishes (aerodynamic plus structural), then such a system can become

unstable by divergence (non-oscillatory static-instability). The actual existence of this instability mechanism has recently been verified by Paidoussis, Price and co-workers in an experimental study on a rotated square array with $P/d = 1.5$ [60]. When the data for the single and multiple-cylinder experiments of this study are considered, a significant decrease in the cross-flow fluidelastic frequency of second and third row cylinders is observed with increasing flow velocity. Typical examples of such a behaviour can be found in Figures 4.5, 4.8 and 4.24. A series of special experiments for cylinders in rows 2 and 3 was designed to investigate, if this loss of total cylinder stiffness can eventually lead to static instability. A schematic example of these experiments, where two flexible cylinders with $\bar{m} = 280$, $f_n = 7$ Hz and $\delta = 0.014$ are located in row 2 (cylinders 2L and 2R), is shown in Figure 4.62. The in- and cross-flow vibrational response of these two cylinders (2L and 2R) are given in Figures 4.63 to 4.68. Certain interesting observations, mainly in the cross-flow direction of both cylinders, can be extracted from these figures.

In the cross-flow direction the main natural frequency exhibits a reduction with increasing flow velocity (Figures 4.63 to 4.65). This reduction becomes substantial for flow velocities greater than approximately 11.5 m/s ($U/f_n d = 61.7$).

- Especially in the cross-flow direction of cylinder 2L, the acceleration magnitude in the primary mode is very low. (less than 0.02 g as seen in Figures 4.64 and 4.66)

Both cylinders 2R and 2L exhibit a static displacement in the cross-flow direction. This displacement starts at the same velocity as that of the frequency reduction and moves the cylinders away from each other. Figure 4.67 shows the increasing magnitude of the static displacement with flow velocity for cylinders 2L and 2R.

- At a flow velocity of ≈ 15.3 m/s ($U/f_n d = 86.1$) cylinder 2L (and to a lesser extent, cylinder 2R) experiences a sudden buckling type of motion in the cross-flow direction as shown in Figure 4.67. The cylinder is displaced, very suddenly,

by a distance of about 6.5 mm relative to the previous point and exhibits an inert vibrational response. The major cross-flow response at this velocity is fairly broadband as seen in the acceleration power spectrum of Figure 4.68 and its magnitude is less than 0.01 g.²⁴ The center of this broadband response can be taken to be slightly less than 4 Hz which corresponds to $\approx 55\%$ of the initial natural frequency value in still-air. Even though the cross flow frequency does not go to zero, as it should in a complete static instability case, loss of substantial rigidity, highly reduced oscillatory motion, significant static deflection and buckling like motion all suggest that cylinder 2L has *undergone a static instability*. Two additional factors lend further support to this argument. Firstly, the only other known case of experimental static instability was detected in another rotated square array, but with a smaller $P/d = 1.5$ [60]. Secondly, when the time averaged-steady forces acting on the static cylinders of this array (rotated square, $P/d = 2.12$) were measured, it was determined that the variation of static lift coefficient with cross-flow displacement ($\partial C_L/\partial y$) is positive. As per the quasi-steady model of Price and Paidoussis [79] this is a *necessary* condition for static instability²⁵. Furthermore, the magnitude of this term is a maximum for cylinders in the second row, where divergence occurred in the flexible cylinder, dynamic experiments.

²⁴a) The peak of ≈ 16 Hz originates from the in-flow direction as shown in Figure 4.61. b) The behaviour of cylinder 2R is somewhat different. Even though a reduction in frequency ($\approx 30\%$) and a static deflection (≈ 6.5 mm in total) is measured, the magnitude of the acceleration at the major mode is still substantial (≈ 0.05 g). Ideally, in a perfect system, both cylinders should exhibit identical behaviour when subject to the same conditions. But it is quite likely that a slight imperfection in array geometry and alignment could possibly trigger and initiate differences.

²⁵When the measured $\partial C_L/\partial y$ term is introduced into the Price and Paidoussis model a major reduction of frequency, similar to that observed in the experiments, is obtained and eventually the cylinder becomes statically unstable at a flow velocity of 15.8 m/s. This is only $\approx 4\%$ different than the above reported experimental value of 15.3 m/sec. Such an excellent agreement between the experimental and the theoretical results gives further support to the existence of static instability and is discussed in detail in Chapter 6.

4.4.2 Three Flexible Cylinders

During most of the three- and four-flexible cylinder experiments performed in the first few upstream rows of the array, a loss of stiffness was noted, prior to *dynamic instability*. In the previous subsection it was seen that this loss of rigidity for two flexible cylinders in the second row eventually leads to *static instability*. These observations lead to the possibility that the threshold for dynamic and static instability can be in the same proximity, at least for some configurations. To check the validity of such a hypothesis, a three-flexible cylinder configuration, known to be dynamically unstable, was tested under different initial conditions. The objective being to suppress the dynamic instability and if possible initiate a static instability. In subsection 4.2.4 it was shown that a combination of three flexible cylinders positioned in the second and third rows (cylinders 2L, 2R and 3) with $\bar{m} = 280$, $f_n = 7$ Hz and $\delta = 0.014$ experiences dynamic instability at a non-dimensional critical velocity of ≈ 105 . The typical oscillatory response of a second row cylinder for such an experiment ending with unstable dynamic behaviour is shown in Figure 4.69. This configuration will be taken as a reference point, and the type of the instability will be altered by changing the initial frequency and/or damping.

In the first experiment to be discussed, the cylinder position, mass and frequency are kept the same, $\bar{m} = 280$, $f_n = 7$ Hz, but the damping is increased 14 times to $\delta = 0.20$. Figures 4.70 to 4.74 illustrates some interesting results of this experiment.

By increasing the damping, the dynamic instability is suppressed²⁶ as shown by the three dimensional acceleration power spectra of Figure 4.70. (Compare this with Figure 4.69, showing the unstable behaviour of the same cylinder at a lower damping value of $\delta = 0.014$).

The motion of the cylinders is uncoupled. So the motion of each cylinder is

²⁶It should be remembered that the critical non-dimensional velocity of ≈ 105 corresponds to the limiting value attainable from the wind tunnel. Even though in this array the critical velocity is weakly dependent on cylinder damping, a major change in damping seems to be sufficient enough to suppress dynamic instability.

similar to that of a single cylinder, with little or no effect from the others. This is in complete contrast to the case where $\delta = 0.014$.

- The maximum vibration amplitude at the major cross-flow mode never exceeds a value of 0.035 g and exhibits a drop after a flow velocity of 11.8 m/s, ($U/f_n d = 66.4$) as shown in Figure 4.70 and 4.72.
- At a flow velocity of 16.9 m/s ($U/f_n d = 95.1$) the vibration at the major cross flow mode becomes broadband and it is quite difficult to distinguish a dominant peak in either the in- or cross-flow directions as shown by Figure 4.70. A closer view of the acceleration power spectra at this flow velocity, Figure 4.73, verifies this argument. The only visible peak is around 17 Hz corresponding to the major in-flow mode. Again, at this flow velocity the cylinder experiences a buckling type motion in the cross-flow direction and undergoes a major static deflection of ≈ 4 mm as shown by Figure 4.74.

All the above observations point to a strong possibility of static instability, at least in the vicinity of a flow velocity of 16.9 m/s ($U/f_n d = 95.1$). This result is quite important in the sense that through the change of a single variable, -damping-, dynamic instability can be suppressed and replaced by a static instability. Such a cohabitation of both dynamic and static instability mechanisms in the same proximity is being reported for the first time. Another similar example will be presented next.

Again a configuration of three flexible cylinders positioned in the second and third rows with $\bar{m} = 280$ is taken as a reference. All the cylinders were set to a damping value of $\delta = 0.14$ (ten times that of the case which resulted in dynamic instability). Cylinders 2L and 2R were tuned to an initial natural frequency of 7 Hz (the same as the case which resulted in dynamic instability) whereas cylinder 3 was tuned to 13.5 Hz. The objective of such an arrangement is to minimise fluidelastic coupling between cylinders by increasing the damping of all the cylinders and the stiffness of the most "energetic" cylinder²⁷ to retard multiple-flexible cylinder type dynamic

²⁷Increasing the fluidelastic natural frequency of flexible cylinder relative to others is termed as

instability to higher flow velocities. Thus static instability, if it exists, will reveal itself. The results for the behaviour of a second row cylinder are as shown in Figures 4.75 to 4.79. Dynamic instability is suppressed and the major cross-flow mode *decreases* both in vibration amplitude and frequency with increasing flow velocity as shown in Figures 4.75 to 4.77. At a flow velocity of 16.1 m/s ($U/f_n d = 91$) the major cross-flow vibrational mode becomes broadband and a distinct peak cannot be detected, as shown in Figure 4.78. Also at this flow velocity a buckling type of motion, similar to the previous ones, is observed. The total static deflection is as much as a third of the cylinder diameter, as shown in Figure 4.79. All these observations point to a static instability.

Therefore, by varying both the damping and/or frequency of the system it is possible to initiate static instability instead of a dynamic instability. Equation 2.5 of Appendix 2 shows that theoretical threshold for static instability is given by

$$U_{cr} = w_0 d \left[\frac{2\bar{m}}{(\partial C/\partial \bar{z})} \right]^{\frac{1}{2}}, \quad (4.3)$$

where w_0 = initial cyclical frequency of the cylinder, d = diameter of the cylinder, \bar{m} = dimensionless cylinder mass and $\partial C/\partial \bar{z}$ = the variation of lift or drag coefficient with displacement. The effect of these parameters upon static instability threshold were investigated by further experiments. Increasing the initial frequency of the cylinder resulted in higher critical velocities. But for $f_n > 9.5$ Hz, probably due to limitations of the wind tunnel, no clear case of static instability was detected. Similarly, experiments with high dimensionless mass ($\bar{m} \geq 490$), prevented static instability and reduced the loss of stiffness in the cross-flow direction. Finally, as will be discussed in Chapter 6, the largest value of $\partial C_L/\partial \bar{y}$ was measured for a second row cylinder, confirming the critical nature of this row as determined by dynamic (vibration) experiments.

"positive detuning". In section 4.3 positive detuning is shown to reduce fluidelastic coupling and retard dynamic instability to higher critical flow velocities

Chapter 5

FORCE MEASUREMENT APPARATUS

5.1 The Force Measurement Insert, the Force Balance and the Associated Instrumentation

Another objective of this study was to investigate the time averaged forces acting on static cylinders; this was done as a function of both the surrounding cylinders displacement and the Reynolds number. Such an investigation enables a better physical understanding of the fluid dynamics in the array and furnishes data for a quasi steady multiple-degree-of-freedom numerical model predicting the instability threshold.

As discussed in section 2.2, the rigid portion of the array was designed to serve in both the vibration and force measurement experiments. By replacing the *vibration measurement insert* with the *force measurement insert* and a *force balance* the apparatus is converted into a form facilitating the measurement of time averaged fluid forces.

The *force measurement insert* consists of eight 25.4 mm (1-in.) diameter, 791 mm (23.25 in.) long, solid aluminum cylinders sandwiched between two equal sided hexagonal 10 mm (0.39 in.) plates, as shown in Figures 5.1 and 5.2. The upper and lower hexagonal plates of the force measurement insert were carefully machined to fit closely into the similar shaped holes in the aluminum base plates of the rigid portion of the array, as shown in Figure 2.2. Thus, when assembled and placed into the

rigid portion of the array, this insert completes a $P/d = 2.12$, rotated square array with the exception of a single cylinder. This cylinder is the so-called "*instrumented cylinder*" which is bolted to the *force balance*, which in turn is attached to the wind tunnel through the arrangement, shown in Figure 5.3. Using a gear arrangement it is possible to move the platform housing the force balance and the instrumented cylinder in the plane parallel to the wind tunnel floor. The instrumented cylinder could be displaced to any desired position within a circle of diameter 46 mm (1.81 in.).

To simulate the effect of the surrounding cylinders motion on the instrumented cylinder, one of the eight cylinders in the insert is designed with the capability of being displaced along a straight slot as much as 25.4 mm (1-in.). As the hexagonal shaped insert is symmetrical, through consecutive turns of 60° each it is possible to locate this cylinder in different rows and positions.

The force balance is instrumented by two Kistler type force transducers mounted orthogonally in the in- and cross-flow directions to measure the fluid forces acting on the instrumented cylinder. The force transducers are calibrated against known weights as shown in Figure 5.4. As observed from this figure, for a load of less than 2.5 lb the relationship between the force and the output voltage of the transducer is linear. The experiments in this study were all performed in this linear range. The in- and cross-flow directional force signals were analysed either via a IIP 3562A or a IIP 5120A dynamic signal analyser. Data analysis is performed on a Hewlett-Packard 9000 310 computer system by utilising the software NEWED, developed by Mark [89] at McGill University

5.2 The Force Measurement Procedure

The force measurements performed in this study can be divided into three main groups.

1) **Measurement of the variation of the drag coefficient (C_D),¹ versus the Reynolds Number Re ².** In this experiment all the cylinders, instrumented and surrounding, were located at non-displaced positions during the course of the whole experiment. The experiment was started at the lowest possible steady upstream flow velocity of 3 m/s and a 10 sec. time trace of the in flow directional fluid force acting on the instrumented cylinder was recorded by the dynamic signal analyzer to calculate an average force. Once this value was stored for future data analysis, the velocity was increased by an increment of ≈ 0.5 m/s to repeat the same measurement. This procedure of measuring time averaged forces at different flow velocities was repeated until the limiting flow velocity of the tunnel was reached. Such measurements were performed in rows 1, 2, 3, 4 and 5 of an eight-row array and in row 7 of a ten-row array. A sample output from this experiment for a cylinder in row 1 can be found in Figure 6.2 in the form of the variation of the drag coefficient, C_D with Reynolds number, Re .

2) **Lift and Drag Maps at constant Reynolds Number** Again all the cylinders were initially located at non-displaced positions. The upstream flow velocity was set to a constant value throughout the experiment. The instrumented cylinder, at the center of the insert, was systematically traversed in a 35.6 mm by 35.6 mm (1.4 in. by 1.4 in.) square. This square can be thought of as a matrix with 361 equally spaced nodes, each of which is a measurement point. The cylinder was displaced to every node and the corresponding in- and cross-flow fluid forces acting on the cylinder measured. These data points were later

¹ Drag coefficient is defined as $C_D = F / \frac{1}{2} \rho U_\infty^2 l d$ where F = Fluid force acting on the cylinder in the direction of the upstream flow, U_∞ = Upstream flow velocity, ρ = Flow density, l = Cylinder Length, d = Cylinder Diameter. In case of the lift coefficient, C_L , the fluid force considered is the one acting on the cylinder perpendicular to flow direction. The typical axis system is as shown in Figure 6.8.

² Reynolds Numbers, Re , is the ratio of inertia to viscous effects and is defined as $Re = \frac{U_\infty d}{\mu}$ where U_∞ = Upstream Flow Velocity, ρ = Flow density, d = characteristic length (cylinder diameter), μ = viscosity.

non-dimensionalised to form contour maps of lift and drag coefficients experienced by the instrumented cylinder as shown in Figures 6.22 and 6.23. The typical velocity chosen for constructing such fluid force coefficient maps was 16.6 m/s, but also some investigations were carried out at flow velocities of 8.3 m/s and 21.4 m/s. In two probing experiments a finer measurement matrix (grid) with 1369 nodes was used. The results, when compared with those from a 361 node matrix, did not exhibit significant difference to warrant the use of a finer measurement matrix requiring nearly four times more experimental effort. The two experimental measurements discussed above, in items 1 and 2, supply data for the analysis of a single flexible cylinder inside an otherwise rigid array. A multiple-flexible-cylinder analysis, further requires the effect of surrounding cylinder motion upon the fluid forces acting on the instrumented cylinder. This measurement was done in the third type of experiment discussed below.

- 3) **Measurement of the variations in lift and drag coefficients of the instrumented cylinder due to surrounding cylinder displacement at constant Reynolds Number.** Again with all the cylinders at their equilibrium positions, a constant flow velocity was chosen and retained throughout the experiment. One of the cylinders in the insert, previously termed the surrounding cylinder, was incrementally displaced either in the in- or cross-flow directions by as much as 25.4 mm (1-in.). At each displaced position the fluid forces acting on the instrumented cylinder, which was kept at its original position, were measured. A typical variation of the drag coefficient of the instrumented cylinder, due to the displacement of a surrounding cylinder is shown in Figure 6.41. By rearranging the apparatus it is possible to measure the effect of displacing the adjacent cylinders, one at a time.

Chapter 6

FORCE MEASUREMENTS

6.1 Variation of The Drag Coefficient, C_D , with Reynolds Number

6.1.1 Variation of The Drag Coefficient, C_D , with Reynolds Number for a Single Cylinder

For a single cylinder in cross-flow, the variation of the steady drag coefficient versus the Reynolds number is well documented. In the Reynolds number range of this study ($6.2 \times 10^3 < Re < 4.5 \times 10^4$) the drag coefficient, C_D , for a single cylinder - with all surrounding cylinders removed - is a constant around 1.15, with a variation of $\approx \pm 10\%$, as shown in Figure 6.1. This figure also shows the drag coefficient values determined in the present study for a single cylinder, exhibiting a good agreement with others.

6.1.2 Variation of the Drag Coefficient, C_D , with Reynolds Number for Cylinders in Different Rows of the Array

These measurements have been performed for cylinders in rows 1, 2, 3, 4 and 5 of an eight-row array and row 7 of a ten row array. During the course of these experiments the instrumented cylinder was kept at a non-displaced position ($\bar{x} = 0, \bar{y} = 0$).

For a cylinder in the first row, the dependence of drag coefficient, C_D , upon

the Reynolds number, Re is very weak as observed in Figure 6.2. Throughout the Reynolds number range considered ($6.2 \times 10^3 < Re < 4.5 \times 10^4$) the drag coefficient is constant, fluctuating around a value of ≈ 2.1 .

The results for the second, third and fourth row cylinders are radically different than that of the first row cylinder. The drag coefficient for cylinders located in these rows exhibits a major decrease with increasing Reynolds number, as shown in Figure 6.3. For an upstream flow velocity range of ≈ 20 m/s, the drag coefficient experiences a reduction of approximately 2-2.5 times, depending upon cylinder position in the array. This is in great contrast to the behaviour of a single cylinder, as well as to the behaviour of the first row cylinder of the array, which are subject to a *constant drag* coefficient in this Reynolds number range of interest. Thus it can be suggested that the velocity dependence of the drag coefficient in the rows 2-4 is an *array-induced* event. This can either be due to a macro change in the flow pattern through the array and/or due to a viscous boundary layer change effecting the separation point, and thus, the size of the wake. Results that will be introduced later¹ do not support the possibility of a major macro level change in the surrounding main flow with Reynolds number. Thus, it is quite likely that a viscous boundary layer event is triggering changes in the wake, and hence, in the drag coefficient.

The drag coefficient for the fifth and seventh row cylinders exhibits a much milder dependence upon Reynolds number as shown in Figure 6.4. It is also of interest that the seventh row shows a striking similarity to the fifth row, in terms of the variation of the drag coefficient with Reynolds number. Such a result suggests the possibility of only a limited change in flow pattern around the cylinders once the upstream entrance rows are traversed. In fact, this observation can be illustrated further by referring to Figure 6.5 which shows the variation of drag coefficient with position in the array at a flow velocity of 16.6 m/s. As seen, after the fourth row, the drag coefficient is only

¹In subsection 6.2 lift and drag maps are obtained by displacing the instrumented cylinder incrementally in a 1.4 m \times 1.4 m. area at different flow velocities. The difference between the *shape* of such maps at three different velocities, $U_\infty = 8.3$ m/s, 16.6 m/s and 21.4 m/s, is only minor. This suggests only a limited change in the flow structure.

weakly related to position in the array. To sum up, it is possible to distinguish three different zones in this array:

- first row where C_D is independent of Re ,
- second, third and fourth rows where C_D is a strong function of both row position and Re ,
- fifth to seventh rows where C_D is a function of Re , but very weakly related to position in the array.

Figures 6.6 and 6.7 display again the variation of the drag coefficient with flow velocity for cylinders in various rows, but in a log-log format. For each row the relationship between drag coefficient and flow velocity can be expressed approximately, as

$$C_D = \alpha Re^\beta \quad (6.1)$$

where α and β are empirical constants. Table 6.1 gives the value of these coefficients for different row cylinders and illustrates the strong effect of Reynolds number and position in the array upon the drag coefficient.

6.2 Lift and Drag Maps

6.2.1 Lift and Drag Maps for a Third Row Cylinder

Once the effect of Reynolds number on the *magnitude* of the drag coefficient was determined, the next step was to resolve the effect of *cylinder displacement* on the force coefficients. A series of drag contours, composed of the fluid forces acting on a third row cylinder in a 361 data point, (1.4 in. \times 1.4 in.) measurement grid for upstream velocities of 8.3 m/s, 16.6 m/s and 21.4 m/s are given, respectively, in Figures 6.8, 6.9 and 6.10. In general, at all flow velocities, when the cylinder is moved either upstream or downstream the drag coefficient increases. Also, cylinder displacement in the cross flow direction, i.e. moving the cylinder more into the channel flow also initiates an increase in the drag coefficient of a third row cylinder. Even though some

important variations are observed between drag contours at different flow velocities, such differences are mainly confined to the peripheries of the maps. The *shape* of each contours' center region is quite similar, even if the *magnitude* of the contours are different.

The lift coefficient maps for a third row cylinder, at the same three flow velocities, are given in Figures 6.11, 6.12 and 6.13. All these maps are quite similar in contour shapes and exhibit a reasonably good symmetry around the $\bar{y} = 0$ axis². Any displacement from the $\bar{y} = 0$ symmetry axis generates a substantial lift force on the cylinder.

Figures 6.14, 6.15 and 6.16 are the force coefficient vector plots obtained from the vector addition of the lift and drag coefficient maps at each velocity. For simplicity such plots will be termed as the *vector plots*. A comparison of the vector plots for $U_\infty = 16.6$ m/s and $U_\infty = 21.4$ m/s (Figures 6.15 and 6.16) shows a strong similarity both in magnitude and direction. Figure 6.14, the vector plot for $U_\infty = 8.3$ m/s exhibits both similarities and differences relative to the vector plots at the other two flow velocities. To better assess these similarities and differences, the force coefficient vectors for $U_\infty = 21.4$ m/s are multiplied by a factor of 1.65³. Then, these *normalised* force coefficient vectors for $U_\infty = 21.4$ m/s and the force coefficient vectors for $U_\infty = 8.3$ m/s are plotted together in Figure 6.17. This figure can be divided into two zones, shown in the figure, by a green-line. Downstream of this line, in an area corresponding to 2/3 of the measurement grid, the vectors for both flow velocities are of similar magnitude and direction. Upstream of this line, neither the magnitudes nor the directions are comparable. Therefore, for a core region in the vicinity of $\bar{x} = 0$ and $\bar{y} = 0$, provided that the variation of the drag coefficient with flow velocity for a cylinder at $\bar{x} = 0$ and $\bar{y} = 0$ is known, force measurements at a *single flow velocity*

²X axis is in the in-flow and y axis is in the cross-flow direction

³The difference in drag coefficient, for a cylinder at $\bar{x} = 0$ and $\bar{y} = 0$, between that measured at a velocity of 8.3 m/s and at $U_\infty = 21.4$ m/s is ≈ 1.65 . So multiplying the drag coefficient value at $\bar{x} = 0, \bar{y} = 0$ for $U_\infty = 21.4$ m/s by a factor of 1.65 can be considered as "normalisation" with respect to $U_\infty = 8.3$ m/s. Such a normalisation can be expected to be reasonably successful in the central core of the vector plots

are sufficient and representative enough to form a data base for modelling purposes.

During the discussion of the dynamic results in Chapter 4, a loss of cylinder rigidity in the cross-flow direction for second, third and fourth row flexible cylinders was reported. Both the lift coefficient and vector plots for the third row cylinder further substantiates the findings of the dynamic experiments. At all flow velocities, the steady fluid forces tend to push the cylinder away from its equilibrium position in the cross-flow direction, as shown in Figures 6.14, 6.15 and 6.16. In this case the fluid forces are acting in an opposing direction to the structural restoring force and will reduce the *overall fluidelastic stiffness* of the cylinder. If the steady fluid stiffnesses ($\partial C_L/\partial \bar{y}$) are large enough to exceed the structural restoring stiffness, then the system will act as if it has a *negative overall fluidelastic stiffness* and static instability (divergence) will occur.

Works of Price and Paidoussis [79, 60] and a simple derivation in Appendix 2 shows that loss of cross-flow stiffness can be expressed by

$$w^2/w_0^2 = 1 - \frac{\bar{U}^2}{2\bar{m}} \frac{\partial C_L}{\partial \bar{y}}, \quad (6.2)$$

where w_0 = initial cyclical frequency of the cylinder, w = in-flow cyclical frequency of the cylinder, \bar{U} = non-dimensional flow velocity, \bar{m} = dimensionless cylinder mass and $\partial C_L/\partial \bar{y}$ = variation of the lift coefficient with cross-flow displacement at $\bar{x} = 0$. Static instability will occur when the LHS of equation (6.2) equals zero. This will take place only if $\partial C_L/\partial \bar{y}$ is positive and \bar{U} is sufficiently large.

From the lift coefficient maps of Figures 6.11, 6.12 and 6.13 the variation of C_L with \bar{y} at $\bar{x} = 0$ can be determined easily. Figures 6.18, 6.19 and 6.20 show this variation for $U_\infty = 8.3$ m/s, 16.6 m/s and 21.4 m/s. In all cases $\partial C_L/\partial \bar{y}$ is *positive* up to a displacement of $\bar{y} = 0.4$, satisfying the condition for static instability at sufficiently high flow velocities. The slope, $\partial C_L/\partial \bar{y}$, at the central position ($\bar{y} = 0$) is not sensitive to flow velocity. A value between 3-3.5 is measured in all cases. But when the cylinder is deflected from the central position in the y-direction a general drop in the magnitude of the slope, increasing with flow velocity, is observed. This can be

seen clearly from the figures where the numbers on each figure, showing the slopes at \bar{y} increments of 0.1 for each velocity, are analysed. For example, at $y = 0.3$ the slope $\partial C_L / \partial \bar{y}$ for $U_\infty = 8.3$ m/s, 16.6 m/s and 21.4 m/s is 2.23, 1.11 and 1.09, respectively (Figures 6.18, 6.19 and 6.20). This variation in slope becomes more significant at large displacements and high velocities. For $U_\infty = 21.4$ m/s and $y = 0.5$ even the sign of the slope changes to *negative*. Such a change indicates an *increase* in the frequency and the possibility of a single degree-of-freedom fluid-damping controlled dynamic instability⁴. The slopes determined at 5 different \bar{y} values for each of three upstream velocities were inserted into equation (6.2), to attain the frequency ratio, w^2/w_0^2 , at different non-dimensional flow velocities and static displacements⁵. Figure 6.21 summarises the results for $\bar{n} = 280$. The contour lines show how the frequency ratio varies with respect to the non-dimensional flow velocity and displacement of the cylinder in the cross-flow direction. In fact this is a map of what may happen to a single flexible cylinder at certain velocities and displacements ($\bar{n} = 280$). Three distinct zones are identifiable in this contour map. The first zone, in the lower left-hand corner, is enveloped by the contour line $w^2/w_0^2 = 0$. Inside this region the cylinder acts as if it has negative overall stiffness and suffers a divergence. So, at sufficiently high velocities it is also possible to have static instability in the third row. The second zone, in the lower right-hand corner, exhibits an entirely different behaviour. In this zone of high flow velocity and large cross-flow directional cylinder displacement the frequency ratio, w^2/w_0^2 , is greater than unity, suggesting the possibility of single degree-of-freedom dynamic instability⁶ at sufficiently high velocities.

In the remaining and major zone ($0 < w^2/w_0^2 < 1$), the cylinder experiences a reduction in its frequency, to an extent related to its displacement and the flow

⁴Paidoussis and Price [79] showed that for a single degree of freedom system dynamic instability occurs when $\partial C_L / \partial \bar{y}$ is negative

⁵The static displacement mentioned in this context is a *predetermined* value inserted into equation 6.2 and is different than the *measured* static displacement discussed in Chapter 4

⁶Inspection of equation 6.2 reveals that w^2/w_0^2 can be greater than unity only when $\partial C_L / \partial y$ is negative. Price and Paidoussis have shown this to be a necessary, but not sufficient, condition for dynamic instability

velocity. It is quite obvious that a third row cylinder will experience a loss of rigidity based on this static analysis.

6.2.2 Lift and Drag Maps for a Second Row Cylinder

The drag and lift coefficient maps and vector plot for a second row cylinder are as shown in Figures 6.22, 6.23 and 6.24 respectively. In general the drag coefficient decreases with cylinder displacement in the upstream and cross-flow directions and increases with displacement in the downstream direction. The lift coefficient is highly sensitive to displacement in the cross-flow direction and shows the tendency to diverge in this direction.

The variation of the lift coefficient versus cross-flow displacement at $\bar{x} = 0$ for a second row cylinder is as shown in Figure 6.25. In a broad range of cylinder displacement the average value of $\partial C_L / \partial \bar{y}$ can be taken as 2.9, a positive and a high value that permits static instability at sufficiently large velocities.

Substituting $\partial C_L / \partial \bar{y} = 2.9$, $\bar{m} = 280$, $f_n = 7$ Hz into equation 6.2, the fluidelastic natural frequency in the cross-flow direction for a flexible cylinder at different velocities can be calculated. The resulting cross-flow frequency variation with flow velocity is as shown in Figure 6.26. At slightly less than 16 m/s, the cylinder totally loses its stiffness and becomes unstable. It is interesting to recall the vibrational behaviour of two flexible cylinders in the second row with $\bar{m} = 280$, $f_n = 7$ Hz and $\delta = 0.014$ as presented in subsection 4.4.1. This configuration, which has identical properties to the above calculated case, becomes unstable at a flow velocity of ≈ 15.3 m/s. The cross-flow frequency variation with flow velocity for this experiment is also plotted in Figure 6.26, for comparison with the calculated results. The difference between the experimental and the calculated critical velocity is only 5%, strongly supporting the existence of static instability in the second row of the $P/d = 2.12$, rotated square array.

6.2.3 Lift and Drag Maps for a First Row Cylinder

In contrast to the behaviour observed in rows 2 and 3, the lift coefficient of a cylinder in row 1 is invariant with displacement unless the cylinder is moved into the vicinity of cylinders 2L and 2R as shown by Figure 6.27. This is in line with the dynamic results showing no loss in the cross-directional rigidity of a first row flexible cylinder. The drag coefficient exhibits a decrease with cylinder displacement in the upstream direction and an increase with displacement in the reverse direction as shown by Figure 6.28. As the cylinder moves upstream of the array, into the free-stream, the drag coefficient should indeed decrease due to the reducing effects of the array. Eventually at a distance sufficiently far upstream, the effects of the array will be minimal on the cylinder and the drag coefficient will approach that of a single cylinder.

Comparing Figure 6.29, the vector plot for a first row cylinder, with those for the second and third rows (Figure 6.21 and 6.14) clearly illustrates the great variation in the flow structure from row to row in the first few upstream rows of the array.

6.2.4 Lift and Drag Maps for Fourth, Fifth and Seventh Row Cylinders

When⁷ the lift coefficient maps (Figures 6.30, 6.31 and 6.32) and the drag coefficient maps (Figures 6.33, 6.34 and 6.35) for fourth, fifth and seventh row cylinders at a flow velocity of $U_\infty = 16.6$ m/s are compared, striking similarities are observed. The lift and drag coefficient maps, as well as the vector plots (Figures 6.36, 6.37 and 6.38) for different rows are nearly identical to each other – both in shape and magnitude. Such a finding implies that, once past the few upstream entrance rows, the fluid forces and hence the flow structure becomes *invariant* with row position inside the array. The results of Price *et al.* in the same array [6], showing that both interstitial velocity and turbulence intensity remain reasonably constant beyond the fourth row lends further support to this finding. This is in sharp contrast to the behaviour observed in the

⁷For this experiment two more rows have been added to the usual eight row array with the objective of protecting the seventh row cylinder from end (exit) effects.

first three entrance rows, where the flow structure exhibits a major variation from row to row

The tendency to diverge in the cross-flow direction is reduced in case of rows 4, 5 and 7. Even though $\partial C'_L/\partial \bar{y}$ is still positive, a necessary condition for divergence, its magnitude is 2.5 - 3 times lower than that recorded in rows 2 and 3. So, loss of stiffness and divergence are delayed to higher velocities, which are outside the limits of the wind tunnel.

The results of the dynamic experiments are in excellent agreement with this observation. No substantial loss of stiffness or divergence was observed for the flexible cylinders in rows 4, 5 or 7. In accordance with row 1, 2 or 3 cylinders, the cylinders in rows 4, 5 and 7 are also *not* prone to damping controlled dynamic instability. As shown in Table 6.2, both $\partial C'_L/\partial y_{1=0}$ ⁸ and $\partial C_D/\partial \bar{x}_{y=0}$ are positive for all rows, barring single degree-of-freedom damping controlled dynamic instability but allowing static instability at sufficiently high flow velocities.

6.3 Effect of the Surrounding Cylinders' Motion

6.3.1 The Effect of Surrounding Cylinder Motion Upon a First Row Cylinder

To determine the effect that motion of the surrounding cylinders have upon the fluid forces acting on a first row cylinder, cylinders 1L, 1R, 2L, 2R and 3 are consecutively displaced in the in- and cross-flow directions. Motion of cylinders 1R and 1L, both in the in- and cross-flow directions, have no effect on the drag or lift coefficients of the first row cylinder, as shown in Figures 6.39 and 6.40⁹. Motion of cylinders 2L and

⁸Table 6.2 shows that static instability is a possibility in the in-flow direction as well as in the cross-flow direction. Equation 6.2, when $\partial C'_L/\partial \bar{y}$ is replaced by $\partial C'_D/\partial \bar{x}$, can be used to calculate the loss of rigidity in the in-flow direction. Setting $f_n = 7$ Hz and $m = 280$, and $\partial C'_D/\partial \bar{x} = 0.69$ (the highest value measured in the array) the critical velocity for in-flow directional static instability is found to be ≈ 32 m/s. As this flow velocity is 50% greater than that available from the wind tunnel, it is not surprising that in-flow static instabilities were not encountered during the experiments.

⁹This observation can be generalised to cover experiments in all rows. For experiments in the rows 1 to 7 the fluid forces acting on the instrumented cylinder are found to be independent of neighbouring cylinder motion in the *same* row.

2R in the cross-flow direction have a limited effect upon the drag coefficient of the instrumented cylinder. But as seen in Figure 6.41 this effect is also marginal. Motion of cylinder 3 in the in-flow direction has a relatively more important effect on the drag coefficient of the instrumented cylinder as shown in Figures 6.42

In general the first row cylinder is insensitive to motion of the surrounding cylinders. Other than a limited effect from the downstream cylinder in its wake, it behaves independently of the motion of the surrounding cylinders. This is in good agreement with vibration (dynamic) test results. In such experiments a flexible cylinder in the first-row always exhibited a substantially lower amplitude vibrational motion relative to the other flexible cylinders and exhibited coupled motion with the flexible cylinder in its wake only at high flow velocities.

6.3.2 The Effect of Surrounding Cylinder Motion Upon a Second Row Cylinder

The cylinders surrounding a second row cylinder can be categorised into three groups as,

- the upstream cylinders (cylinders 1L and 1R),
- the side cylinders (cylinders 2L and 2R),
- the downstream cylinders (cylinders 3L, 3R and 4).

Motion of the side cylinders, have sensibly no effect on the instrumented cylinder. This is most likely due to the considerable distance between the instrumented and the side cylinders.

The displacement of the upstream cylinders (cylinders 1L and 1R) in the in flow direction also has little effect on either the lift and drag coefficients of the row 2 cylinder. In contrast, as shown in Figure 6.43 the cross-flow motion of these cylinders induce a major effect on the fluid forces acting upon the instrumented cylinder. For example, a 0.4 d. displacement of cylinder 1L or 1R in the cross-flow direction changes the lift coefficient from 0 to 1.0 and the drag coefficient from 2.65 to 2.3 for an

instrumented cylinder in the second row. Another major effect is induced by the in-flow directional motion of cylinders 3L, 3R and 4 in the in-flow direction, as shown in Figure 6.44.

Therefore, the second row cylinder is strongly affected by motion of the upstream cylinders and to a lesser, but still important, extent by motion of the downstream cylinders. This finding is in good agreement with two important results obtained during multi-flexible cylinder vibration experiments.

1. When two first row flexible cylinders are located in front of a second row flexible cylinder, the three flexible cylinders experience dynamic instability after a highly coupled vibrational motion. If the two upstream flexible cylinders are replaced by rigid cylinders, the second row flexible cylinder stabilises. Thus, the upstream flexible cylinders have a major effect on the second row flexible cylinder as verified by the force measurements.
2. If two flexible cylinders are located in the second row, at sufficiently high non-dimensional flow velocities static instability occurs. Force measurements verify the critical velocity for static instability obtained from vibration experiments with a difference of 5%. Also, force measurements show that flexible cylinders in the same row do not affect each other. Therefore, due to lack of coupled motion dynamic instability cannot develop.

6.3.3 The Effect of Surrounding Cylinder Motion Upon a Third Row Cylinder

Once again, the surrounding cylinders will be categorised into three groups; the upstream cylinders (cylinder 1, 2L and 2R), side cylinders (3L and 3R) and downstream cylinders (cylinders 4L, 4R and 5). Up to this point the effect of the surrounding cylinders upon the instrumented cylinder was monitored at a flow velocity of 16.6 m/s only. In this row, to observe the effect of the surrounding cylinders at different Reynolds numbers, experiments were also performed at a flow velocity of 8.3 m/s.

The effect of the upstream cylinders is critically important and each will be discussed separately. It should be noted that cylinders 1, 2L and 2R, together with the third row instrumented cylinder, represent the typical four flexible cylinder configuration used in many vibration experiments. Cylinder 1, the upstream cylinder of the four flexible cylinder configuration in the vibration experiments, is the one with the greatest influence on the downstream instrumented cylinder. The motion of this cylinder in the cross-flow direction creates a major change in both the drag and lift coefficients of the third row cylinder – both at $U_\infty = 8.3$ m/s and $U_\infty = 16.6$ m/s, as shown in Figure 6.45. For example, the lift coefficient of the row 3 cylinder varies between 1.7 and -1.7 when cylinder 1 is displaced $\pm 0.5 d$ about its original position. In addition, these figures display the variation of the fluid force coefficient versus displacement at $U_\infty = 8.3$ m/s, normalised¹⁰ with respect to the properties at $U_\infty = 16.6$ m/s. Normalisation is reasonably successful in the $y = \pm 0.25 d$ interval and will be used in the remainder of this subsection.

Based on the above measurements, it is to be expected that a flexible cylinder in row 1 will have a substantial effect on a flexible cylinder in row 3 in a vibration experiment. In fact, the experiment, with two flexible cylinders introduced in subsection 4.2.2, (Figures 4.6 to 4.12) testifies to such an intimate relationship between the motion of flexible cylinders in these locales. The vibrational motion of these cylinders is highly coupled, and coherences as high as 90% are monitored between cylinder vibration signals.

The next echelon of upstream cylinders, 2L and 2R, also incite a significant effect on the forces acting upon the row 3 cylinder. Again, the cross-flow motion of cylinders 2L and 2R induces a greater change in the fluid force coefficients of the row 3 cylinder compared to that induced by the in-flow motion, as shown in Figures 6.46 and 6.47.

Finally¹¹ the effect of displacing the downstream cylinders (4L, 4R and 5) is shown in Figures 6.48 to 6.50; this effect is much less than that induced by the motion of

¹⁰The normalisation technique is identical to that used in subsection 6.2.1

¹¹Side cylinders have no effect as usual.

the upstream cylinders. Therefore, the four flexible cylinder array utilised in the vibration experiments includes the flexible cylinders that will have the major impact on the oscillatory behaviour of a row 3 cylinder—if cascading effects are not included.

Also, in most cases discussed above, *normalisation*¹² has been quite successful in a broad range of static displacements. Thus surrounding cylinder data acquired at a single Reynolds number can be used in theoretical models, if normalised through utilisation of curves like Figures 6.2 to 6.4.

6.3.4 The Effect of Surrounding Cylinder Motion Upon Fourth, Fifth and Seventh Row Cylinders

A general inspection of the data (Figures 4.51 to 4.53), shows that the motion of the surrounding cylinders have a very limited effect upon the fluid forces acting upon fourth, fifth and seventh¹³ row cylinders. This becomes more obvious when the surrounding cylinder effect for a third and fifth row cylinder are compared as shown in Figures 6.54 to 6.56. The differences between the third and fifth¹⁴ row cylinder response to surrounding cylinder motion is indeed striking. The row 5 cylinders' drag and lift coefficients are virtually independent of the surrounding cylinder motion, in strong contrast to what has been observed in row 3. This is in excellent agreement with vibration experiment results presented in Chapter 4. While a set of four flexible cylinders experienced dynamic instability in the entrance rows with highly coupled motion, the same array was quite stable *deep* inside the array. When inside the array, the individual flexible cylinders of the four flexible cylinder configuration acted like

¹²In subsection 6.2.1 it has been determined that the *shape* of the lift and drag contours, especially in the core region, vary very little with Reynolds number, Figures 6.8 to 6.16. Therefore, if the variation of the drag coefficient versus the Reynolds number at $\bar{x} = 0$ and $\bar{y} = 0$ is known (Figure 6.2 to 6.4), then a normalisation factor can be obtained from this data to predict the *magnitude* of the contours at different Reynolds numbers, even if only the contours at a single Reynolds number is available.

Even though, there is only limited justification, the same approach has been used to normalise the effect that surrounding cylinders have upon an instrumented cylinder at different Reynolds numbers. The result, as seen in Figures 6.45 to 6.50, is surprisingly good.

¹³For this experiment two more rows have been added to the usual eight row array.

¹⁴The response of the fifth row cylinder to surrounding cylinder motion is sensibly the same as that experienced by the fourth and seventh row cylinders.

single flexible cylinders, without any interaction with each other.

Therefore, both vibration and force measurements indicate that the instability, in this array is due to a multiple-flexible-cylinder, stiffness-controlled mechanism. Lack of interaction between cylinders *inside* the array prevents coupled motion between cylinders, - a necessary condition for the existence of this type of instability mechanism. Thus, in this array, instability is confined to the entrance rows¹⁵.

¹⁵It should be once again recalled that single-cylinder, damping-controlled mechanism is ineffective in this array

Chapter 7

THEORETICAL MODEL

7.1 Introduction

In Chapter 1, the merits and disadvantages of various theoretical modelling approaches, taken by different researchers, were discussed. A modified quasi-steady model, developed by Price and Paidoussis [74-80], was shown to deliver an excellent understanding of the instability mechanisms, while only requiring a reasonable amount of experimental data. This model, as mentioned in section 1.5, has the capability to predict dynamic instability in both single degree-of-freedom [74, 75] and multiple degree-of-freedom systems [76-80], in contrast to some other models [61, 63, 64, 65]. Using this model, Price and Paidoussis analysed systems with as many as twelve flexible cylinders¹ (twenty-four degrees-of-freedom) [76]. Later, to reduce the magnitude of the computational work, they introduced a so-called “constrained-mode” method, where a specific pattern of motion² is prescribed for the cylinders in the array [77-80]. This helped to reduce the analysis for an array of flexible cylinders to four-degrees of freedom. Comparison of the critical flow velocities obtained using the “long-row” and “constrained mode” solutions, for the same geometry, showed a

¹Later they named this approach, developed for a two-row array, as the “long-row” solution.

²In a recent study [80] the same authors introduced a *variable* phase difference between the motion of adjacent cylinders

good agreement for $10 < \bar{m}\delta < 10^5$ [77].

In the present study, to investigate the effects of various parameters upon the instability threshold of the rotated square array, an approach similar to the "long row" method of Price and Paidoussis is adopted³. The heat exchanger tube bank is modelled by up to four flexible cylinders (eight degrees-of-freedom) in an array of otherwise rigid cylinders. The objective of such an approach is to test the theoretical model against the various multiple-flexible-cylinder vibration experiments discussed in previous chapters. It should be stressed that the four flexible cylinders are *not* thought to be representative of a complete array of flexible cylinders.

7.2 Equations of Motion

Assuming equal mechanical damping in all modes and no mechanical coupling, the equations of motion of the four flexible cylinders, see Figure 7.1(a), can be written as

$$\mathbf{F} = [E]\mathbf{z} + [C]\dot{\mathbf{z}} + [M]\ddot{\mathbf{z}}, \quad (7.1)$$

where;

\mathbf{F} = the fluid force vector;

$\mathbf{z} = \{x_1, y_1, x_2, y_2, x_3, y_3, x_4, y_4\}^T$, the displacement vector;

$[E] = [k]$, the mechanical stiffness matrix with $k_{ij} = 0$ for all terms other than $i = j$, (the diagonal terms, k_{ii} , can be different from each other to introduce differences between the mechanical stiffness of adjacent flexible cylinders);

³The "constrained-mode" method assumes the pattern of cylinder motion to be constant throughout the array. Such an approach, imposes an additional initial restriction to the solution. Therefore in this case, where a maximum of eight degrees-of-freedom is desired, the "long row" type of solution is computationally feasible and is expected to be more accurate.

$[C] = b[I_{8 \times 8}]$, the mechanical damping matrix, b being an equivalent viscous damping coefficient;

$[M] = ml[I_{8 \times 8}]$, the mass matrix, m being the mass per unit length of the cylinder and ℓ the cylinder length.

In the following sections the expressions for the fluid force vector, \mathbf{F} , will be obtained.

7.3 Fluid Forces

As seen in Figure 7.1(b), due to the vibrational motion of a flexible cylinder the resultant velocity vector for cylinder i is at an induced incidence, α_i , to the upstream velocity. Neglecting higher order terms, the angle of induced incidence α_i and the resultant velocity vector U_r can be defined as

$$\alpha_i \simeq \frac{\dot{y}}{U_r}, \quad (7.2)$$

and

$$U_r \simeq U_G - \dot{x}, \quad (7.3)$$

Where U_G is the so-called "reference gap velocity". This velocity can be obtained from continuity to be

$$U_G = U_\infty a, \quad (7.4)$$

where $a = T/(T - 0.5d)$ and U_∞ is the upstream velocity.

Using quasi-steady aerodynamics the fluid forces on cylinder i in the x - and y -directions can be expressed as

$$\begin{aligned} F_{x_i} &= \frac{1}{2} \rho U_r^2 \ell d [\bar{C}_D \cos \alpha_i + \bar{C}_L \sin \alpha_i], \\ F_{y_i} &= \frac{1}{2} \rho U_r^2 \ell d [\bar{C}_L \cos \alpha_i - \bar{C}_D \sin \alpha_i], \end{aligned} \quad (7.5)$$

where \bar{C}_L and \bar{C}_D are lift and drag coefficients, non-dimensionalised with respect to the local approach velocity. However, the measured force coefficients are based on the upstream velocity U_∞ and not U_G . Realising that $U_\infty^2 C_L = U_G^2 C_L$, where C_L is now based on the upstream velocity, enables C_L to be written as

$$\bar{C}_L = C_L/a^2, \quad (7.6)$$

and similarly for the drag coefficient.

By non-dimensionalising the displacement vector with respect to the cylinder diameter and combining equations (7.2) to (7.6), the resulting expression for the fluid forces can then be written as

$$\begin{aligned} F_{x_i} &= \frac{1}{2} \rho U_\infty^2 \ell d [C_D - 2C_D \dot{x}_i d / U_G + C_L \dot{y}_i d / U_G], \\ F_{y_i} &= \frac{1}{2} \rho U_\infty^2 \ell d [C_L - 2C_L \dot{x}_i d / U_G - C_D \dot{y}_i d / U_G], \end{aligned} \quad (7.7)$$

For a flexible cylinder in the first row of the array U_G in equation (7.7) is replaced by U_∞ . In this analysis C_L and C_D are functions of both the Reynolds number⁴ and cylinder displacements. Assuming that they can be expressed in a linear form, C_L and C_D can be written as

$$\begin{aligned} C_{L_i} &= C_{L_{i0}} + \Delta \bar{U} \frac{\partial C_{L_{i0}}}{\partial \bar{U}} + \sum_{k=1}^4 \left(\xi_k \frac{\partial C_{L_i}}{\partial \xi_k} + \eta_k \frac{\partial C_{L_i}}{\partial \eta_k} \right), \\ C_{D_i} &= C_{D_{i0}} + \Delta \bar{U} \frac{\partial C_{D_{i0}}}{\partial \bar{U}} + \sum_{k=1}^4 \left(\xi_k \frac{\partial C_{D_i}}{\partial \xi_k} + \eta_k \frac{\partial C_{D_i}}{\partial \eta_k} \right), \end{aligned} \quad (7.8)$$

where the derivation of the Reynolds number dependent terms, is given in Appendix 3. ξ and η , respectively, are directions parallel and normal to gap flow as shown in Figure 7.2. Next, various time delay terms introduced into this analysis, are discussed

⁴In previous analysis, due to lack of data, the developers of the model neglected the effect of Reynolds number on C_D and C_L

7.4 Time Delays and Apparent Displacements

It is assumed that the fluid forces acting on a flexible cylinder (i.e. cylinder 4) are affected by its own motion and that of its three other neighbouring flexible cylinders (i.e. cylinders 1, 2 and 3). However, the effect induced by the neighbouring flexible cylinders will not be instantaneous and will involve a time delay, τ_i , necessary for the disturbance to traverse the distance between the cylinders. Thus, following Simpson and Flower [91], Price and Paidoussis [76] stated that the apparent displacement of cylinders 1, 2 or 3 in the in-flow (x) direction, as viewed from cylinder 4, will be

$$c_i(t - \tau_i) + \tau_i \dot{c}_i(t - \tau_i) \quad (7.9)$$

where $i = 1$ to 3 in this case⁵. The corresponding displacement of cylinder 4 will be only

$$x_4(t) . \quad (7.10)$$

The exact magnitude of the time delay τ_i , is as yet unknown⁶, but following the work of Price and Paidoussis it can be approximated as

$$\tau_i = S_i / U_G \quad (7.11)$$

where S_i is the distance between the center of cylinder 4 and the three other flexible cylinders. U_G , the so-called "gap velocity", has already been defined by equation (7.4) in section 7.3.

Another effect of cylinder motion is to produce a change in the angle of incidence of the oncoming flow, as seen in Figure 7.1. Assuming \dot{x} and $\dot{y} \ll U_G/d$ and neglecting second order terms, the induced angles of incidence, α_i , for cylinders 1, 2 or 3 are

⁵The analysis will be developed as viewed from cylinder 4 and later generalised

⁶A current research program in McGill is aimed at having a better understanding of this time delay

given by

$$\alpha_i(t - \tau_i) = \dot{y}_i(t - \tau_i)/U_G , \quad (7.12)$$

and for cylinder 4 by

$$\alpha_4(t) = \dot{y}_4(t)/U_G . \quad (7.13)$$

The result of this induced incidence is to reorganize the direction of the interstitial gap velocity and produce apparent displacements of cylinders 1, 2 and 3 as viewed from cylinder 4. The apparent displacements-parallel and normal to the realigned gap velocity, ξ_i and η_i - can be determined from Figure 7.2 as

$$\begin{aligned} \Delta\eta_1 &= -2L\alpha_1, \quad \Delta\xi_1 = 0, \\ \Delta\eta_2 &= -L\alpha_2, \quad \Delta\xi_2 = T\alpha_2, \\ \Delta\eta_3 &= -L\alpha_3, \quad \Delta\xi_3 = -T\alpha_3. \end{aligned} \quad (7.14)$$

In order to express the variables in equation (7.14) in terms of time t instead of $t - \tau_i$, the cylinder motion is assumed to be harmonic, such that

$$x_i(t) = x_{i0}\exp(\lambda t) , y_i(t) = y_{i0} \exp(\lambda t) \quad (7.15)$$

where x_{i0} and y_{i0} are the amplitude of oscillation of cylinder i in the in- and cross-flow directions, and λ is an eigenvalue of the final solution. Therefore, variables at $t - \tau_i$ can be expressed at time t as

$$\begin{aligned} x_i(t - \tau_i) &= x_i(t)\exp(-\tau_i\lambda) = g_i x_i(t) , \\ \dot{x}_i(t - \tau_i) &= g_i \dot{x}_i(t) = g_i \lambda x_i(t) , \end{aligned} \quad (7.16)$$

where $g_i = \exp(-\tau_i\lambda)$.

In addition to above discussed time delay terms, Simpson and Flower [91] determined that another delay term, due to the flow retardation effect around the stag-

nation region of the cylinder is important in arrays where large changes in the fluid force coefficients may occur as a result of small cylinder displacements. This term is especially important as it can lead to fluid-dynamic damping forces which can be either stabilising or destabilising. If the flow retardation is ignored, then the time for a fluid particle to traverse from $x = x_1$ to $R + \Delta R$ is $t = [x_1 - (R + \Delta R)]/U$, where R is the cylinder radius and U the constant flow velocity. But, as the flow approaches the cylinder, it slows down. Therefore, the approach velocity has to be taken as a variable to have a realistic estimate of the time required to traverse the distance from x_1 to $R + \Delta R$. This time can be expressed as

$$t + \Delta t = \int_{R+\Delta R}^{x_1} \frac{1}{U_a} dx, \quad (7.17)$$

where U_a is the variable approach velocity. As a first approximation this velocity can be taken to be $U_a = U(1 - R^2/x^2)$, as that given by potential flow theory⁷ for flow around a single cylinder to yield

$$\Delta t = \frac{R}{2U} \left[\ell n \left(\frac{x_1 - R}{x_1 + R} \right) - \ell n \left(\frac{\Delta R}{2R + \Delta R} \right) \right]. \quad (7.18)$$

Taking x_1 as large compared to ΔR simplifies the above equation further, to the form

$$\Delta t = \frac{R}{2U} \ell n \left[\frac{2R}{\Delta R} \right]. \quad (7.19)$$

A typical value of ΔR is yet unknown, but Simpson and Flower [91] by varying ΔR from $0.1R$ to $0.01R$ calculated $\Delta t = 0.75(d/U)$ and $\Delta t = 1.32(d/U)$, respectively. Therefore an equation of the form

$$\Delta t = \frac{\mu d}{U}, \quad (7.20)$$

where μ is of order unity can be taken to be an acceptable representation of the delay

⁷Price and Paidoussis [76] recognised this not be totally correct, but in view of other assumptions, did not pursue a more exact expression

induced by flow retardation until further understanding of the problem is gained⁸.

Assuming harmonic motion, Price and Paidoussis [76] stated that this flow retardation will induce a y-directional apparent displacement of the cylinder in the form

$$\Delta y = y(t)[1 - \bar{g}] , \quad (7.21)$$

where

$$\bar{g} = \exp(-\lambda\Delta t) . \quad (7.22)$$

The *final* apparent displacement of cylinders 1 to 4, as viewed from cylinder 4 at time t can be obtained by substituting equations (7.12), (7.13) and (7.16) into (7.14) and multiplying the outcome by equation (7.22). The results are given below,

$$\begin{aligned} \xi_1 &= g_\infty g_1 x_1 (1 + \tau_1 \lambda), & \eta_1 &= g_\infty g_1 y_1 (1 - 2L\lambda/U_\infty), \\ \xi_2 &= g_G g_2 [x_2 (1 + \tau_2 \lambda) + T\lambda y_2 / U_G], & \eta_2 &= g_G g_2 y_2 (1 - \lambda L / U_G), \\ \xi_3 &= g_G g_3 [x_3 (1 + \tau_3 \lambda) - T\lambda y_3 / U_G], & \eta_3 &= g_G g_3 y_3 (1 - \lambda L / U_G), \\ \xi_4 &= g_G x_4, & \eta_4 &= g_G y_4. \end{aligned} \quad (7.23)$$

Based on the apparent displacements shown in Figures 7.2 and using the procedure detailed above, the final apparent displacements, as viewed from the perspective of all *other* cylinders can also be determined. Thus the apparent displacements of cylinders 1, 2, 3 and 4, as viewed from cylinder 1, at time t are determined to be

$$\begin{aligned} \xi_1 &= g_\infty x_1, & \eta_1 &= g_\infty y_1, \\ \xi_2 &= g_G g_2 x_2 (1 + \lambda\tau_2) + T\lambda y_1 / U_\infty, & \eta_2 &= g_G g_2 y_2 + L\lambda y_1 / U_\infty, \\ \xi_3 &= g_G g_3 x_3 (1 + \lambda\tau_3) - T\lambda y_1 / U_\infty, & \eta_3 &= g_G g_3 y_3 + L\lambda y_1 / U_\infty, \\ \xi_4 &= g_G g_4 x_4 (1 + \lambda\tau_4), & \eta_4 &= g_G g_4 y_4 + 2L\lambda y_1 / U_\infty. \end{aligned} \quad (7.24)$$

Similarly, the apparent displacements of cylinders 1, 2, 3 and 4, as viewed from

⁸Price, Paidoussis and co-workers are presently pursuing an involved experimental study to have a deeper understanding of the time delays involved

cylinder 2, at time t are

$$\begin{aligned}
 \xi_1 &= g_\infty g_1 x_1 (1 + \lambda \tau_1) + g_\infty g_1 T \lambda y_1 / U_\infty, & \eta_1 &= g_\infty g_1 y_1 - g_\infty g_1 L \lambda y_1 / U_\infty, \\
 \xi_2 &= g_G x_2, & \eta_2 &= g_G y_2, \\
 \xi_3 &= g_G g_3 x_3 (1 + \lambda \tau_3) + g_G g_3 T \lambda y_3 / U_G, & \eta_3 &= g_G g_3 y_3, \\
 \xi_4 &= g_G g_4 x_4 (1 + \lambda \tau_4) + g_G T \lambda y_2 / U_G, & \eta_4 &= g_G g_4 y_4 + g_G L \lambda y_2 / U_G.
 \end{aligned} \tag{7.25}$$

Finally, the apparent displacements of cylinders 1,2,3 and 4 as viewed from cylinder 3, at time t are,

$$\begin{aligned}
 \xi_1 &= g_\infty g_1 x_1 (1 + \lambda \tau_1) - g_\infty g_1 T \lambda y_1 / U_\infty, & \eta_1 &= g_\infty g_1 y_1 - g_\infty g_1 L \lambda y_1 / U_\infty \\
 \xi_2 &= g_G g_2 x_2 (1 + \lambda \tau_2) - g_G g_2 T \lambda y_2 / U_G, & \eta_2 &= g_G g_2 y_2, \\
 \xi_3 &= g_G x_3 & \eta_3 &= g_G y_3, \\
 \xi_4 &= g_G g_4 x_4 (1 + \lambda \tau_4) - g_G T \lambda y_3 / U_G, & \eta_4 &= g_G g_4 y_4 + g_G L \lambda y_3 / U_G.
 \end{aligned} \tag{7.26}$$

Before substituting the apparent displacements given by equations (7.23) to (7.26), into equation (7.8), it is possible to introduce certain simplifications arising from geometric symmetry of the present array. The force measurements discussed in chapter 6 have substantiated the validity of these simplifications, shown below

$$\begin{aligned}
 C_{L_{10}} &= C_{L_{20}} = C_{L_{30}} = C_{L_{40}} = 0, \\
 C_{D_2} &= C_{D_3}, \\
 \frac{\partial C_{L_4}}{\partial \xi_4} &= \frac{\partial C_{L_3}}{\partial \xi_3} = \frac{\partial C_{L_2}}{\partial \xi_2} = \frac{\partial C_{L_1}}{\partial \xi_1} = 0, \\
 \frac{\partial C_{D_4}}{\partial \eta_4} &= \frac{\partial C_{D_3}}{\partial \eta_3} = \frac{\partial C_{D_2}}{\partial \eta_2} = \frac{\partial C_{D_1}}{\partial \eta_1} = 0, \\
 \frac{\partial C_{D_4}}{\partial \xi_2} &= \frac{\partial C_{D_4}}{\partial \xi_3} \quad \frac{\partial C_{D_4}}{\partial \eta_2} = -\frac{\partial C_{D_4}}{\partial \eta_3}, \\
 \frac{\partial C_{L_4}}{\partial \xi_2} &= \frac{\partial C_{L_4}}{\partial \xi_3} \quad \frac{\partial C_{L_4}}{\partial \eta_2} = \frac{\partial C_{L_4}}{\partial \eta_3}, \\
 \frac{\partial C_{L_4}}{\partial \xi_1} &= \frac{\partial C_{D_4}}{\partial \eta_1} = 0, \\
 \tau_2 &= \tau_3.
 \end{aligned} \tag{7.27}$$

By substituting equations (7.23) to (7.27) into equation (7.8) the lift and drag coefficients for each flexible cylinder as a function of the Reynolds number, its own motion and the motion of the other flexible cylinders can be obtained. The results are presented in Appendix 4. Once the lift and drag coefficients are determined, they in turn can be substituted into equation (7.7) to obtain the fluid forces acting on each cylinder in the x- and y-directions. The complete set of fluid forces acting on the four flexible cylinders can be written as

$$\mathbf{F} = [K]\mathbf{z} + [B]\dot{\mathbf{z}} \quad (7.28)$$

where

$\mathbf{z} = \{x_1, y_1, x_2, y_2, x_3, y_3, x_4, y_4\}^T$, the displacement vector;

$[K]$ = the fluid-stiffness matrix;

$[B]$ = the fluid-damping matrix.

Finally, equations (7.1) and (7.28) are combined to form the complete equations of motion as

$$[M]\ddot{\mathbf{z}} + \{[C] - [B]\}\dot{\mathbf{z}} + \{[E] - [K]\}\mathbf{z} = 0 . \quad (7.29)$$

Substituting the expanded form of the matrices

$$\begin{aligned} [M] &= m\ell[I_{8 \times 8}] , \\ [C] &= \frac{m\ell w_o \delta}{\pi} [I_{8 \times 8}] , \\ [E] &= w_o^2 m\ell [h] , \\ [B] &= \frac{\rho d \ell U}{2a} [B] , \\ [K] &= \frac{\rho \ell U^2}{2} [K] , \end{aligned} \quad (7.30)$$

into equation (7.29) yields

$$m\ell[I_{8 \times 8}]\ddot{\mathbf{z}} + \left\{ \frac{m\ell\omega_o\delta}{\pi}[I_{8 \times 8}] - \frac{\rho d\ell U}{2a}[\bar{B}] \right\} \dot{\mathbf{z}} + \left\{ \omega_o^2 m\ell[h] - \frac{\rho\ell U^2}{2}[\bar{K}] \right\} \mathbf{z} = 0. \quad (7.31)$$

Introducing a non-dimensional displacement vector, $\bar{\mathbf{z}} = \frac{\mathbf{z}}{d}$, and a non-dimensional time, $\bar{t} = \omega_o t$, into the equation of motion leads to

$$[I_{8 \times 8}]\ddot{\bar{\mathbf{z}}} + \left\{ \frac{\delta}{\pi}[I_{8 \times 8}] - \frac{\bar{U}}{2\bar{m}a}[\bar{B}] \right\} \dot{\bar{\mathbf{z}}} + \left\{ [h] - \frac{\bar{U}^2}{2\bar{m}}[\bar{K}] \right\} \bar{\mathbf{z}} = 0$$

where $\bar{U} = \frac{U}{\omega_o d}$ and $\bar{m} = \frac{m}{\rho d^2}$. (7.32)

The individual terms in $[\bar{K}]$ and $[\bar{B}]$ are as given in Appendix 5 and 6.

In this analysis a solution of the form $\bar{\mathbf{z}} = \bar{\mathbf{z}}_o \exp(\lambda t)$ is assumed, where λ is a complex eigenvalue. At the dynamic instability boundary λ will be purely imaginary, indicating zero damping. The eigenvalues and eigenvectors are obtained through standard numerical procedures.

Chapter 8

THEORETICAL RESULTS

8.1 Multiple-Flexible Cylinder Fluidelastic Instability

8.1.1 Four Flexible Cylinders and The Instability Threshold

The stability of a $P/d = 2.12$ rotated square array housing a four-flexible-cylinder configuration was investigated using the fluid force coefficients and their variation with displacement, presented in Appendix 1. To compare with the experimental results discussed in section 4.2, the flexible cylinder configuration was located in different rows of the array. Figure 8.1 shows the variation of the non-dimensional critical velocity, $U_c/f_n d$, versus the dimensionless mass, \bar{m} , for four flexible cylinder configurations with the upstream of the four cylinders located in each of the first five rows of the array. The damping parameter, δ , was kept at 0.014 and no frequency detuning between the cylinders was introduced. The results of Figure 8.1 show that the four-flexible-cylinder configuration has the lowest instability threshold when its upstream cylinder is in the second row¹. Then configurations with their upstream

¹An exception to this is $\bar{m} < 75$, where the four flexible-cylinder configuration with its upstream cylinder in the third row has the lowest critical velocity.

cylinders in rows 1, 3, 4 and 5, respectively, have increasing instability thresholds. This *trend* is in agreement with the experimental results of section 4.2.

Experimental results of Chapter 4 showed that, an equation of the form

$$U_c/f_n d \propto (\bar{m})^\beta \dots \delta = \text{constant} \quad (8.1)$$

was not applicable for the $P/d = 2.12$, rotated square array. Even, in a relatively narrow range of dimensionless mass, $195 \leq \bar{m} \leq 980$, the exponent in equation (8.1) β , exhibited a substantial variation from 0.38 to 1.55. For the same configuration and the same range of dimensionless mass, the theoretical calculations resulted in a β value varying between 0.19 and 0.27. This low value leads to the conclusion that the theoretical model utilised, *fails to predict* the experimentally determined strong dependence of critical velocity upon the dimensionless mass.

Also in Chapter 4, it was experimentally determined that the critical velocity is only *weakly* related to the initial damping of the cylinder, δ . For $0.014 < \delta < 0.25$, the relationship between the two variables was proposed to be in the form

$$U_c/f_n d \propto \delta^\alpha \dots \bar{m} = \text{constant} \quad (8.2)$$

where $\alpha = 0.06$ and 0.07 , respectively for $\bar{m} = 280$ and 490 . Figure 8.2 shows the theoretically determined effect of initial cylinder damping upon the critical velocity for $\bar{m} = 75, 280$ and 1500 . For $0.014 < \delta < 0.35$, the theoretically determined relationship between critical velocity and damping can be approximated by equation (8.2), where α varies between 0.10 and 0.39 , depending upon the value of the dimensionless mass. Therefore, the theoretical model predicts a greater dependence of critical velocity upon the cylinder damping than the experimentally determined one.

Again in Chapter 4, for a four-flexible cylinder configuration ($\bar{m} = 280$ and $\delta = 0.014$), the variation of the stability threshold with position in the array had been

discussed. Figure 8.3 compares both the experimental and theoretical² results for the variation of the nondimensional critical velocity with cylinder position in the array at $\bar{m} = 280$ and $\delta = 0.014$. Both the experimental and theoretical curves are quite similar in *shape*. In both cases the entrance rows are found to be the least stable, whereas the rows deeper in the array, are found to be more stable due to lack of coupled motion between flexible cylinders. Figure 8.3 also shows a major shortcoming of the model, which is a difference of an order of magnitude between the experimental and theoretical critical velocities. Therefore, the present model, at least for the rotated square array, is more likely to deliver a general physical understanding of fluidelastic instability rather than predicting instability threshold with precision³.

8.1.2 Sensitivity of Four Flexible Cylinder Motion to “Unsteady Effects”

The “unsteady effects” included in this model are: the time delay/flow retardation effect, accounted for by equation (7.20); the delay between the motion of cylinders, accounted for by equation (7.11); the wake inclination effect, accounted for by equations (7.12) and (7.13).

In a recent study [79] Paidoussis and Price showed that the time delay factor, μ , defined by equation (7.20) has a major effect in the stability behaviour of single flexible cylinder models, especially in the lower $m\delta$ range where the fluid-damping controlled instability mechanism attains importance. To assess its importance in this array, the time delay factor, μ , has been varied between 3.0 and 0.0. As shown in Figure 8.4, for $\bar{m} > 7400$ ($\bar{m}\delta > 104$), the value of μ has no effect on the non-dimensional critical velocity. However, for $\bar{m} < 740$ ($\bar{m}\delta < 10$), the effect of changing μ induces a change in the non-dimensional critical velocity. For $\bar{m} = 74$ ($\bar{m}\delta = 1$), at $\mu = 0$ and $\mu = 3$ the non-dimensional critical velocities are approximately 50% less and 75% greater, respectively, than the value at $\mu = 1$. Therefore, the fluid-damping terms generated

²These results can be obtained from Figure 8.1 at $\bar{m} = 280$ for each position in the array

³There is, as yet, no such model

by μ are stabilising⁴, rather than destabilising in the region of $\bar{m} < 740$ ($\bar{m}\delta < 10$). This is in general agreement with the results of Price and Paidoussis [76] obtained through their "long row" solution for a different array.

The effect of the time delay term, τ_1 , and the wake inclination terms, α_1 and α_4 , are determined to be negligible in this array. Setting these terms equal to zero generates no sensible change in the instability threshold.

Therefore the insensitivity of the critical flow velocity to both time delays Δt and τ_1 , defined by equations (7.20) (7.11), and to the wake inclination terms, α_1 and α_4 , defined by equations (7.12) and (7.13) allows major simplifications in the theoretical model adopted.

The effect of the variation of drag coefficient with Reynolds number⁵, has been included in the model as per equation (7.8). Numerical investigations revealed that inclusion of this factor has sensibly no effect⁶ on the non-dimensional critical velocity. This result is not surprising when it is noted that the Reynolds number dependent terms are a part of the fluid damping matrix⁷ which has practically no contribution to the instability mechanism prevailing in this array. Omission of the Reynolds number dependent terms introduces further simplification into the model.

8.1.3 Sensitivity of Four Flexible Cylinder Motion to Fluid Force Coefficients

To assess the sensitivity of the instability threshold to variations in the fluid force coefficients, a series of calculations have been performed with modified coefficients, specifically, reduced by 50% and increased by 50%. Tables 8.1 and 8.2 summarize the critical velocities obtained with increased and decreased fluid coefficients as well

⁴This is not surprising in the light of the fluid force coefficients presented in Chapter 6. For instrumented cylinders in rows 2, 3, 4, 5 and 7, $\partial C_L/\partial \bar{y}$ and $\partial C_D/\partial \bar{x}$ are both *positive*, advocating stabilising fluid-damping terms

⁵This approach only considers the change in the value of the drag coefficient of each flexible cylinder with R_c . In Chapter 6 it is shown that the variation of fluid force coefficients with respect to displacement is only weakly dependent upon velocity and such an effect is neglected in this model.

⁶For $\bar{m} \geq 750$ the critical velocity is unchanged, however, for $m < 350$ a change less than 5% has been noted.

⁷Appendix 6

as with the original force coefficients. As expected, reducing the force coefficients generates an increase in the critical velocity and vice versa. In all cases the change in the critical velocity is less than the change in the fluid coefficients. This signifies the critical velocity for this array not to be over sensitive to the small changes in the fluid force coefficients.

8.1.4 Multiple Instability Boundaries

Multiple instability boundaries at low $\bar{m}\delta$ values have been encountered in various theoretical models [63-65] and [74-80] as well as in a recent experimental study [59]. Inspection of Figure 8.1, for the case of upstream cylinder of the four-flexible-cylinder configuration located in rows 3 and 4, exhibits a sudden drop in the critical non-dimensional velocity for $\bar{m} < 300$ that could possibly be due to existence of multiple instability boundaries. Figure 8.5 summarises a "numerical search" for such multiple instability boundaries at low values of \bar{m} . It is seen that for $\bar{m} = 1$ and 15 as the velocity is decreased, the eigenvalue of the solution changes sign at $\bar{U} \simeq 2.3$ and the array becomes stable. If the eigenvalue is monitored at lower non-dimensional velocities it is observed that at $\bar{U} \simeq 0.2$ the eigenvalue changes its sign once more and the system becomes unstable again. Eventually further reduction of U restabilises the system. A similar display of instability bands has also been detected for a four flexible cylinder configuration with its upstream cylinder in row 4.

Existence of multiple instability band for this array is, somewhat unexpected, as the damping controlled mechanism is stabilising rather than destabilising⁸. As suggested by Price *et al.* [80] even at such low $\bar{m}\delta$ values, the fluid-stiffness controlled mechanism can be dominant enough to generate instability bands through the effect of fluid stiffness terms oscillating harmonically.

The results presented in this section strongly suggest that, by far, the dominant instability mechanism in a rotated square array with $P/d = 2.12$ is the multiple-

⁸Even though stabilising, it is still oscillatory

flexible-cylinder, fluid-stiffness controlled one. As shown by the magnitude of the non-dimensional critical velocity for instability to occur, the fluid-stiffness effects are most dominant in the first few upstream rows relative to downstream positions. Time delay terms, associated with flow retardation and adjacent cylinder response lag, have been found to have no effect on the stability threshold of the array and can be neglected.

8.1.5 Three Flexible Cylinders and The Instability Threshold

Theoretical results for the stability threshold of a three- and four-flexible-cylinder configuration are compared in Figure 8.6. The three-flexible cylinder configuration has cylinders in positions 2L, 2R and 3, whereas the four-flexible-cylinder configuration has cylinders in positions 1, 2L, 2R and 3. The only difference between the two configurations is an additional flexible cylinder in the row 1. As expected the three-cylinder configuration is more stable in the range $75 \leq \bar{m} \leq 750,000$ ($\delta = 0.014$) when the three-flexible-cylinder configuration is placed deeper in the array, the stability threshold increases further, as shown in Figure 8.7. For example, the non-dimensional critical velocity for a configuration with upstream cylinders in row 5 is approximately two orders of magnitude higher than that of the same configuration with upstream cylinders in row 1.

8.2 The Effect of Frequency detuning Upon the Instability Threshold

8.2.1 The Effect of the Mass-Damping Parameter

In Chapter 4 it was shown that frequency detuning between the cylinders of a $P/d = 2.12$ rotated square array incites substantial variations in the instability threshold.

In a numerical study, frequency detuning can be realised by introducing differences between the diagonal terms of the mechanical stiffness matrix defined by equation (7.1).

To enable comparison with experimental results, a four flexible cylinder configuration is located in the three upstream rows of the array (cylinders 1, 2L, 2R and 3). The initial natural frequency of the row 3 cylinder is kept constant, while that of the other cylinders, collectively, are varied.

Typical results, for $\bar{m}\delta^9 = 3.92$ and $\bar{m}\delta = 10500$, are as shown in Figures 8.8 and Figure 8.9. A quick inspection of these figures suggests that effect of frequency detuning upon the non-dimensional critical velocity is not only a function of $m\delta$, but of δ and \bar{m} separately. This observation is especially pronounced in the positive detuning region ($f_{1,2L,2R}/f_3 > 1$).

The numerical results for $\bar{m} = 280$ and $\delta = 0.014$ shown by a solid line in Figure 8.8 can be compared with Figure 4.58 displaying the experimental results for the same conditions. Both results¹⁰, reproduced in Figure 8.10, shows a general agreement in the region $f_{1,2L,2R}/f_3 > 1$. However, for $0.8 < f_{1,2L,2R}/f_3$, the numerical solution exhibits a sharp increase in the instability threshold, in contrast to the experimental results. Finally for $f_{1,2L,2R}/f_3 < 0.8$ both experimental and numerical trends are the same, but a magnitude difference still exist, probably due to the sharp increase experienced in the previous zone. In general the agreement between experimental and numerical detuning results are not satisfactory.

8.2.2 The Effect of Cylinder Damping

In this section the effect of detuning on the non-dimensional critical velocity at three damping values, $-\delta = 0.14, 0.014$ and 0.0014 -, is presented. The other initial

⁹In Chapter 4, it has been shown that lumping \bar{m} and δ together in form of a single dimensionless parameter is not applicable in this array. So it should be stressed that, this approach is adopted here just to show that it does not give satisfactory results.

¹⁰The physical understanding attained from this curve has been discussed in Chapter 4 and will not be repeated in this context.

conditions are identical to those of the previous subsection. As observed both in Figure 8.11 ($\bar{m} = 280$) and Figure 8.12 ($\bar{m} = 750000$) changing damping by two-orders of magnitude has no significant effect on the non-dimensional critical velocity in the positive detuning region, $f_{1,2L,2R}/f_3 > 1$. Whereas in the negative detuning region, $f_{1,2L,2R}/f_3 < 1$, especially for the higher dimensionless mass, $\bar{m} = 750000$, a substantial effect of damping on the stability threshold is observed. In general, it can be proposed that, in the operational range of actual heat exchangers¹¹ the instability threshold of a detuned rotated square array with $P/d = 2.12$ is weakly related to the initial damping of the cylinders, especially in the positive detuning region. A similar insensitivity of instability threshold of detuned arrays to initial cylinder damping has also been reported by Price et. al. [77].

8.2.3 The Effect of Dimensionless-Cylinder Mass

Again, for a four-flexible-cylinder configuration, located in the three upstream rows of the array, the initial natural frequency of the row 3 cylinder is kept constant while that of the others is varied. Figures 8.13 to 8.15 very clearly show that, at all damping values, changing the dimensionless cylinder mass has a large effect on the non-dimensional critical velocity across the whole detuning range. This result is not surprising in light of the experimental findings presented in Chapter 4, showing the dominant effect of cylinder mass upon the instability threshold. Therefore the numerical results verify the critical velocity of this array to be more sensitive to dimensionless mass than damping.

8.2.4 The Effect of Flexible Cylinder Position

In Chapter 4, it was shown experimentally that the effect of frequency detuning, on the instability threshold decreases if a flexible cylinder configuration is located in the

¹¹A damping value of 0.0014 is an order of magnitude lower and a dimensionless mass of 750000 is at least two orders of magnitude higher than that of an actual heat-exchanger. Such extreme values are used to assess the effect of these variables in the broadest range possible

inner rows of the array rather than the upstream rows. Dynamic tests have revealed this to be due to a major deficit of coupled motion inside the array.

In this context a four-flexible-cylinder configuration ($\bar{n} = 280, \delta = 0.011$) is numerically first located in positions 1, 2L, 2R and 3 and then in positions 4, 5L, 5R and 6. The numerical results, shown in Figure 8.16, are in agreement with vibration experiment results. Inside the array the effect of detuning, especially in the negative detuning range, is less relative to the upstream rows.

Chapter 9

A GENERAL DISCUSSION & CONCLUSIONS

In this thesis, the flow-induced vibrational behaviour of a rotated-square array, with $P/d = 2.12$, was investigated both experimentally and theoretically to introduce further insight into the nature of fluidelastic instability mechanisms.

The experimental studies were comprised of extensive dynamic (vibration) and static (fluid force) measurements, whereas the theoretical studies focused on introducing limited changes into an existing quasi-steady model and applying it for comparison with experimental results.

9.1 Single and Two Flexible Cylinders

In the dynamic experiments, a *single flexible cylinder* retained its stability throughout the entire non-dimensional velocity range, in agreement with previous results [6]. When the fluid forces acting on such a cylinder, both at equilibrium and displaced positions, were measured and introduced into the quasi-steady model, the stability of a single flexible cylinder was also verified theoretically. Therefore, it was firmly concluded that, a single-degree-of-freedom¹, galloping type instability mechanism, is incapable of inducing dynamic instability in this array.

¹In all experiments, the in- and cross-flow vibrational motion of a single flexible cylinder was found to be uncoupled

Dynamic experiments *with two flexible cylinders*, although stable for all experimental conditions², revealed that the vibrational motion of one cylinder could affect and synchronise the motion of the other cylinder through fluidelastic coupling. The strength of such interaction between cylinders was determined to be a function of position in the array and relative location of the flexible cylinders with respect to each other. The highest level of coherence was measured between two flexible cylinders, arranged in tandem in the upstream rows of the array. When positioned in rows deeper inside the array, or with a different relative position, the coupling between the motion of the flexible cylinders reduced dramatically and each behaved as a single flexible cylinder. In support of these observations, the time averaged fluid force measurements revealed that displacing the cylinders in the entrance rows sharply affected the fluid forces acting on the surrounding cylinders, especially when the cylinders were placed in tandem. Deeper inside the array, displacement of cylinders had practically no effect on the fluid forces of neighbouring cylinders.

9.2 Three and Four Flexible Cylinders

Dynamic experiments with *three and four flexible cylinder* configurations, first produced a highly coupled and synchronised motion, and eventually *fluidelastic instability*. This result has a great importance, in the sense that arrays *stable* when housing a single flexible cylinder can become fluidelastically *unstable* in the presence of multiple flexible cylinders. For the first time, this furnishes experimental evidence, for the existence of a multiple-flexible-cylinder type fluidelastic instability mechanism, necessitating fluidelastically coupled motion between adjacent cylinders. The instability threshold for this mechanism was found to be related to the number of flexible cylinders. For the same mechanical properties, four flexible cylinders became unstable at a 40% lower non-dimensional velocity than that of three flexible cylinders.

When the four flexible cylinder configuration was moved deeper into the array,

²Static instability excluded

the instability threshold increased in association with reduced fluidelastic coupling. Beyond the fourth row, instability would not develop within the velocity range of the wind tunnel. Also the motion of the flexible cylinders were totally independent of the other, each behaving as a single flexible cylinder.

Force measurements supplied similar results. Displacement of cylinders located in the three upstream rows affected the fluid forces acting on adjacent cylinders to a significant extent. Especially the motion of upstream cylinders in the first and second rows, induced major changes in the flow field around the third row cylinder and the fluid forces acting on it. In contrast, the motion of downstream cylinders was determined to have no significant effect on the upstream cylinders fluid forces. Fluid forces acting on cylinders in the fourth to seventh rows were relatively insensitive to the displacement of neighbouring cylinders. Both dynamic and static results detected two major regions in the array.

1. *The upstream rows* of the array, where flexible cylinders were capable of generating major changes in the flow field, through their vibrational motion and so to affecting the magnitude and direction of fluid forces acting upon neighbouring flexible cylinders. At sufficiently high flow velocities, the motion of the cylinders was synchronised through strong fluidelastic coupling, which subsequently, induced violent unstable motion. The instability threshold for this multiple-flexible cylinder, stiffness-controlled instability mechanism requiring coupled motion, was experimentally determined to be a strong function of the number of flexible cylinders and the extent of coupling between the cylinders.
2. *The inner-rows* of the array, where flexible cylinders were sensibly unaffected by each others motion and acted as single isolated cylinders. Thus, a multiple-flexible-cylinder type instability could not occur in this region. Similarly, the single degree-of-freedom fluid-damping controlled instability mechanism by itself, as shown in the present and previous studies, was insufficient to induce fluidelastic instability in this region of the array. Therefore stability prevailed

in the inner rows of the rotated square array with $P/d = 2.12$

Another interesting result, obtained from the static measurements, was the variation of the fluid force coefficients of cylinders in the array with the Reynolds number. In a similar range ($6 \times 10^3 < Re < 4.5 \times 10^4$) the drag coefficient of a *single cylinder* was determined to be virtually constant, $C_D = 1.2 \pm 5\%$. Therefore, the variation of the fluid force coefficients for the cylinders in the array *is induced by the presence of the array itself*. In general, the fluid forces were found to be functions of both position and Reynolds number.

The theoretical results for fluidelastic instability were in qualitative agreement with the experimental ones. Three and four flexible cylinder configurations became unstable, while single and two flexible cylinder configurations retained their stability. The major shortcoming of the theoretical model was an order of magnitude difference between the experimental and theoretical critical velocities. Therefore, the present theoretical model, is more likely to deliver a general physical understanding of instability mechanisms rather than predicting the instability threshold of the present array with precision. Even with such a shortcoming, the theoretical model delivered important results, in agreement with the dynamic and static experiments.

1. The instability threshold for a three and a four flexible cylinder configuration increased sharply when the cylinders were located in the inner rows of the array. For example, the instability threshold of a four flexible cylinder configuration³ was an order-of-magnitude lower when located at 1, 2R, 2L, 3 rather than at 5, 6R, 2L, 3.
2. The variation of the fluid force coefficients with Reynolds number, discussed above, was included in the theoretical model. In fact, this was one of the main changes to the quasi-steady model, already developed by Price and Paidoussis.

³The variation in the instability threshold of a *three flexible cylinder* configuration with respect to position was even greater. The critical velocity difference between the positions 1, 2R, 2L and 5, 6R, 6L was *two orders-of-magnitude*.

Considering such an effect, introduced additional fluid-damping terms into the theoretical model. These additional terms had no sensible effect on the numerically determined critical velocity. This is in excellent agreement with the experimental results which showed a single-degree-of-freedom, damping-controlled mechanism to be ineffective in this array. It should be stressed that even though unimportant in this case, Reynolds number dependent terms can be very important in arrays where a single degree-of-freedom, damping-controlled mechanism is the main contributor to dynamic instability.

3. In a recent publication [79], Paidoussis and Price showed that if the time delay factor, μ , was neglected (i.e. $\mu = 0$), then the destabilising/stabilising fluid-damping terms would be suppressed. In the present study, solutions with $\mu = 0$ resulted in a small change in the critical velocity, once again substantiating the unimportance of the fluid-damping controlled mechanism in this array.

9.3 Applicability of a "Connors' type" Instability Criterion

Dynamic results with multiple-flexible-cylinders showed that a "Connor's type" instability criterion,

$$\bar{U}_c = K(\bar{m}\delta)^\beta$$

or a modified form of it,

$$\bar{U}_c = K\bar{m}^{\alpha_1}\delta^{\alpha_2}$$

could not be applicable in the rotated square array, with $P/d = 2.12$.

1. α_1 , the exponent of dimensionless mass, was determined to be a function of dimensionless mass itself. The α_1 values at $\bar{m} = 195$ and 980 was 0.38 and 1.55 , respectively. It should be appreciated that this substantial variation was recorded in a limited range of dimensionless mass and can be expected to be

more pronounced in a wider range.

2. A value of α_1 , as high as 1.55, was recorded for the first time. There is a likelihood that such a *strong* dependence of critical velocity upon cylinder mass is a generic property of arrays for which fluidelastic instability is induced by the multiple-flexible cylinder, stiffness controlled mechanism.
3. The instability threshold for a multiple-flexible-cylinder configuration was determined to be only *marginally* affected by changes in the mechanical damping of the cylinders. In a relatively broad range of mechanical damping, ($0.0135 < \delta < 0.25$), the value of α_2 was determined to be only 0.06. Such a *low* α_2 value is being reported for the first time and may well be a characteristic of arrays where multiple-flexible cylinder type instability mechanism is dominant.

In the light of the above findings it is obvious that neither equation (1.3) nor equation (1.5) can be used to predict the instability threshold of this array. Whether this conclusion can be generalised for all other arrays, in which the instability is induced by a multiple-flexible cylinder, stiffness-controlled mechanism, is yet to be determined through further studies..

9.4 Frequency Detuning

In actual heat exchangers, variations between the natural frequencies of tubes, termed as *frequency detuning* or simply *detuning*, is a common phenomenon. The information available on the effects of this phenomenon is inconclusive and in some cases contradictory. Therefore an extensive experimental work was undertaken to shed further insight into the instability behaviour of detuned arrays.

Various forms of frequency variation were introduced between the cylinders of a four-flexible cylinder configuration and some important results are itemised below.

1. Cylinders with different natural frequencies, are capable of imposing on each other, different modes of vibrations through fluid coupling at flow velocities

which can be as low as 50% of the critical velocity. To emphasize the strong interaction between the vibrational motion of such cylinders, it should be mentioned that in some experiments as many as eleven frequencies common to at least two cylinders were monitored. In the vicinity of the critical velocity, the effect of fluid coupling was determined to be domineering enough to synchronise the motion of all the cylinders at a single frequency (and possibly its harmonics). Therefore, some of the cylinders – in many cases *all* – completely “lost” or “forgot” their original natural frequencies.

2. Such an exchange of frequencies between detuned cylinders was *reciprocal*. While, through fluidelastic coupling, higher-frequency cylinders imposed greater rigidity on lower-frequency cylinders, the lower-frequency cylinders in return, inflicted lower frequencies on high-frequency cylinders. This mutual exchange of frequencies altered the *fluidelastic natural frequency* of all the cylinders in such a fashion that lower frequency cylinders acted as if they were tuned to a *higher initial natural frequency* than they actually were and higher frequency cylinders responded as if they were tuned to a *lower initial natural frequency*.
3. Therefore, if one or more flexible cylinders of an array are tuned to a *higher-frequency* than the others, then the whole array will become unstable at a critical velocity, *greater* than that experienced when all the cylinders were at the same frequency. Similarly, if one or more flexible cylinders of an array are tuned to a *lower-frequency* than the others, then the whole array will become unstable at a critical velocity, *less* than that experienced when all the cylinders were at the same frequency. This simple criterion can be expected to be applicable for all arrays in which the multiple flexible-cylinder type instability mechanism is the dominant one.

The quantitative agreement between the experimental and theoretical detuning results was unsatisfactory, especially in the negative detuning region⁴. Still, the theo-

⁴As defined in section 4.3

retical results showed the critical velocity of detuned arrays to be a strong function of dimensionless mass and a weak function of damping. Even though the dimensionless mass had been determined to be the variable with the greatest effect on the critical velocity of non-detuned arrays, due to set-up limitations, the magnitude of its effect in *detuned* arrays could not be assessed experimentally. This, still remains, to be verified through further experiments.

9.5 Static Displacement and Instability.

In most of the dynamic experiments with multiple flexible-cylinders, a fluidelastic loss of stiffness in the cross-flow direction had been observed in the second and third rows. Special dynamic experiments with two flexible cylinders in the second row determined;

- a loss of cross-flow stiffness, that in some cases, could be as much as 50%,
- a major reduction in the cross-flow vibrational motion, correlated to the loss of stiffness,
- a static displacement of the cylinder in the cross-flow direction increasing with flow velocity and finally taking the form of a "buckling" type motion.

The above give support to the possibility of a static instability (divergence) in this array.

On the other hand, static experiments found fluid force coefficients favouring static instability ($\partial C_L / \partial y > 0$ and large) in the second and third rows. When these coefficients were introduced into a simple equation of motion, it was possible to verify the second row static instability threshold measured in the dynamic experiments with a deviation of only 5%. Such an agreement between dynamic, static and theoretical results solidly verified the existence of static instability in this array. Therefore the present rotated square array, with $P/d = 2.12$ is the only array so far, in which both

multiple-flexible-cylinder, stiffness-controlled dynamic instability and static instability exist with critical flow velocities of the same order of magnitude. In fact, by altering the mechanical properties (i.e. frequency and/or damping) of a three-flexible cylinder configuration located in the second and third rows of the array it has been possible to suppress dynamic instability and initiate static instability.

BIBLIOGRAPHY

- [1] Paidoussis, M.P. 1980, "Flow-induced Vibrations in Nuclear Reactors and Heat Exchangers. Practical Experiences and State of Knowledge" *Practical Experiences with Flow-Induced Vibrations*, eds. E. Naudascher & D. Rockwell, Springer-Verlag, Berlin, pp. 1-81.
- [2] Paidoussis, M.P. 1981, "Fluidelastic Vibration of Cylinder Arrays in Axial and Cross-flow: State of the Art", *Journal of Sound and Vibration*, Vol. 76, pp. 329-360.
- [3] Paidoussis, M.P. 1983, "A Review of the Flow- Induced Vibrations in Reactors and Reactor Components", *Nuclear Engineering and Design*, Vol. 74, pp. 31-60.
- [4] Chen, S.S. 1987, "*Flow-Induced Vibration of Circular Cylindrical Structures*", Hemisphere Publishing.
- [5] Fitzpatrick, J.A., Donaldson, I.S. 1980, "Row Depth Effects on Turbulence Spectra and Acoustic Vibrations in Tube Banks", *Journal of Sound and Vibration*, Vol 73, pp. 225- 237.
- [6] Pnce, S.J., Paidoussis, M.P., Macdonald, R., Mark. B. 1987. "The Flow-Induced Vibration of a Single Flexible Cylinder in a Rotated Square Array of Rigid Cylinders with Pitch- to-Diameter Ratio of 2.12" *Journal of Fluids and Structures*, Vol. 1, pp. 359-378.

- [7] Sandifer, J.B., Bailey, R.T. 1984, "Turbulent Buffeting of Tube Arrays in Liquid Crossflow", *ASME Symposium on Flow Induced Vibrations*, (Paidoussis, M.P. Principal Editor), ASME WAM, New Orleans, Vol. 2, pp. 211-226.
- [8] Gorman, D.J. 1980, "The Effect of Artificially Induced Upstream Turbulence on Liquid Cross-flow Induced Vibration of Tube Bundles", *ASME Symposium Flow-Induced Vibration in Power Plant Components*, (Au-Yang, M.K. Editor), PVP Vol. 41, pp. 33-43.
- [9] Gorman, D.J. 1982 "Further Experimental Studies of the Vibration of Multi-Span Heat Exchanger Tubes Subjected to Liquid Cross-Flow." *Proceedings of BNES International Conference on Vibration in Nuclear Plant*, Keswick, pp. 88-100.
- [10] Pettigrew, M.J., Gorman, D.J. 1978, "Vibration of Heat Exchanger Tube Bundles in Liquid and Two-Phase Cross-Flow". *ASME Flow-Induced Vibration Design Guidelines*, Chen, N.Y. New York, PVP Vol. 52, pp. 89-110.
- [11] Price, S.J., Paidoussis, M.P. 1987, "The Flow- Induced Response of a Single Flexible Cylinder in an In-line Array of Rigid Cylinders", *Proceedings of International Conference on Flow Induced Vibrations*, Bowness-on-Windermere, Vol. 1, pp. 51-63.
- [12] Pettigrew, M.J , Sylvestre, Y., Compagna, A.O 1978, "Vibration Analysis of Heat Exchanger and Steam Generator Designs", *Nuclear Engineering and Design*, Vol. 48, pp. 97- 115.
- [13] Blevins, R.D., Gibert, R.J , Villard, B. 1981, "Experiments on Vibration of Heat Exchanger Tube Array in Cross- flow " *Transactions of 6th International Conference on Structural Mechanics in Reactor Technology*, paper B 6/9.

- [14] Taylor, C.E., Pettigrew, M.J., Axisa, F., Villard, B. 1988, "Experimental Determination of Single and Two-Phase Cross Flow-Induced Forces on Tube Rows", *Journal of Pressure Vessel Technology*, Vol. 110, pp. 22-28.
- [15] Chen, S.S., Jendrzejczyk, J.A. 1986, "Fluid Excitation Forces Acting on a Tube Array", *ASME Publication FED-40*, New York, pp. 45-55.
- [16] Weaver, D.S., Fitzpatrick, J.A. 1988, "A Review of Cross-flow Induced Vibrations in Heat Exchanger Tube Arrays", *Journal of Fluids and Structures*, Vol. 2, pp. 73-93.
- [17] Chen, S.S. 1978 "Vibration of a Group of Circular Cylinders Subject to Fluid Flow", *ASME Flow-Induced Vibration Design Guidelines*, (Chen, P.Y.), New York, PVP Vol. 52, pp. 76-88.
- [18] Chen, Y.N. 1968, "Flow-Induced Vibration and Noise in Tube Bank Heat Exchangers Due to Von Karman Sheets", *ASME Journal of Engineering for Industry*, Vol. 90, pp. 134-148.
- [19] Chen, Y.N. 1980, "Turbulence as Excitation Source in Staggered Tube Bundle Heat Exchangers", *ASME Publication*, PVP Vol. 41, pp. 45-63.
- [20] Owen, P.R. 1965, "Buffeting Excitation of Boiler Tube Vibration", *Journal of Mechanical Engineering Science*, Vol. 7, pp. 431-439.
- [21] Axisa, F., Villard, B., Gibert, R.J., Heteroni, G., Sundheimer, P. 1984, "Vibration of Tube Bundles Subjected to Air-Water and Steam-Water Cross-flow: Preliminary Results in Fluidelastic Instability" *ASME Symposium on Flow Induced Vibrations*, New Orleans, Vol. 2, pp. 269-284.
- [22] Pettigrew, M.J., Tromp, J.H., Mastcrakos, J. 1985, "Vibration of Tube Bundles Subjected to Two-Phase Cross-Flow." *ASME Journal of Pressure Vessel Technology*, Vol. 107, pp. 335-343.

- [23] Savkar, S.D., Litzinger, T.A. 1982, "Buffeting Forces Induced by Cross Flow Through Arrays of Cylinders." *Proceedings of the BNES International Conference on Vibration in Nuclear Plant*, Keswick, pp. 64-87.
- [24] Savkar, S.D. 1984, "Buffeting of Cylindrical Array in Cross Flow." *ASME Symposium on Flow Induced Vibrations*, New Orleans, Vol. 2, pp. 195-210.
- [25] Fitzpatrick, J.A., Donaldson, I S., McKnight, W. 1986, "The Structure of the Turbulence Spectrum of Flows in Deep Tube Array Models." *ASME Symposium on Flow Induced Vibrations*, PVP 104, pp. 193-200.
- [26] Weaver, D.S., Abd Rabbo, A. 1985, "A Flow Visualization Study of a Square Array of Tubes in Water Cross-flow." *ASME Journal of Fluids Engineering*, Vol. 107, pp. 354-363.
- [27] Abd Rabbo, A., Weaver, D.S. 1986, "A Flow Visualization Study of Flow Development in Staggered Tube Array." *Journal of Sound and Vibration*, Vol. 106, pp. 241-256.
- [28] Mureithi, N.W. 1988, "An Experimental Study of the Flow Structure and Dynamics of a Flexible Cylinder Within an Array of Rigid Cylinders Subjected to Water Cross-flow." *Masters Thesis*, McGill University.
- [29] Oengoren, A., Buhlmann, E.T. 1989, "On Acoustical Resonance in Tube Arrays, Part I: Experiments." *ASME Symposium on Flow-Induced Vibration*, Chicago, Vol. 5, pp. 219-243.
- [30] Mark, B., Mureithi, N.W. 1990, Unpublished results on "Rotated Square Arrays in Water Flow and Private Communications", McGill University.
- [31] Fitz-Hugh, J.S. 1973, "Flow Induced Vibration in Heat Exchangers", *U.K.A.E.A. Internal Report*, Harwell.
- [32] Chen, Y.N. 1977, "The Sensitive Tube Spacing Region of The Tube Bank Heat Exchangers for Fluid-elastic Coupling in Cross-flow." *ASME Symposium on*

Fluid-Structure Interaction Phenomena in Pressure Vessel and Piping Systems, pp. 1-18.

- [33] Bryce, W.B., Murray, B.G. 1980, "Design Criteria for Flow Induced Vibration in Heat Exchangers" *Symposium on Practical Experiences with Flow Induced Vibrations*, Karlsruhe, pp. 77-84.
- [34] Murray, B.G., Rae, G., Bryce, W.B. 1982, "Strouhal Numbers in Tube Arrays." *Proceedings of the BNES International Conference on Vibration in Nuclear Plant*, Keswick, pp. 231-243.
- [35] Weaver, D.S., Fitzpatrick, J.A., El-Kashlan, M. 1986, "Strouhal Numbers for Heat Exchanger Tube Arrays in Cross Flow." *ASME Symposium on Flow Induced Vibrations*, PVP 104, pp. 193-200.
- [36] Zukauskas, A., Katinas, V. 1980, "Flow Induced Vibration in Heat Exchanger Tube Banks." *Symposium on Practical Experiences with Flow Induced Vibrations*, Karlsruhe, pp. 188-196.
- [37] Roberts, B.W. 1962, "Low Frequency Self-excited Vibration in a Row of Circular Cylinders Mounted in an Air- stream." *Ph.D. Thesis*, University of Cambridge.
- [38] Connors, H.J. 1970, "Fluidelastic Vibration of Tube Arrays by Cross Flow." *ASME Flow Induced Vibration in Heat Exchangers*, New York, pp. 42-56.
- [39] Chen, S.S. 1984, "Guidelines for the Instability Flow Velocity of Tube Arrays in Cross-Flow." *Journal of Sound and Vibration*, Vol 93, pp. 439-455.
- [10] Gibert, R J., Sagner, M., Doyen, R. 1981, "Vibration of Tube Arrays in Transversal Flow." *Transactions of the 6th International Conference on Structural Mechanics in Reactor Technology*, Paris, Paper B6/6.
- [41] Heilker, W.J., Vincent, R Q 1981, "Vibration in Nuclear Heat Exchangers Due to Liquid and Two-phase Flow." *ASME Journal of Engineering for Power*, Vol. 103, pp. 358-366.

- [42] Chen, S.S., Jendrzejczyk, J.A. 1981, "Experiments on Fluid Elastic Instability in Tube Banks Subjected to Liquid Cross Flow." *Journal of Sound and Vibration*, Vol. 78, pp. 355-381.
- [43] Soper, B.M.H. 1980, "The Effect of Tube Layout on the Fluidelastic Instability of Tube Bundles in Cross Flow." *ASME Flow-Induced Heat Exchanger Tube Vibration*, New York, pp. 1-9.
- [44] Grover, L.K., Weaver, D.S. 1978, "Cross-Flow Induced Vibrations in a Tube Bank-Turbulent Buffeting and Fluid Elastic Instability", *Journal of Sound and Vibration*, Vol. 59, pp. 277-294.
- [45] Tanaka, H., Takahara, S. 1981, "Fluid Elastic Vibration of Tube Array in Cross Flow." *Journal of Sound and Vibration*, Vol. 77, pp. 19-37.
- [46] Weaver, D.S., El-Kashlan, M. 1981, "The Effect of Damping and Mass Ratio on the Stability of a Tube Bank." *Journal of Sound and Vibration*, Vol. 76, pp. 283-294.
- [47] Connors, H.J. 1978, "Fluidelastic Vibration of Heat Exchanger Tube Arrays." *Journal of Mechanical Design*, Vol. 100, pp. 347-353.
- [48] Savkar, S.D. 1977, "A Brief Review of Flow Induced Vibration of Tube Arrays in Cross-Flow." *Journal of Fluids Engineering*, Vol. 99, pp. 517-519.
- [49] Chen, Y.N. "The Orbital Movement and the Damping of the Fluidelastic Vibration of Tube Banks Due to Vortex Formation, Part 2. Criterion for the Fluidelastic Orbital Vibration of Tube Arrays." *Transactions of The American Society of Mechanical Engineers*, Vol. 95, Series B, pp. 1065- 1077.
- [50] Price, S J., Mark, B., Paidoussis, M.P. 1986 "An Experimental Stability Analysis of a Single Flexible Cylinder Positioned in an Array of Rigid Cylinders and Subject to Cross-flow." *ASME Symposium on Flow-Induced Vibrations*, Vol. 2, pp. 179-194.

- [51] Southworth, P.J., Zdravkovich, M.M. 1975, "Cross- Flow-Induced Vibrations of Finite Tube Banks in In-line Arrangements." *Journal of Mechanical Engineering Science*, Vol. 17, pp. 190-198.
- [52] Zdravkovich, M.M., Namork, J.E. 1979, "Structure of Interstitial Flow Between Closely Spaced Tubes in Staggered Array." *ASME Flow Induced Vibration*, New York, pp. 41- 46.
- [53] Zdravkovich, M.M., Namork, J.E. 1980, "Excitation Amplification and Suppression of Flow Induced Vibrations in Heat Exchangers." *Practical Experiences with Flow Induced Vibration*, Berlin, pp. 109-117.
- [54] Zdravkovich, M.M. 1987, "The Effects of Interference Between Circular Cylinders in Cross Flow." *Journal of Fluids and Structures*, Vol. 1, pp. 239-261.
- [55] Chen, S.S., Jendrzejczyk, J.A. 1981, "Flow Velocity Dependence of Damping in Tube Arrays Subjected to Liquid Cross-Flow." *Journal of Pressure Vessel Technology*, Vol. 103, pp. 130-135.
- [56] Pettigrew, M.H., Goyder, H.G.D., Qiao, Z.L., Axisa, F. 1986, "Damping of Multispan Heat Exchanger Tubes Part 1: In Gases." *ASME Flow Induced Vibration*, New York, PVP. Vol. 104, pp. 81-87.
- [57] Pettigrew, M.J., Rogers, R.j., Axisa, F. 1986, "Damping of Multispan Heat Exchanger Tubes: Part 2: In Liquids." *ASME Flow Induced Vibration*, New York PVP, Vol 104, pp 89-98.
- [58] Kim, B.S., Pettigrew, M J., Tromp, J.H. 1988, "Vibration Damping of Heat Exchanger Tubes in Liquids: Effects of Support Parameters." *Journal of Fluids and Structures*, Vol. 2, pp. 593-614.
- [59] Andjelic, A., Popp.K. 1989, "Stability Effects in a Normal Triangular Cylinder Array." *Journal of Fluids and Structures*, Vol. 3, pp. 165-186.

- [60] Paidoussis, M.P., Price, S.J., Nakamura, T., Mark, B., Njuki, W. 1988, "Flow-Induced Vibrations and Instabilities in a Rotated-Square Cylinder Array in Cross Flow." *ASME International Symposium on Flow-Induced Vibration and Noise*, New York, Vol. 3, pp. 111-137.
- [61] Paidoussis, M.P., Mavriplis, D., Price, S.J. 1984, "A Potential Flow Theory for the Dynamics of Cylinder Arrays in Cross Flow." *Journal of Fluid Mechanics*, Vol. 148, pp. 227-252.
- [62] Paidoussis, M.P., Price, S.J., Mavriplis, D., 1985, "A Semipotential Flow Theory for the Dynamics of Cylinder Arrays in Cross Flow." *Journal of Fluids Engineering*. Vol. 107, pp. 500-506.
- [63] Lever, J.H., Weaver, D.S. 1982, "A Theoretical Model for Fluid-Elastic Instability in Heat Exchanger Tube Bundles." *Journal of Pressure Vessel Technology*, Vol. 104, pp. 147-158.
- [64] Lever, J.H., Weaver, D.S. 1986, "On the Stability of Heat Exchanger Tube Bundles, Part I: Modified Theoretical Model." *Journal of Sound and Vibration*, Vol. 107, pp. 375-392.
- [65] Lever, J.H., Weaver, D.S. 1986, "On the Stability of Heat Exchanger Tube Bundles, Part II: Numerical Results and Comparison with Experiments." *Journal of Sound and Vibration*, Vol. 107, pp. 393-401.
- [66] Tanaka, H., Takahara, S. 1980, "Unsteady Fluid Dynamic Forces on Tube Bundle and its Dynamic Effect on Vibration." *ASME Flow Induced Vibration of Power Plant Component*, PVP 41, pp. 77-92.
- [67] Tanaka, H., Takahara, S. 1981, "Fluidelastic Vibration of Tube Arrays in Cross Flow", *Journal of Sound and Vibration*, Vol. 77, pp. 19-37.

- [68] Tanaka, H., Takahara, S., Ohta, K. 1982, "Flow- Induced Vibration of Tube Arrays With Various Pitch-to-Diameter Ratios." *Journal of Pressure Vessel Technology*, Vol. 104, pp. 168-174.
- [69] Chen, S.S. 1983, "Instability Mechanisms and Stability Criteria of a Group of Circular Cylinders Subjected to Cross-Flow. Part 1: Theory." *Journal of Vibration, Acoustics, Stress and Reliability in Design*, Vol. 105, pp. 51- 58.
- [70] Chen, S.S. 1983, "Instability Mechanisms and Stability Criteria of a Group of Circular Cylinders Subjected to Cross-Flow. Part 2: Numerical Results and Discussions." *Journal of Vibration, Acoustics, Stress and Reliability in Design*, Vol. 105, pp. 253-260.
- [71] Blevins, R.D. 1974, "Fluid Elastic Whirling of a Tube Row." *Journal of Pressure Vessel Technology*, Vol. 96, pp. 263-267.
- [72] Blevins, R.D. 1977, "Fluid Elastic Whirling of Tube Rows and Tube Arrays." *Journal of Fluids Engineering*, Vol. 99, pp. 457-461.
- [73] Whiston, G.S., Thomas, G.D. 1982, "Whirling Instabilities in Heat Exchanger Tube Arrays." *Journal of Sound and Vibration*, Vol. 81, pp. 1-13.
- [74] Price, S.J., Paidoussis, M.P. 1986, "A Single- Flexible-Cylinder Analysis for the Fluidelastic Instability of an Array of Flexible Cylinders in Cross-Flow." *Journal of Fluids Engineering*, Vol. 108, pp. 193-199.
- [75] Price, S.J , Paidoussis, M.P. 1986. "A Theoretical Investigation of the Fluidelastic Instability of a Single Flexible Cylinder Surrounded by Rigid Cylinders." *Proceedings of ASME The Symposium on Flow-Induced Vibrations*, pp. 117-133.
- [76] Price, S.J., Paidoussis, M.P. 1984, "An Improved Mathematical Model for the Stability of Cylinder Rows Subject to Cross-Flow." *Journal of Sound and Vibration*, Vol. 97, pp. 615-640.

- [77] Price, S.J., Paidoussis, M.P. 1986, "A Constrained-Mode Analysis of the Fluidelastic Instability of a Double Row of Flexible Circular Cylinders Subject to Cross-flow: A Theoretical Investigation of System Parameters." *Journal of Sound and Vibration*, Vol. 105, pp. 121-142.
- [78] Price, S.J., Paidoussis, M.P. 1987. "Fluidelastic Instability of a Full Array of Flexible Cylinders Subject to Cross-flow." *ASME Symposium on Fluid-Structure Interaction and Aerodynamic Damping*, Vol. 171-192.
- [79] Paidoussis, M.P., Price, S.J. 1988, "The Mechanisms Underlying Flow-Induced Instabilities of Cylinder Arrays in Crossflow." *Journal of Fluid Mechanics*, Vol. 187, pp. 45-59.
- [80] Price, S.J., Paidoussis, M.P., Giannias, N. 1990, "A Generalized Constrained-Mode Analysis for Cylinder Arrays in Cross-Flow." *Journal of Fluids and Structures*, Vol. 4, pp. 171-202.
- [81] Price, S.J., Valerio, N.R., 1989, "A Non-Linear Investigation of Single-Degree-of-Freedom Instability in Cylinder Arrays Subject to Cross-Flow." *Journal of Sound and Vibration*, Vol. 137, pp. 419-432.
- [82] Axisa, F., Antunes, J., Villard, B. 1986, "Overview of Numerical Methods for Predicting Flow-Induced Vibration and Wear of Heat Exchanger Tubes." *ASME Symposium on Flow-Induced Vibration*, Chicago, pp. 147-159.
- [83] De Longre, E., Doveil, F., Porcher, G., Axisa, F. 1990, "Chaotic and Periodic Motion of a Non-Linear Oscillator in Relation With Flow-Induced Vibrations of Loosely Supported Tubes." *ASME Symposium on Flow-Induced Vibration*, Nashville, PVP. Vol. 189, pp. 119-125.
- [84] Fricker, A.J. 1988, "Numerical Analysis of the Fluidelastic Vibration of a Steam Generator Tube with Loose Supports." *ASME Symposium on Flow-Induced Vibration*, Chicago, Vol. 5, pp. 105-120.

- [85] Weaver, D.S., Koroyannakis, D. 1982, "Flow-Induced Vibrations of Heat Exchanger U-Tubes: A Simulation to Study the Effects of Asymmetric Stiffness", *Journal of Vibration, Acoustics, Stress and Reliability in Design*, Vol. 105, pp. 67-75.
- [86] Mark, B. 1986, "An Experimental Study of the Vibration Response of a Flexibly-mounted Cylinder Within a Rigid Array Subject to Air Cross-flow", *Masters Thesis*, McGill University.
- [87] Collar, A.R., Simpson, A. 1987, *Matricies and Engineering Dynamics*, Ellis Harwood, Chichester.
- [88] Mark, B. 1987, Unpublished results on "Measurement of Cylinder Vibrational Motion by Magnets", McGill University.
- [89] Mark, B. 1987, "NEWED", *User's Manual*, Department of Mechanical Engineering, McGill University.
- [90] Macdonald, R. 1986, *Undergraduate Project*, Department of Mechanical Engineering, McGill University.
- [91] Simpson, A., Flower, J.W. 1977, "An Improved Mathematical Model for the Aerodynamic Forces on Tandem Cylinders With Aeroelastic Applications", *Journal of Sound and Vibration*, Vol. 51, pp. 183-217.

TABLES

	Reference	K	α
Blevins <i>et al.</i>	[13]	2.5	0.5
Gibert <i>et al.</i>	[40]	2.7	0.34
Heilker and Vincent	[41]	5.0	0.5
Chen and Jendrezjczyk	[42]	2.43-6.03	0.20-1.08
Soper	[43]	1.25-1.78	0.5
Grover and Weaver	[44]	7.1	0.21
Tanaka and Takahara	[45]	3.0	0.75

Table 1.1: Empirical Values of the Constants in Equation (1.3)

	Reference	K	α_1	α_2
Tanaka & Takahara	[45]	-	0.33-0.5	0.2-0.5
Weaver & El-Kashlan	[46]	4.6	0.29	0.21
Price & Paidoussis	[11]	0.68-15.4	0.19-0.57	0.15-0.57
Grover & Weaver	[44]	-	0.5	< 0.5

Table 1.2: Empirical Values of the Constants in Equation (1.5)

Cylinder Type	Cylinder Material	Dimensionless Cylinder Cylinder Mass ($\bar{m} = m/\rho d^2$)
1	Steel	980 ± 7
2	Aluminum	490 ± 5
3	Drafting paper/epoxy	280 ± 3
4	Drafting paper/epoxy	195 ± 3

Table 3.1: Certain Characteristics of Flexible Cylinders Used.

Accelerometer Model	Charge Sensitivity (pC/g)	Charge Amp Model	Capacitance
Endevco 2229C	3.196	27218	365
Endevco 2229C	3.207	27218	392
Endevco 2229C	3.260	27218	384
Endevco 2229C	2.785	27218	356
Endevco 2221D	17.2	27218	384
Endevco 2221D	17.7	27218	845

Table 3.2: Characteristics of Accelerometers Used.

Experiment Reference	Flexible Cylinder Position	$\frac{m}{\rho d^2}$	$f_n [Hz]$	δ	$U_c/f_n d$
S -1	1	280	10	0.014	stable for $U_c/f_n d \leq 83$
S -2	3	280	10	0.014	stable for $U_c/f_n d \leq 83$
S -3	3	280	7	0.014	stable for $U_c/f_n d \leq 118$
S -4	3	195	7.4	0.014	stable for $U_c/f_n d \leq 112$

Table 4.1: Summary of the Dynamic Response of a Single Flexible Cylinder in Different Rows of the Array

Experiment Reference	Flexible Cylinder Position	$\frac{m}{\rho d^2}$	$f_n [Hz]$	δ	$U_c/f_n d$
T -1	1,3	280	10.0	0.014	stable for $U_c/f_n d \leq 80$
T -2	4,5	280	10.0	0.014	stable for $U_c/f_n d \leq 77$
T -3	2L, 2R ¹	280	7.0	0.014	stable for $U_c/f_n d \leq 87$
T -5	1, 2L	280	10.0	0.014	stable for $U_c/f_n d \leq 80$
T -6	5, 6L ²	280	10.0	0.014	stable for $U_c/f_n d \leq 77$
T -4	2L, 2R ¹	195	5.0	0.014	stable for $U_c/f_n d \leq 165$
T -7	4,6	280	10.0	0.014	stable for $U_c/f_n d \leq 77$

Table 4.2: Summary of the Dynamic Response of Two Flexible Cylinders for Different Positions in the Array. Notes: (1) This arrangement is stable in terms of dynamic instability, but unstable in terms of static instability. (2) An extra row of cylinders was added to the array in this experiment.

		f_1 (Hz)	f_2 (Hz)	f_3 (Hz)	f_4 (Hz)	f_5 (Hz)	f_6 (Hz)	f_7 (Hz)	f_8 (Hz)	f_9 (Hz)
Cylinder 1	in-flow	-	-	-	-	12.3	12.6 ¹	13.0	-	15.6
	cr-flow	-	-	-	11.5	-	12.6 ¹	-	-	15.6
Cylinder 2L	in-flow	-	-	-	11.5	12.3	12.6 ¹	-	12.8	15.6
	cr-flow	-	-	9.3	11.5	-	12.6 ¹	-	-	-
Cylinder 2R	in-flow	-	-	-	-	-	12.6 ¹	-	-	15.5
	cr-flow	-	-	9.3	-	-	12.6 ¹	-	-	15.6
Cylinder 3	in-flow	-	-	-	-	12.2	12.6 ¹	-	-	-
	cr-flow	5.7	6.8	9.3	-	12.3	12.7 ¹	-	-	-

Table 4.3: Major Peaks in The In- and Cross-flow Acceleration Power Spectra of Four Flexible Cylinders Located in the Three Upstream Pows for $U_c/f_n d \approx 57.5$. Note: (1) This peak, observed in all cylinders, is a periodicity corresponding to $Su = 0.022$

Experiment Reference	Flexible Cylinder Position	$\frac{m}{\rho d^2}$	f_n [Hz]	δ	$U_c/f_n d$
A -1	2L, 2R, 3	280	7.0	0.014	2L = 2R = 105; 3 = 97
A -2	2L, 2R, 3	280	10.0	0.014	stable for $U_c/f_n d \leq 79$
A -3	2L, 2R 3 ¹	280	7.00	0.200	stable for $U_c/f_n d \leq 112$
A -4	2L, 2R, 3	280	10.8	0.014	stable for $U_c/f_n d \leq 73$

Table 4.4: Summary of the Dynamic Response of Three Flexible Cylinders Positioned in the Second and the Third Rows. Note: (1) a static instability possibly occurred in this experiment.

Experiment Reference	Flexible Cylinder Position	$\frac{m}{\rho d^2}$	f_n [Hz]	δ	$U_c/f_n d$
Z -1	1, 2L, 2R, 3	280	13.5	0.014	stable for $U_c/f_n d \leq 57$
Z -2	1, 2L, 2R, 3	280	13.0	0.014	stable for $U_c/f_n d \leq 65$
Z -3	1, 2L 2R, 3	280	12.5	0.014	1 = 2L = 2R = 65; 3 = 63
Z -4	1, 2L 2R, 3	280	10.0	0.014	1 = 2L = 2R = 62; 3 = 59
Z -5	2, 3L, 3R, 4	280	10.0	0.014	2 = 52; 3L = 3R = 53; 4 = 52
Z -6	3, 4L, 4R, 5	280	10.0	0.014	stable for $U_c/f_n d \leq 83$
Z -7	3, 4L, 4R, 5	280	7.0	0.014	3 = 67; 4L = 74; 4R = 70; 5 = 82
Z -8	3, 4L, 4R, 5 ¹	280	8.25	0.014	3 = 70; 4R = 74;
Z -9	4, 5L, 5R, 6 ²	280	7.00	0.014	stable for $U_c/f_n d \leq 110$

Table 4.5: Summary of the Dynamic Response of Four Flexible Cylinders Positioned In Different Rows of the Array [$\bar{m} = 280, \delta = 0.014$]. Notes: (1) cylinders 4L and 5 did not go unstable. (2) An extra row of cylinders was added to the array to eliminate downstream effects.

Experiment Reference	Flexible Cylinder Position	$\frac{m}{\rho d^2}$	$f_n [Hz]$	δ	$U_c/f_n d$
Z -10	1, 2L, 2R, 3	195	13.5	0.014	1 = 2L = 53; 2R = 3 = 51
Z -11	1, 2L, 2R, 3	195	6.75	0.014	1 = 2L = 2R = 53; 3 = 52
Z -1	1, 2L, 2R, 3	280	13.5	0.014	stable for $U_c/f_n d \leq 57$
Z -2	1, 2L, 2R, 3	280	13.0	0.014	stable for $U_c/f_n d \leq 65$
Z -3	1, 2L, 2R, 3	280	12.5	0.014	1 = 2L = 2R = 65; 3 = 63
Z -4	1, 2L, 2R, 3	280	10.0	0.014	1 = 2L = 2R = 62; 3 = 59
Z -12	1, 2L, 2R, 3	490	5.00	0.014	1 = 77; 2L = 90; 2R = 79; 3 = 87
Z -13	1, 2L, 2R, 3	490	7.00	0.014	1 = 93; 2L = 2R = 3 = 91
Z -14	1, 2L, 2R, 3	980	4.88	0.014	stable for $U_c/f_n d \leq 165$
Z -15	1, 2L, 2R, 3 ¹	980	3.40	0.014	1 = 2L = 2R = 3 = 236

Table 4.6: The Effect of Dimensionless Cylinder Mass on the Dynamic Response of Four Flexible Cylinders Positioned in the First Three Rows of the Array [$\delta = 0.014$]. Note: (1) In this experiment it is not clear if instability has occurred or if it is just impending.

Experiment Reference	Flexible Cylinder Position	$\frac{m}{\rho d^2}$	$f_n [Hz]$	δ	$U_c/f_n d$
Z -4	1, 2L, 2R, 3	280	10.0	0.014	1 = 2L = 2R = 62; 3 = 59
Z -16	1, 2L, 2R, 3	280	10.0	0.10	1 = 2L = 2R = 67; 3 = 64
Z -17	1, 2L, 2R, 3 ¹	280	10.0	0.20	2L = 2R = 72; 3 = 69
Z -18	1, 2L, 2R, 3 ²	280	10.0	0.45	stable for $U_c/f_n d \leq 76$
Z -1	1, 2L, 2R, 3	280	13.5	0.014	stable for $U_c/f_n d \leq 57$
Z -2	1, 2L, 2R, 3	280	13.0	0.014	stable for $U_c/f_n d \leq 65$
Z -3	1, 2L, 2R, 3	280	12.5	0.014	1 = 2L = 2R = 65; 3 = 63
Z -12	1, 2L, 2R, 3	490	5.00	0.014	1 = 77; 2L = 90, 2R = 79, 3 = 87
Z -13	1, 2L, 2R, 3	490	7.00	0.014	1 = 93, 2L = 2R = 3 = 91
Z -19	1, 2L, 2R, 3	490	7.00	0.24	1 = 2L = 2R = 3 = 108
Z -20	1, 2L, 2R, 3 ³	490	7.00	0.07	1 = 2L = 2R = 3 = 105

Table 4.7: The Effect of Initial Cylinder Damping on the Dynamic Response of Four Flexible Cylinders Positioned in the First Three Rows of the Array [$m = 280$ and 490]. Notes: (1) Cylinder 1 was not instrumented in this experiment, (2) a static instability possibly occurred in these experiments; (3) no detailed measurements made in this experiment, U_c based on visual observations only.

			f_1 [Hz]	f_2 [Hz]	f_3 [Hz]	f_4 [Hz]	f_5 [Hz]	f_6 [Hz]	f_7 [Hz]
$U_c/f_n d = 18$	Cylinder 1	in-flow	-	-	-	6.87	-	-	-
		cr-flow	6.03	-	6.75	-	-	-	-
	Cylinder 2L	in-flow	-	-	-	6.87	-	-	-
		cr-flow	-	6.44	-	-	-	-	-
	Cylinder 2R	in-flow	-	6.44	-	6.87	7.5	-	-
		cr-flow	-	-	-	6.87	-	-	-
	Cylinder 3	in-flow	-	-	-	6.87	-	-	9.56
		cr-flow	-	6.44	-	-	-	9.31	-

			f_1 [Hz]	f_2 [Hz]	f_3 [Hz]	f_4 [Hz]	f_5 [Hz]	f_6 [Hz]	f_7 [Hz]
$U_c/f_n d = 39$	Cylinder 1	in-flow	-	11.81	-	-	-	-	-
		cr-flow	-	11.81	-	-	-	-	-
	Cylinder 2L	in-flow	-	11.81	-	-	-	-	-
		cr-flow	5.9	11.81	-	-	-	-	-
	Cylinder 2R	in-flow	5.9	11.81	17.72	-	-	-	-
		cr-flow	5.9	11.81	-	-	-	-	-
	Cylinder 3	in-flow	5.9	11.81	17.72	-	-	-	-
		cr-flow	5.9	11.81	17.72	-	-	-	-

Table 4.8: Major Peaks in the In- and Cross-Flow Acceleration Power Spectra of a -36% Detuned Four Flexible Cylinder Configuration Located in The Three Upstream Rows, $\bar{m} = 280$, $\delta = 0.014$, $f_1 = f_{2R} = f_{2L} = 6.375$ Hz and $f_3 = 10$ Hz.

			f_1 [Hz]	f_2 [Hz]	f_3 [Hz]	f_4 [Hz]	f_5 [Hz]	f_6 [Hz]	f_7 [Hz]
$U_c/f_n d = 33$	Cylinder 1	in-flow	-	-	-	-	13.56	-	-
		cr-flow	-	-	-	-	13.56	-	-
	Cylinder 2L	in-flow	-	-	-	-	-	13.75	-
		cr-flow	-	-	12.91	-	-	-	-
	Cylinder 2R	in-flow	-	-	-	-	-	-	13.84
		cr-flow	-	-	-	13.40	-	-	-
	Cylinder 3	in-flow	9.40	10.47	-	-	-	-	-
		cr-flow	9.40	-	-	-	-	-	-

			f_1 [Hz]	f_2 [Hz]	f_3 [Hz]	f_4 [Hz]	f_5 [Hz]	f_6 [Hz]	f_7 [Hz]	f_8 [Hz]	f_9 [Hz]
$U_c/f_n d = 65$	Cylinder 1	in-flow	-	-	-	-	12.80	-	14.5	-	-
		cr-flow	-	-	-	-	-	-	-	-	-
	Cylinder 2L	in-flow	-	-	-	-	-	13.00	-	14.90	-
		cr-flow	-	-	11.60	-	-	13.09	-	-	-
	Cylinder 2R	in-flow	-	-	-	-	-	13.00	-	-	17.10
		cr-flow	-	-	-	12.60	-	-	-	-	17.0
	Cylinder 3	in-flow	-	7.25	-	-	12.80	13.00	-	-	-
		cr-flow	5.87	7.25	11.60	-	-	13.00	-	-	-

Table 4.9: Major Peaks in the In- and Cross-Flow Acceleration Power Spectra of a +35% Detuned Four Flexible Cylinder Configuration Located in The Three Upstream Rows, $\bar{m} = 280$, $\delta = 0.014$, $f_1 = f_{2R} = f_{2L} = 13.5$ Hz and $f_3 = 10$ Hz.

Exper Ref	f_1 (Hz)	f_{2L} (Hz)	f_{2R} (Hz)	f_3 (Hz)	$(f_1 = f_{2L} = f_{2R})/f_3$	U_{1c} (m/s)	U_{2Lc} (m/s)	U_{2Rc} (m/s)	U_{3c} (m/s)	$U_{3c}/f_3 d$	$U_{3c(det)}/U_{3c}$
D-1	13.5	13.5	13.5	10.00	1.35	n.a.	n.a.	n.a.	17.65	69.5	1.18
D-2	13.5	13.5	13.5	10.00	1.35	17.80	17.80	17.80	17.80	70.0	1.19
D-3	12.37	12.37	12.37	10.00	1.237	n.a.	n.a.	n.a.	16.90	66.50	1.13
D-4	11.44	11.44	11.44	10.00	1.444	n.a.	n.a.	n.a.	16.25	64.0	1.08
D-5	10.80	10.80	10.80	10.00	1.080	n.a.	n.a.	n.a.	15.65	61.5	1.04
D-6	10.00	10.00	10.00	10.00	1.00	n.a.	n.a.	n.a.	15.00	59.0	1.00
D-7	9.00	9.00	9.00	10.00	0.90	n.a.	n.a.	n.a.	12.35	48.5	0.82
D-8	8.12	8.12	8.12	10.00	0.812	n.a.	n.a.	n.a.	10.15	40.0	0.68
D-9	6.37	6.37	6.37	10.00	0.637	n.a.	n.a.	n.a.	9.80	38.5	0.65
D-10	6.00	6.00	6.00	10.00	0.600	9.90	9.50	8.75	8.40	33.0	0.56

Table 4.10: Initial Natural Frequency (f_i), Natural Frequency Ratio (f_1/f_3), Critical Velocity (U_{ic}) and Non-dimensional Critical Velocity of Cylinder 3 $\frac{U_{3c(det)}}{U_{3c}}$ for Various Detuning Experiments with Four Flexible Cylinders Located in The Three Upstream Rows of the Array (1, 2L, 2R and 3), $\bar{m} = 280, \delta = 0.014$. Note: (1) n.a. = not available (not measured).

Experiment Reference	f_1 (Hz)	f_{2L} (Hz)	f_{2R} (Hz)	f_3 (Hz)	U_{1c} (m/s)	U_{2Lc} (m/s)	U_{2Rc} (m/s)	U_{3c} (m/s)
D-11	10.00	10.00	10.00	10.00	15.8	15.8	15.8	15.80
D-12	8.00	8.00	8.00	8.00	11.5	11.5	11.5	11.5
D-13	12.50	12.50	12.50	12.50	20.4	20.4	20.4	20.4
D-14	10.00	12.50	12.50	10.00	17.6	16.1	15.0	17.90
D-15	8.00	12.50	12.50	8.00	17.1	16.5	17.5	14.00
D-16	12.50	8.00	8.00	12.50	18.0	18.7	18.7	18.5
D-17	13.00	8.50	8.50	13.00	16.0	16.0	16.0	16.0

Table 4.11: Initial Natural Frequency (f_i) and Critical Flow Velocity (U_i) for Various Detuning Experiments With Four Flexible Cylinders Located in the Three Upstream Rows of the Array (1, 2L, 2R and 3), $\bar{m} = 280, \delta = 0.014$.

Exper. Ref.	Flexible Cylinder Position	f_1 (Hz)	f_2 (Hz)	f_3 (Hz)	f_4 (Hz)	U_{1cr} (m/s)	U_{2cr} (m/s)	U_{3cr} (m/s)	U_{4cr} (m/s)
D-17	1, 2L, 2R, 3	8.00	9.50	11.00	12.50	18.60	18.00	14.00	16.50
D-18	1, 2L, 2R, 3	12.50	11.00	9.50	8.00	13.20	13.00	10.60	10.40
D-20	2, 3L, 3R, 4	10.00	10.00	10.00	10.00	13.45	13.45	13.45	13.45
D-21	2, 3L, 3R, 4	8.50	13.00	13.00	8.50	18.50	15.50	20.72	20.72
D-22	2, 3L, 3R, 4	8.50	8.50	8.50	13.50	13.50	15.20	14.20	15.20
D-23	3, 4L, 4R, 5	10.00	10.00	10.00	10.00	stbl	stbl	stbl	stbl
D-24	3, 4L, 4R, 5	7.00	10.00	10.00	10.00	12.20	12.45	12.45	13.20
D-25	3, 4L, 4R, 5	8.15	8.15	8.15	10.00	16.50	18.05	18.30	17.50
D-26	3, 4L, 4R, 5	8.25	8.25	8.25	8.25	14.65	15.50	???	???
D-27	3, 4L, 4R, 5	13.00	13.00	13.00	8.00	stbl	stbl	stbl	stbl
D-28	3, 4L, 4R, 5	7.00	7.00	7.00	7.00	11.90	12.35	13.15	14.50
D-29	3, 4L, 4R, 5	13.00	7.00	7.00	7.00	17.95	19.00	19.00	stbl

Table 4.12: Further Detuning Experiments With Four Flexible Cylinders ($\tilde{m} = 280$, $\delta = 0.014$)

Cylinder Position (Row)	α	β
1	2.1	0
2	300	-0.46
3	400	-0.55
4	130	-0.46
5	90	-0.45
7	38	-0.38

Table 6.1: The Values of Constants in the Equation $C_D = \alpha Re^\beta$ for a Cylinder Located in the Different Rows of the Array

Cylinder Position (Row)	$\partial C_L / \partial \bar{y}_{\bar{x}=0}$	$\partial C_D / \partial \bar{x}_{\bar{y}=0}$
1	≈ 0	0.40
2	2.90	0.43
3	2.75	≈ 0
4	1.35	0.45
5	1.15	0.41
7	1.04	0.69

Table 6.2: Variation of the Lift and Drag Coefficients With Displacement at a Flow Velocity of 16.63 m/s.

\bar{m}	Non-dimensional Critical Velocity (\bar{U})		
	Case A	Case B	Case C
50	3.80	3.50	4.30
280	4.60	4.10	5.60
1500	6.80	6.00	9.00
7500	12.40	10.40	16.75
75000	34.00	28.00	47.50
750000	103.00	84.00	145.00

Table 8.1: The Effect of Varying the fluid Force Coefficients on the Non-dimensional Critical Velocity of the Array. Case A is for the Coefficients Given in Appendix 1. Case B is for the Same Coefficients Increased by 50% and Case C is for the Same Coefficients Decreased by 50% ($\delta = 0.014$).

δ	Non-dimensional Critical Velocity (\bar{U})		
	Case A	Case B	Case C
0.0014	5.70	5.00	7.20
0.014	12.40	10.40	16.75
0.14	34.50	28.50	47.00

Table 8.2: The Effect of Varying the Fluid Force Coefficients on the Non-dimensional Critical Velocity of the Array. Case A is for the Coefficients Given in Appendix 1. Case B is for the Same Coefficients Increased by 50% and Case C is for the Same Coefficients Decreased by 50% ($\bar{m} = 7500$).

Figures

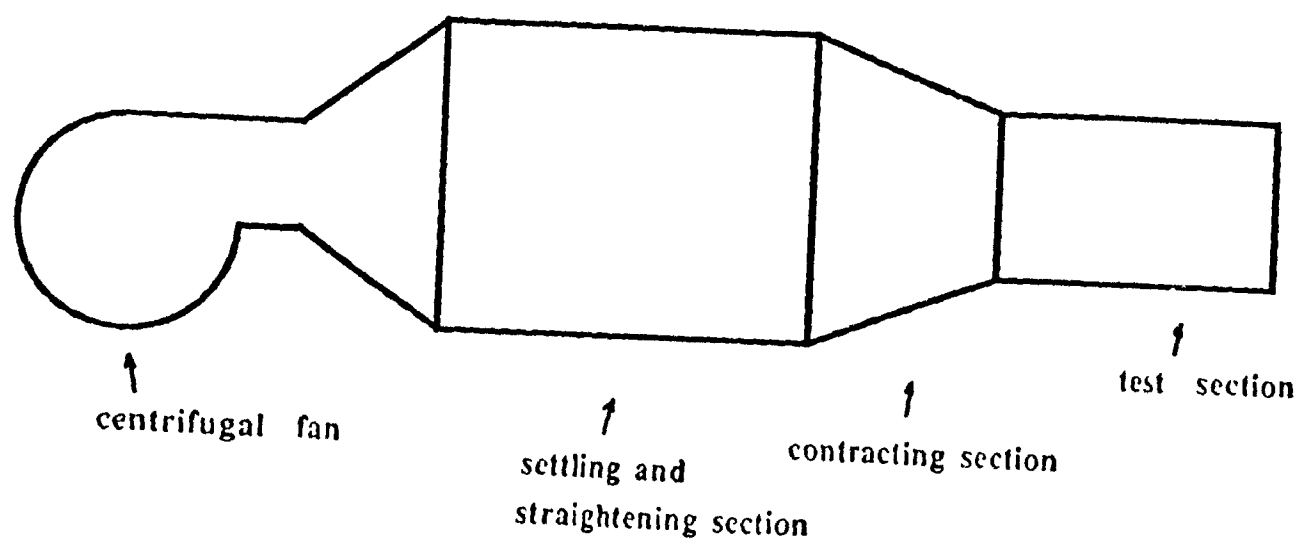


Figure 2.1: Schematic of the wind tunnel

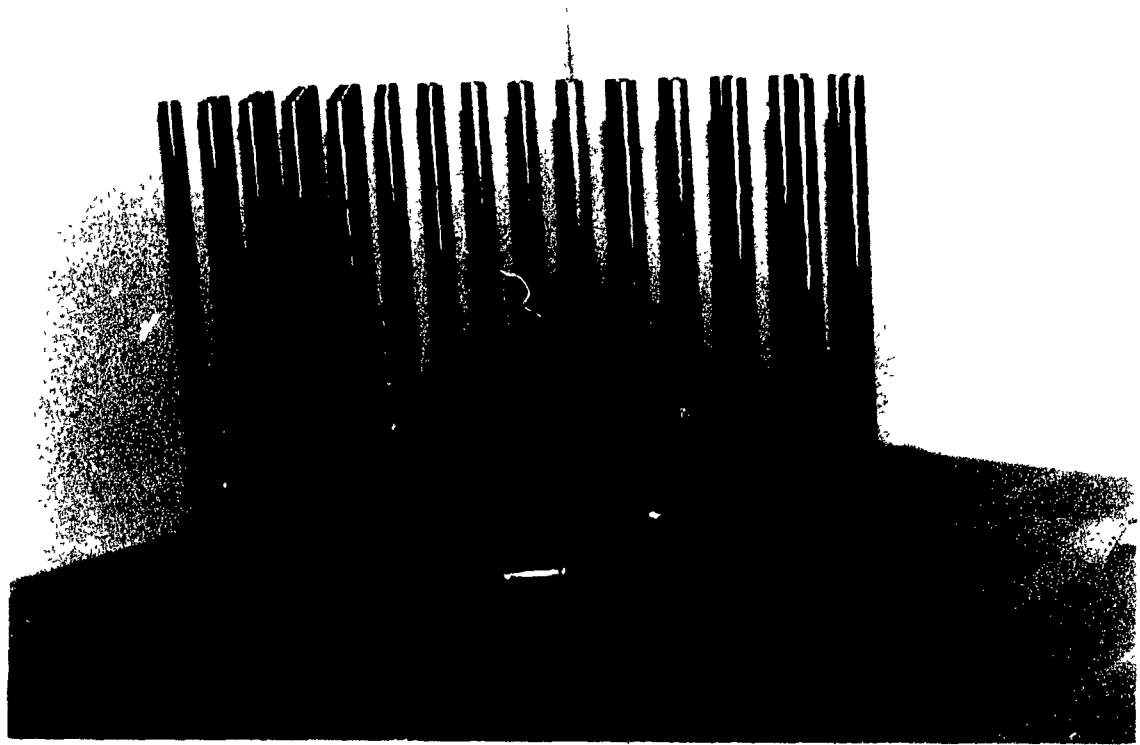


Figure 2.2. The rigid portion of the array (the upper plate is removed for a better view)

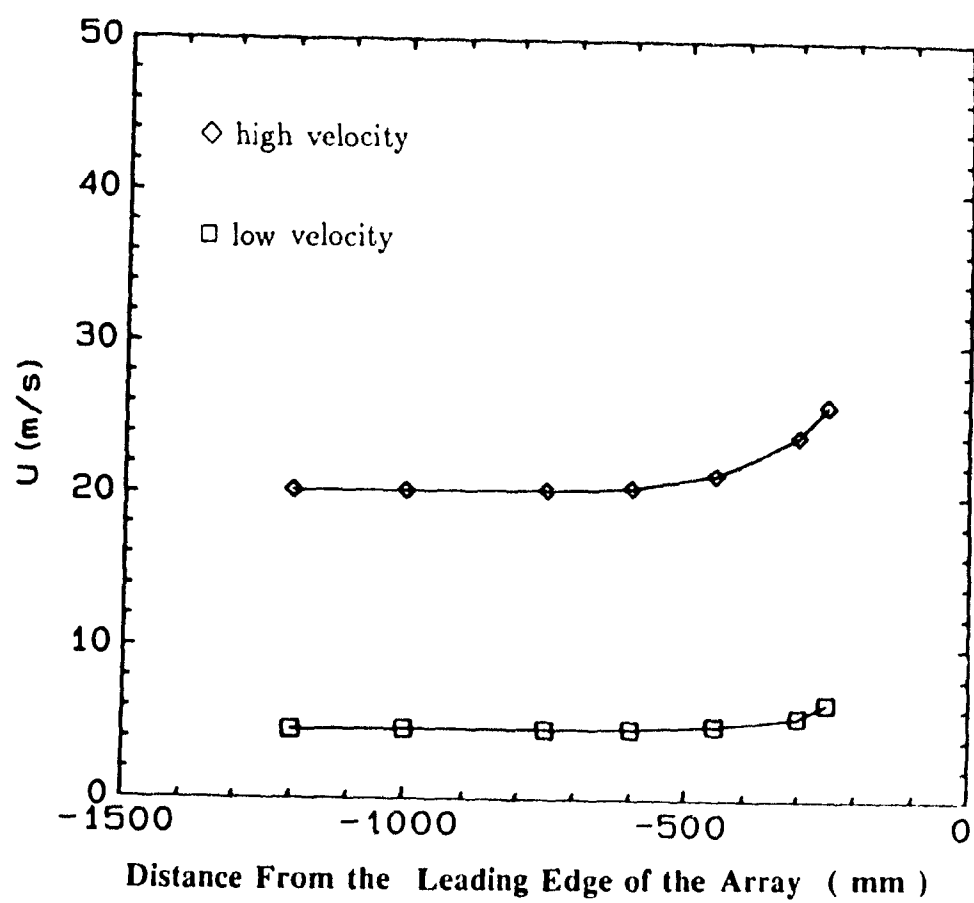


Fig 2.3: Variation of the upstream velocity magnitude with distance from the leading edge of the array.



Figure 3.1: The vibration insert (The rigid portion of the array has been removed in this instance for a better view)



Figure 3.2: Upper portion of the vibration insert.

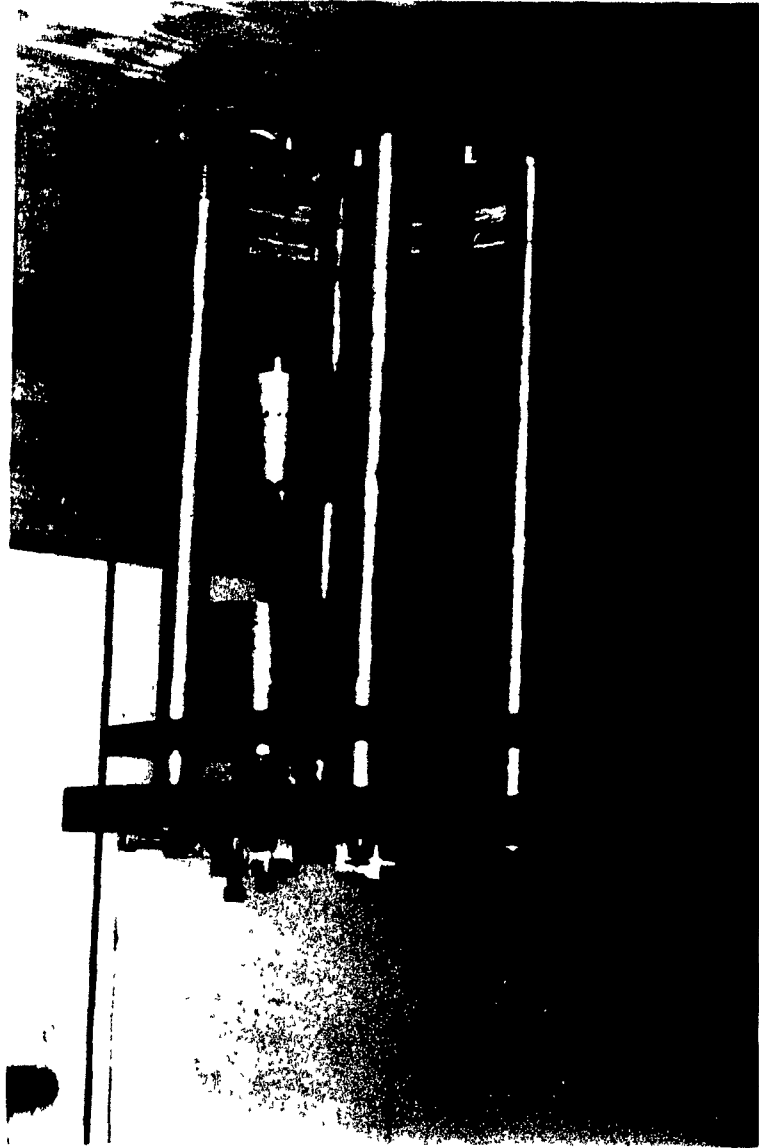


Figure 3 3. Lower portion of the vibration insert.

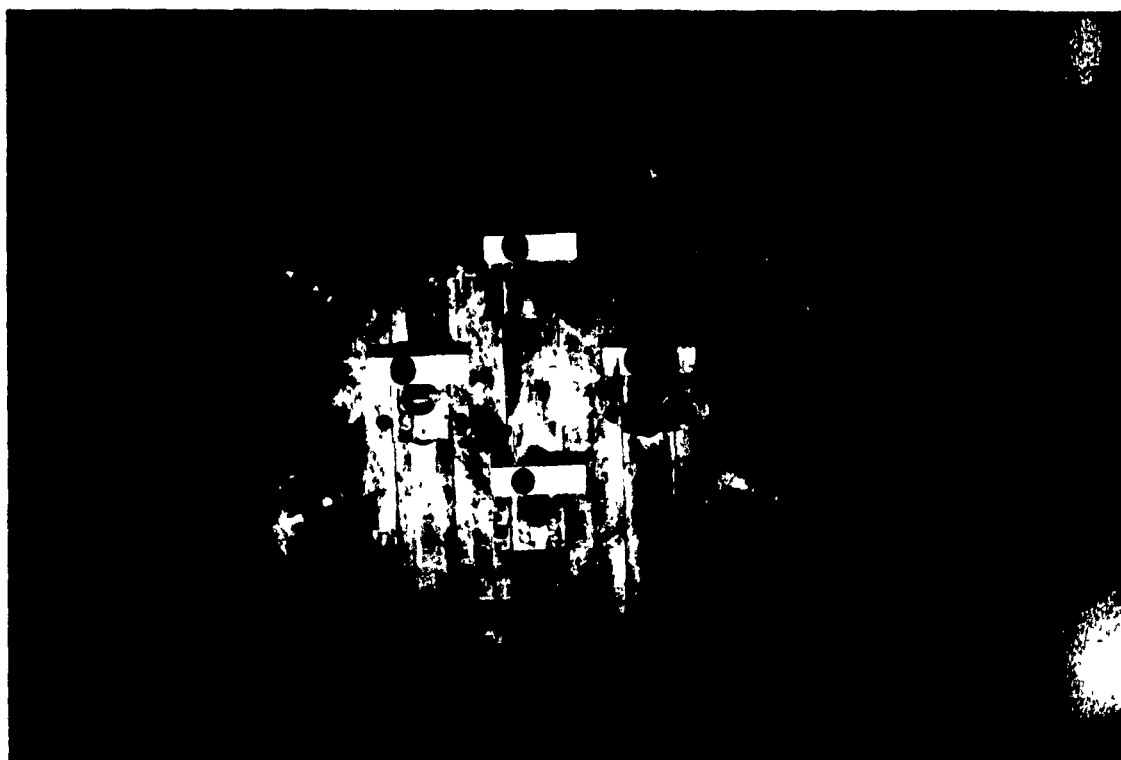


Figure 3.4: The lower platform with sliders.

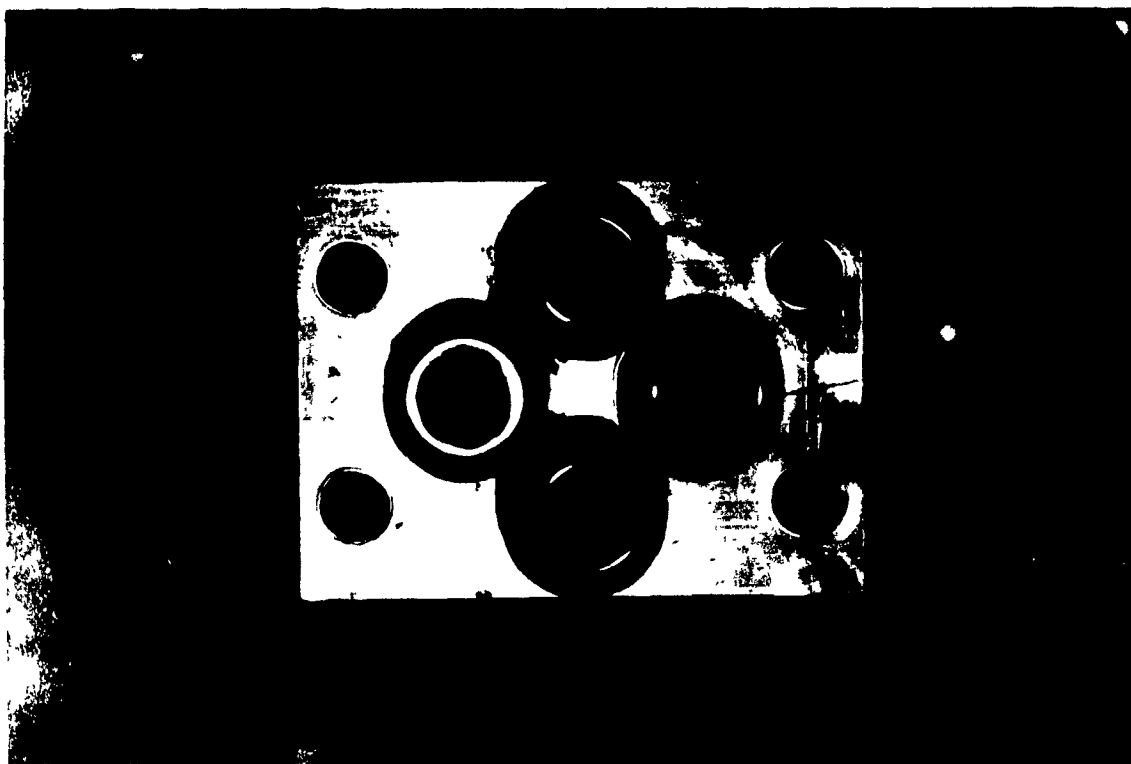


Figure 3.5. Platform holding oil pots.

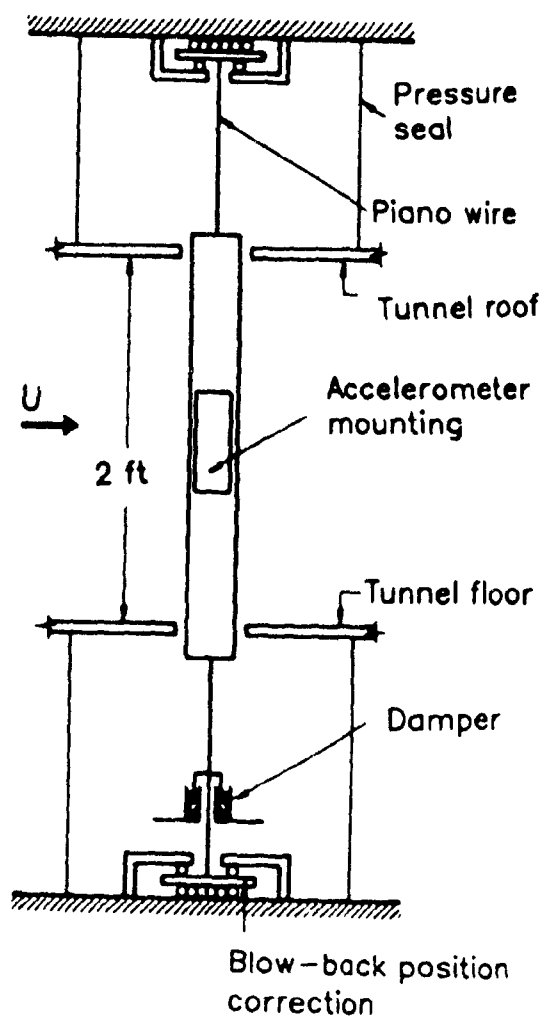


Figure 3.6: A typical flexible cylinder and its mounting system (reproduced from ref. [6])

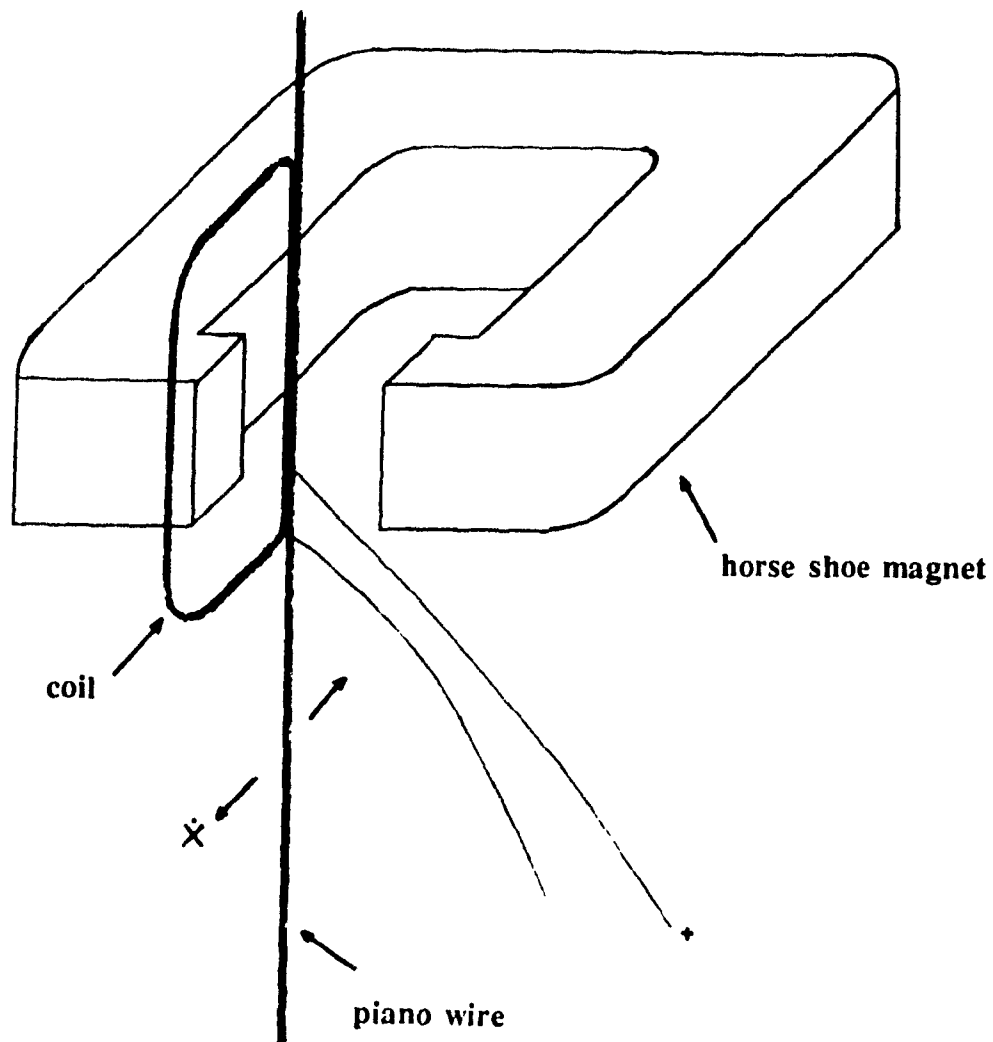


Figure 37 The velocity pick-up.

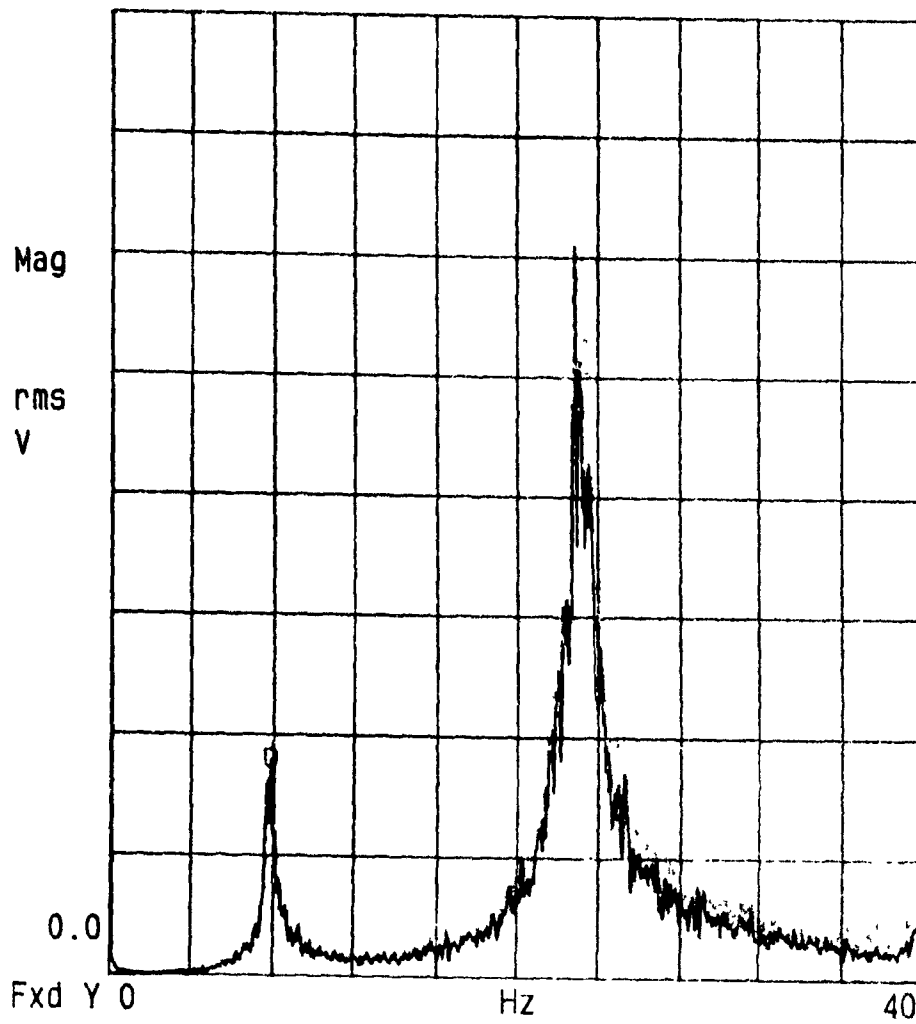


Figure 3 S: Comparison of accelerometer (black) and velocity pick-up (red) signals (differentiated).

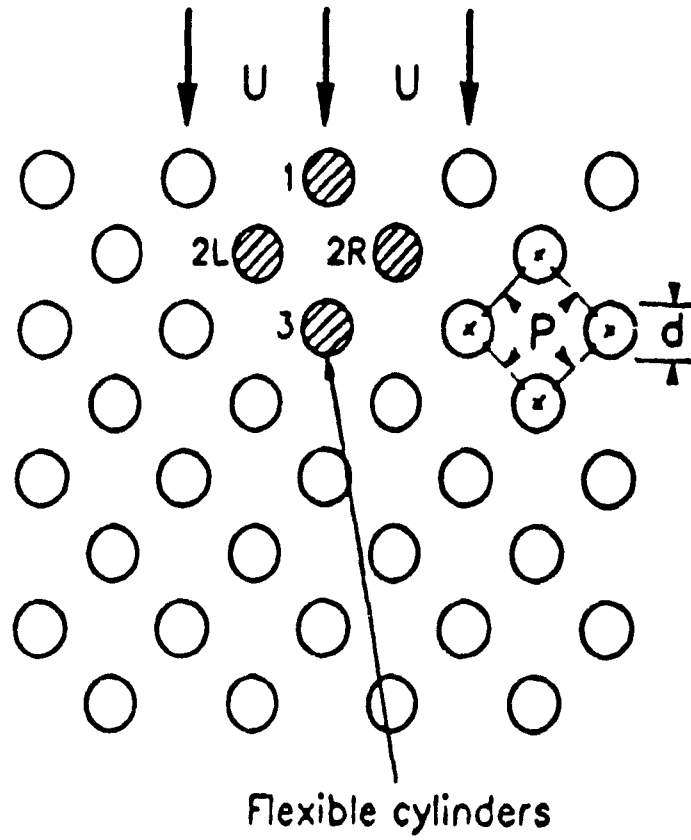


Figure 4-1. Schematic drawing of the middle portion of the cylinder array.

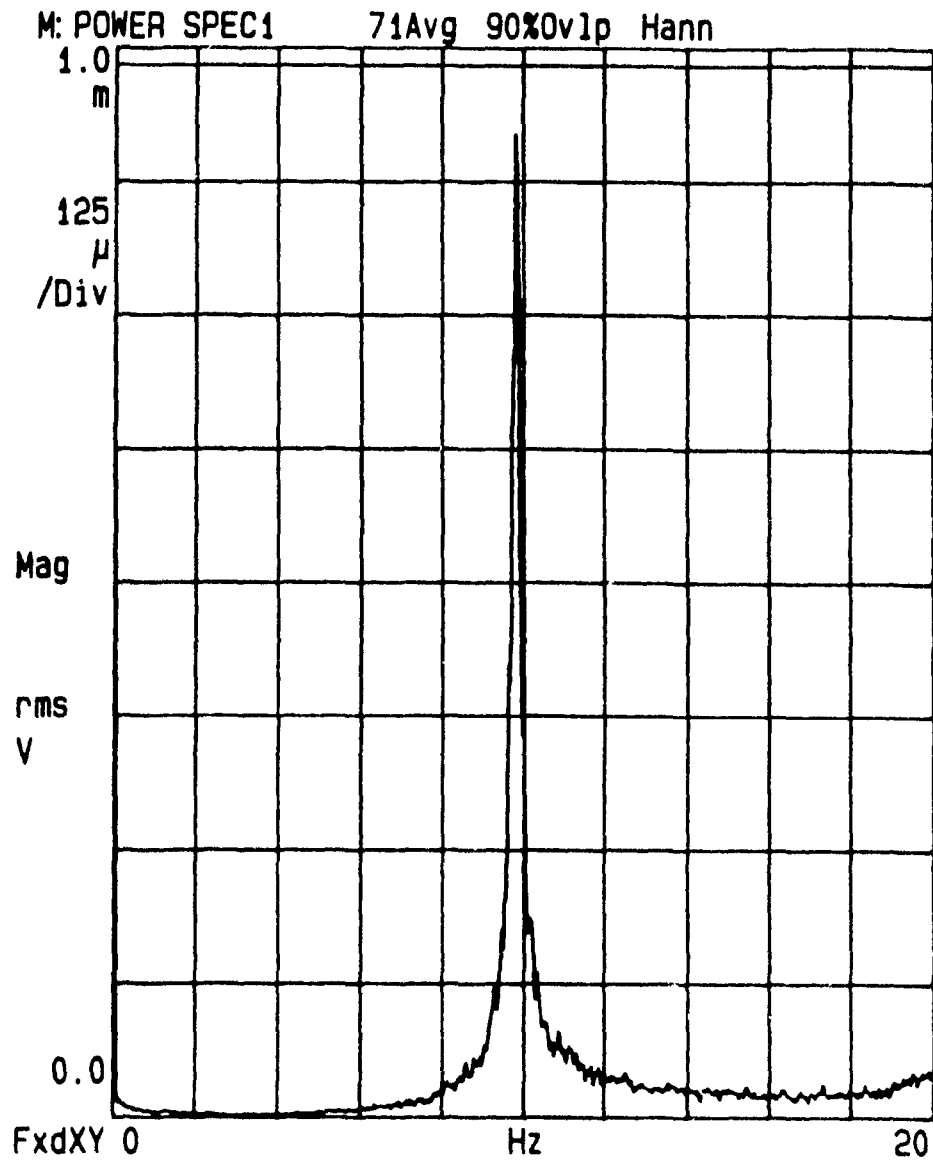


Figure 4.2: Typical vibrational acceleration power spectra for a single flexible cylinder

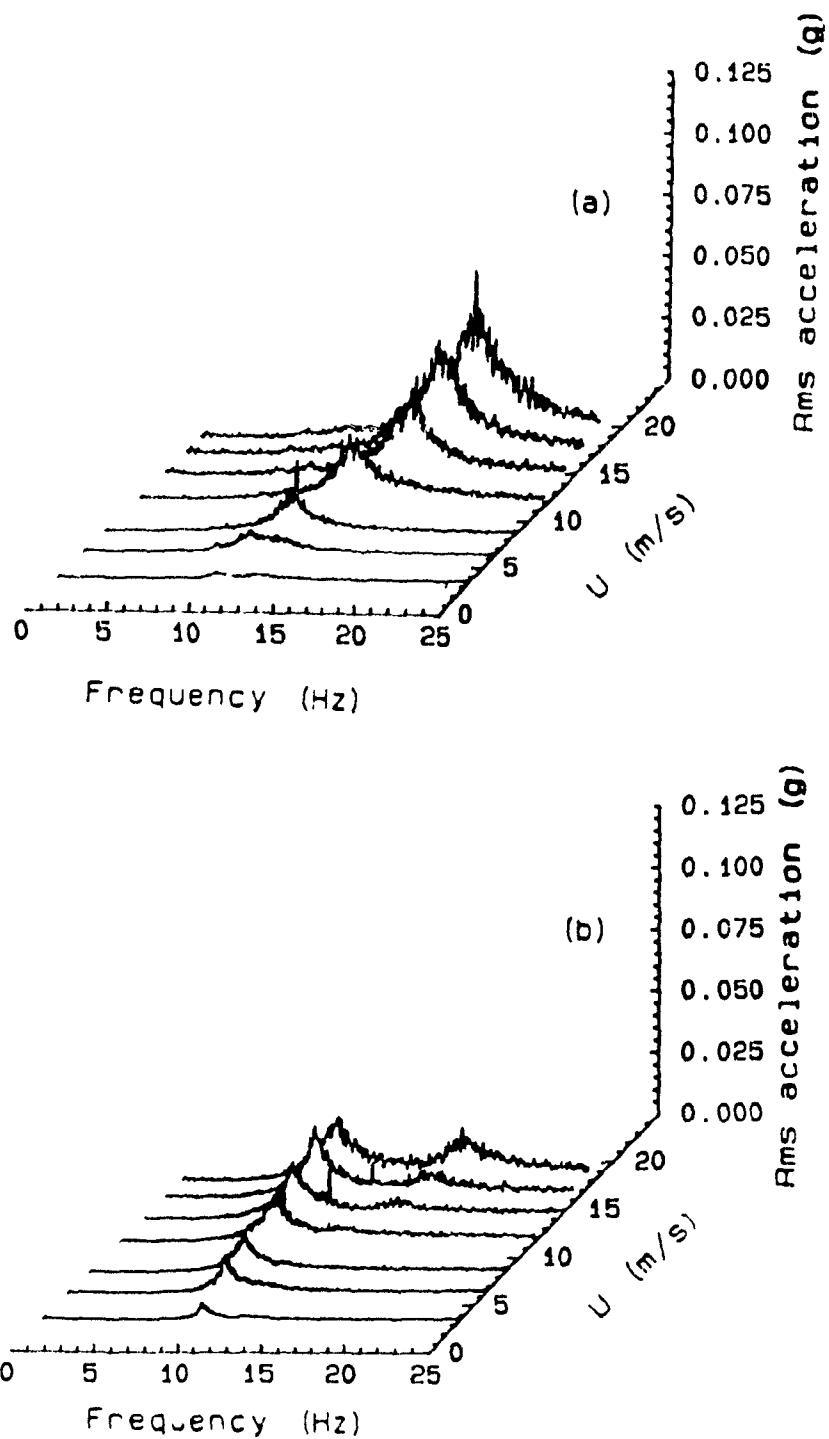


Figure 1.3. Variation of the in-flow (a) and cross-flow (b) vibrational power spectra with flow velocity, ($U_{\infty}/f_n d$ (single-flexible-cylinder in the fourth row, $\bar{m} = 280$, $f_3 = 10$ Hz and $\delta = 0.014$).

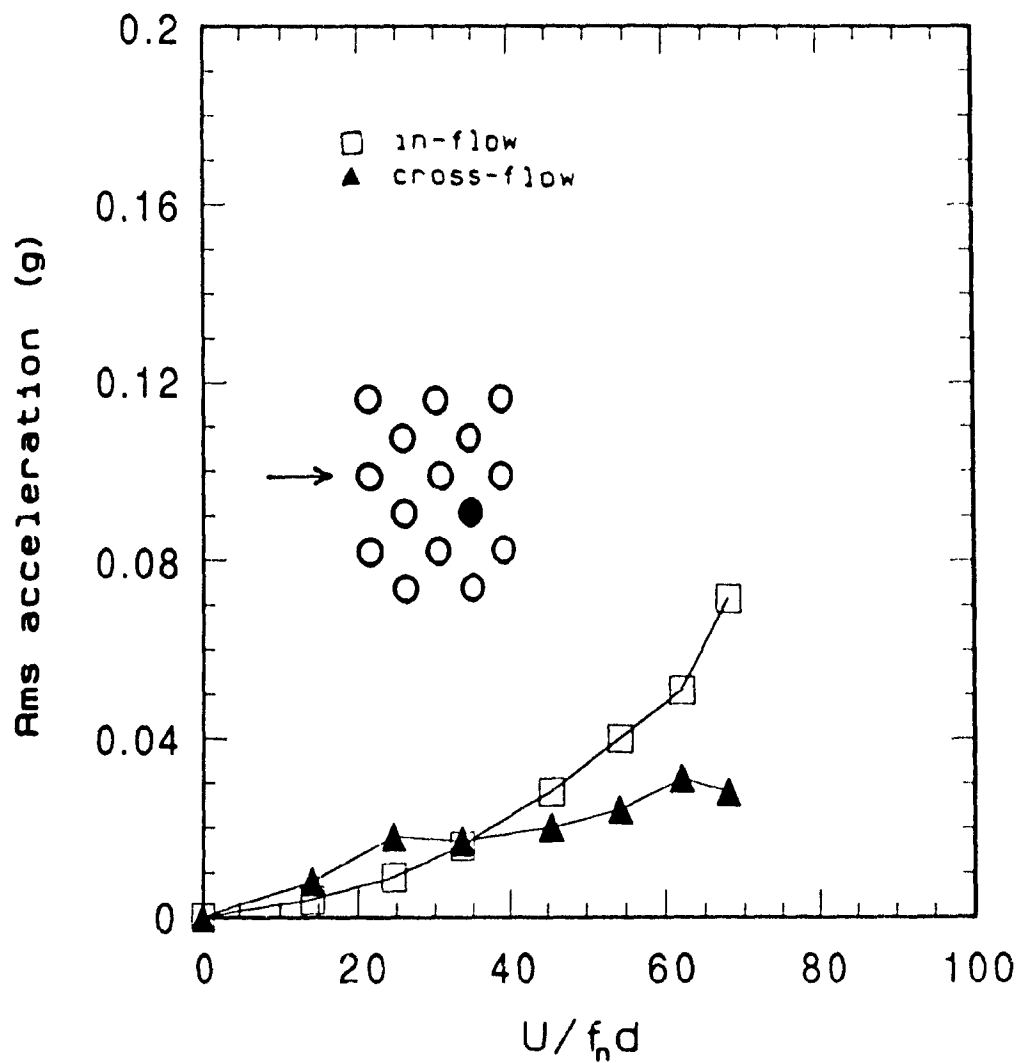


Figure 4.4: Rms vibrational acceleration of cylinder 1 as a function of the non-dimensional flow velocity, $U/f_n d$ (single flexible cylinder in the fourth row $m = 280$, $f_3 = 10$ Hz and $\delta = 0.014$).

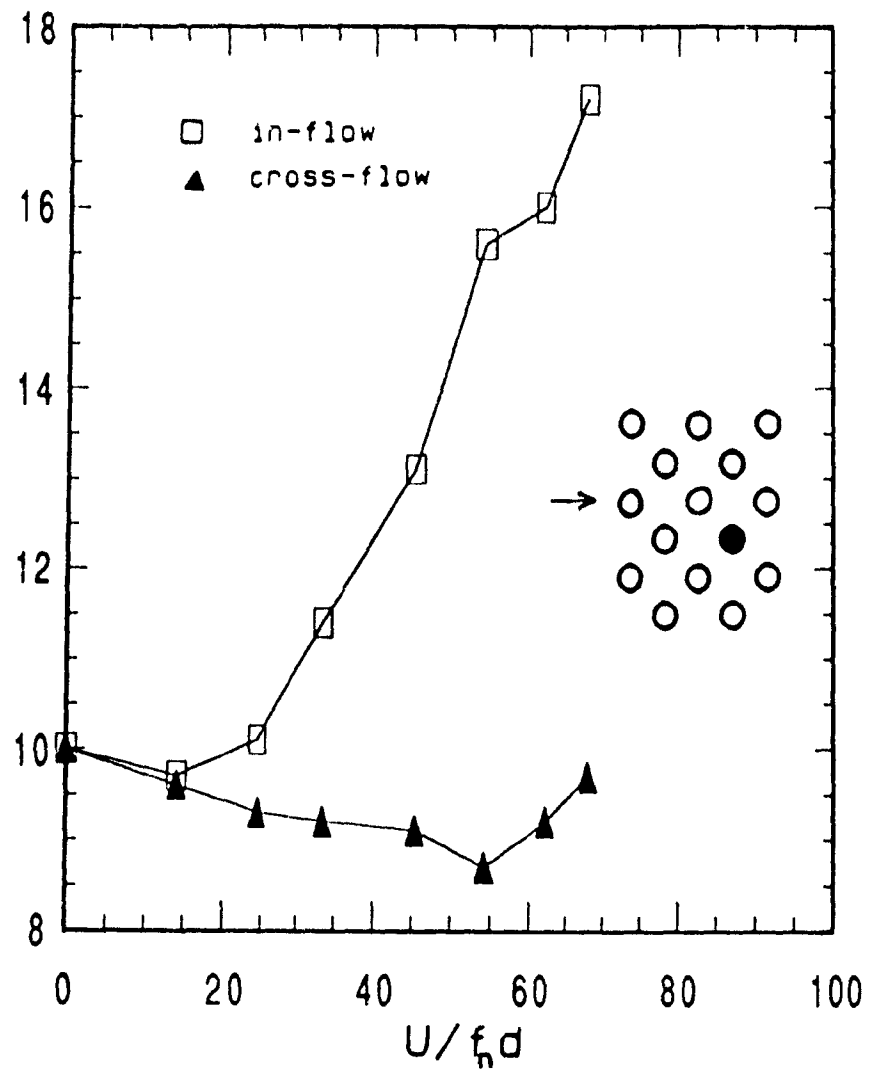


Figure 4.5 Variation of the fluidelastic frequencies of cylinder 3 with the non-dimensional flow velocity, $U/f_n d$ (single flexible cylinder in the fourth row, $\bar{m} = 280$, $f_3 = 10$ Hz and $\delta = 0.014$).

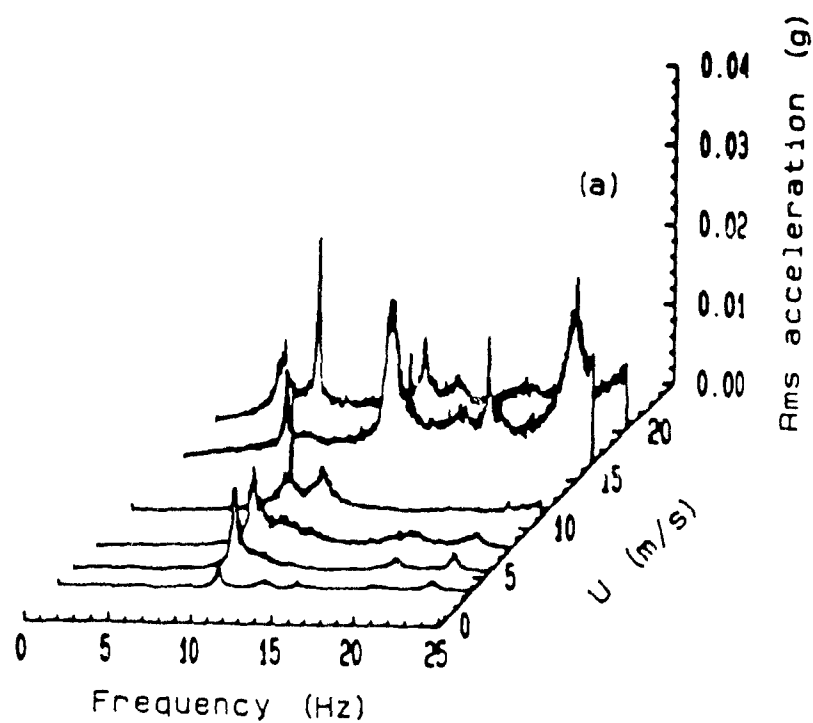


Figure 1.6: Variation of the in-flow vibrational power spectra with flow velocity for cylinder 1 (two-flexible cylinders - 1 and 3 -, $\bar{m} = 280$, $f_1 = f_3 = 10$ Hz and $\delta = 0.014$).

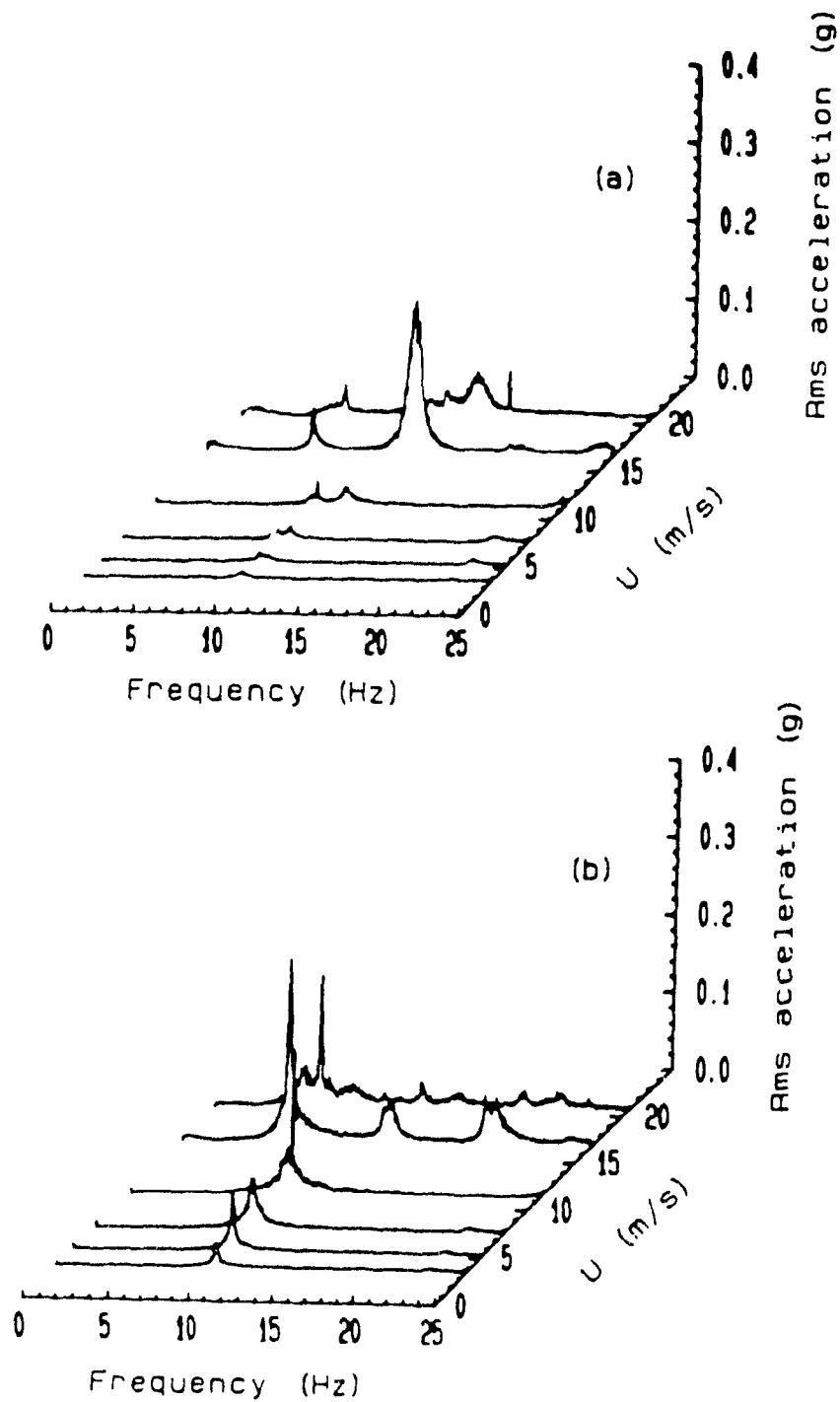


Figure 17 Variation of the in-flow (a) and cross-flow (b) vibration power spectra with flow velocity for cylinder 3 (two-flexible cylinders - 1 and 3 -, $\bar{m} = 280$, $f_1 = f_3 = 10$ Hz and $\delta = 0.014$).

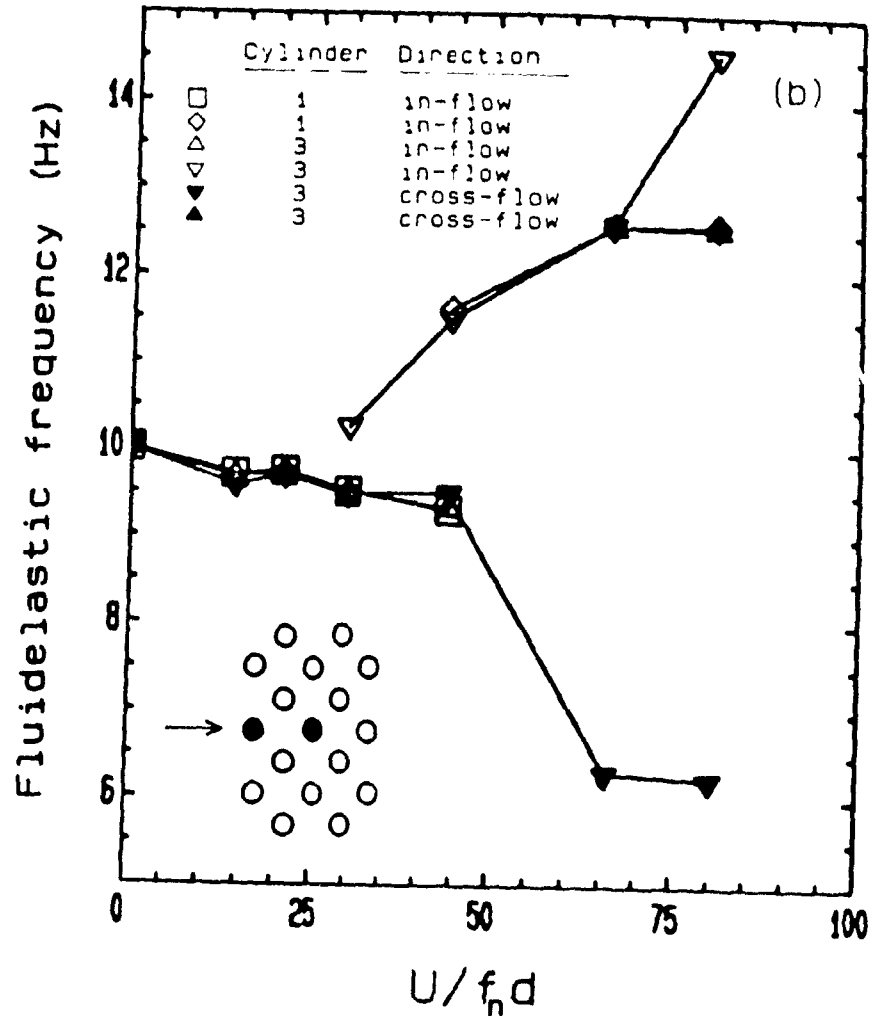


Figure 4.8: Variation of the major fluidelastic frequencies of cylinders 1 and 3 with non-dimensional flow velocity (two-flexible cylinders 1 and 3, $m = 280$, $f_1 = f_3 = 10$ Hz and $\delta = 0.011$)

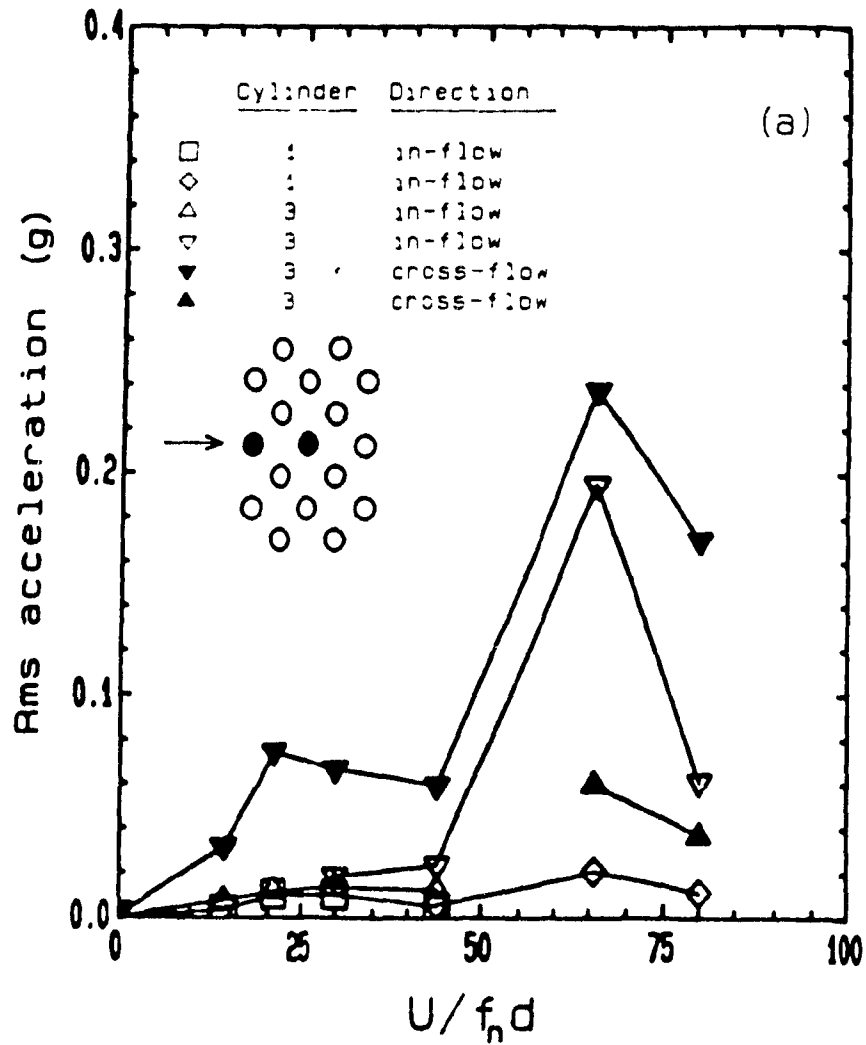


Figure 19. Rms acceleration of cylinders 1 and 3 at major fluidelastic frequencies as a function of the non-dimensional flow velocity. (Two-flexible cylinders - 1 and 3 -, $m = 280$, $f_1 = f_3 = 10$ Hz and $\delta = 0.014$.)

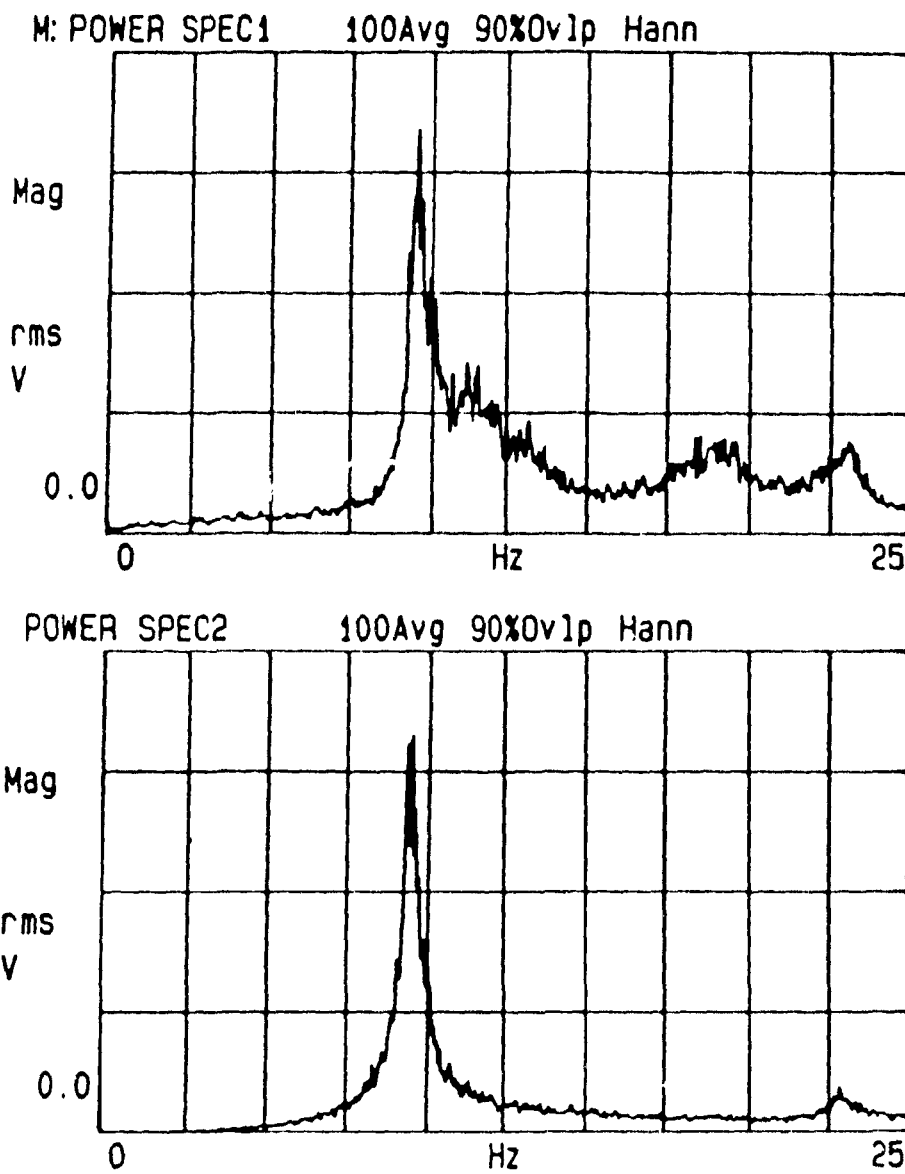


Figure 4.10: vibrational acceleration power spectra of cylinders 1 and 3 at $U_{\infty} = 7.8$ m/s (two-flexible cylinders - 1 in-flow -, - 3 cross-flow -, $m = 280$, $f_1 = f_3 = 10$ Hz and $\delta = 0.014$).

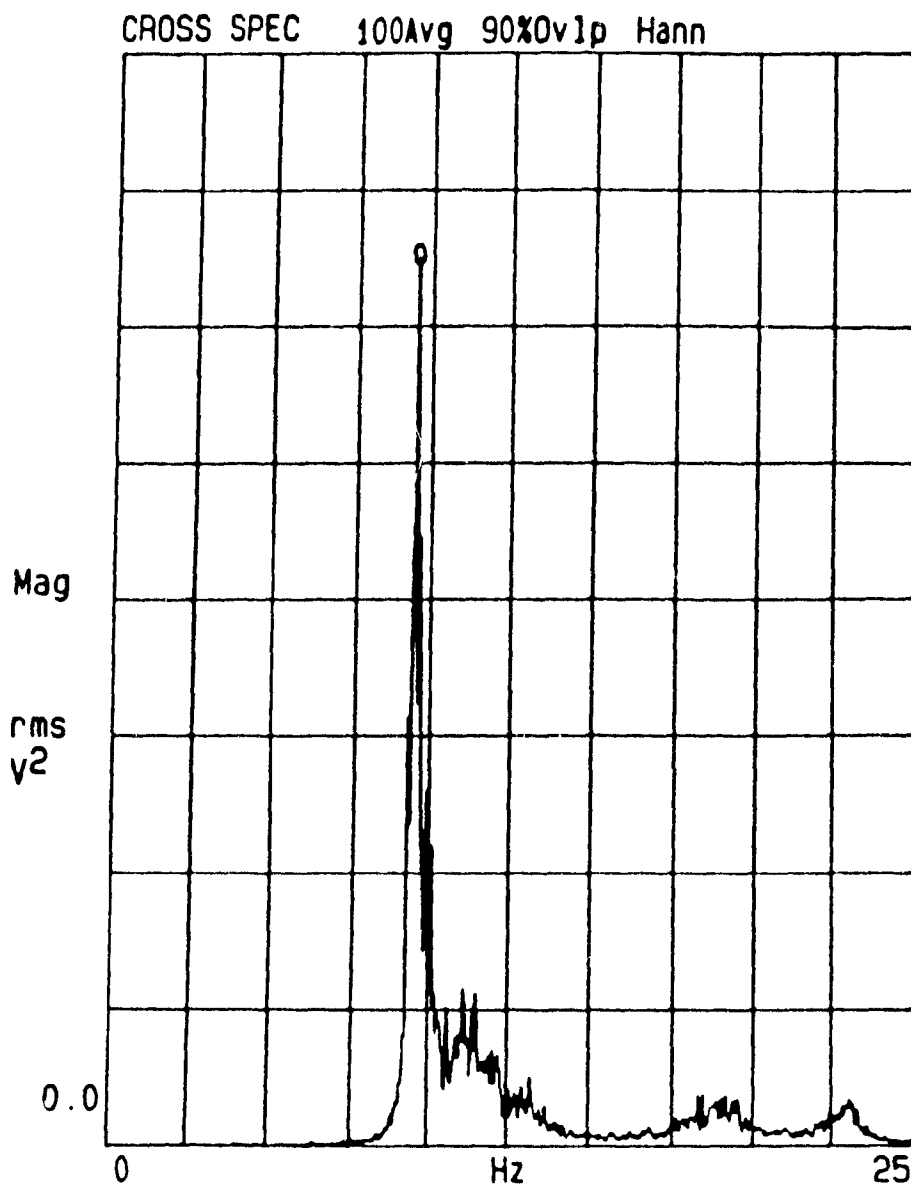


Figure 4.11. acceleration cross-spectra of cylinders 1 and 3 at
 $U_{\infty} = 7.8$ m/s (two-flexible cylinders -1 in-flow -, - 3 cross-flow -, $\bar{m} = 280$,
 $f_1 = f_3 = 10$ Hz and $\delta = 0.014$).

X=9.531 Hz

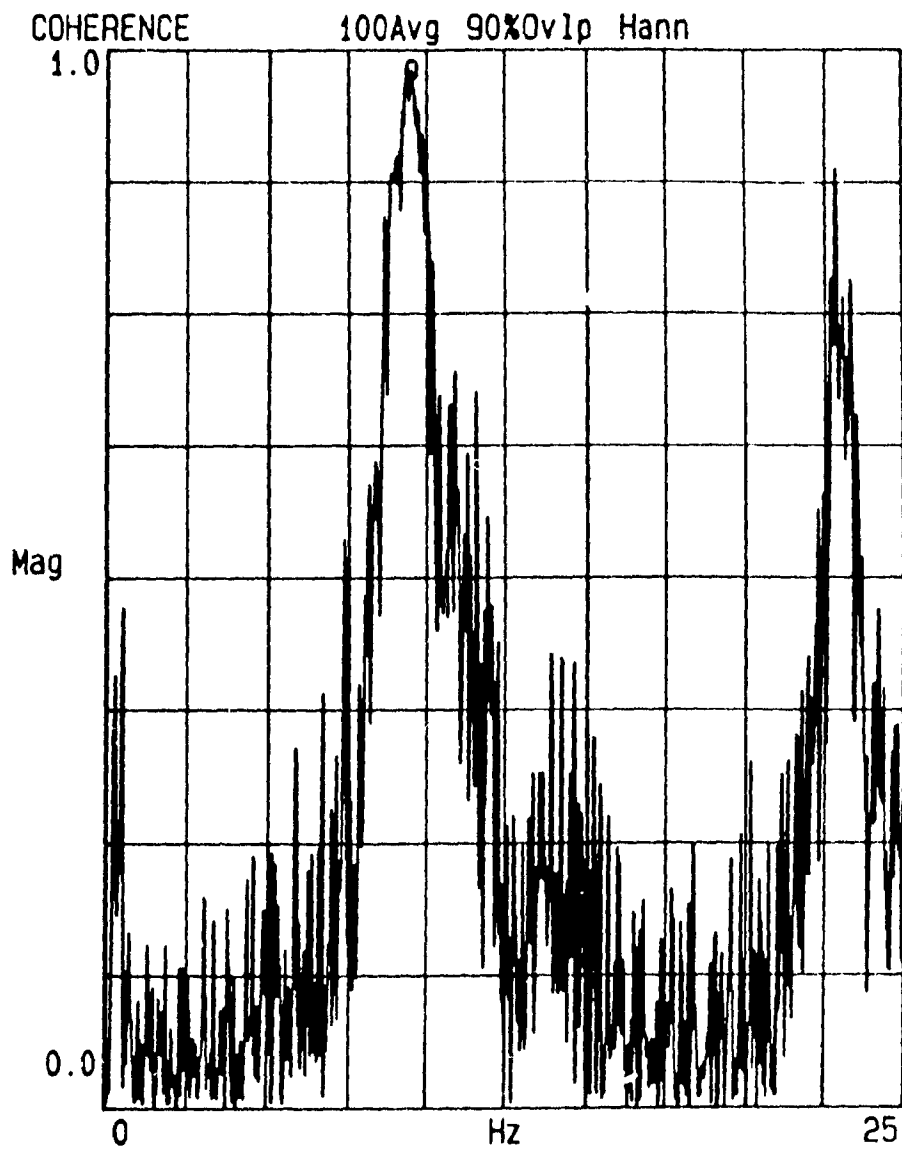


Figure 4.12: Coherence between the signals of cylinders 1 and 3 at $U_{\infty} = 7.8$ m/s (two-flexible cylinders -1 in-flow -, - 3 cross-flow -, $m = 280$, $f_1 = f_3 = 10$ Hz and $\delta = 0.014$).

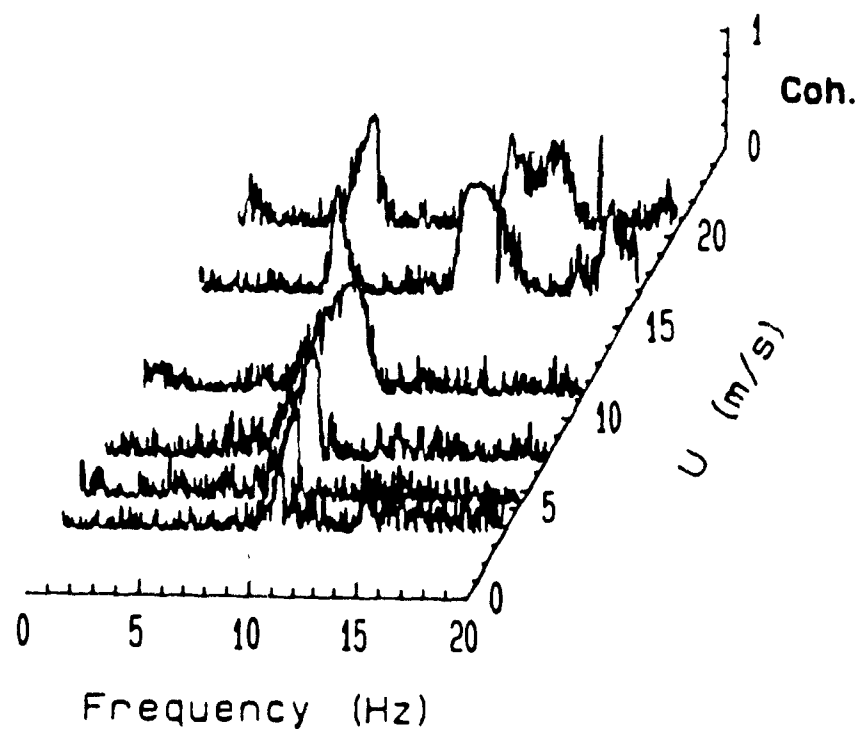


Figure 4.13: Coherence between the in-flow vibration signals of cylinders 1 and 3 at different flow velocities (two-flexible cylinders - 1 and 3 -, $\bar{m} = 280$, $f_1 = f_3 = 10$ Hz and $\delta = 0.011$).

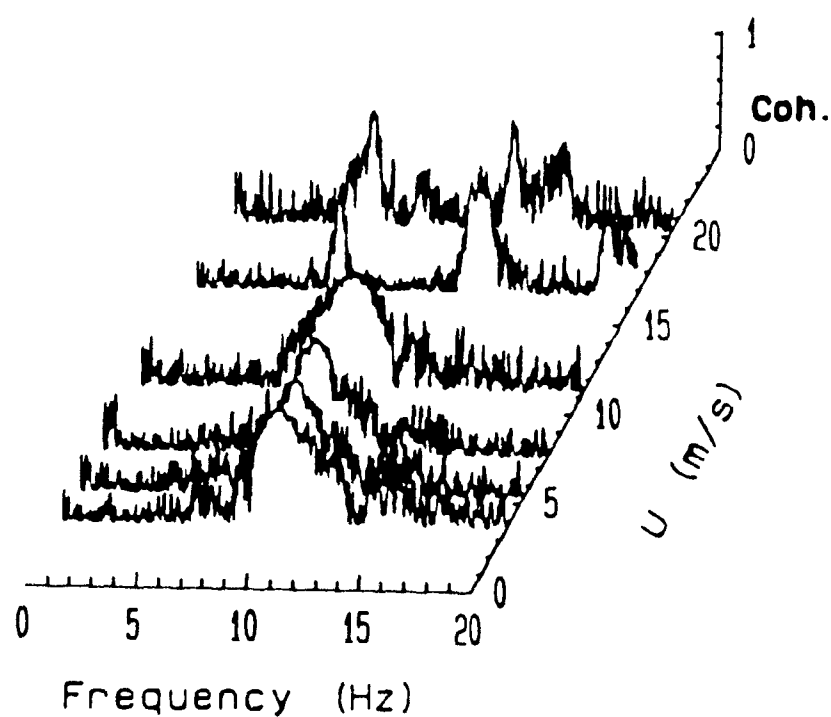


Figure 4.14: Coherence between the in-flow signal of cylinder 1 and the cross-flow signal of cylinder 3 at different flow velocities (two-flexible-cylinders 1 and 3, $\bar{m} = 280$, $f_1 = f_3 = 10$ Hz and $\delta = 0.014$).

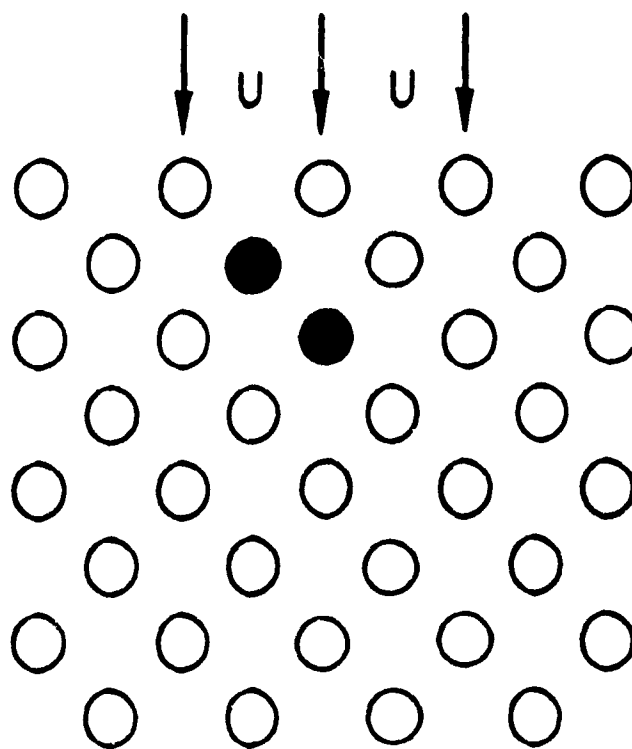


Figure 4.15: A two-flexible cylinder configuration with flexible cylinders in the second and third rows of the array.

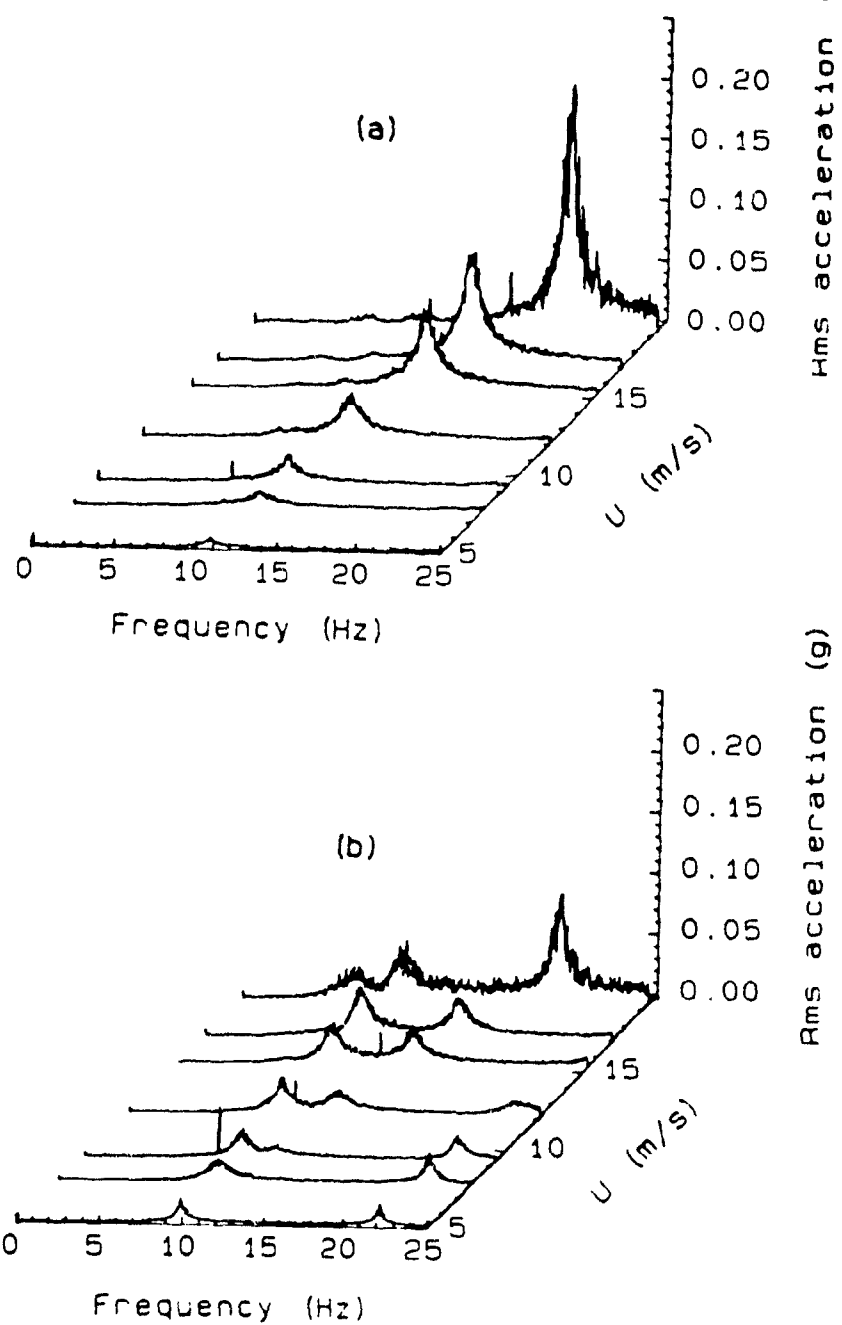


Figure 4.16. Variation of the in-flow (a) and cross-flow (b) vibration power spectra with flow velocity for cylinder 2 (two-flexible cylinders -2 and 3 -, $m = 280$, $f_2 = f_3 = 10$ Hz and $\delta = 0.014$).

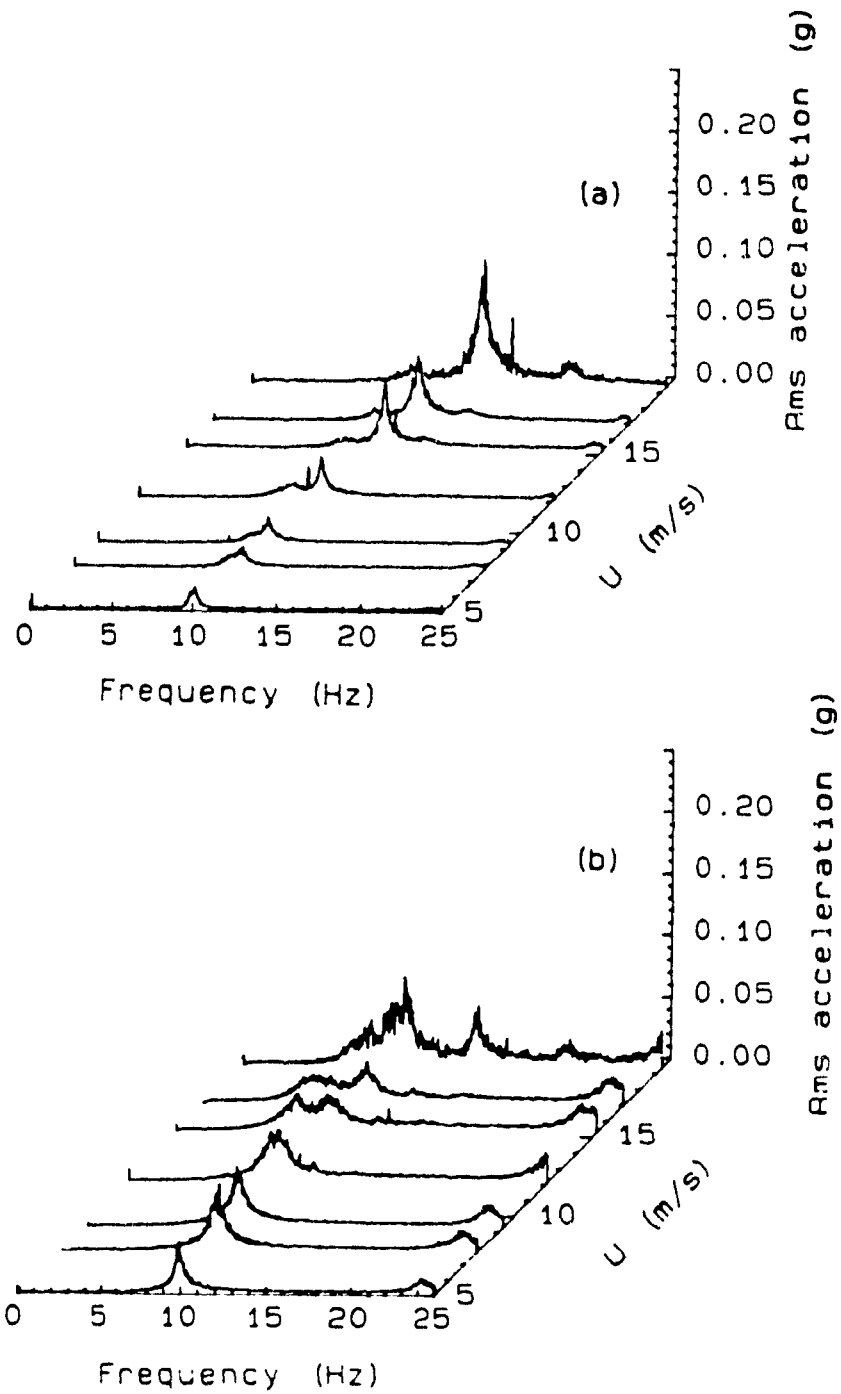


Figure 4.17: Variation of the in-flow (a) and cross-flow (b) vibration power spectra with flow velocity for cylinder 3 (two-flexible cylinders - 2 and 3, $m = 280$, $f_2 = f_3 = 10$ Hz and $\delta = 0.014$).

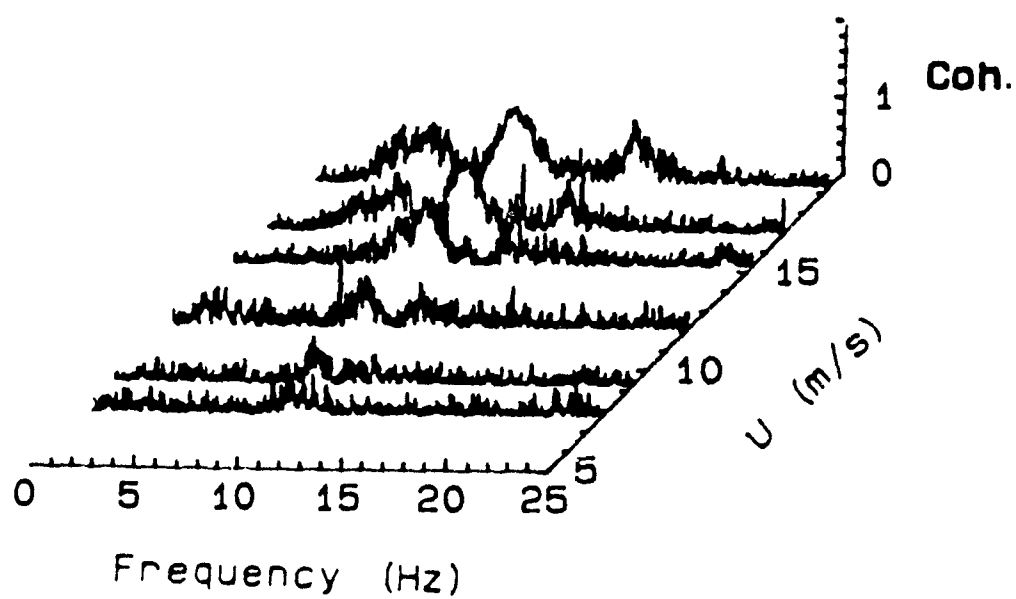


Figure 4.18: Coherence between the cross-flow vibration signals of cylinders 2 and 3 at different flow velocities (two-flexible cylinders - 2 and 3 -, $\bar{m} = 280$, $f_2 = f_3 = 10$ Hz and $\delta = 0.014$).

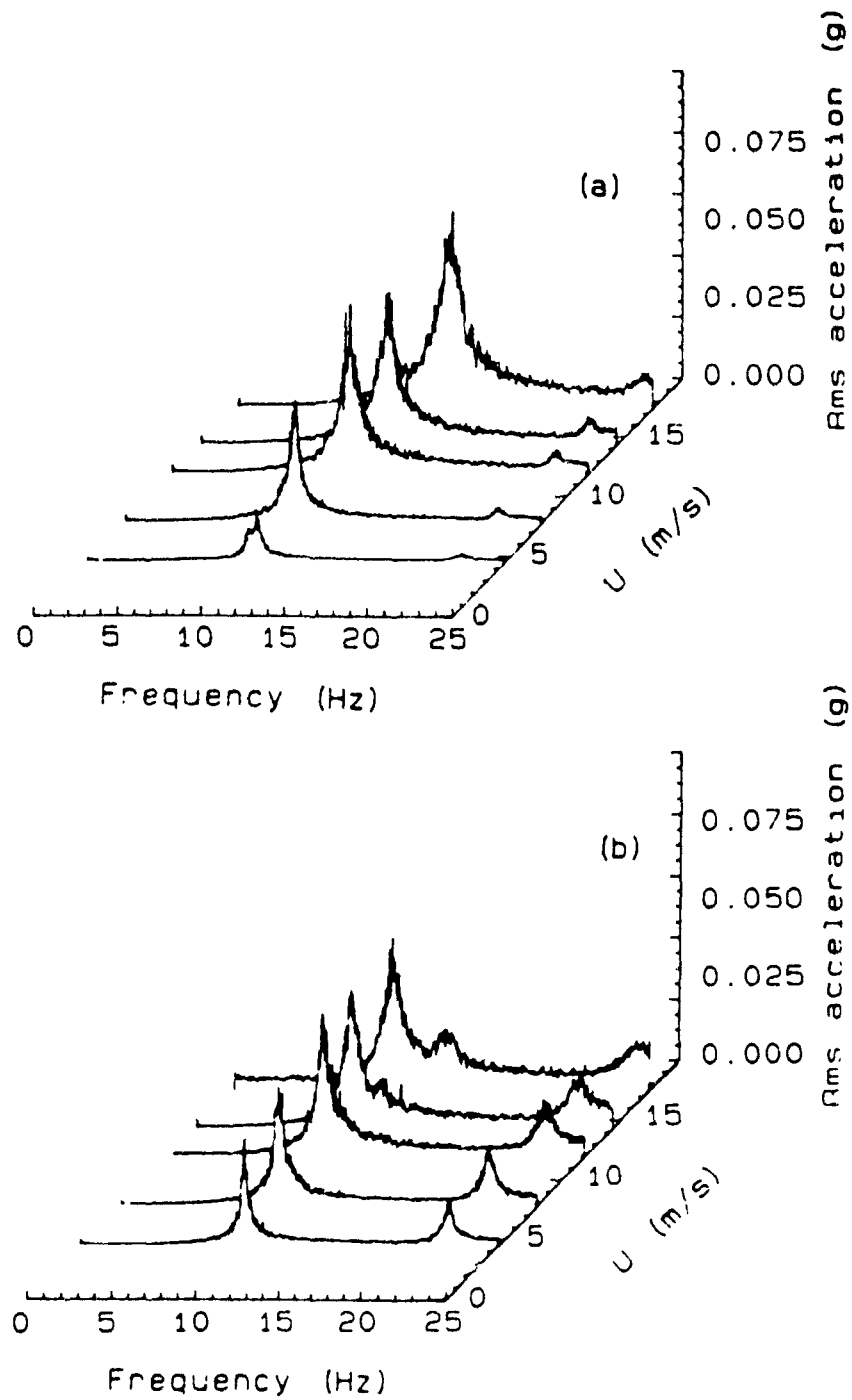


Figure 4.19: Variation of the in-flow (a) and cross-flow (b) vibration power spectra with flow velocity for cylinder 4 (two-flexible cylinders -4 and 6 -, $\bar{m} = 280$, $f_4 = f_6 = 10$ Hz and $\delta = 0.014$).

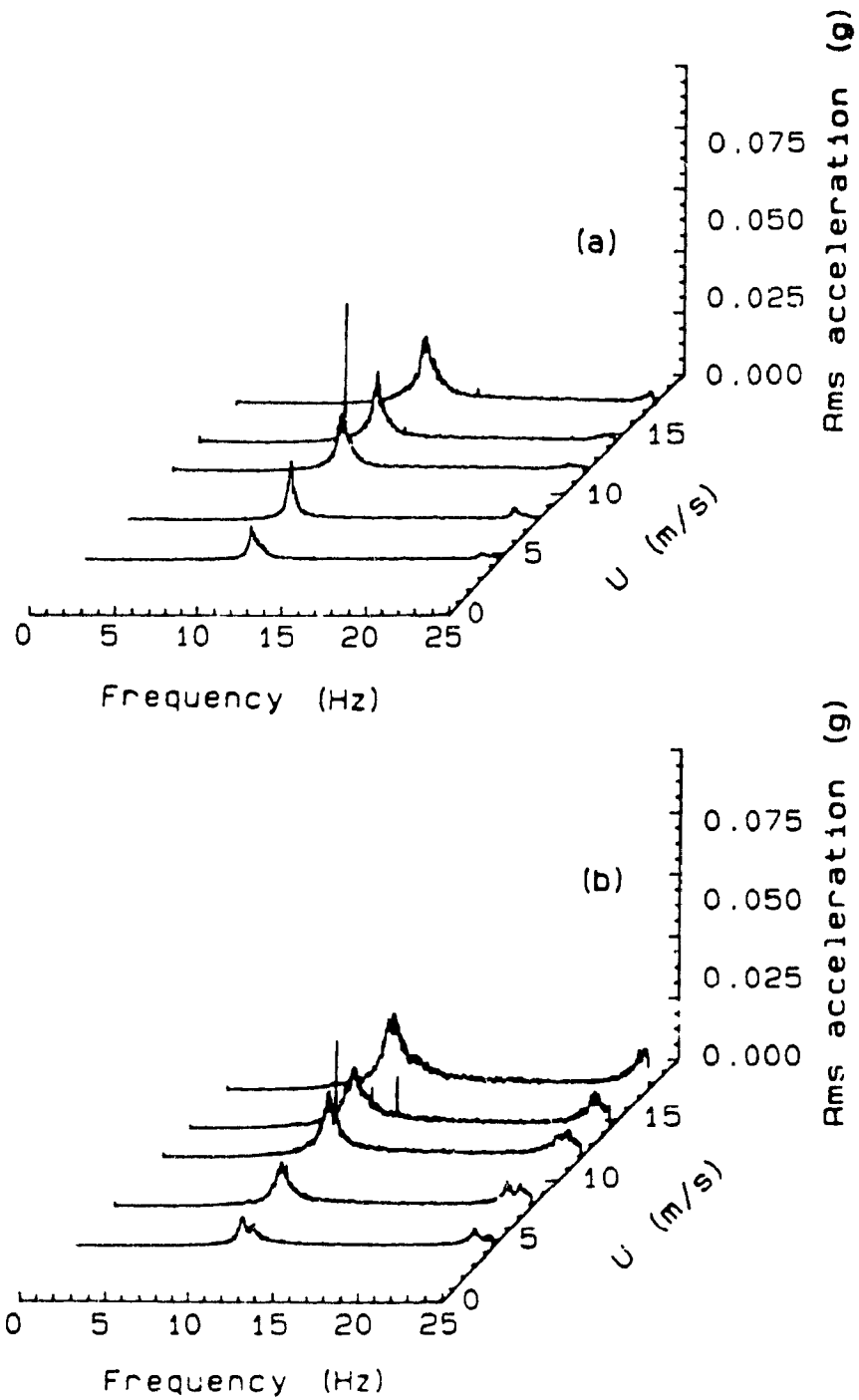


Figure 1.20: Variation of the in-flow (a) and cross-flow vibration power spectra with flow velocity for cylinder 6 (two-flexible cylinders - 4 and 6 -, $\bar{m} = 280$, $f_4 = f_6 = 10$ Hz and $\delta = 0.014$).

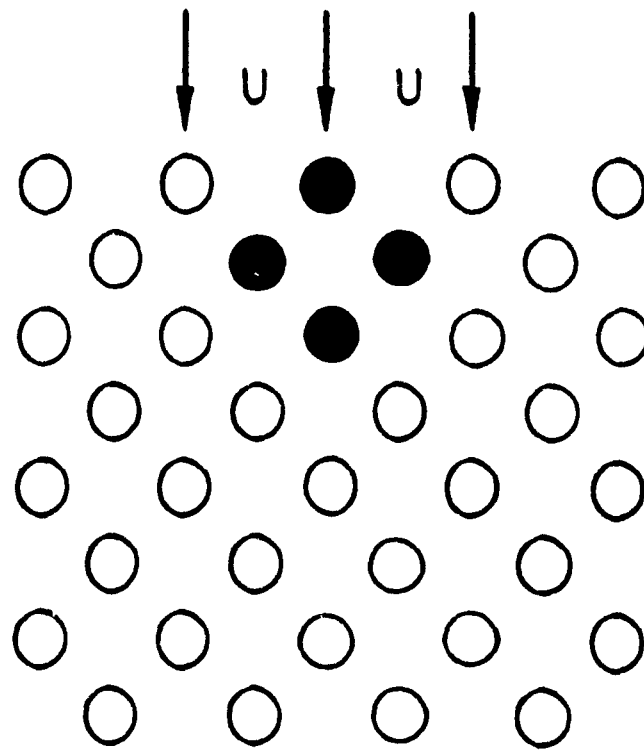


Figure 4 21 A four-flexible cylinder configuration in the upstream rows of the array

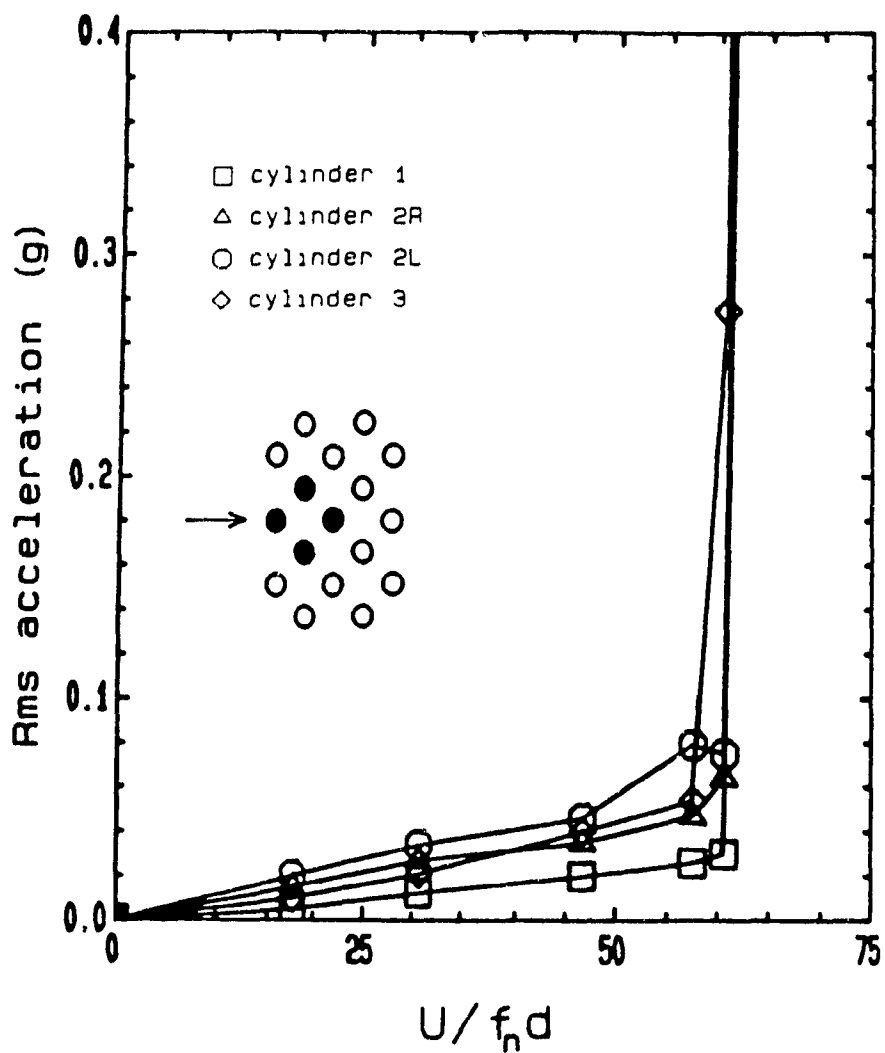


Figure 4.22: In-flow directional rms acceleration of cylinders 1, 2R, 2L and 3 at their major fluidelastic frequencies as a function of the non-dimensional flow velocity (four-flexible cylinders - 1, 2R, 2L and 3 -, $\bar{m} = 280$, $f_1 = f_{2R} = f_{2L} = f_3 = 10$ Hz and $\delta = 0.014$)

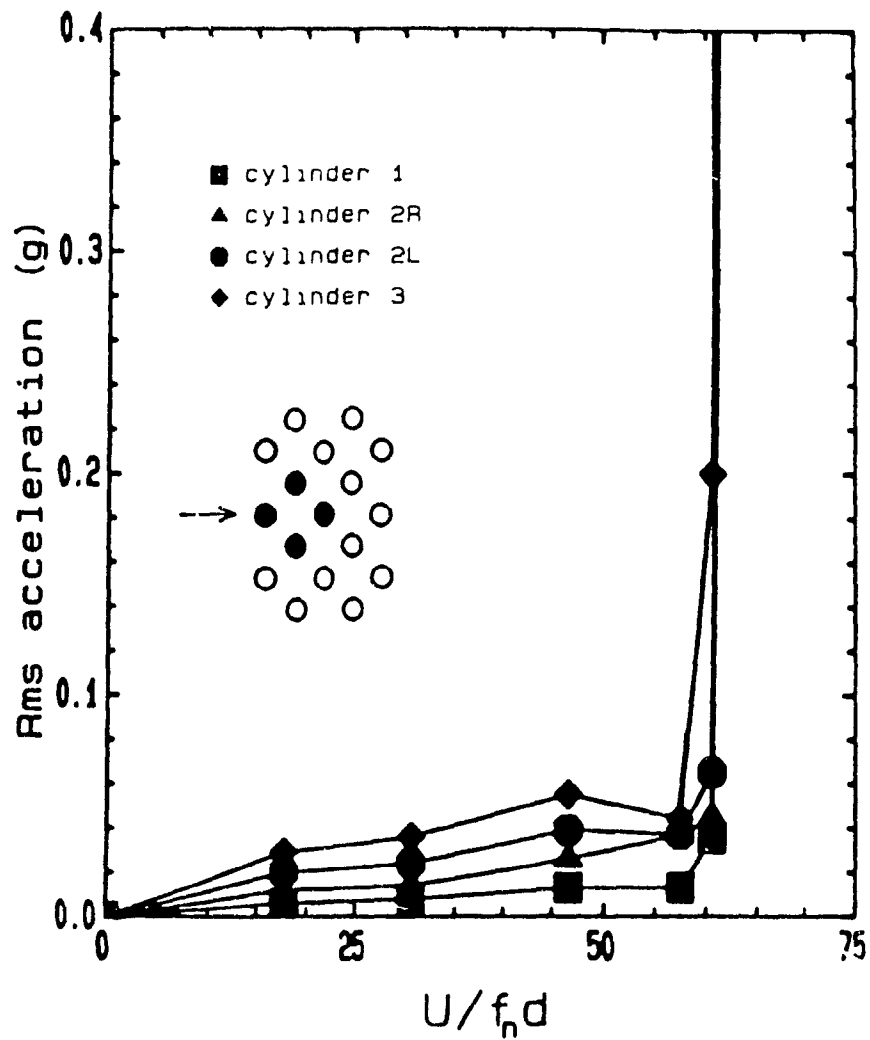


Figure 4.23: Cross-flow directional rms acceleration of cylinders 1, 2R, 2L and 3 at their major fluidelastic frequencies as a function of the non-dimensional flow velocity (four-flexible cylinders - 1, 2R, 2L and 3 -, $\bar{m} = 280$, $f_1 = f_{2R} = f_{2L} = f_3 = 10$ Hz and $\delta = 0.014$).

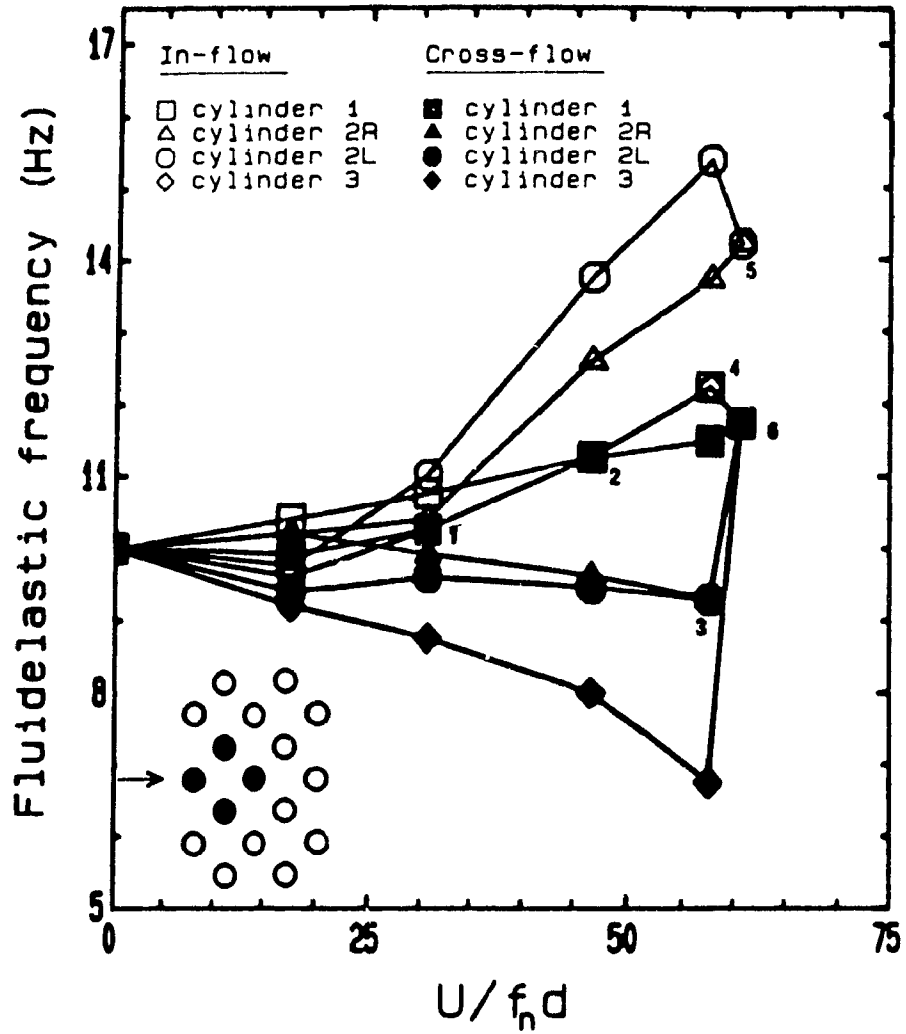


Figure 4.24: Variation of the major fluidelastic frequencies of cylinders 1, 2R, 2L and 3 with non-dimensional flow velocity (four-flexible cylinders - 1, 2R, 2L and 3 -, $\bar{m} = 280$, $f_1 = f_{2R} = f_{2L} = f_3 = 10$ Hz and $\delta = 0.014$).

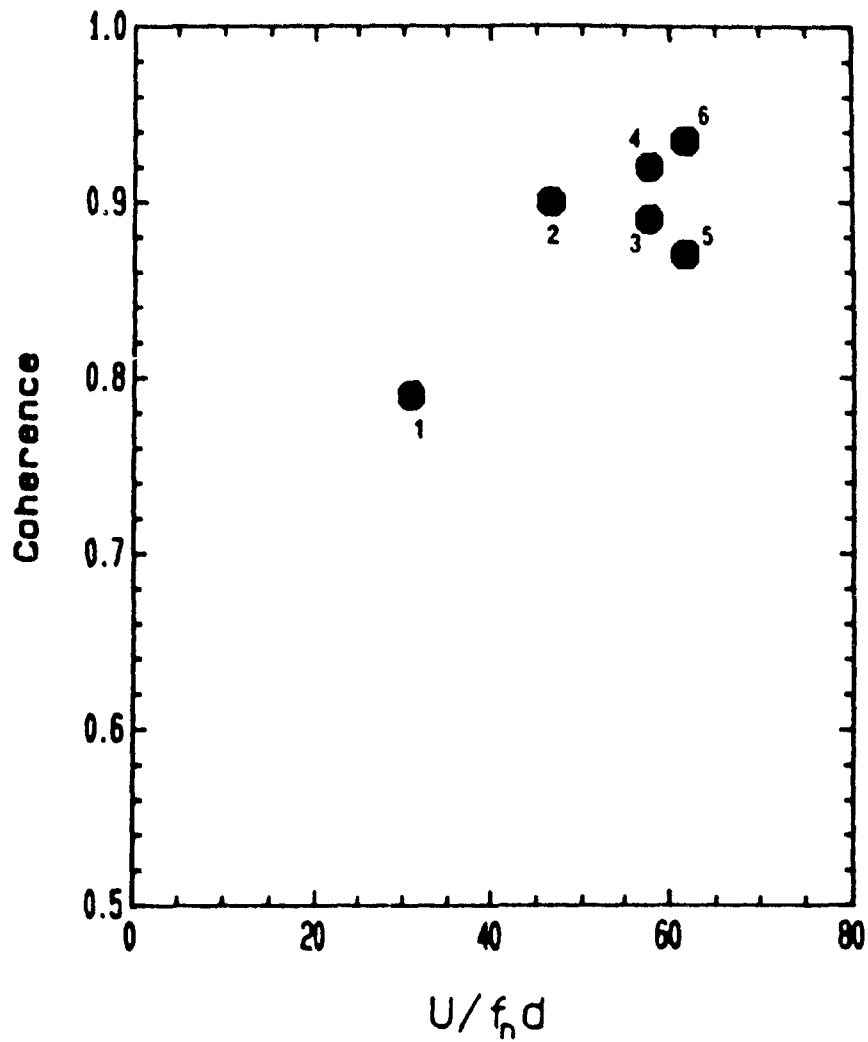


Figure 4.25. Coherence between the motion of flexible cylinders at different non-dimensional flow velocities (four-flexible cylinders = 1, 2R, 2L, and 3; $m = 280$, $f_1 = f_{2R} = f_{2L} = f_3 = 10$ Hz and $\delta = 0.014$).

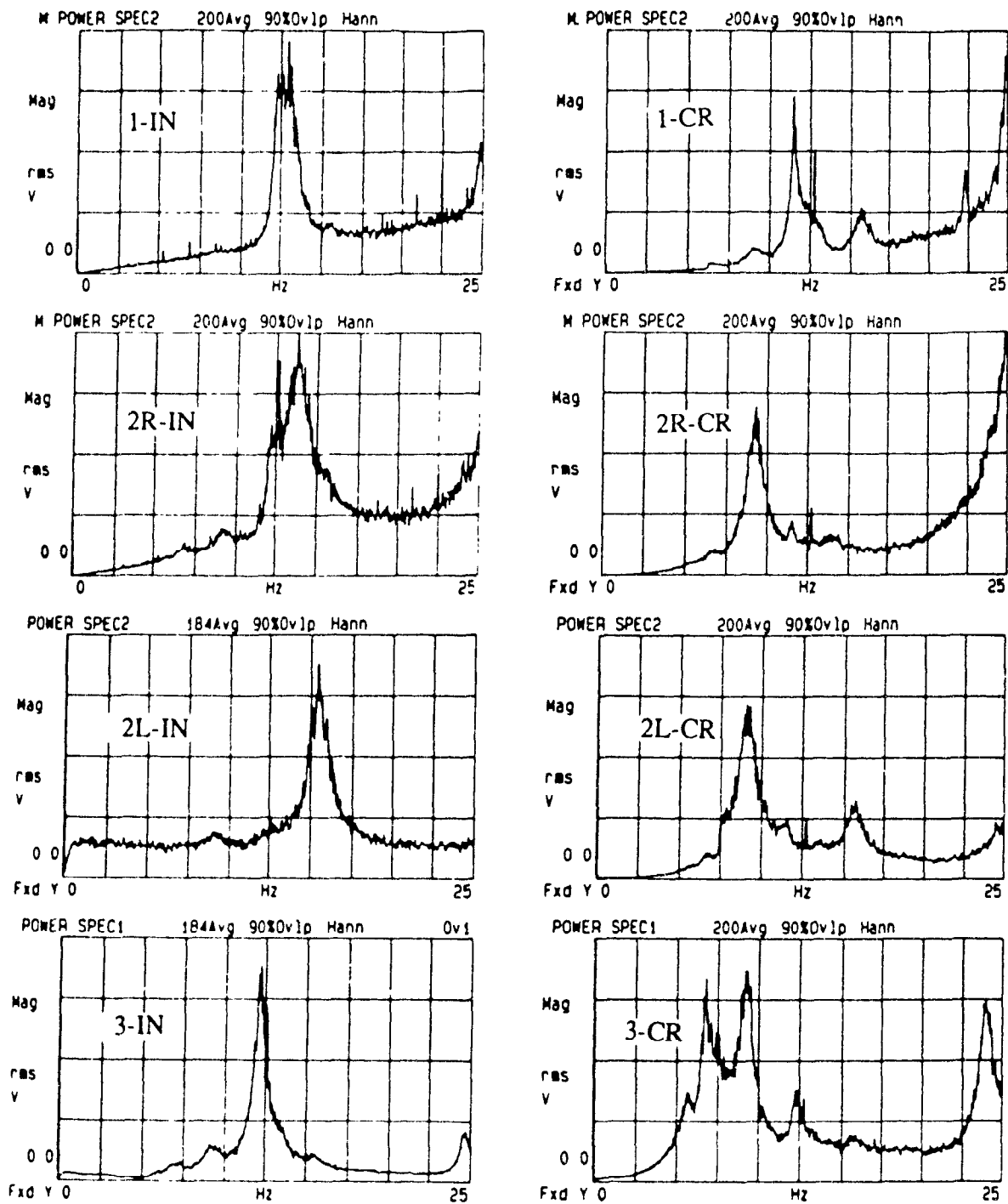


Figure 4.26 Acceleration power spectra of cylinders 1, 2R, 2L and 3 in the in- and cross-flow directions at $U/f_n d \approx 57.5$ (four-flexible cylinders - 1, 2R, 2L and -, $\bar{m} = 280$, $f_1 = f_{2R} = f_{2L} = f_3 = 10$ Hz and $\delta = 0.014$).

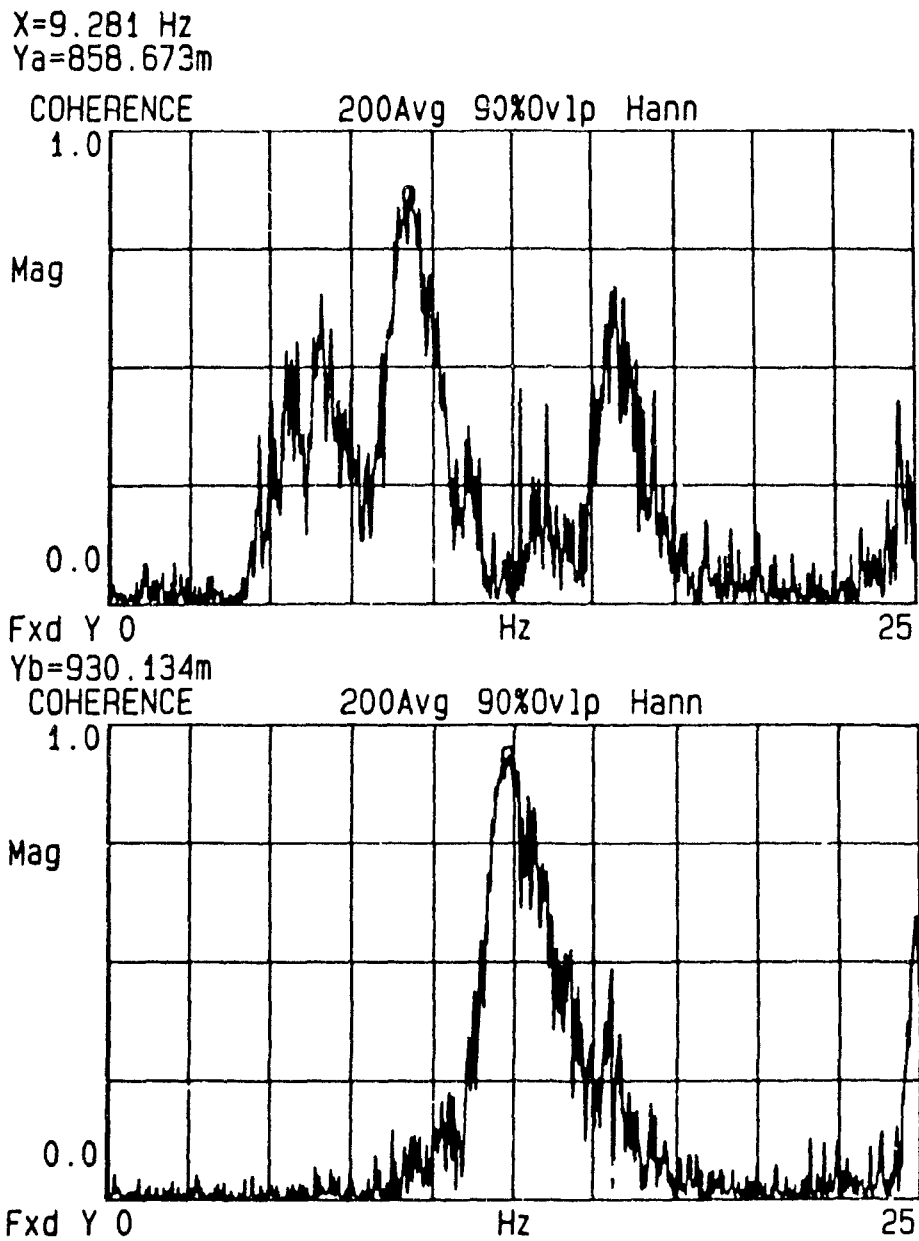


Figure 1.27: Coherence between the cross-flow signals of cylinders 3 and 2L (a) and between in-flow signals of cylinders 3 and 1 at $U/f_n d \approx 57.5$ (four-flexible cylinder - 1, 2R, 2L and 3 -, $\bar{m} = 280$, $f_1 = f_{2R} = f_{2L} = f_3 = 10$ Hz and $\delta = 0.014$)

X=9.281 Hz

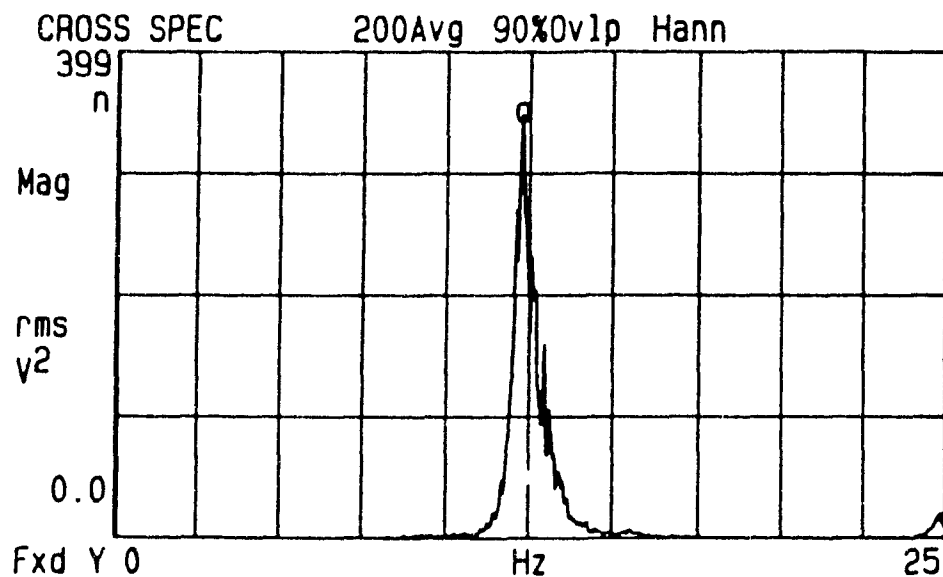
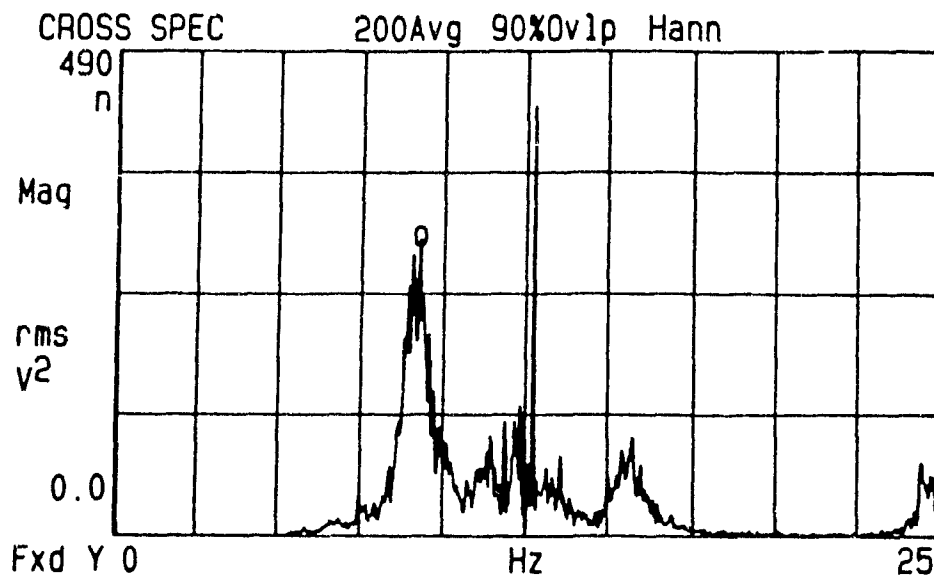


Figure 128 Cross-spectra between the cross-flow signals of cylinders 3 and 2L (a) and between the in-flow signals of cylinders 3 and 1 at $U/f_n d \approx 57.5$ four-flexible cylinders - 1, 2R, 2L and 3 -, $\bar{m} = 280$, $f_1 = f_{2R} = f_{2L} = f_3 = 10$ Hz and $\delta = 0.014$).

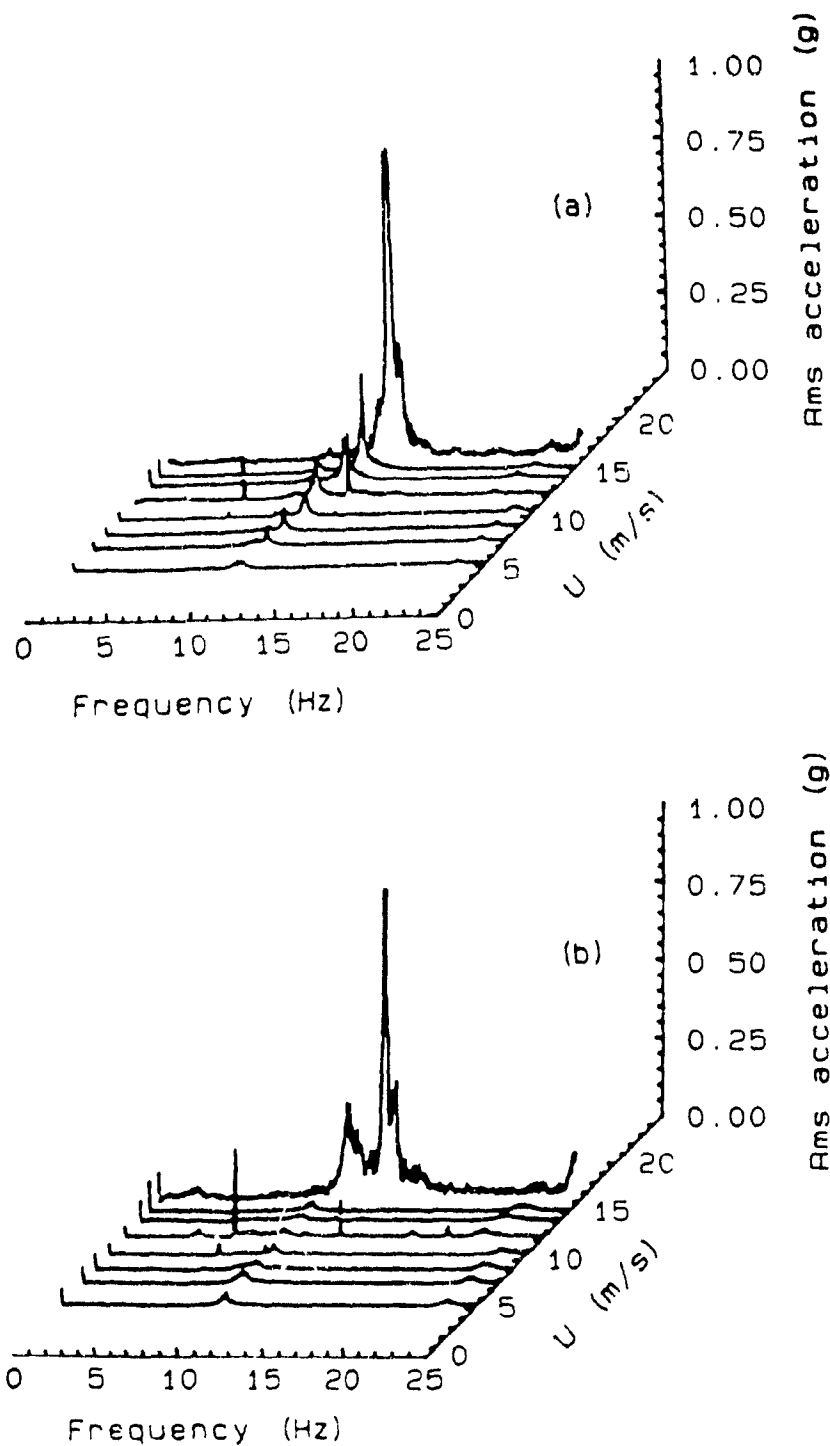


Figure 4.29: Variation of the in-flow (a) and cross-flow (b) power spectra with flow velocity for cylinder 3 (four-flexible cylinders - 1, 2R, 2L and 3, $m = 280$, $f_1 = f_{2R} = f_{2L} = f_3 = 10$ Hz and $\delta = 0.014$).

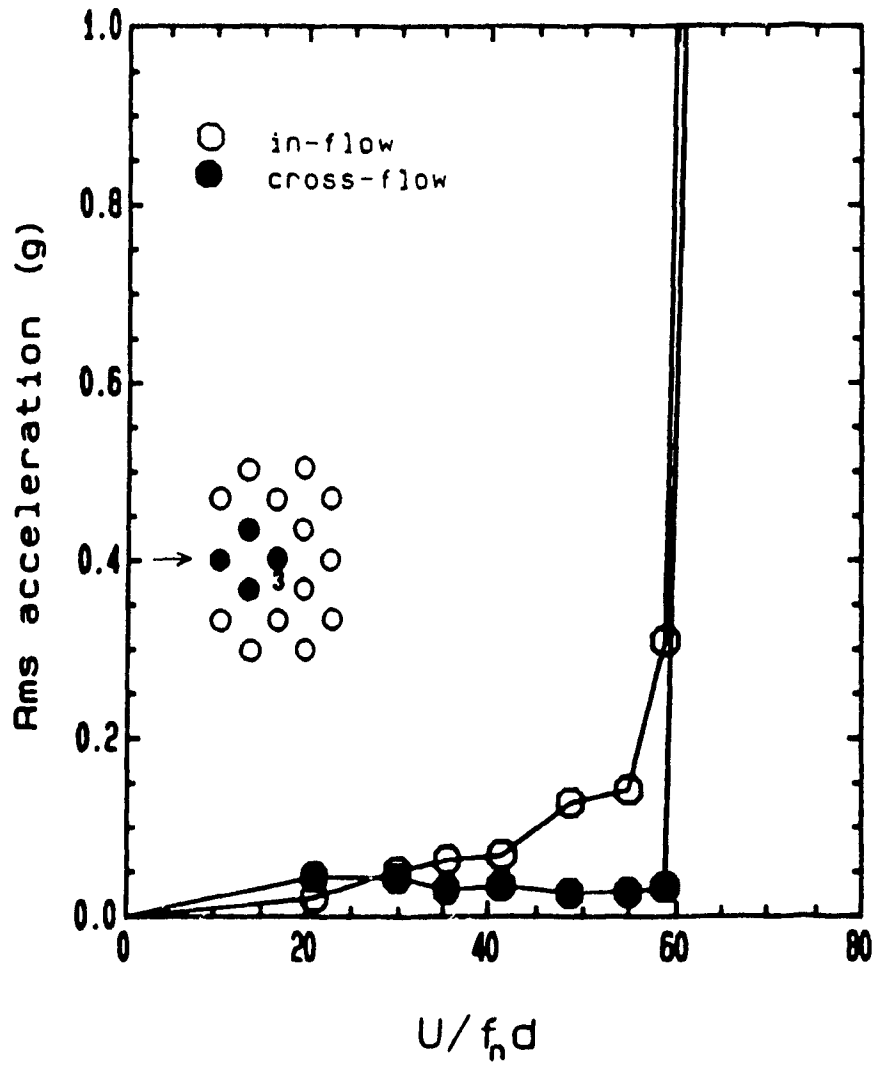


Figure 4.30: Rms acceleration of cylinder 3 at its major fluidelastic frequencies as a function of the non-dimensional flow velocity (four-flexible cylinders - 1, 2R, 2L and 3 -, $\bar{m} = 280$, $f_1 = f_{2R} = f_{2L} = f_3 = 10$ Hz and $\delta = 0.014$).

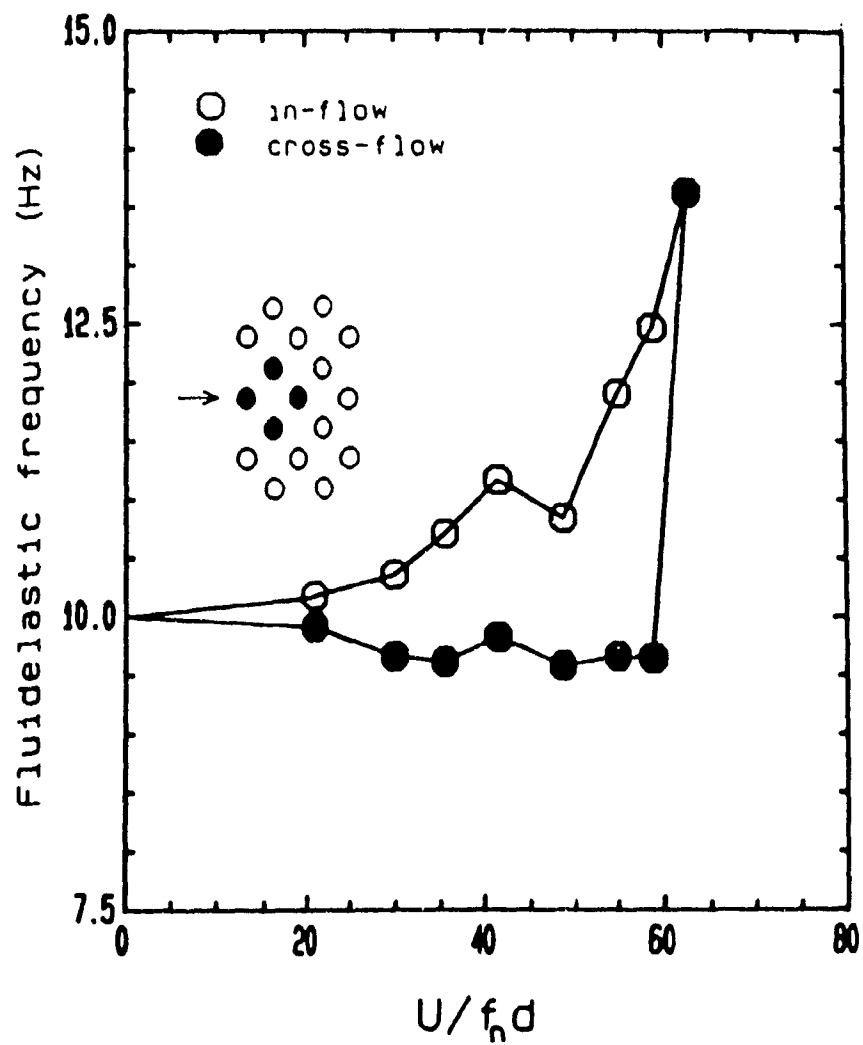


Figure 4.31: Variation of the major fluidelastic frequencies of cylinder 3 with non-dimensional flow velocity (four-flexible cylinders - 1, 2R, 2L and 3 -, $\bar{m} = 280$, $f_1 = f_{2R} = f_{2L} = f_3 = 10$ Hz and $\delta = 0.014$).

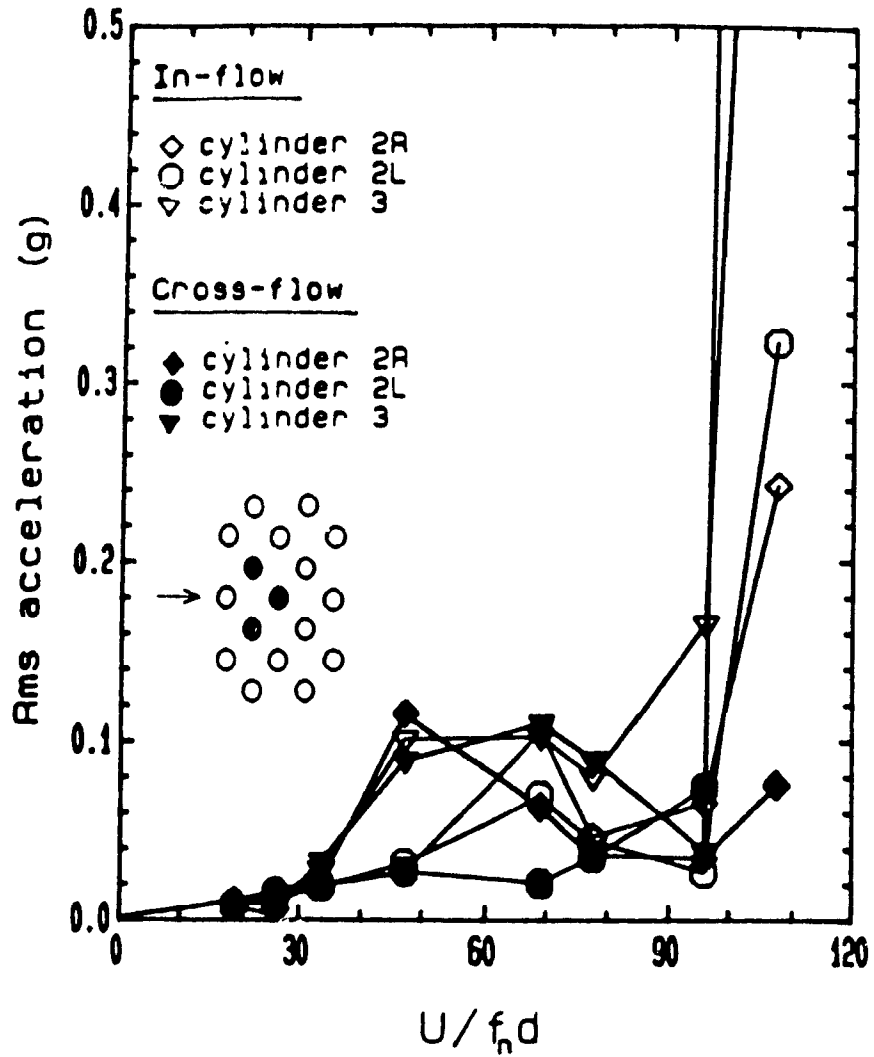


Figure 4 32: In- and cross-flow directional rms acceleration of cylinders 2R, 2L and 3 at their major fluidelastic frequencies as a function of the non-dimensional flow velocity (three-flexible cylinders - 2R, 2L and 3 -, $\bar{m}l = 280$, $f_{2R} = f_{2L} = f_3 = 7$ Hz and $\delta = 0.014$).

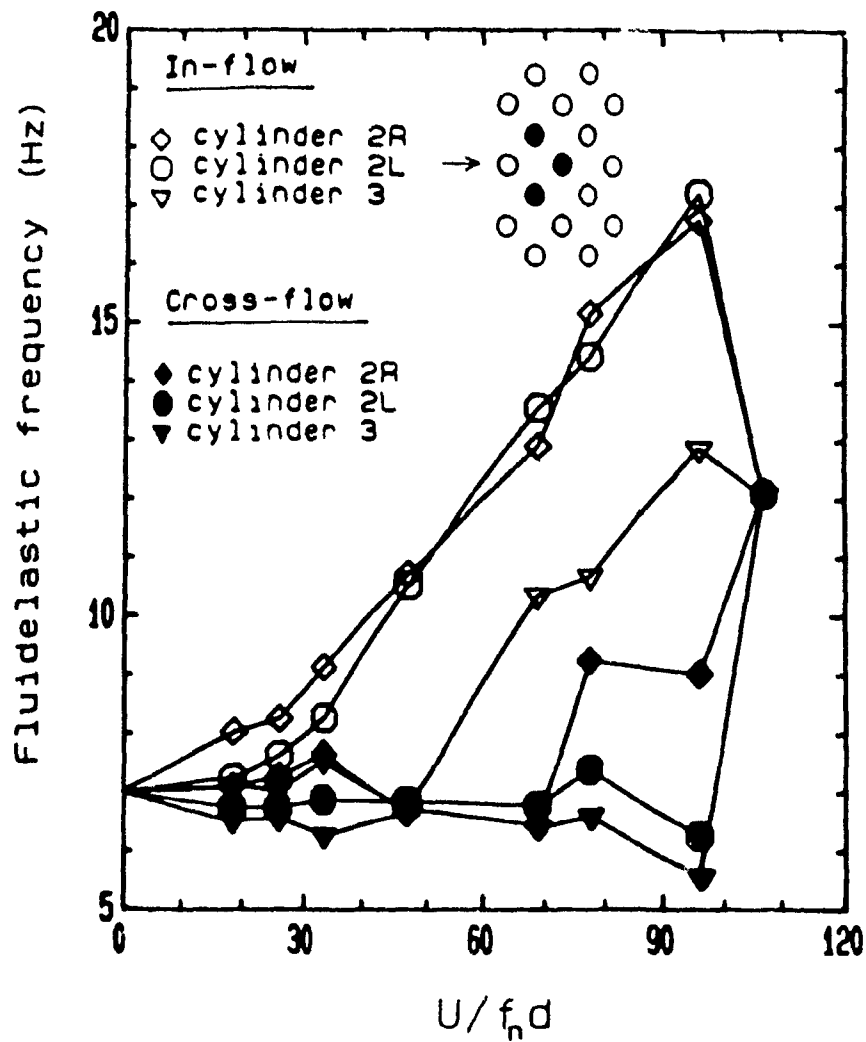


Figure 4.33: Variation of the major fluidelastic frequencies of cylinders 2R, 2L and 3 with non-dimensional flow velocity (three-flexible cylinders - 2R, 2L and 3, $\bar{m} = 280$, $f_{2R} = f_{2L} = f_3 = 7$ Hz and $\delta = 0.014$)

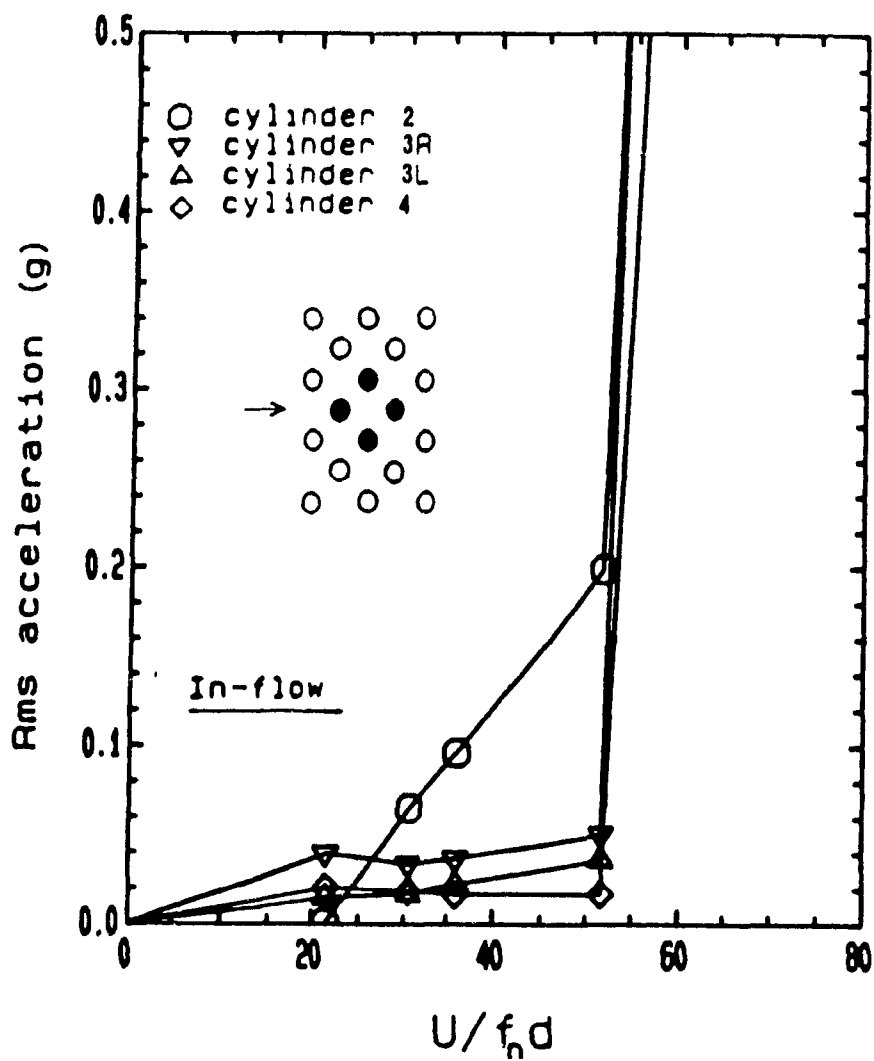


Figure 4.34: In-flow directional rms acceleration of cylinders 2, 3R, 3L and 4 at their major fluidelastic frequencies as a function of the non-dimensional flow velocity (four-flexible cylinders - 2, 3R, 3L and 4 -, $\bar{m} = 280$, $f_2 = f_{3R} = f_{3L} = f_4 = 10$ Hz and $\delta = 0.014$).

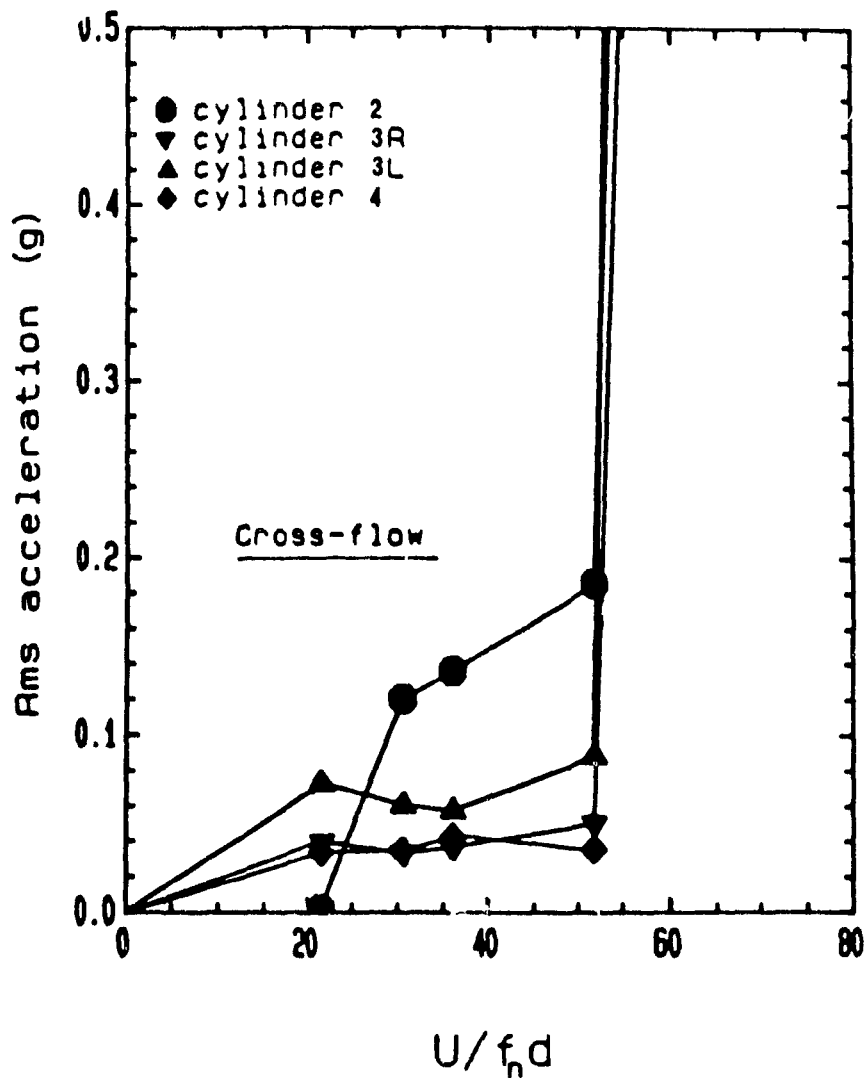


Figure 4.35: Cross-flow directional rms acceleration of cylinders 2, 3R, 3L and 4 at their major fluidelastic frequencies as a function of the non-dimensional flow velocity (four flexible cylinders - 2, 3R, 3L and 4 -, $\bar{m} = 280$, $f_2 = f_{3R} = f_{3L} = f_4 = 10$ Hz and $\delta = 0.014$).

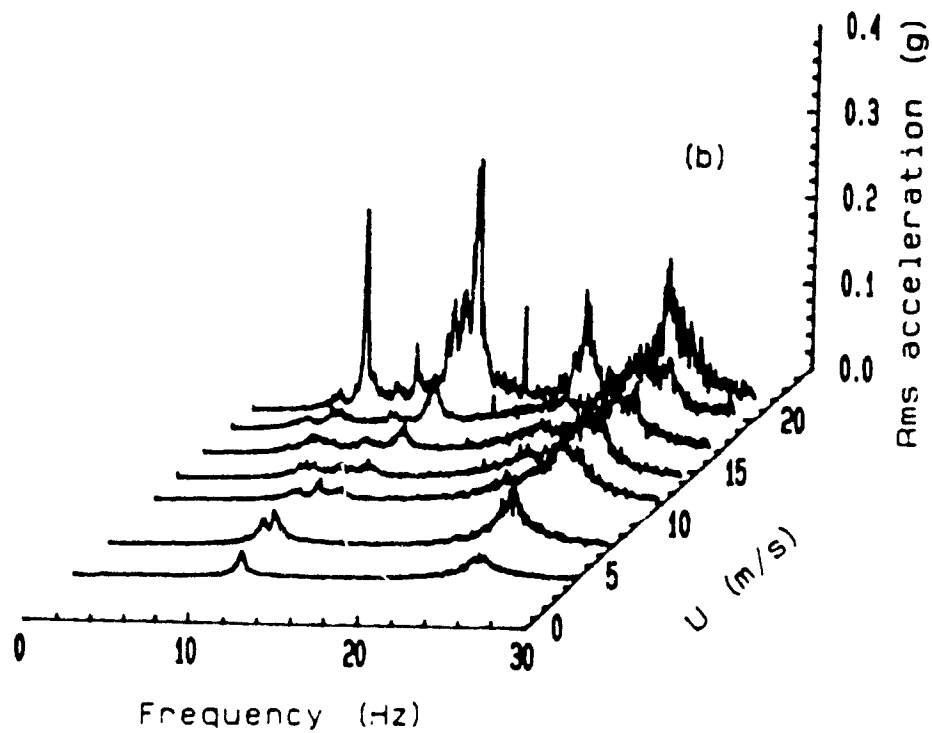
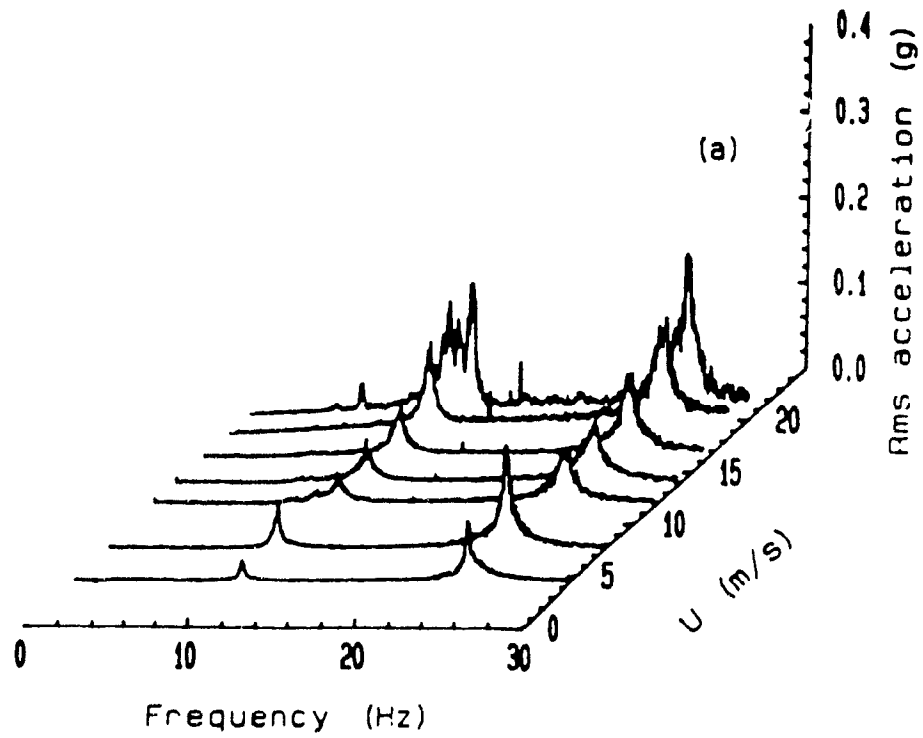


Figure 1.36: Variation of the in-flow (a) and cross-flow (b) vibration power spectra with flow velocity for cylinder 3 (four-flexible cylinders - 3, 4R, 4L and 5 -, $\bar{m} = 280$, $f_3 = f_{4R} = f_{4L} = f_5 = 10$ Hz and $\delta = 0.014$).

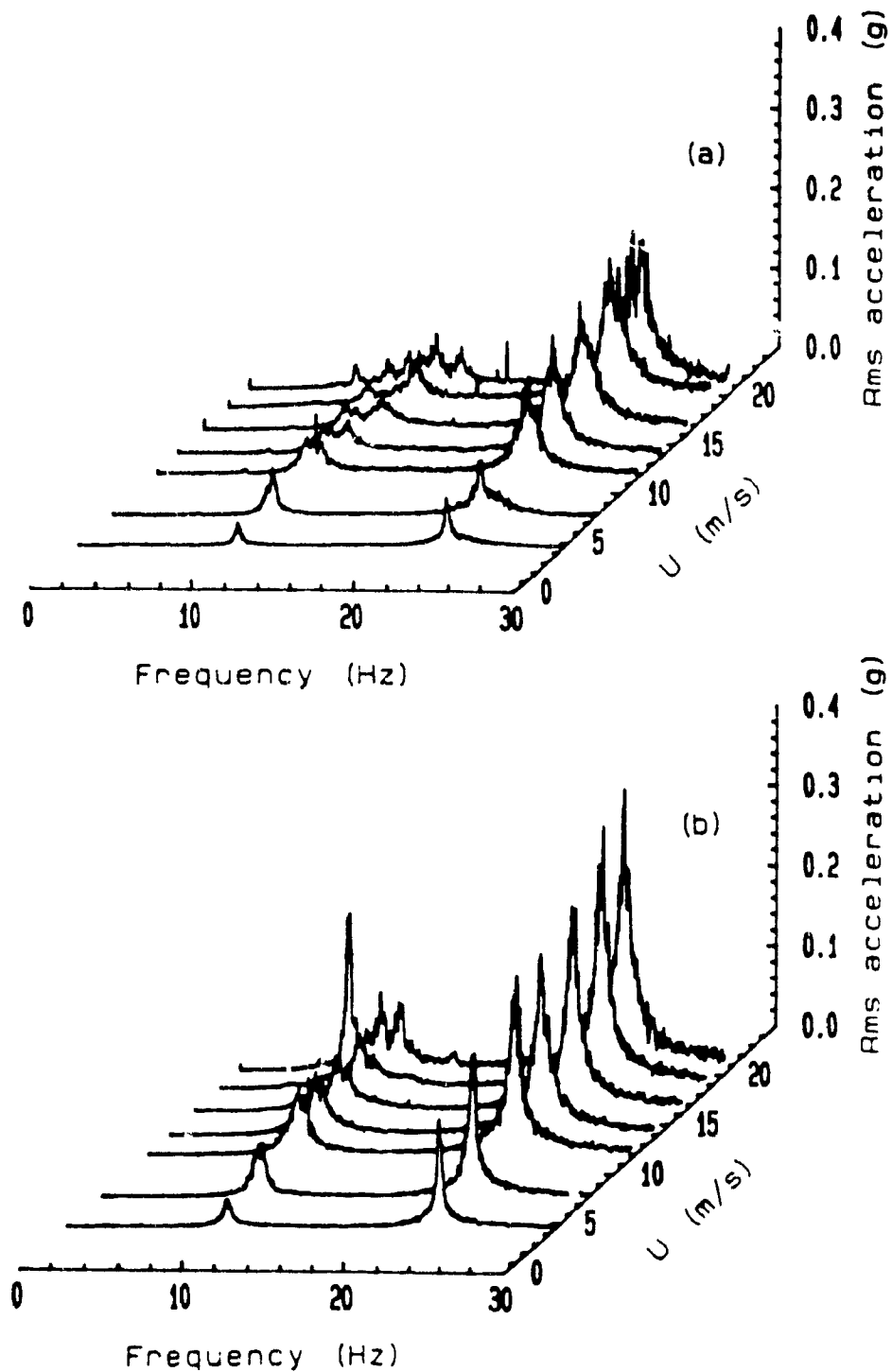


Figure 4.37: Variation of the in-flow (a) and cross-flow (b) vibration power spectra with the flow velocity for cylinder 4R (four-flexible cylinders - 3, 4R, 4L and 5, $\bar{m} = 280$, $f_3 = f_{4R} = f_{4L} = f_5 = 10$ Hz and $\delta = 0.014$).

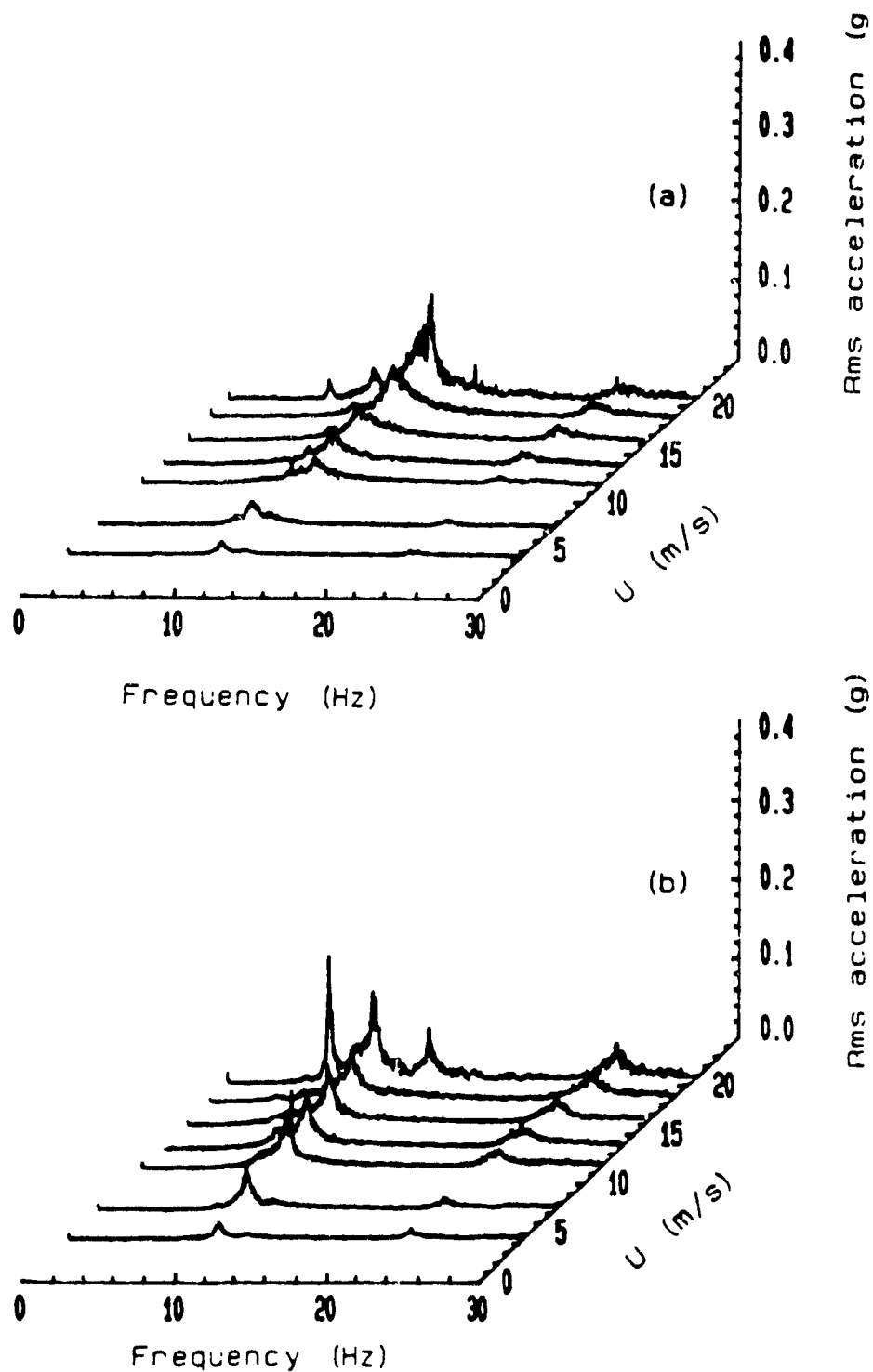


Figure 4.38: Variation of the in-flow (a) and cross-flow (b) vibration power spectra with the flow velocity for cylinder 4L (four-flexible cylinders - 3, 4R, 4L and 5 -, $\dot{m} = 280$, $f_3 = f_{4R} = f_{4L} = f_5 = 10$ Hz and $\delta = 0.014$).

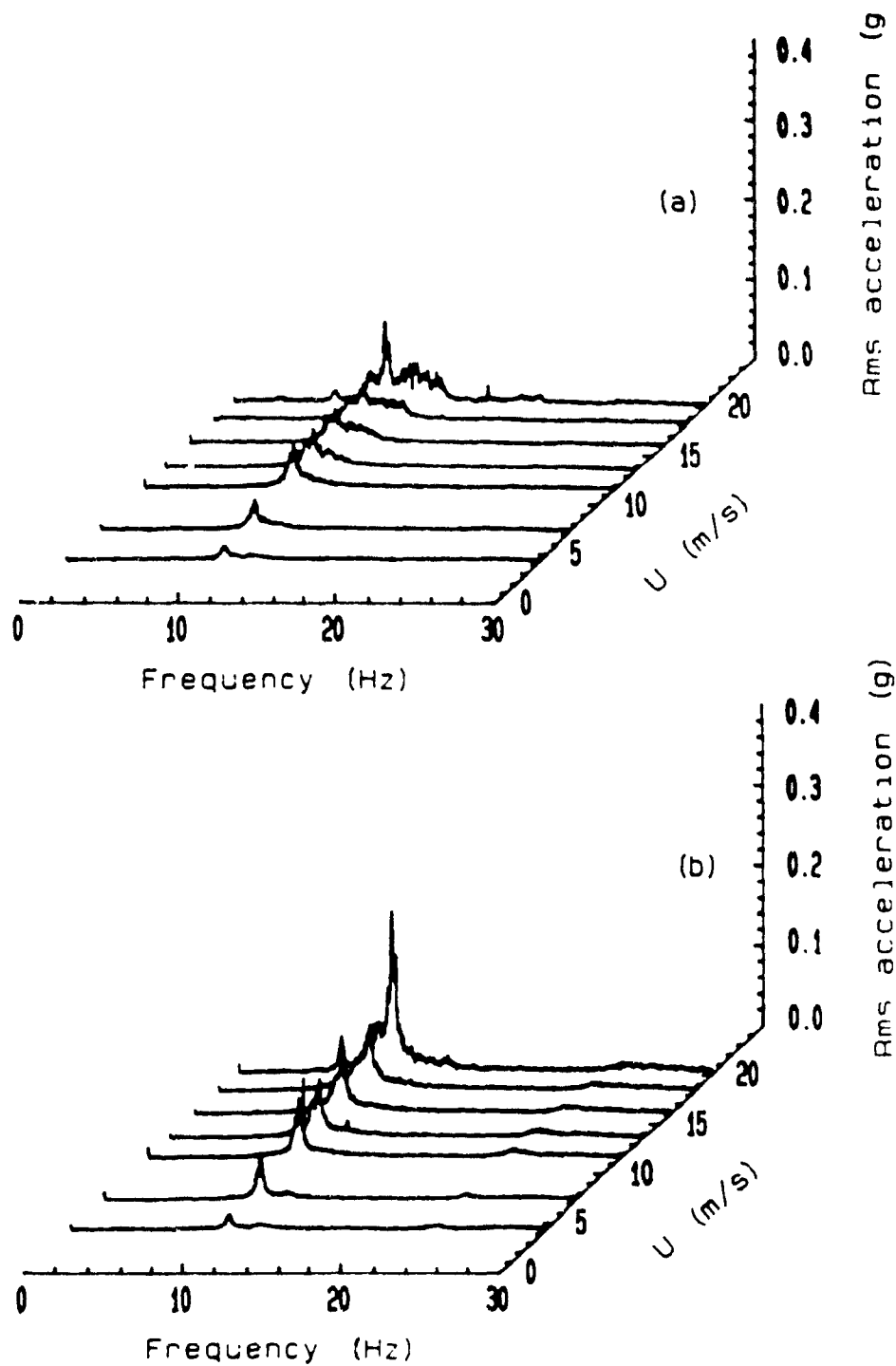


Figure 4.39: Variation of the in-flow (a) and cross-flow (b) vibration power spectra with the flow velocity for cylinder 5 (four-flexible cylinders - 3, 4R, 4L and 5, $\bar{m} = 280$, $f_3 = f_{4R} = f_{4L} = f_5 = 10$ Hz and $\delta = 0.014$).

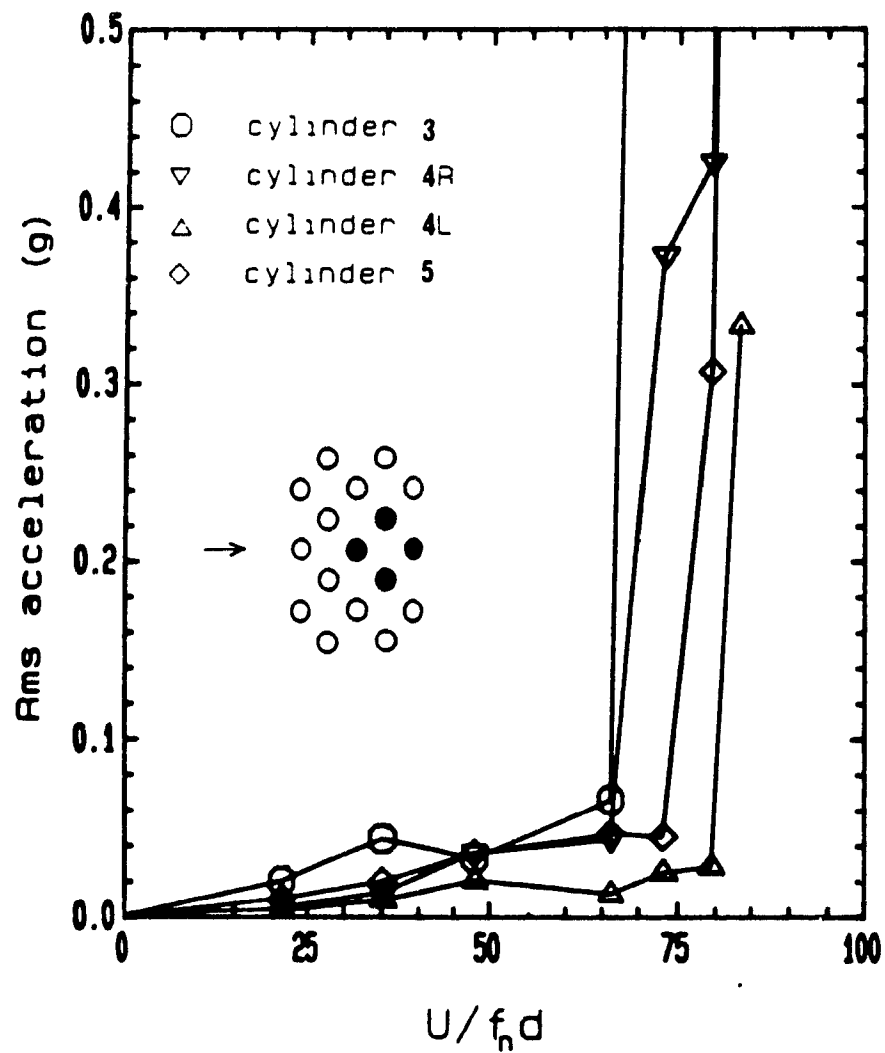


Figure 4.40: In-flow directional rms acceleration of cylinders 3, 4R, 4L and 5 at their major fluidelastic frequencies as a function of the non-dimensional flow velocity (four flexible cylinders - 3, 4R, 4L and 5 -, $\bar{m} = 280$, $f_3 = f_{4R} = f_{4L} = f_5 = 7$ Hz and $\delta = 0.014$).

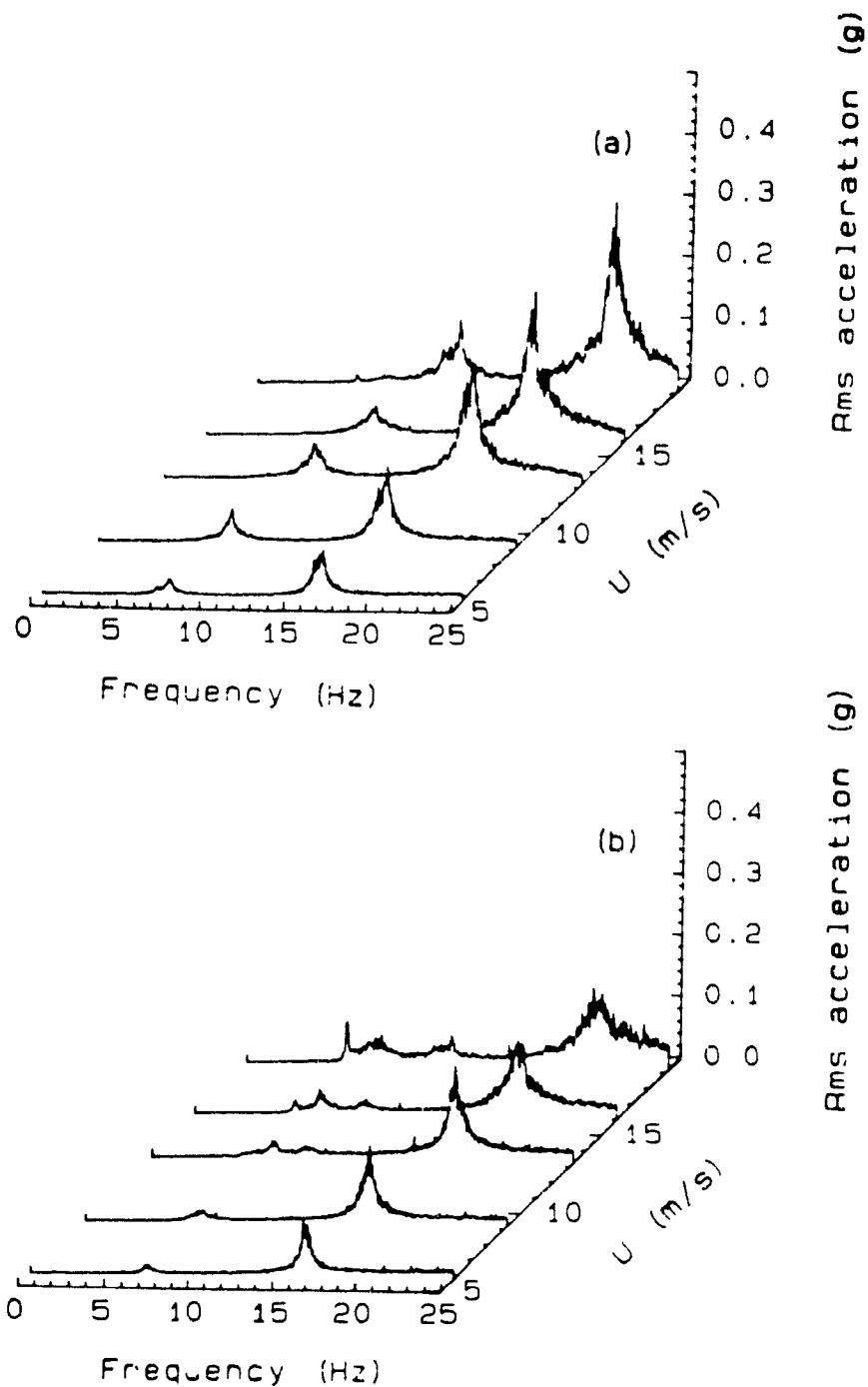


Figure 4.41: Variation of the in-flow (a) and cross-flow (b) vibration power spectra with the flow velocity for cylinder 4 (four-flexible cylinders - 4, 5R, 5L and 6, $\bar{m} = 280$, $f_A = f_{5R} = f_{5L} = f_b = 7$ Hz and $\delta = 0.011$)

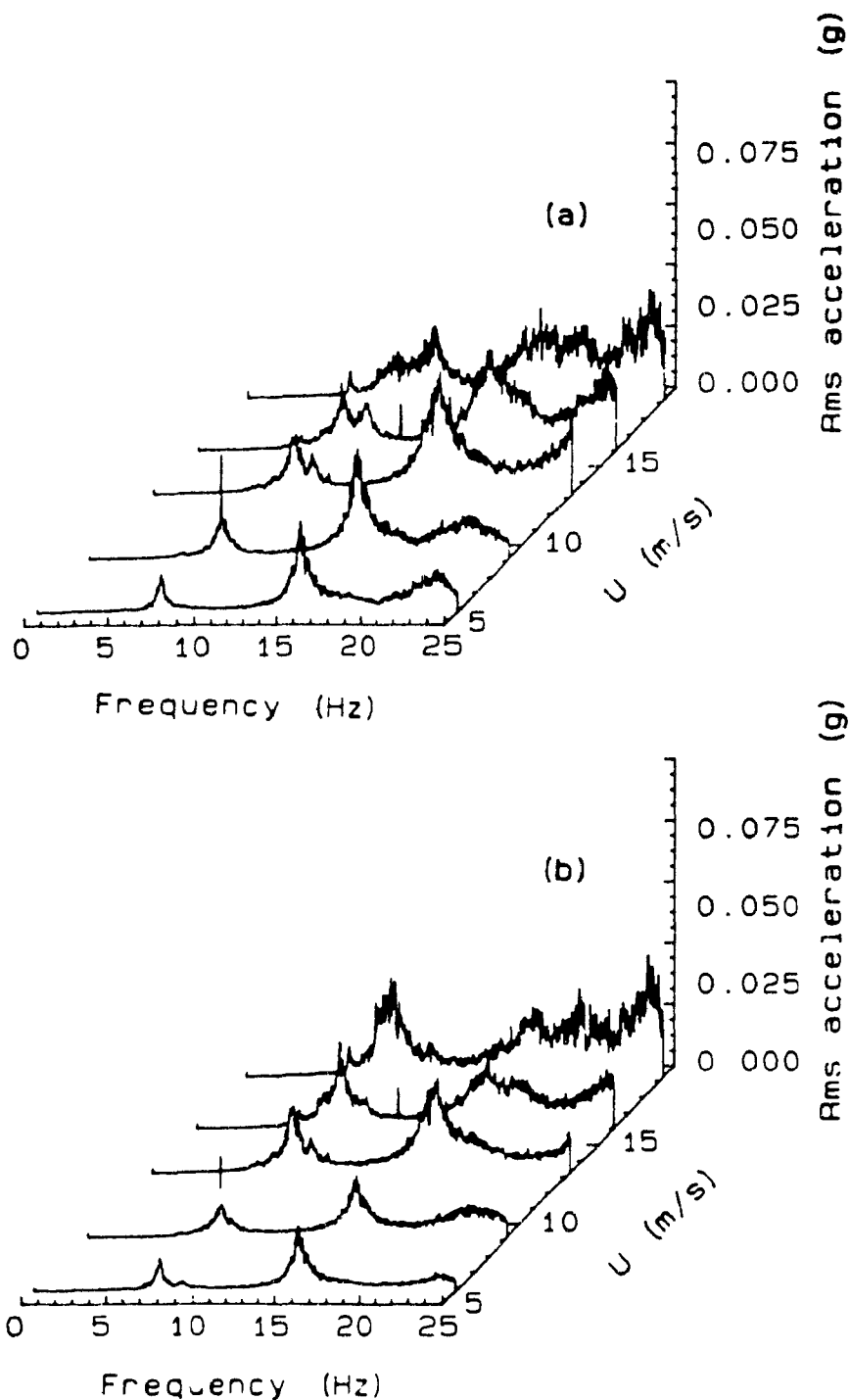


Figure 1.12 Variation of the m-flow (a) and cross-flow (b) vibration power spectra with the flow velocity for cylinder 5R (four flexible cylinders - 4, 5R, 5L and 6 -, $m = 280$, $f_1 = f_{5R} = f_{5L} = f_6 = 7$ Hz and $\delta = 0.014$).

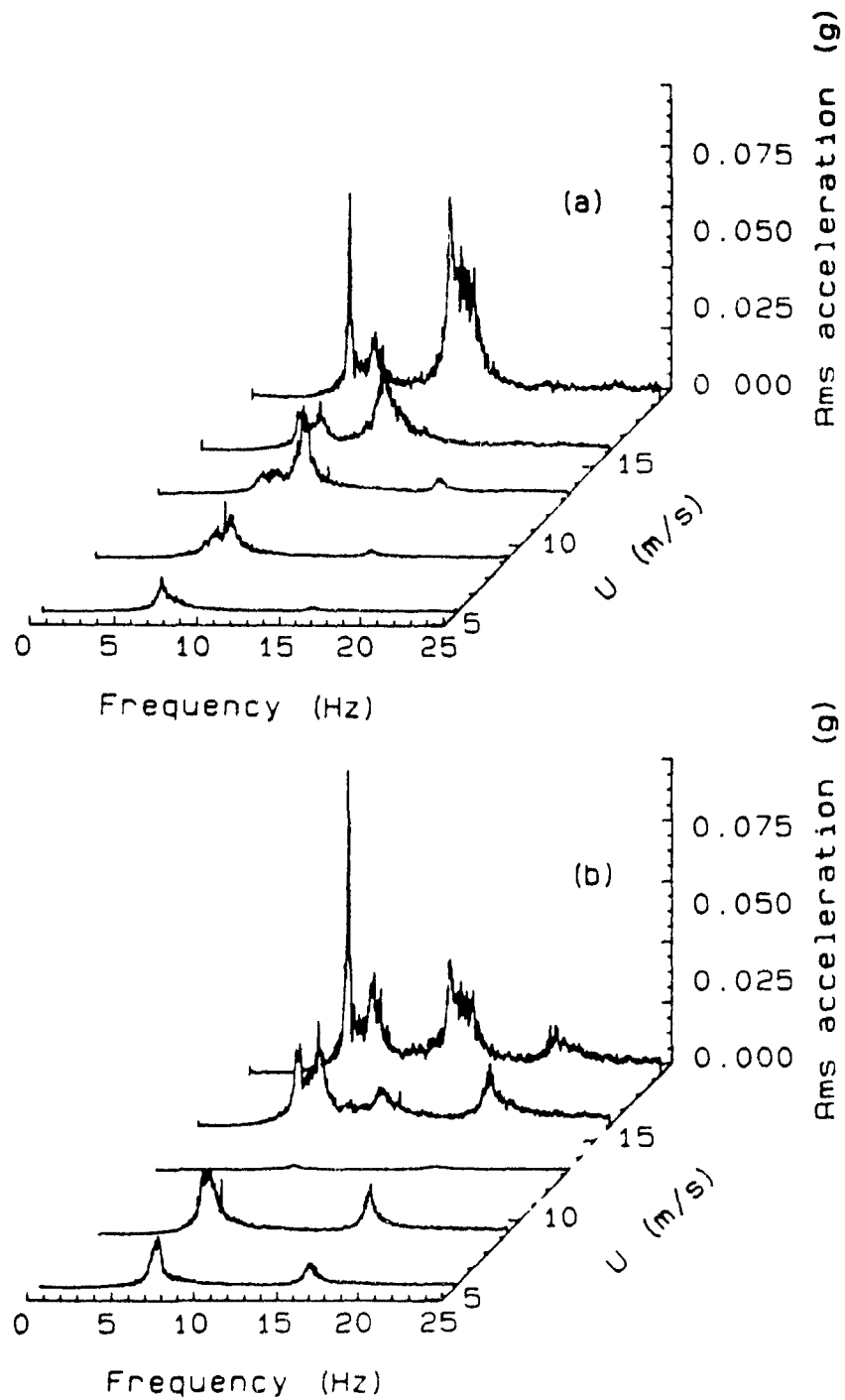


Figure 4.43: Variation of the in-flow (a) and cross-flow (b) vibration power spectra with the flow velocity for cylinder 5L (four flexible cylinders 4, 5R, 5L and 6, $\bar{m} = 280$, $f_4 = f_{5R} = f_{5L} = f_6 = 7$ Hz and $\delta = 0.014$).

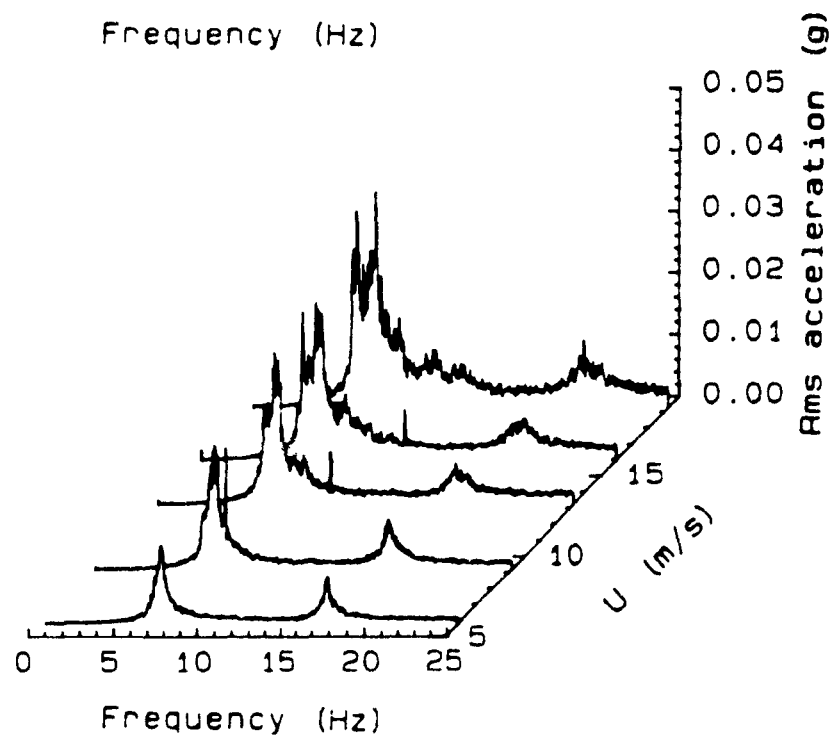
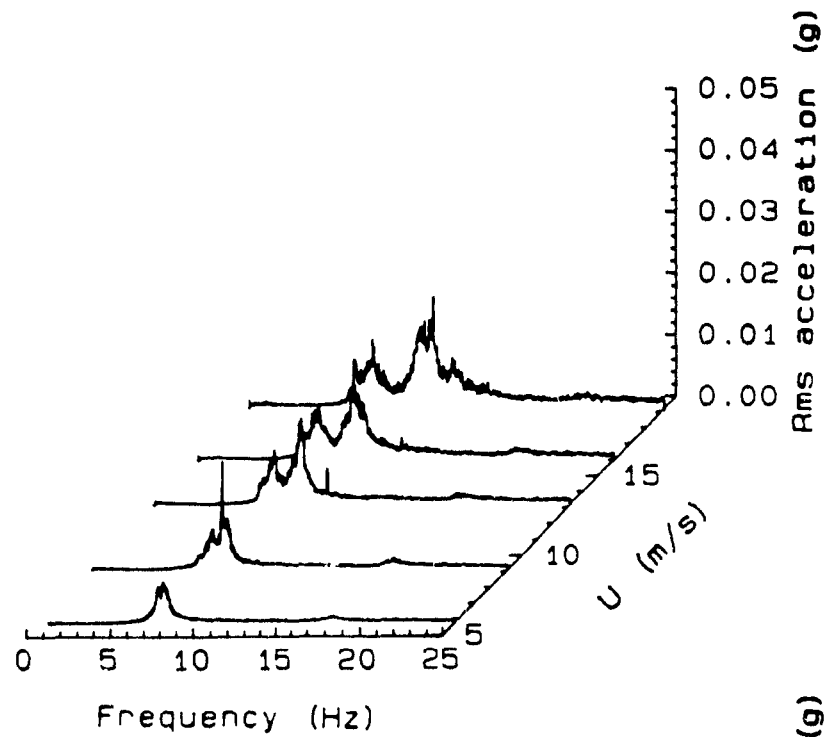


Figure 1.44: Variation of the in-flow (a) and cross-flow (b) vibration power spectra with the flow velocity for cylinder 6 (four flexible cylinders - 4, 5R, 5L and 6 -, $m = 280$, $f_4 = f_{5R} = f_{5L} = f_6 = 7$ Hz and $\delta = 0.014$).

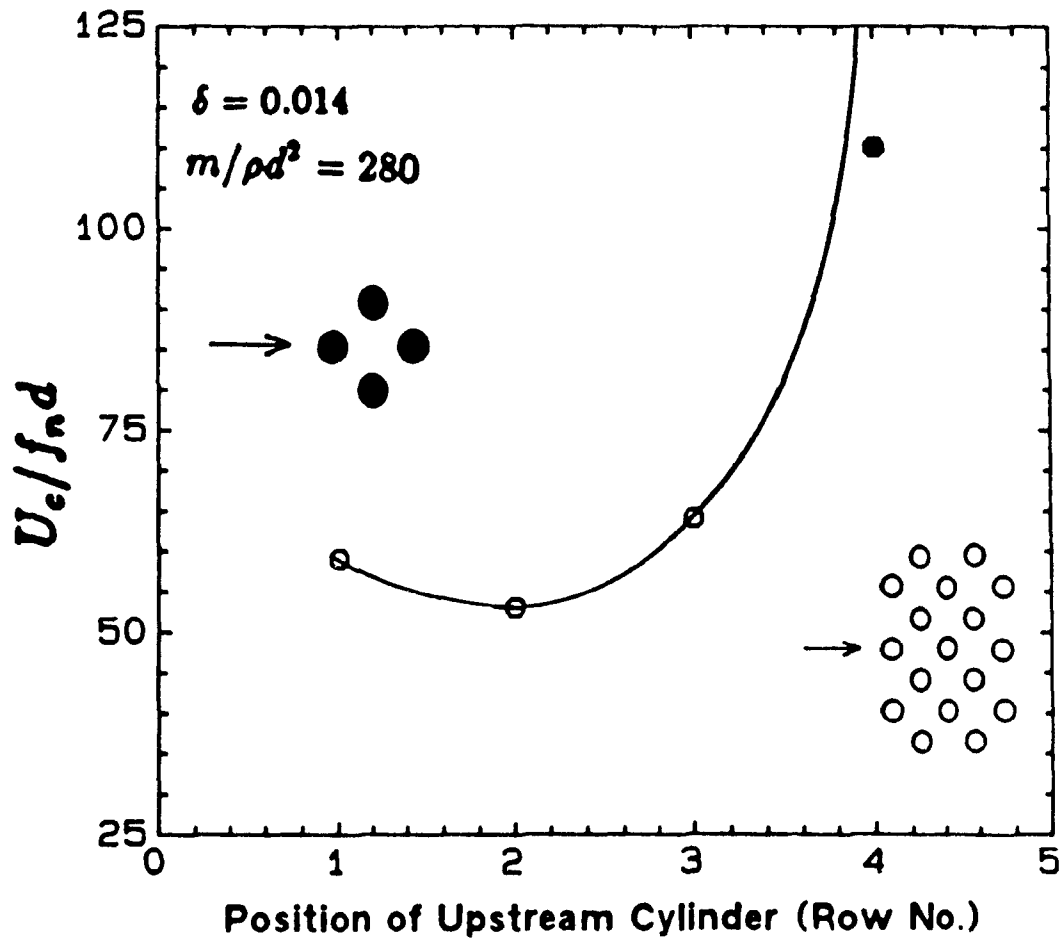


Figure 4.45: Variation of non-dimensional critical velocity with flexible cylinder position in the array (four-flexible cylinders, $\bar{m} = 280$ $\delta = 0.014$, \bigcirc = unstable, and \bullet = stable).

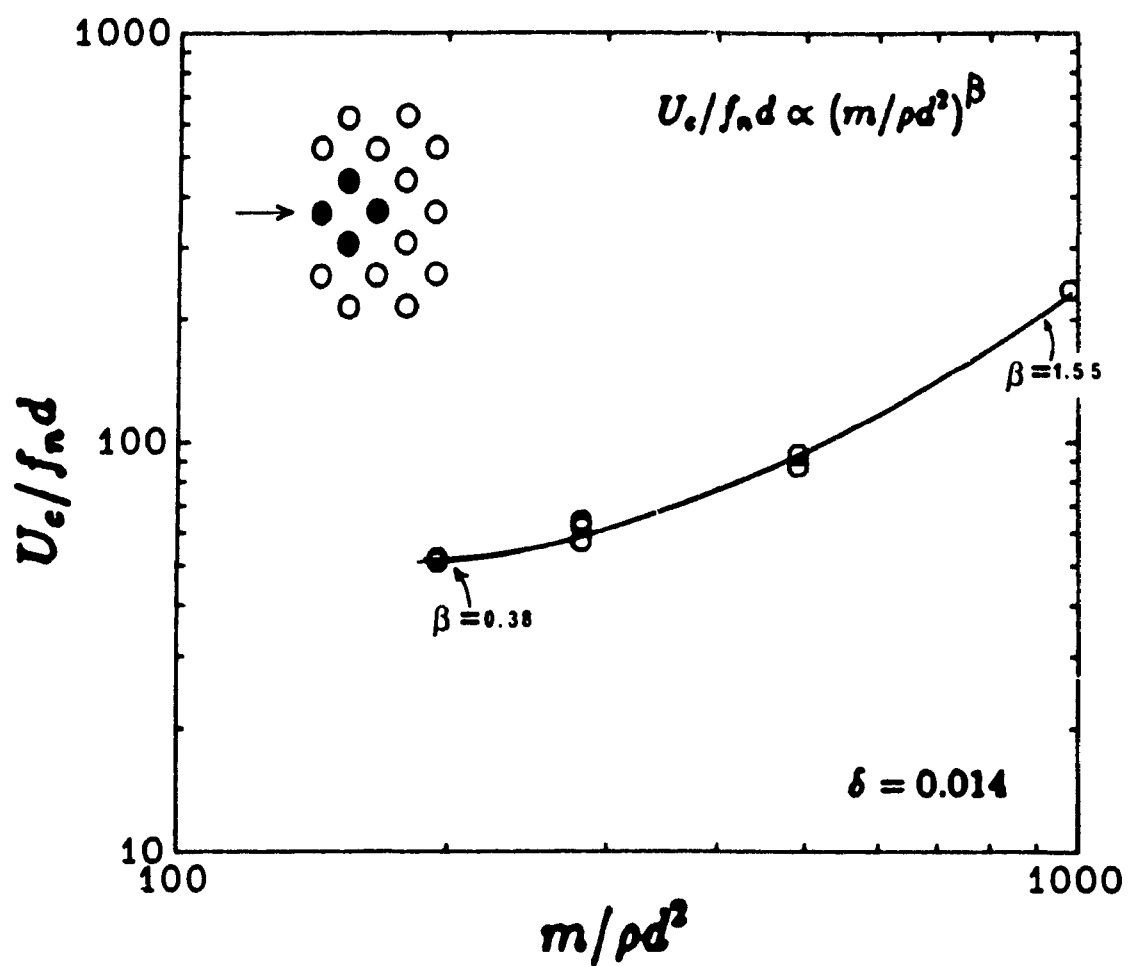


Figure 4.46: Variation of non-dimensional critical velocity with dimensionless cylinder mass for four flexible cylinders (cylinders 1, 2R, 2L and 3 and $\delta = 0.014$).

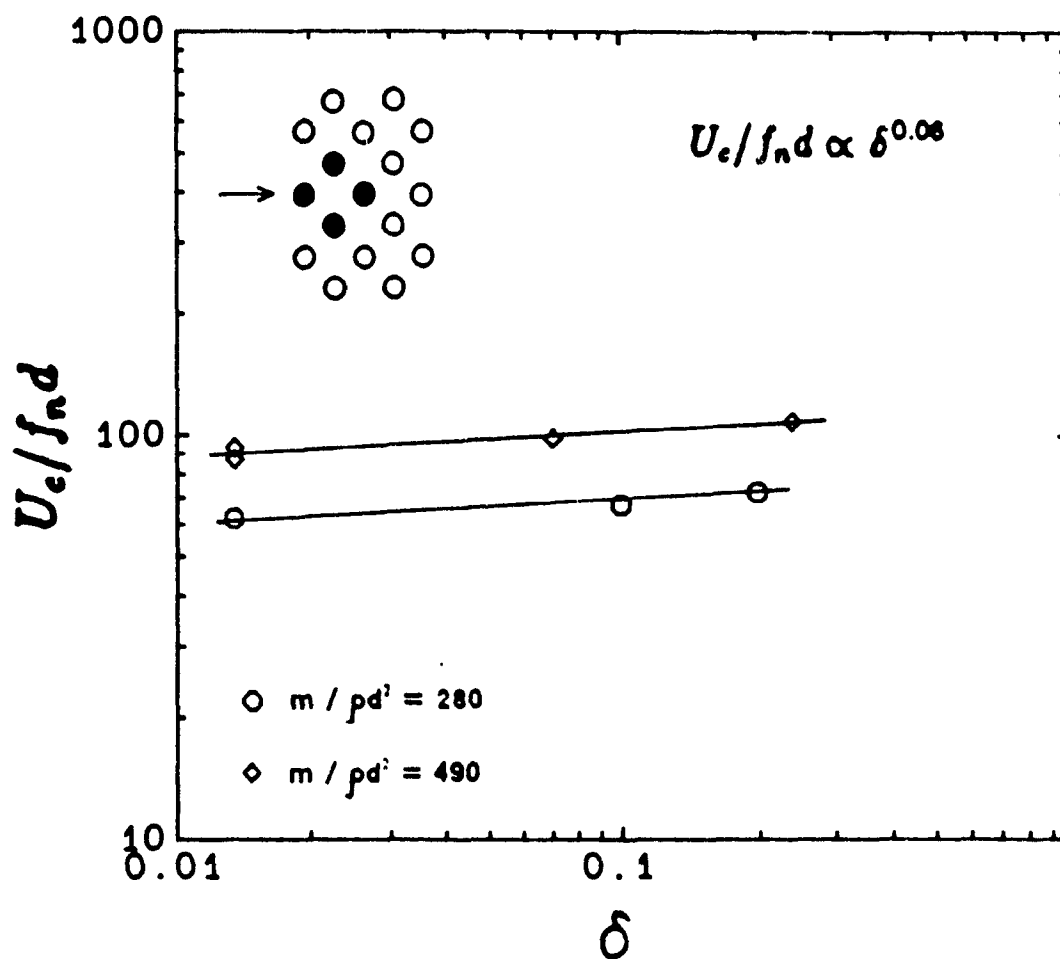


Figure 4.47: Variation of non-dimensional critical velocity with cylinder damping for four flexible cylinders (cylinders 1, 2R, 2L and 3, $\bar{m} = 280$ and 490).

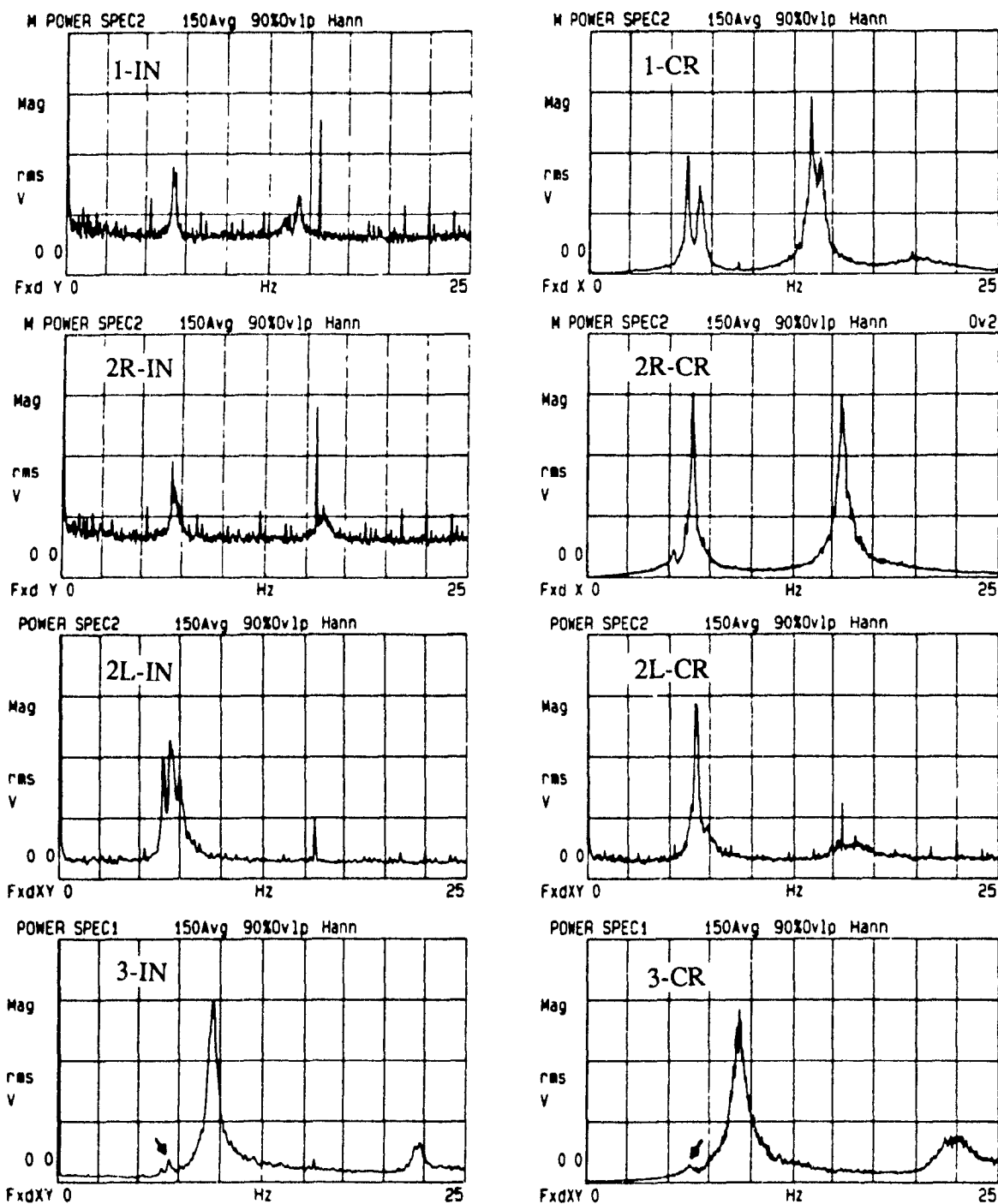


Figure 1.48: Acceleration power spectra of cylinders 1, 2R, 2L and 3 in the in- and cross-flow directions at $U/f_n d \approx 18$ (four-flexible cylinders – 1, 2R, 2L and 3 –, $\dot{m} = 280$, $f_1 = f_{2R} = f_{2L} = 6.375$ Hz, $f_3 = 10$ Hz and $\delta = 0.014$).

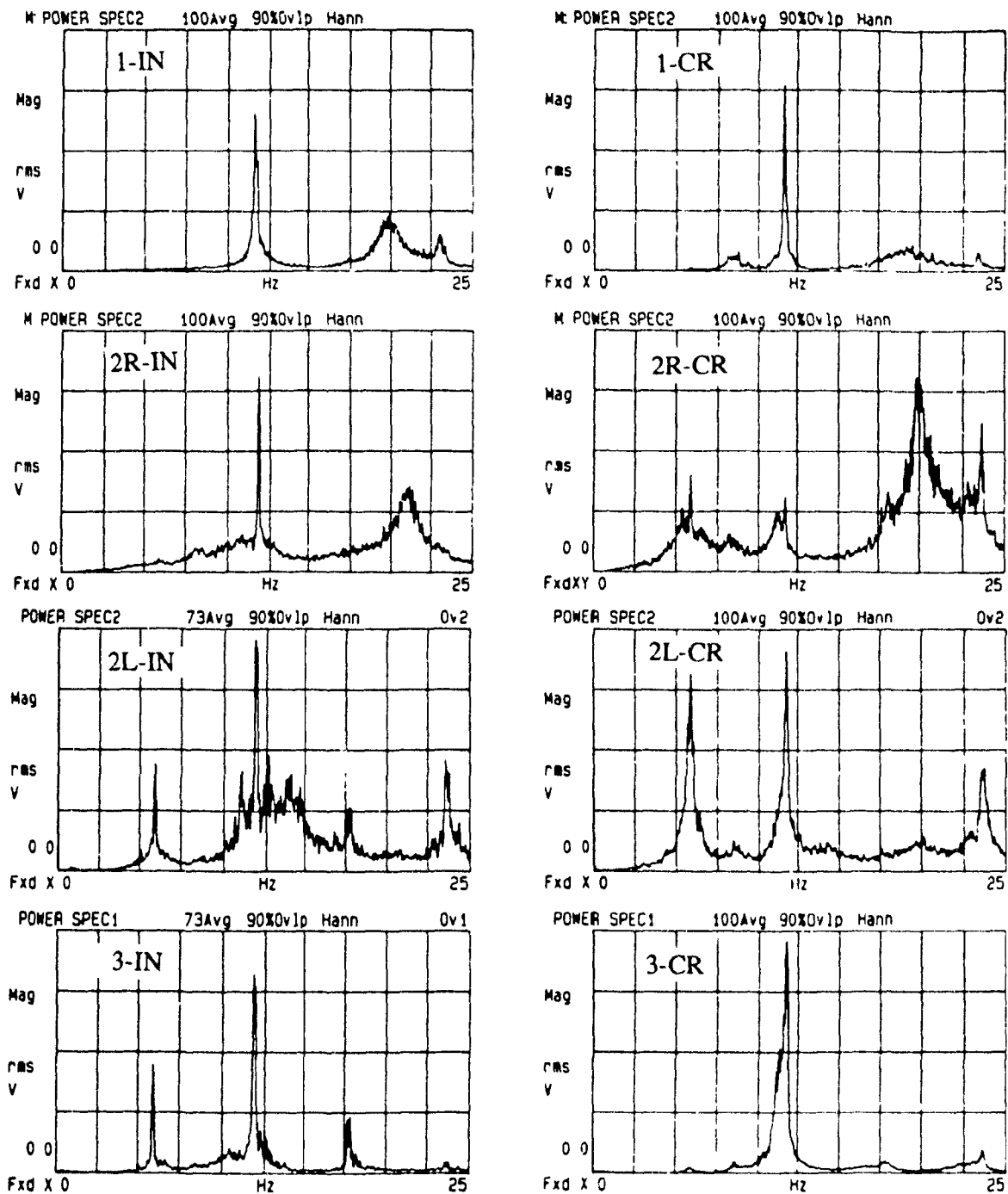


Figure 4.49: Acceleration power spectra of cylinders 1, 2R, 2L and 3 in the in- and cross-flow directions at $U/f_n d \approx 39$ (four-flexible cylinders - 1, 2R, 2L and 3, $\bar{m} = 280$, $f_1 = f_{2R} = f_{2L} = 6.375$ Hz, $f_3 = 10$ Hz and $\delta = 0.014$)

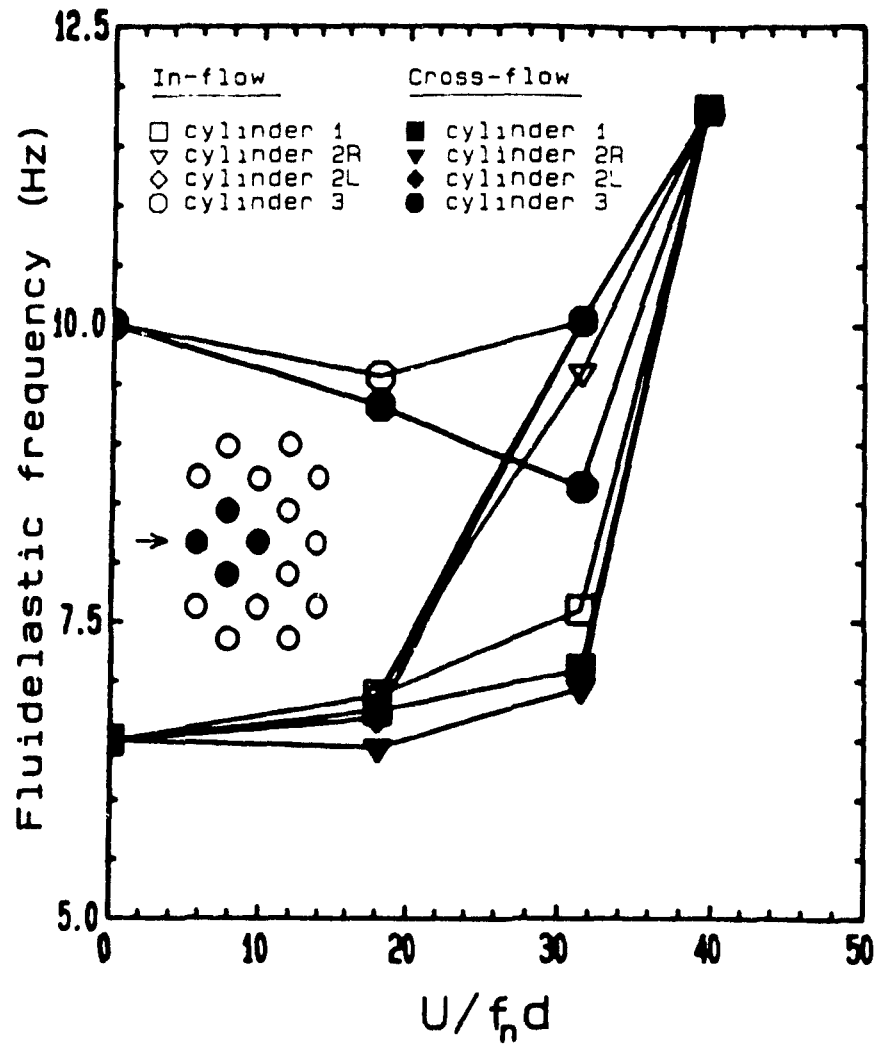


Figure 4.50: Variation of the major fluidelastic frequencies of cylinders 1, 2R, 2L and 3 with non-dimensional flow velocity (four-flexible cylinders - 1, 2R, 2L and 3 -, $\bar{m} = 280$, $f_1 = f_{2R} = f_{2L} = 6.375$ Hz, $f_3 = f_n = 10$ Hz and $\delta = 0.014$).

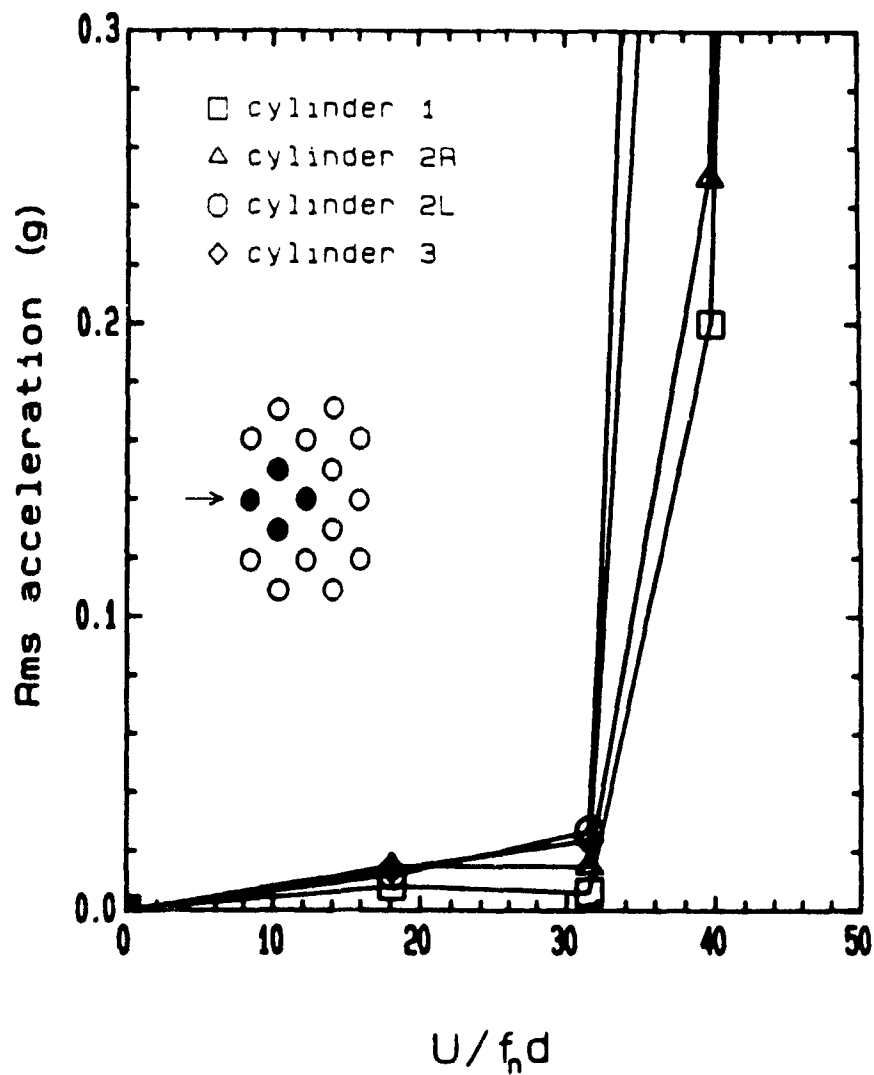


Figure 4.51: In-flow directional rms acceleration of cylinders 1, 2R, 2L and 3 at their major fluidelastic frequencies as a function of the non-dimensional flow velocity (four-flexible cylinders - 1, 2R, 2L and 3 -, $\bar{m} = 280$, $f_1 = f_{2R} = f_{2L} = 6.375$ Hz, $f_3 = f_n = 10$ Hz and $\delta = 0.014$).

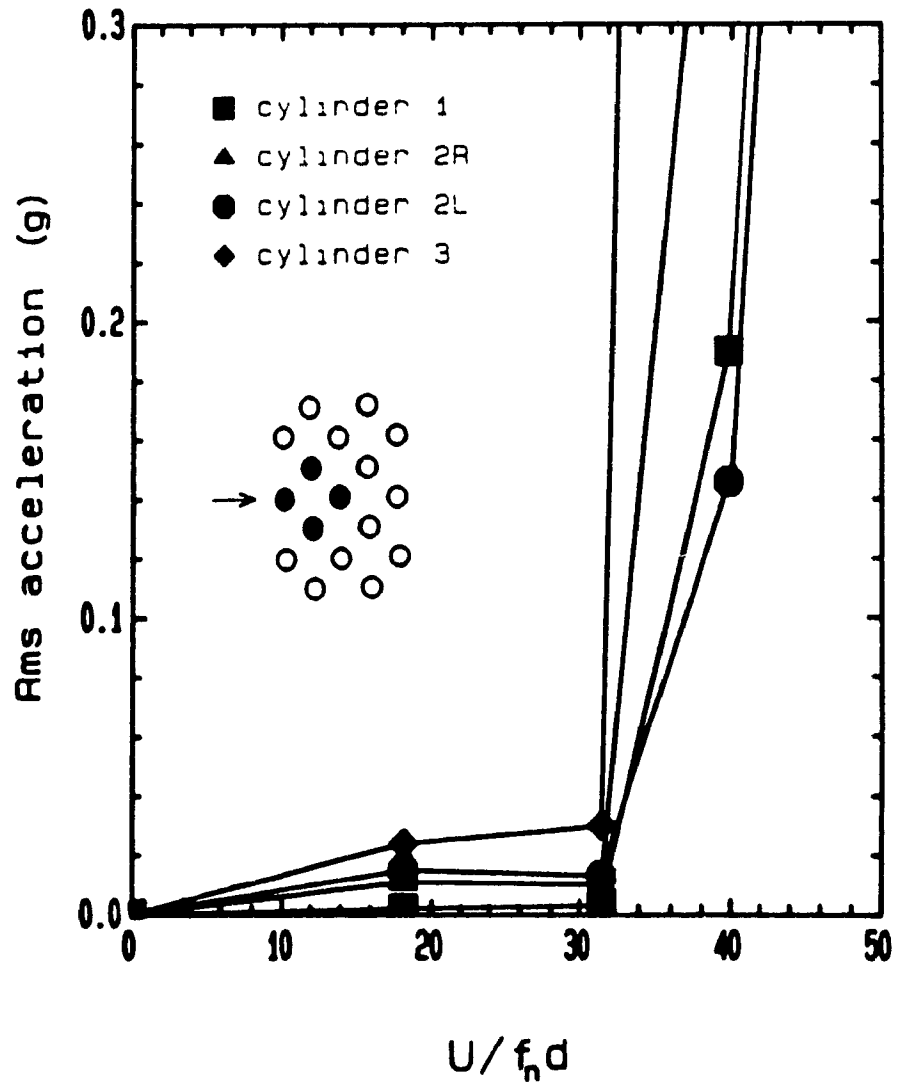


Figure 4.52: Cross-flow directional rms acceleration of cylinders 1, 2R, 2L and 3 at their major fluidelastic frequencies as a function of the non-dimensional flow velocity (four-flexible cylinders - 1, 2R, 2L and 3 -, $\bar{m} = 280$, $f_1 = f_{2R} = f_{2L} = 6.375$ Hz, $f_3 = f_n = 10$ Hz and $\delta = 0.014$).

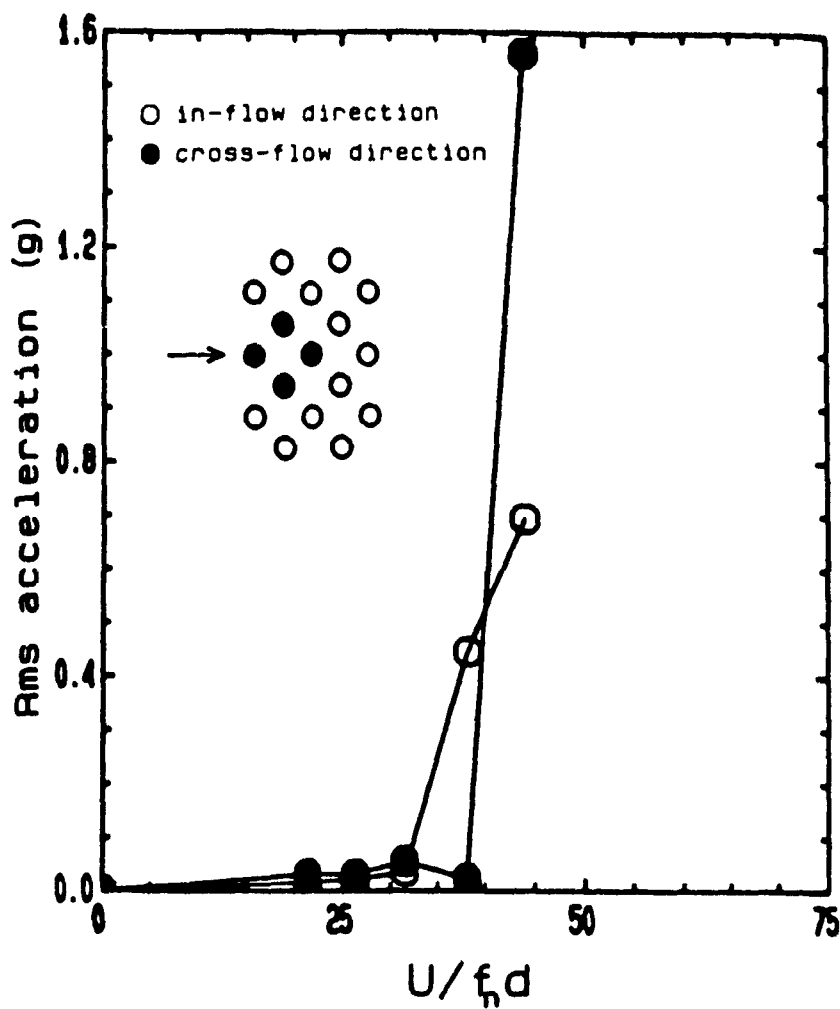


Figure 4.53: Rms acceleration of cylinder 3 at its major fluidelastic frequencies as a function of the non-dimensional flow velocity (four-flexible cylinders - 1, 2R, 2L and 3 -, $\bar{m} = 280$, $f_1 = f_{2R} = f_{2L} = 6.5$ Hz, $f_3 = 10$ Hz and $\delta = 0.014$).

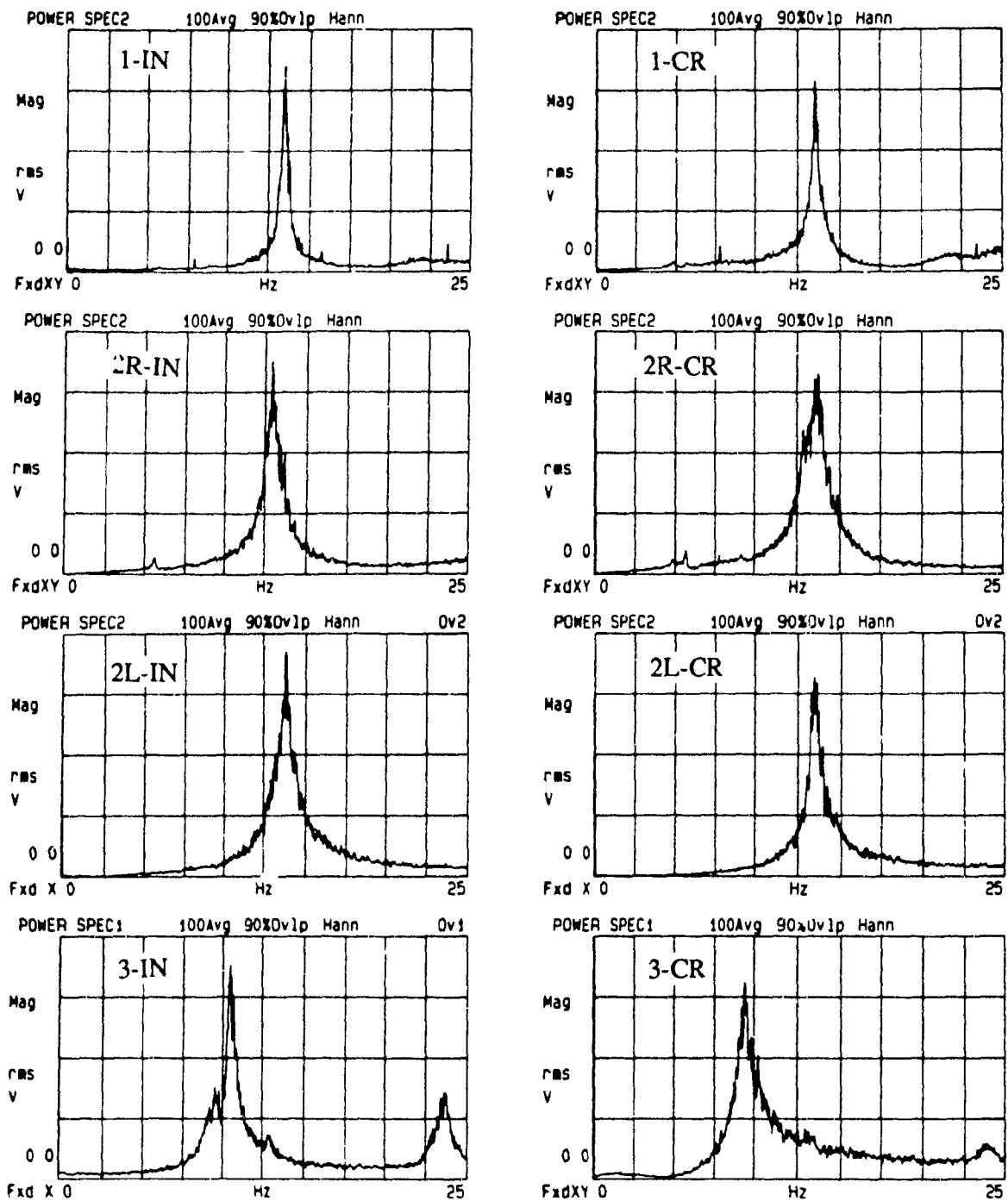


Figure 1.54: Acceleration power spectra of cylinders 1, 2R, 2L and 3 in the in- and cross-flow directions at $U/f_n d \approx 33$ (four-flexible cylinders - 1, 2R, 2L and 3 -, $m = 280$, $f_1 = f_{2R} = f_{2L} = 13.5$ Hz, $f_3 = 10$ Hz and $\delta 0.014$).

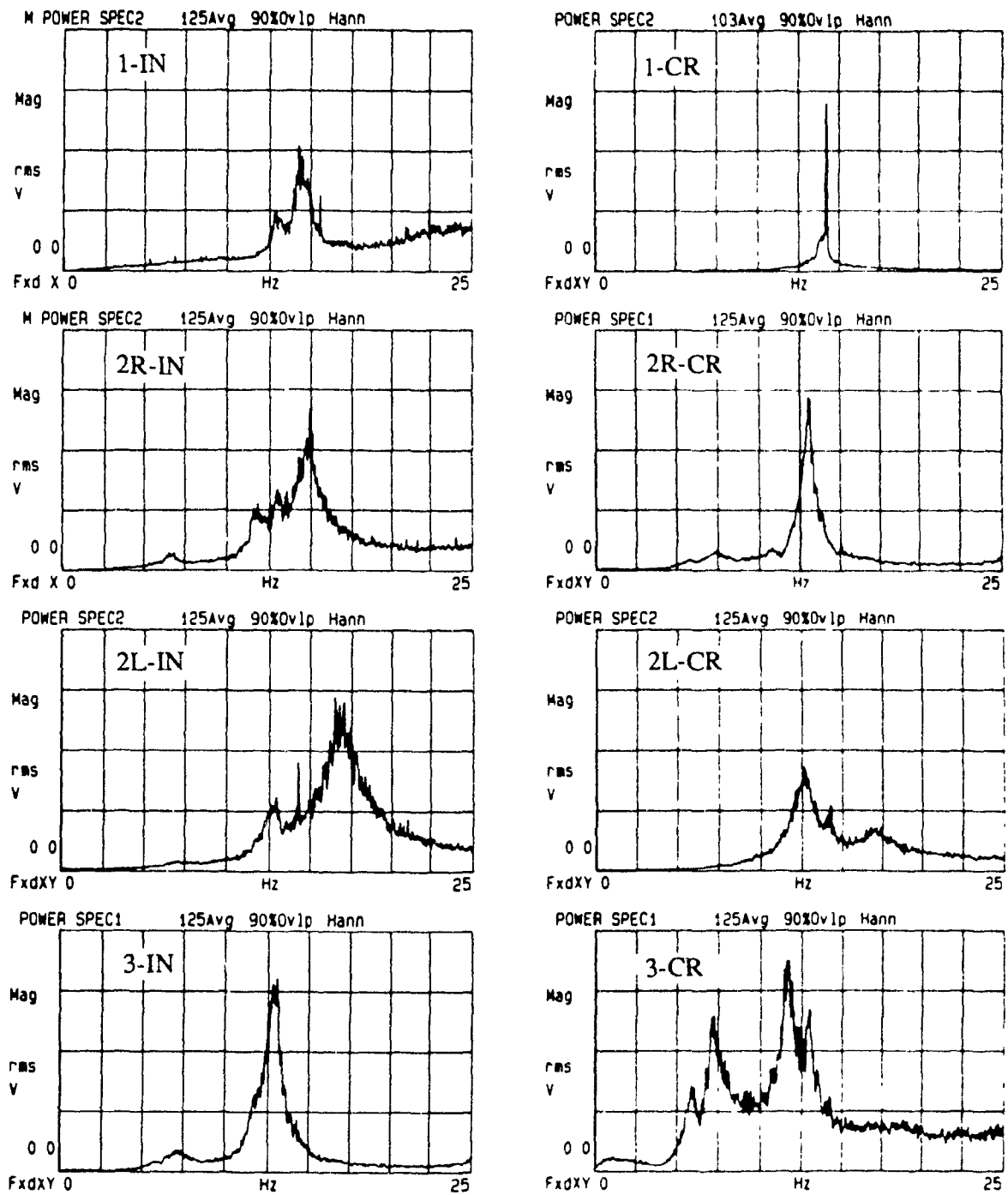


Figure 4.55: Acceleration power spectra of cylinders 1, 2R, 2L and 3 in the in- and cross-flow directions at $U/f_n d = 65$ (four-flexible cylinders - 1, 2R, 2L and 3, $\bar{m} = 280$, $f_1 = f_{2R} = f_{2L} = 13.5$ Hz, $f_3 = 10$ Hz and $\delta = 0.014$).

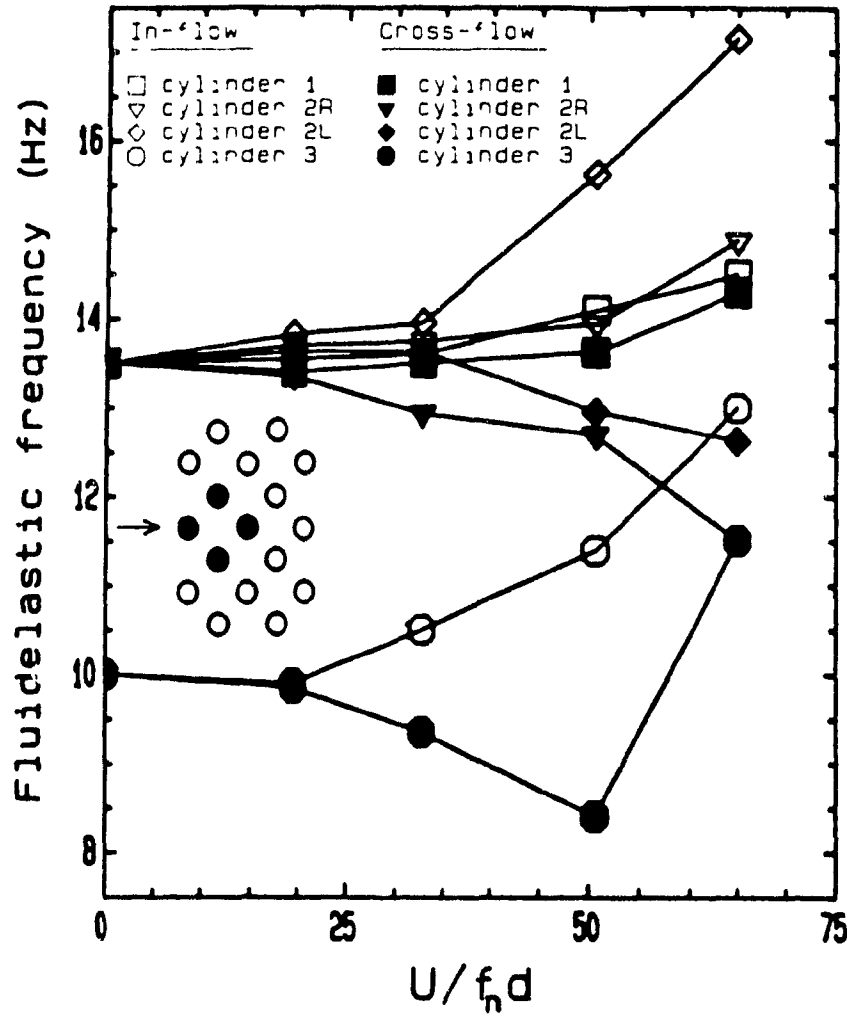


Figure 4.56: Variation of the major fluidelastic frequencies of cylinders 1, 2R, 2L and 3 with non-dimensional flow velocity (four-flexible cylinders - 1, 2R, 2L and 3 -, $\dot{m} = 280$, $f_1 = f_{2R} = f_{2L} = 13.5$ Hz, $f_3 = 10$ Hz and $\delta = 0.014$).

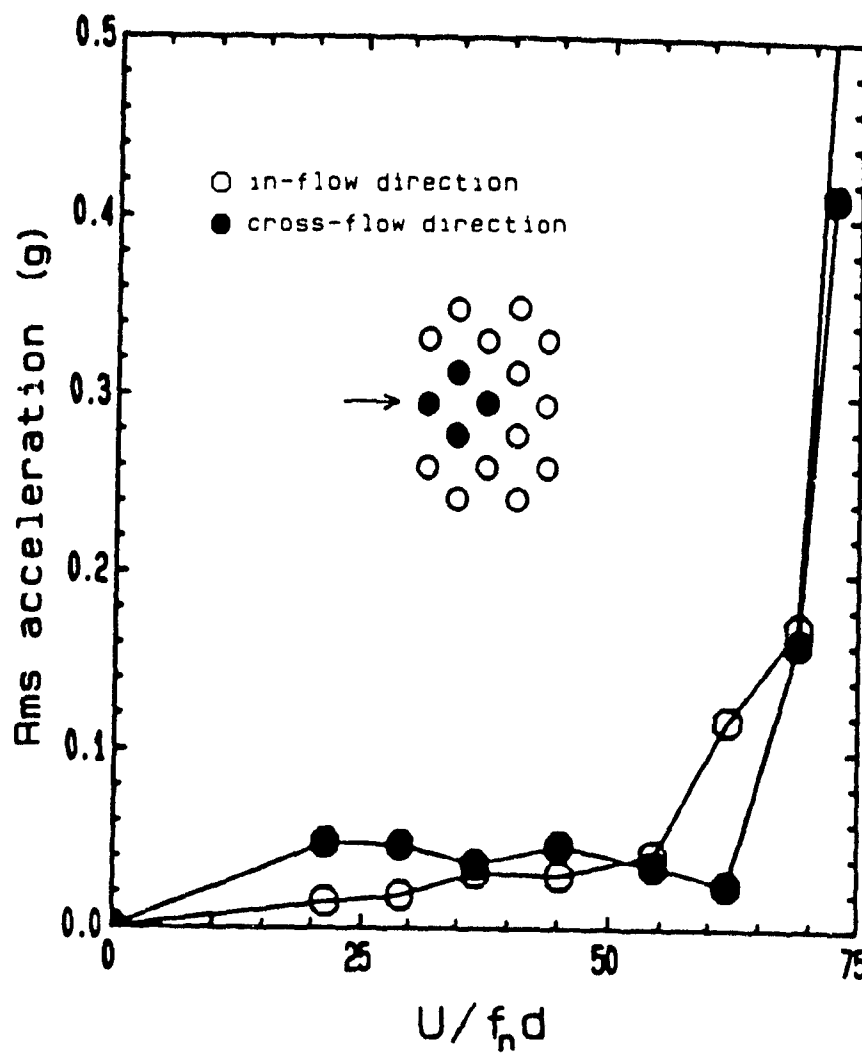


Figure 4.57: Rms acceleration of cylinder 3 at its major fluidelastic frequencies as a function of the non-dimensional flow velocity (four-flexible cylinders - 1, 2R, 2L and 3 -, $\bar{m} = 280$, $f_1 = f_{2R} = f_{2L} = 13.5$ Hz, $f_3 = f_n = 10$ Hz and $\delta = 0.014$).

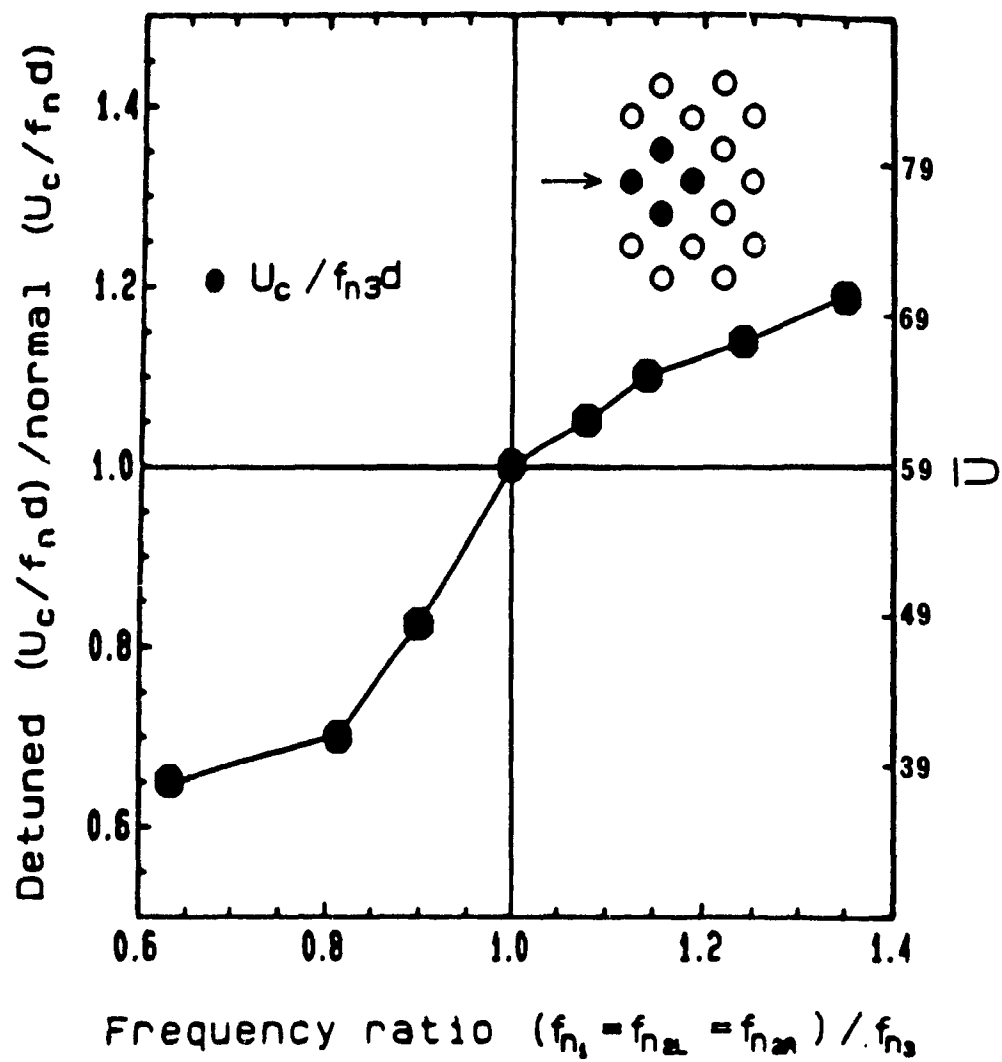


Figure 4.58: Effect of frequency detuning between adjacent cylinders on non-dimensional critical flow velocity (four-flexible cylinders - 1, 2R, 2L and 3 -, $\bar{m} = 280$, $f_1 = f_{2R} = f_{2L} = 13.5$ Hz, $f_3 = 10$ Hz and $\delta = 0.014$).

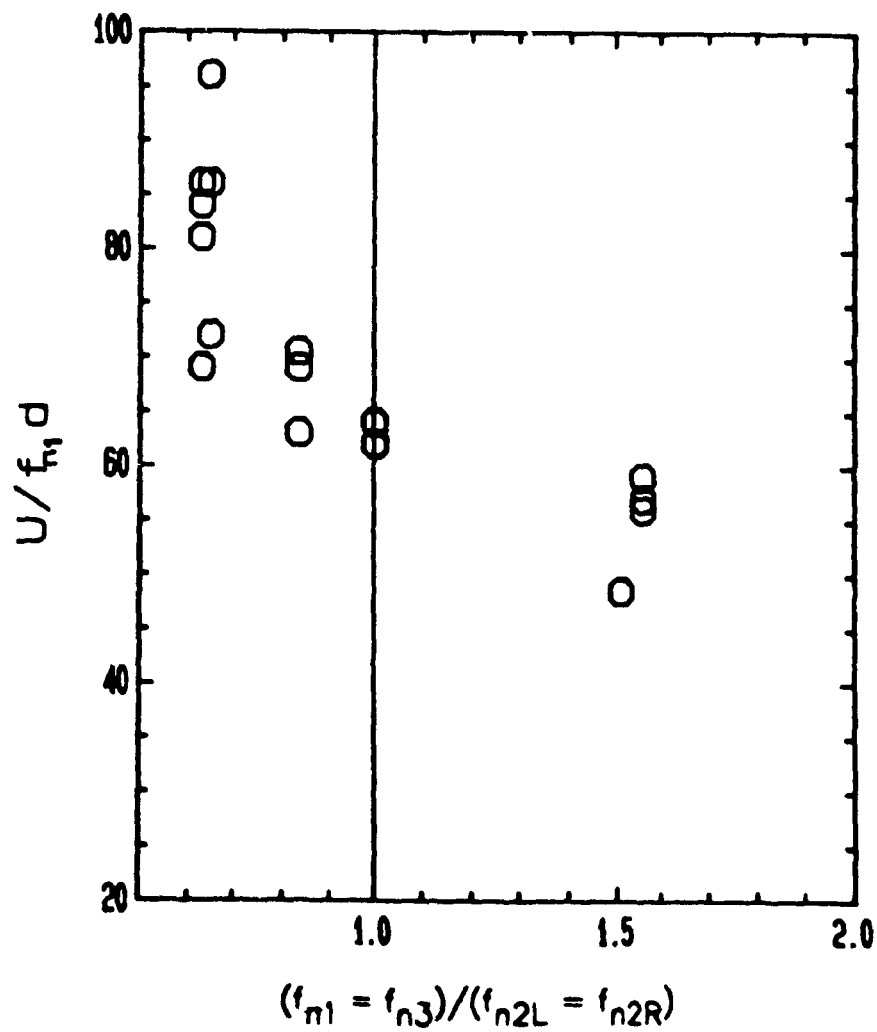


Figure 4.59: Effect of frequency detuning on $U_c/f_{n1}d$ (four-flexible cylinders - 1, 2R, 2L and 3 -, $\bar{m} = 280$, $[f_1 = f_3] \neq [f_{2R} = f_{2L}]$, and $\delta = 0.014$).

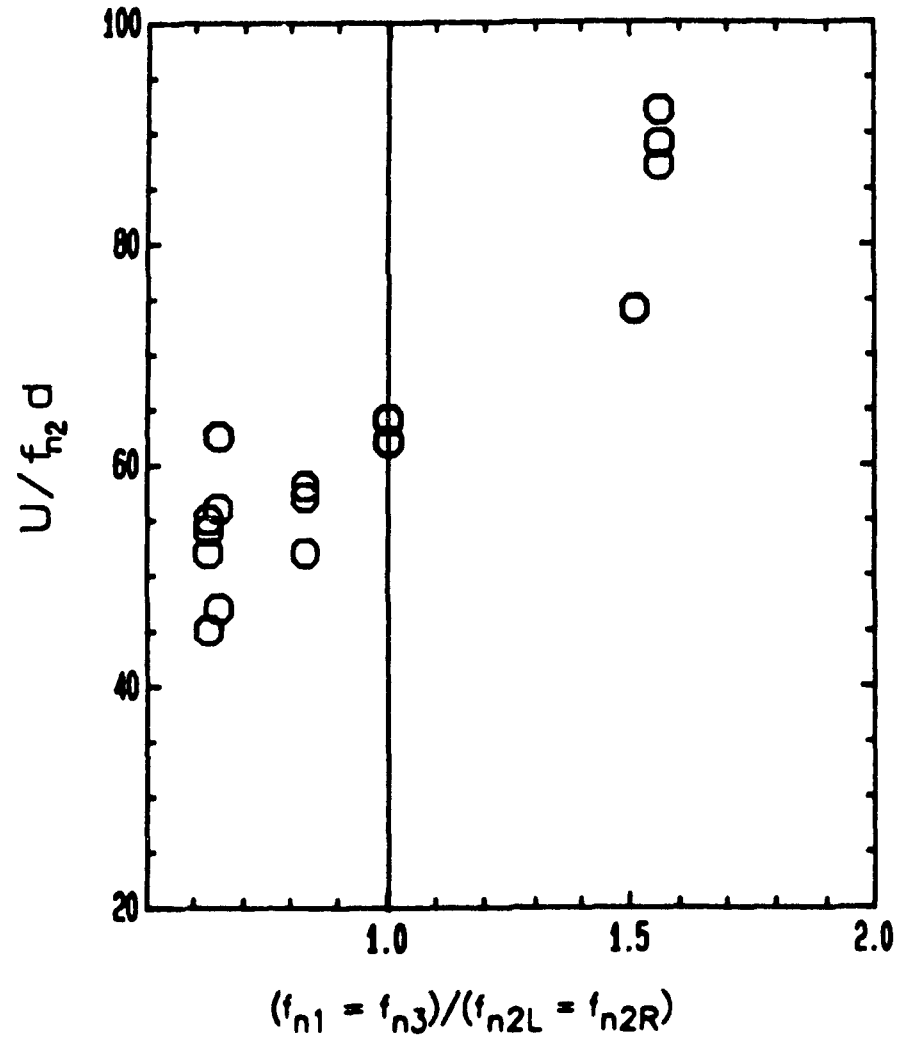


Figure 4.60: Effect of frequency detuning on $U_c/f_{n_2}d$ (four-flexible cylinders - 1, 2R, 2L and 3 -, $\bar{m} = 280$, $[f_1 = f_3] \neq [f_{2R} = f_{2L}]$, and $\delta = 0.014$).

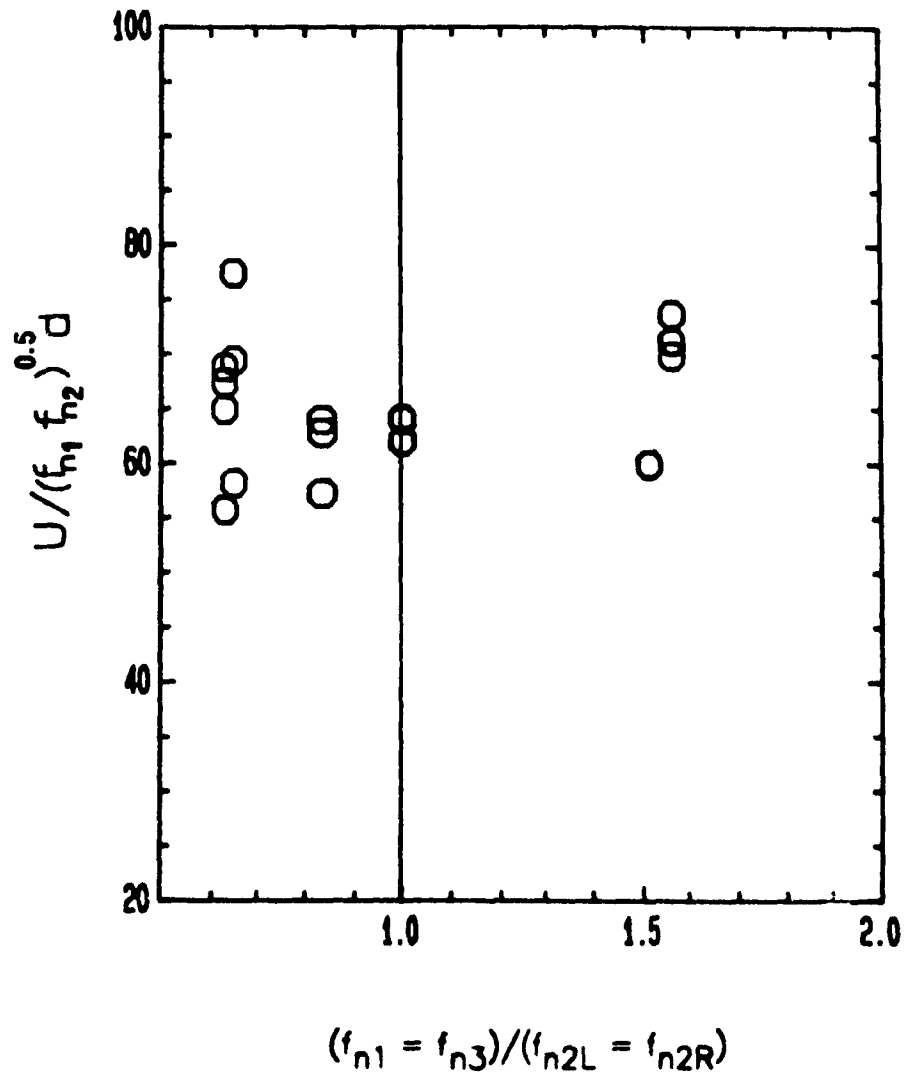


Figure 4.61: Effect of frequency detuning on $U_c / (f_{n1} f_{n2})^{0.5} d$ (four-flexible cylinders 1, 2R, 2L and 3 -, $\bar{m} = 280$, $[f_1 = f_3] \neq [f_{2R} = f_{2L}]$, and $\delta = 0.014$).

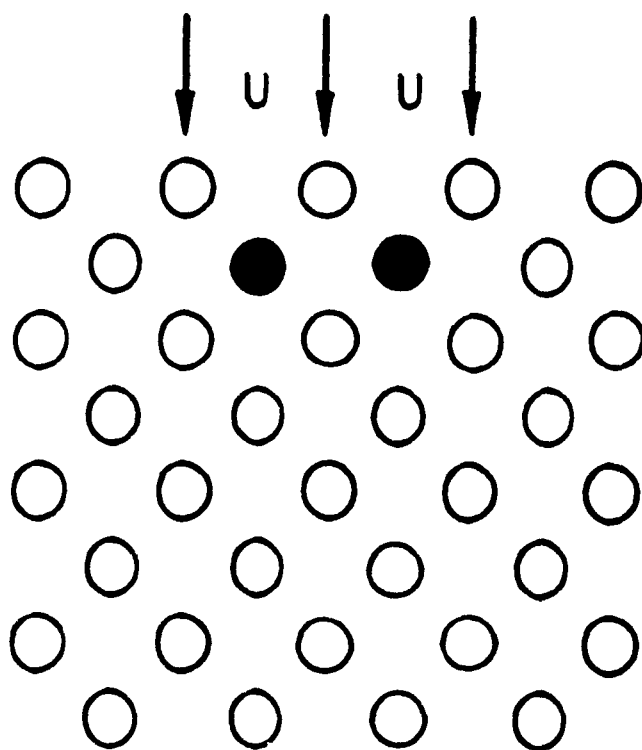


Figure 4.62: A two-flexible cylinder configuration in the second row of the array.

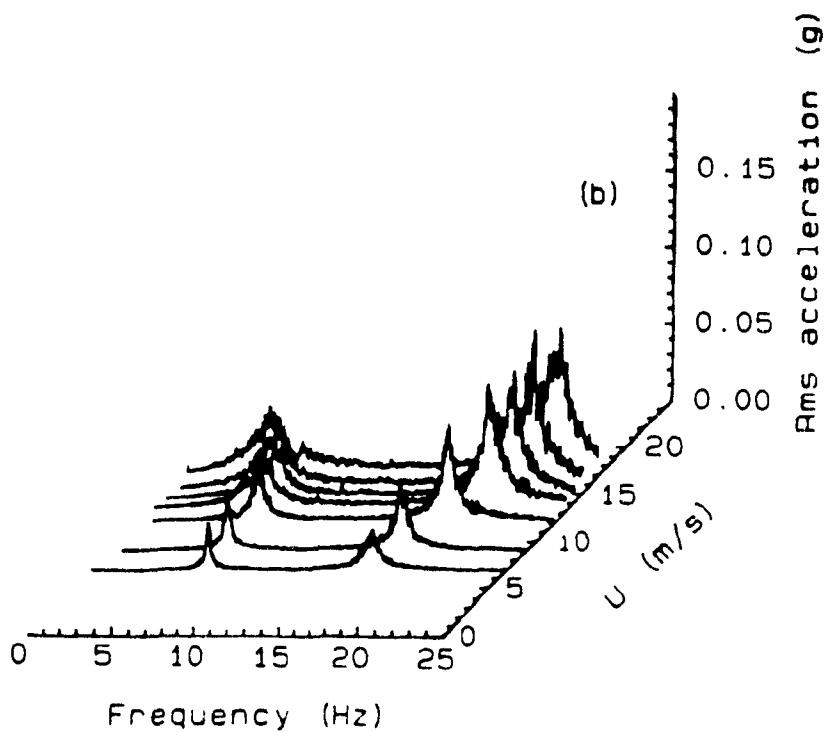
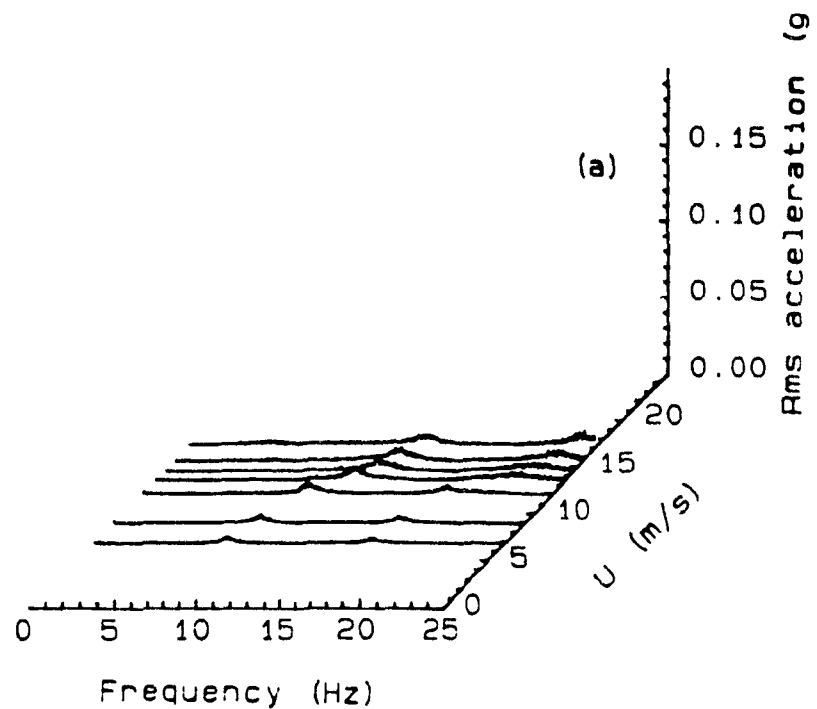


Figure 4.63: Variation of the in-flow (a) and cross-flow (b) vibration power spectra with the flow velocity for cylinder 2R (two-flexible cylinders - 2R, and 2L -, $m = 280$, $f_{2R} = f_{2L} = 7$ Hz and $\delta = 0.014$).

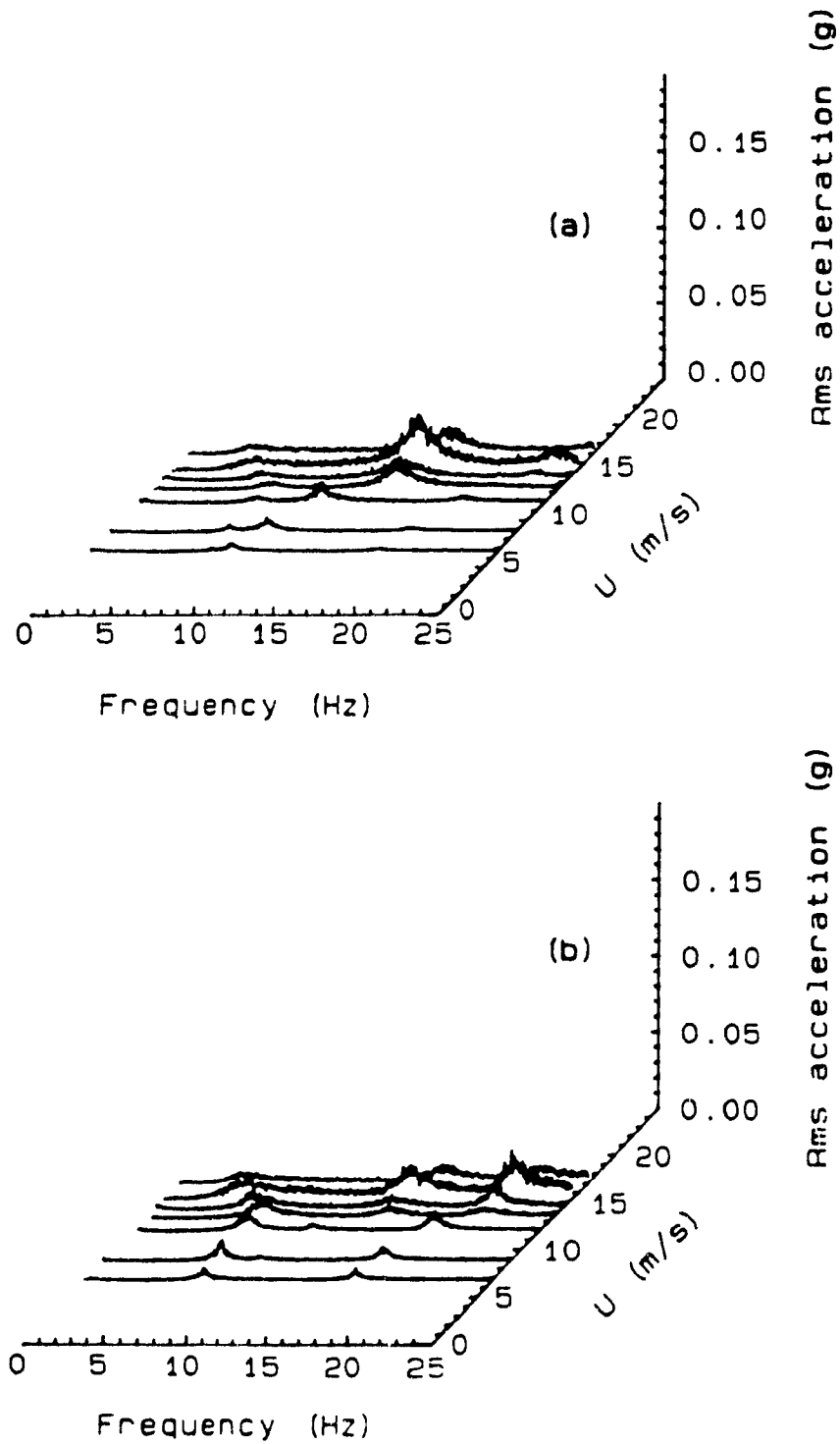


Figure 4.64: Variation of the in-flow (a) and cross-flow (b) vibration power spectra with the flow velocity for cylinder 2L (two-flexible cylinders - 2R, and 2L -, $\bar{m} = 280$, $f_{2R} = f_{2L} = 7$ Hz and $\delta = 0.014$).

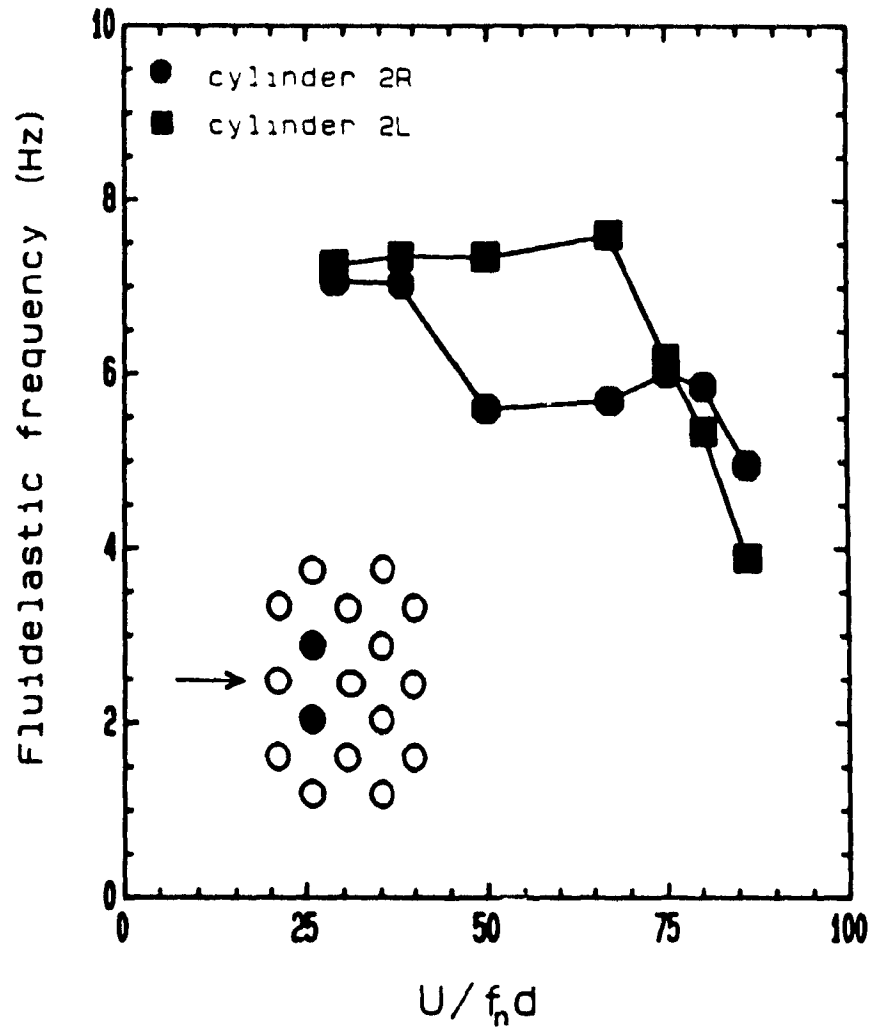


Figure 4.65: Variation of the major cross-flow fluidelastic frequencies of cylinders 2R and 2L with non-dimensional flow velocity (two-flexible cylinders 2R, and 2L, $\bar{m} = 280$, $f_{2R} = f_{2L} = 7$ Hz and $\delta = 0.014$).

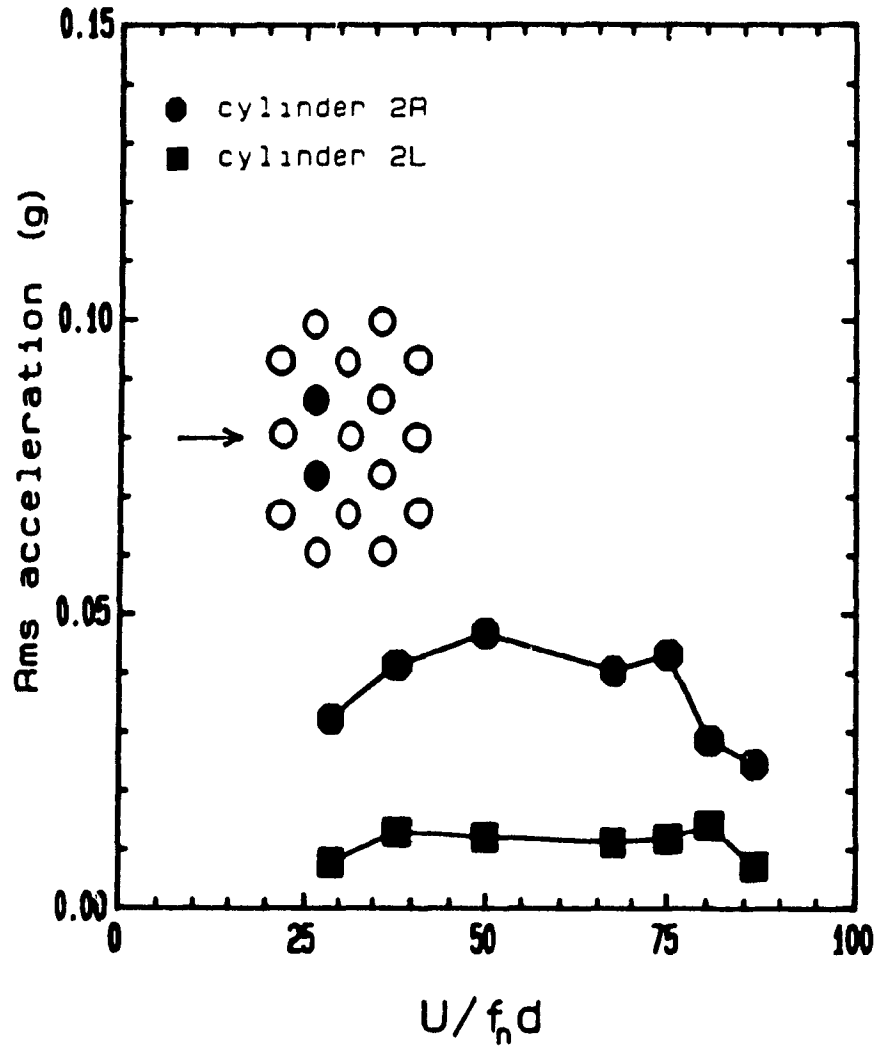


Figure 4.66: Rms acceleration of cylinders 2R and 2L at their major cross-flow frequencies as a function of the non-dimensional flow velocity (two-flexible cylinders - 2R, and 2L -, $\bar{m} = 280$, $f_{2R} = f_{2L} = 7$ Hz and $\delta = 0.014$).

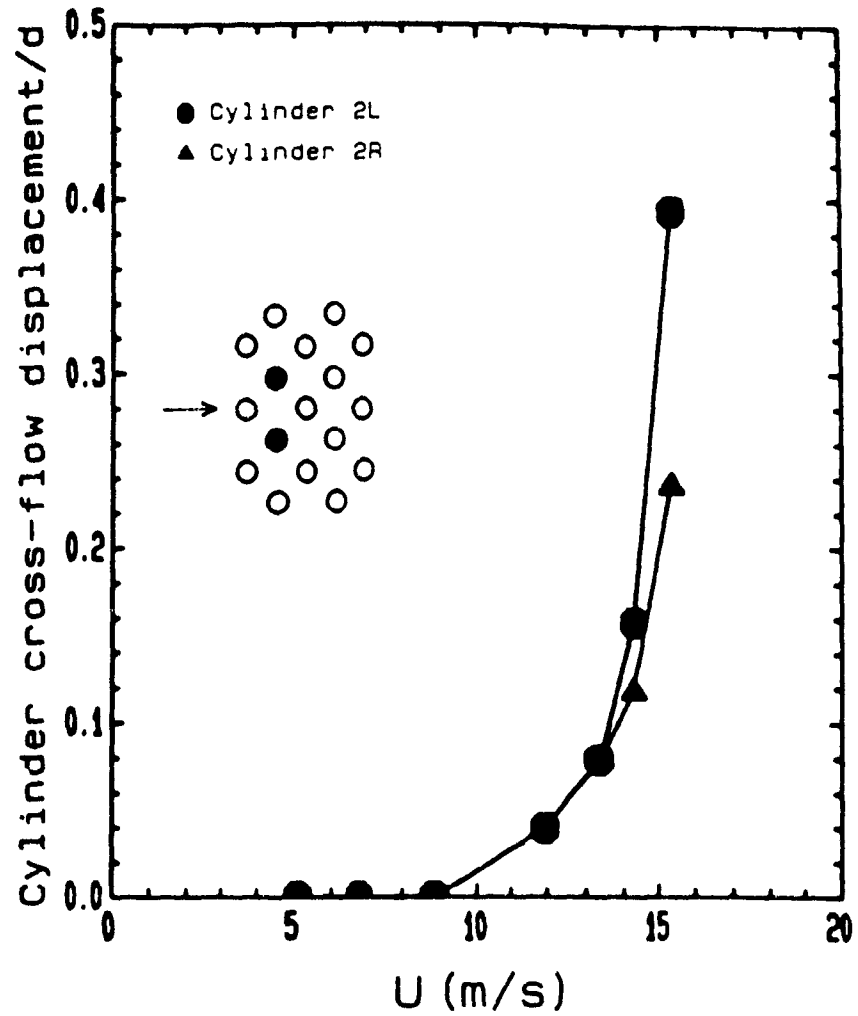


Figure 4.67: Variation of the cylinder cross-flow displacement with non-dimensional flow velocity (two-flexible cylinders - 2R, and 2L -, $\bar{m} = 280$, $f_{2R} = f_{2L} = 7$ Hz and $\delta = 0.014$).

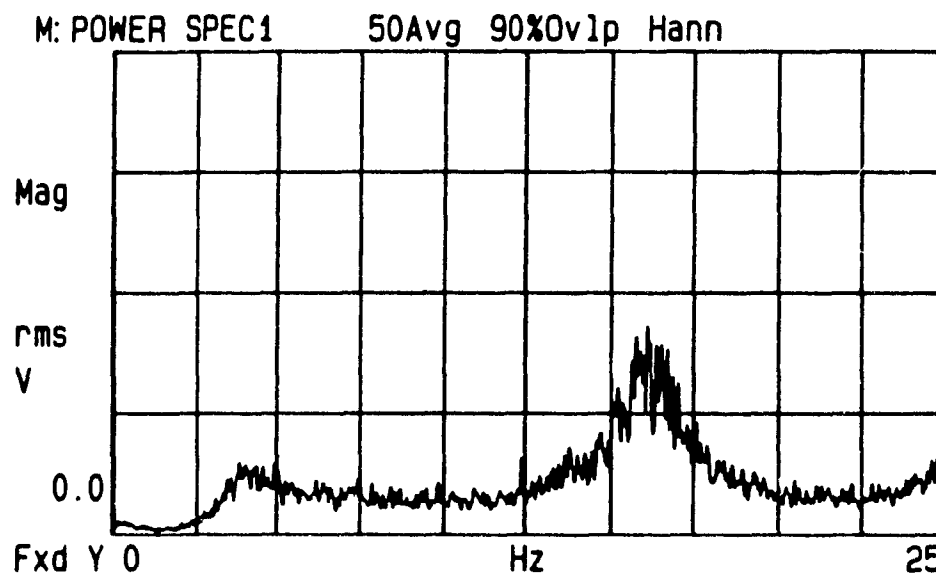


Figure 4.68: Vibrational power spectra of cylinder 2L at $U_\infty \approx 15.3$ m/s. (two-flexible cylinders - 2R, and 2L -, $\bar{m} = 280$, $f_{2R} = f_{2L} = 7$ Hz and $\delta = 0.014$).

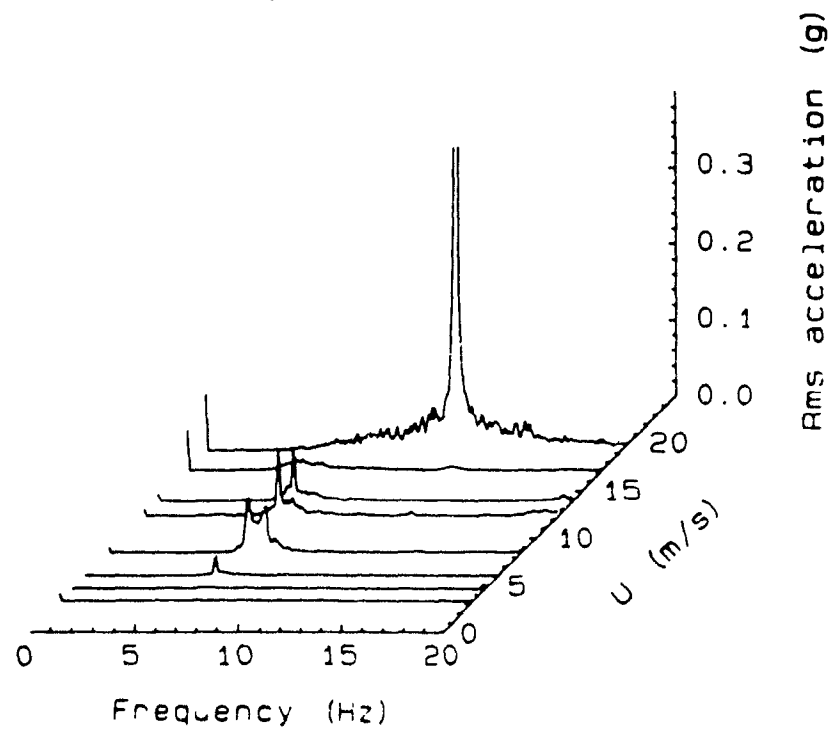
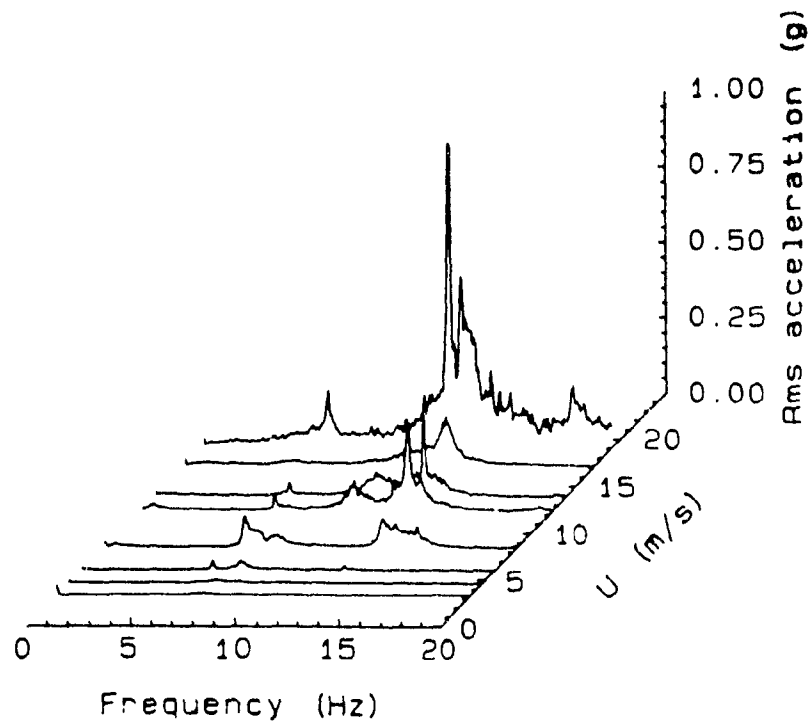


Figure 4.69: Variation of the in-flow (a) and cross-flow (b) vibration power spectra with the flow velocity for cylinder 2L (three-flexible cylinders - 2R, 2L and 3, $\bar{m} = 280$, $f_{2R} = f_{2L} = f_3 = 7$ Hz and $\delta = 0.014$).

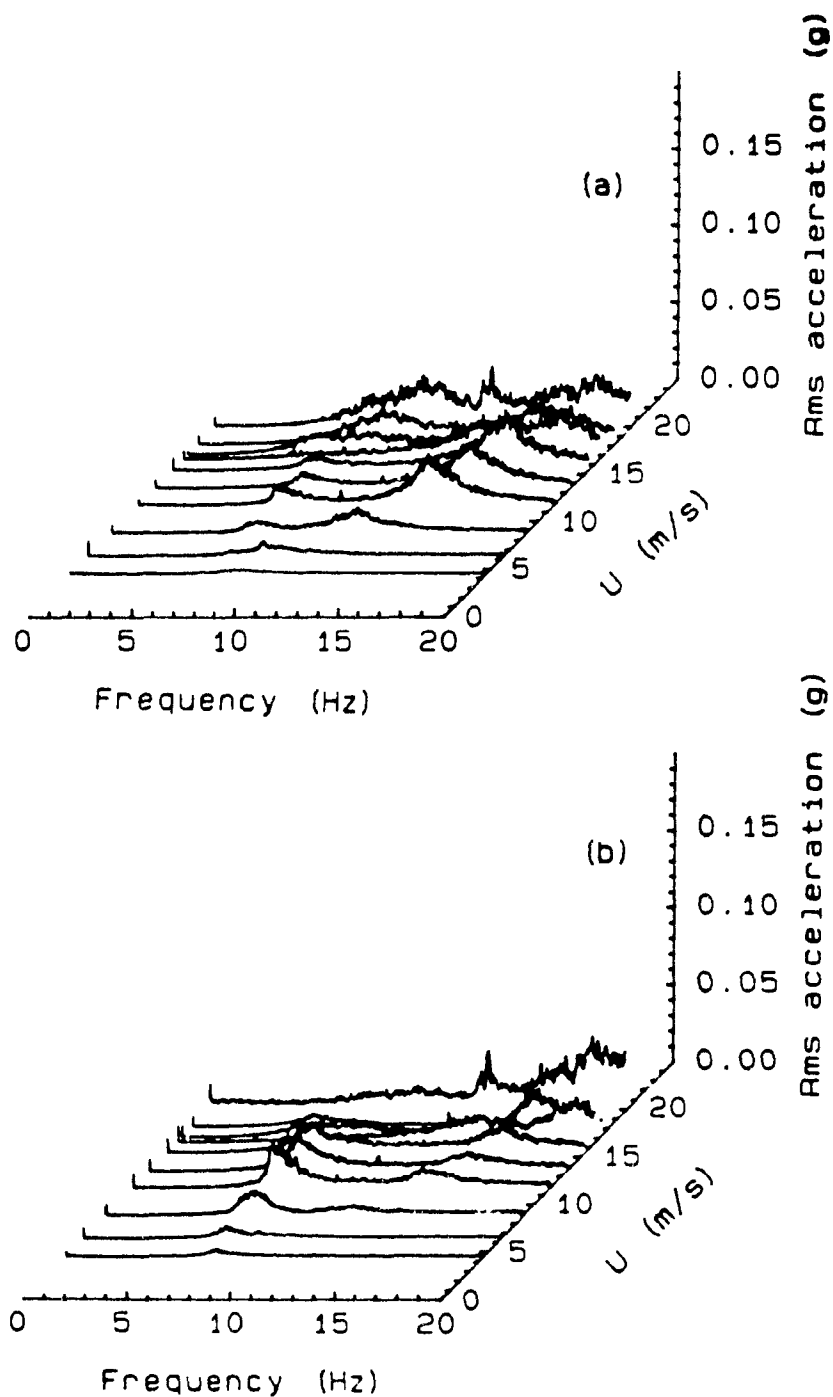


Figure 4 70: Variation of the in-flow (a) and cross-flow (b) vibration power spectra with the flow velocity for cylinder 2L (three-flexible cylinders - 2R, 2L and 3 -, $\bar{m} = 280$, $f_{2R} = f_{2L} = f_3 = 7$ Hz and $\delta = 0.20$).

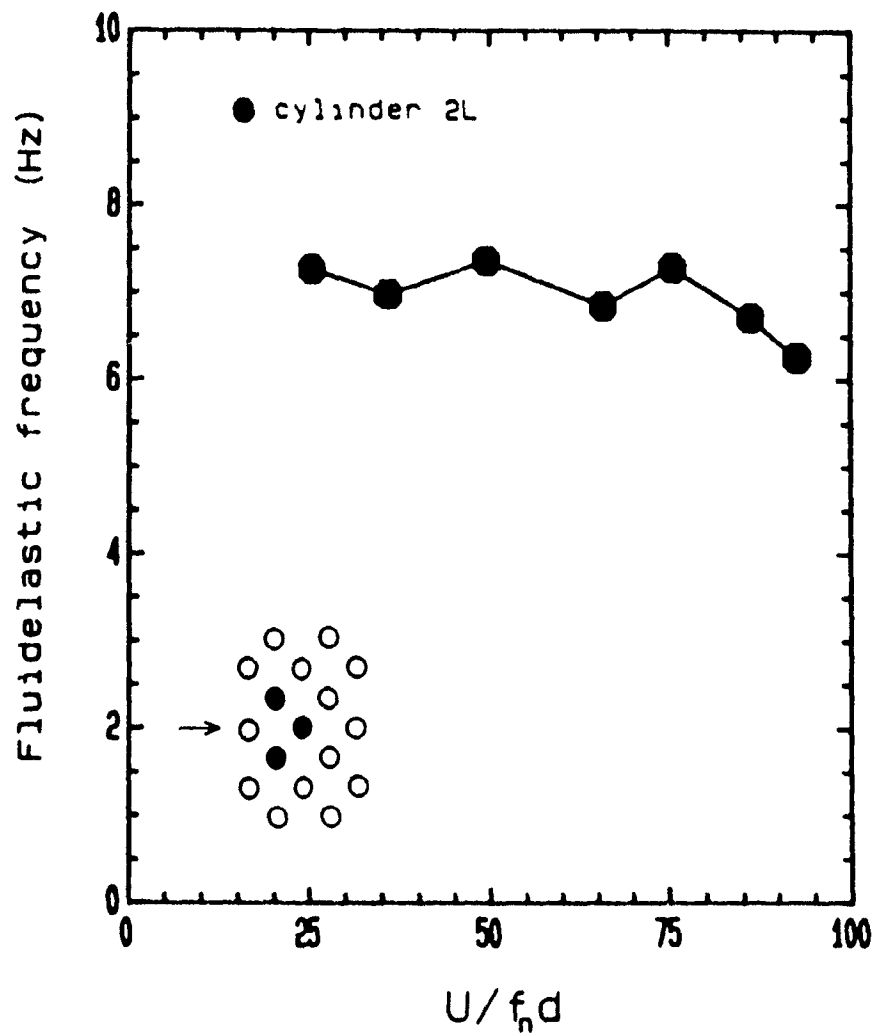


Figure 4.71: Variation of the major cross-flow fluidelastic frequency of cylinder 2L with non-dimensional flow velocity (three-flexible cylinders - 2R, 2L and 3, $m = 280$, $f_{2R} = f_{2L} = f_3 = 7$ Hz and $\delta = 0.20$).

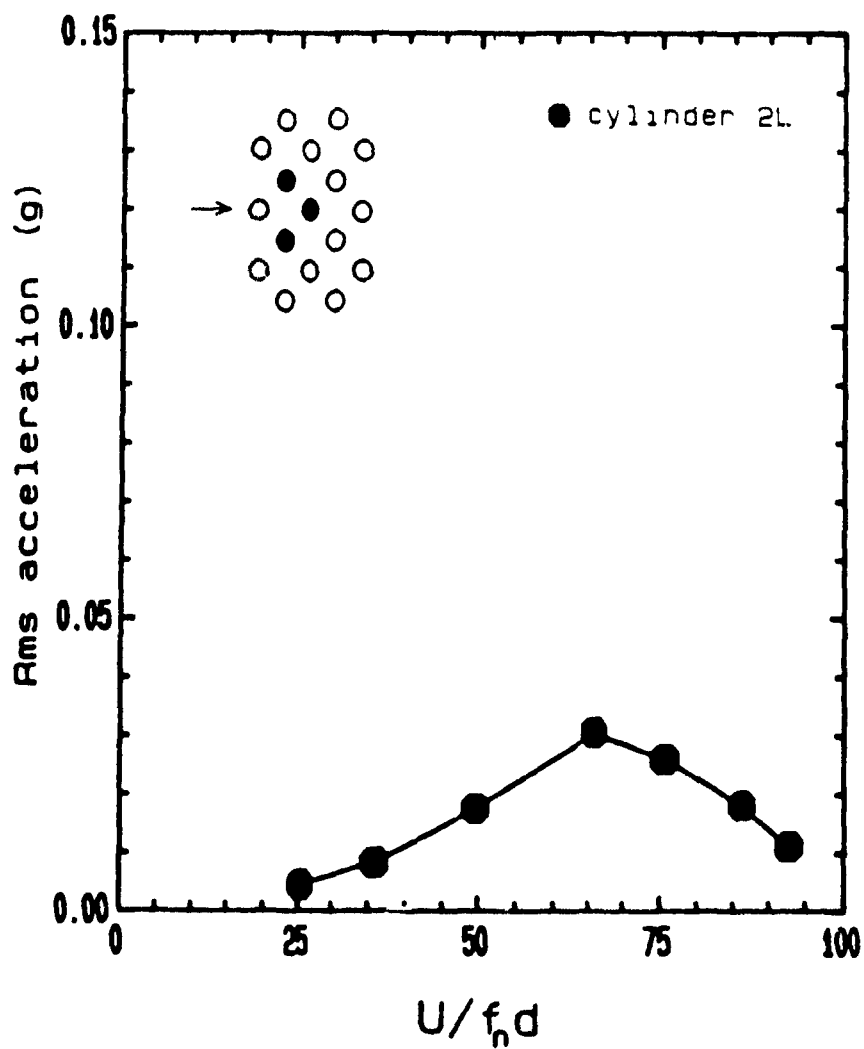


Figure 4.72: Rms acceleration of cylinder 2L at its major cross-flow frequency as a function of non-dimensional flow velocity (three-flexible cylinders - 2R, 2L and 3 -, $m = 280$, $f_{2R} = f_{2L} = f_3 = 7$ Hz and $\delta = 0.20$).

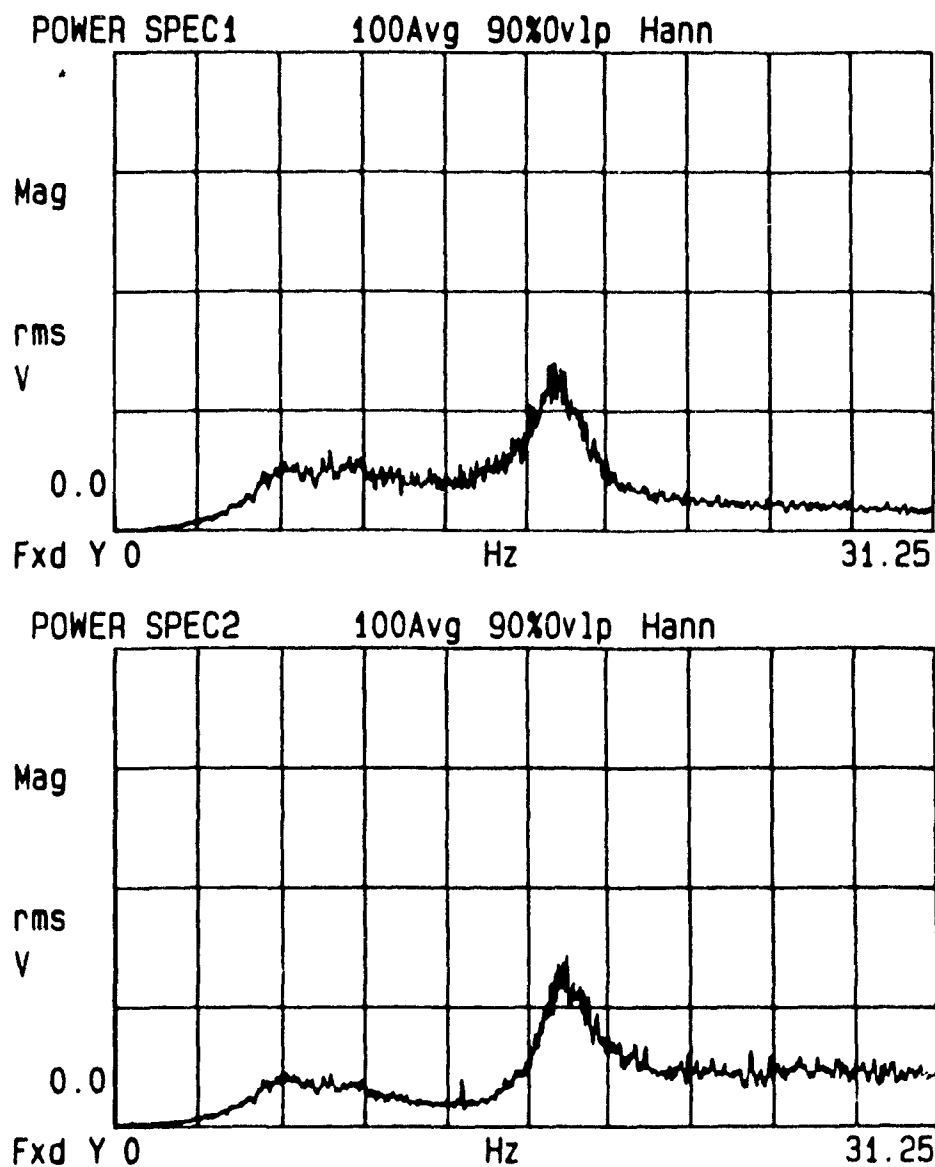


Figure 4.73: In- and Cross-flow vibrational power spectra of cylinder 2L at $U_\infty = 16.9$ m/s (three-flexible cylinders - 2R, 2L and 3 -, $\bar{m} = 280$, $f_{2R} = f_{2L} = f_3 = 7$ Hz and $\delta = 0.20$).

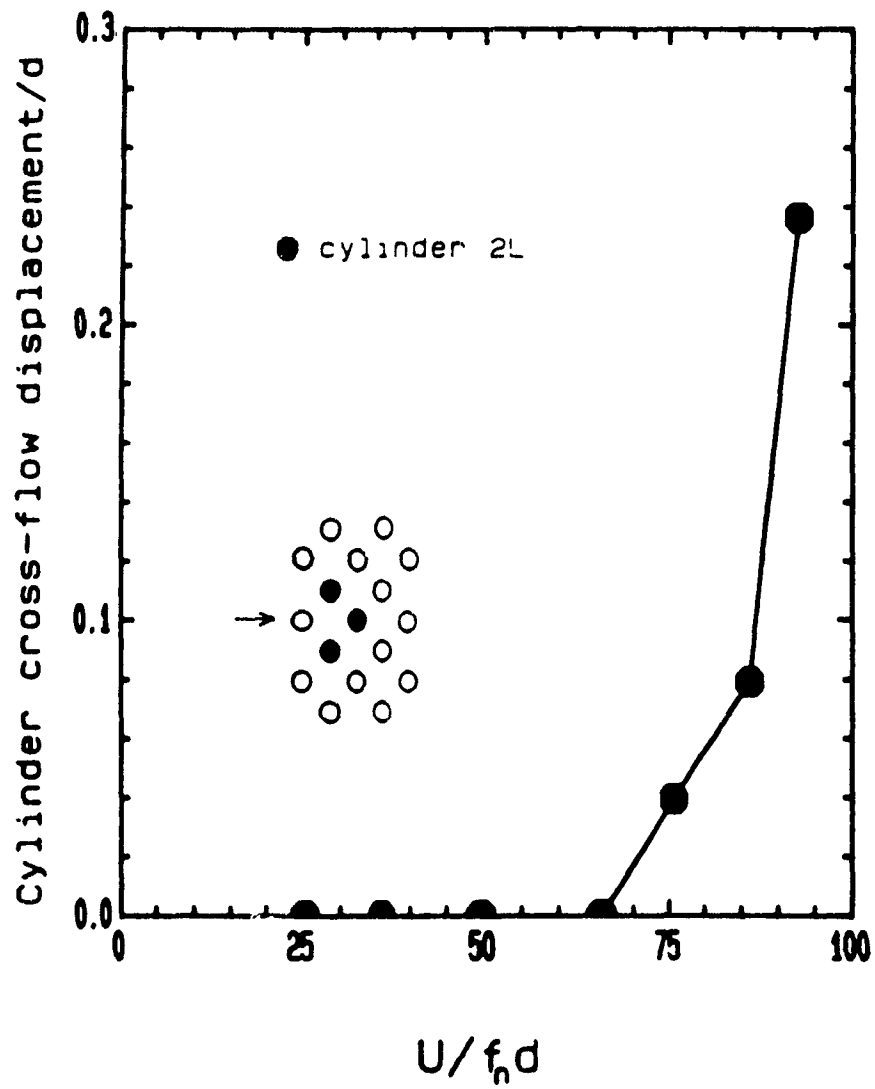


Figure 4.74: Variation of the cylinder cross-flow displacement with non-dimensional flow velocity (three-flexible cylinders - 2R, 2L and 3 -, $\bar{m} = 280$, $f_{2L} = f_{2R}f_3 = 7$ Hz and $\delta = 0.20$).

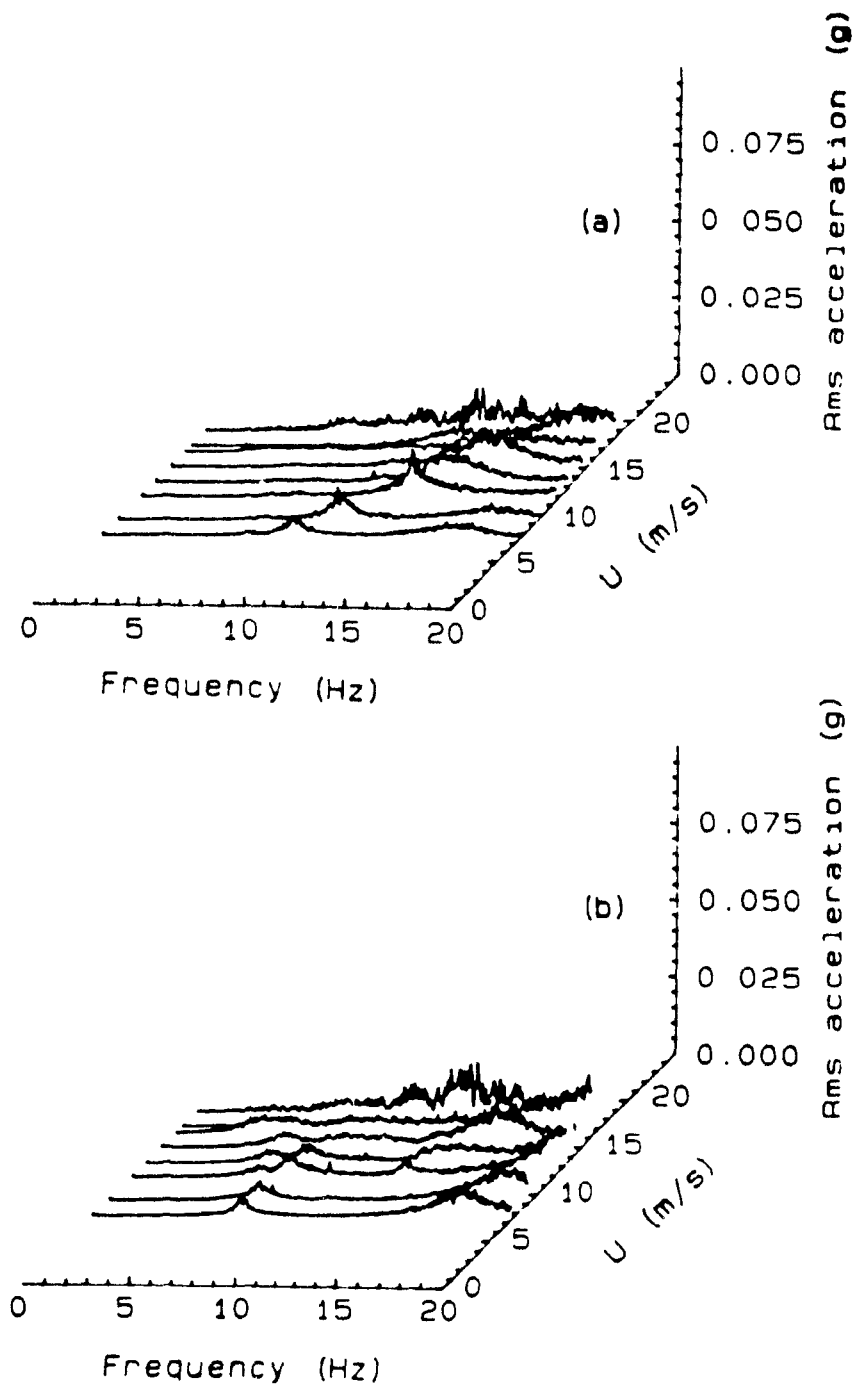


Figure 4.75: Variation of the in-flow (a) and cross-flow (b) vibration power spectra with flow velocity for cylinder 2L (three-flexible cylinders 2R, 2L and 3, $\bar{m} = 280$, $f_{2R} = f_{2L} = 7$ Hz, $f_3 = 13.5$ Hz and $\delta = 0.14$).

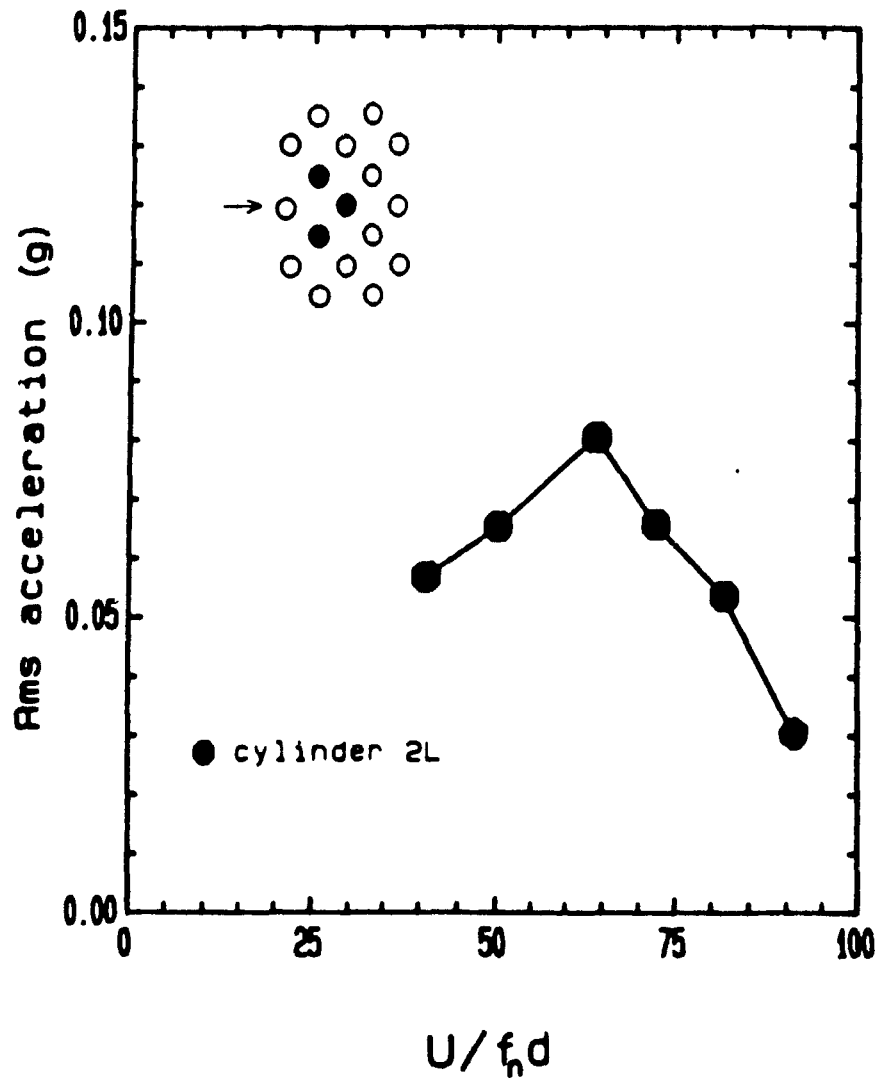


Figure 4.76: Rms acceleration of cylinder 2L at its major cross-flow frequency as a function of non-dimensional flow velocity (three-flexible cylinders - 2R, 2L and 3 -, $\bar{m} = 280$, $f_{2L} = f_{2R} = 7$ Hz, $f_3 = 13.5$ Hz and $\delta = 0.14$).

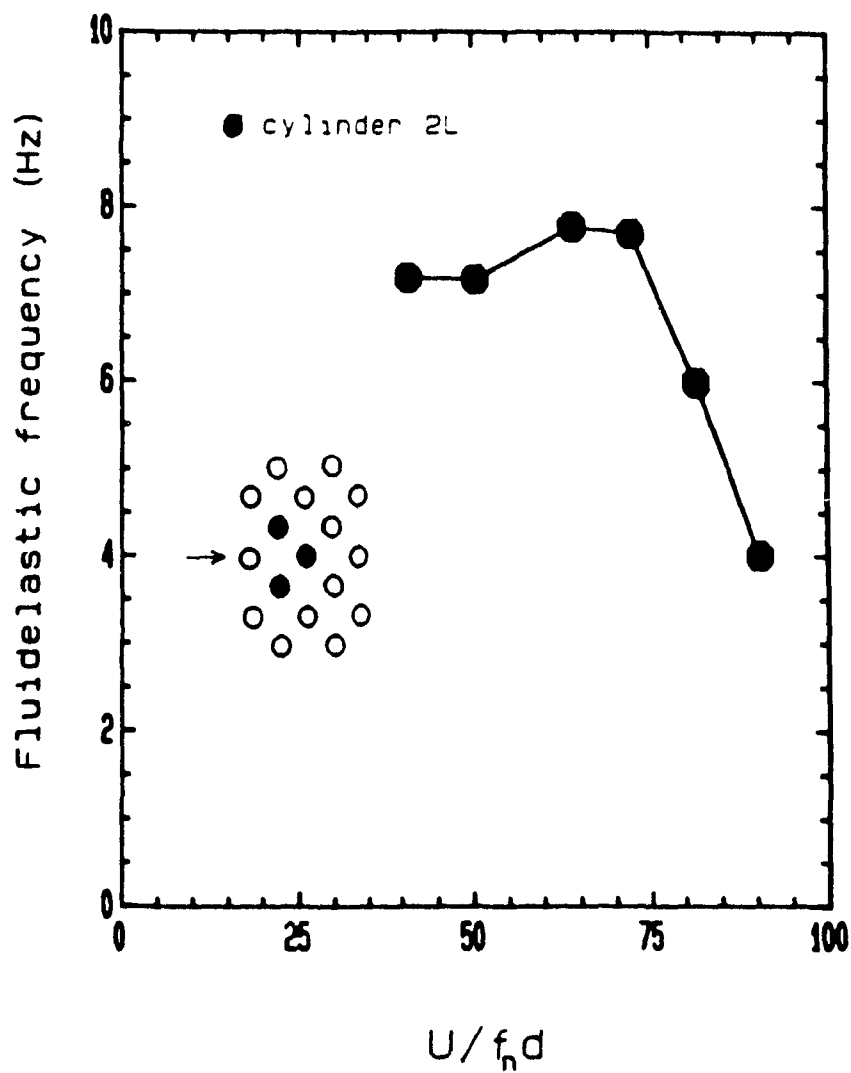


Figure 4.77: Variation of the major cross-flow fluidelastic frequency of cylinder 2L with non-dimensional flow velocity (three-flexible cylinders - 2R, 2L and 3, $m = 280$, $f_{2R} = f_{2L} = 7$ Hz, $f_3 = 13.5$ Hz and $\delta = 0.14$).

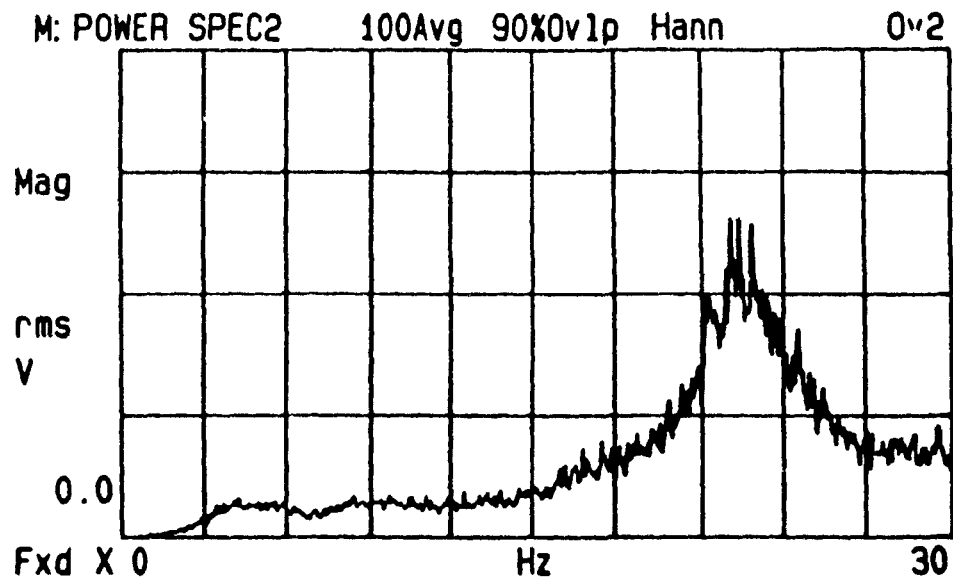


Figure 4.78: cross-flow vibrational power spectra of cylinder 2L at $U_\infty = 16.1$ m/s (three-flexible cylinders - 2R, 2L and 3 -, $\bar{m} = 280$, $f_{2R} = f_{2L} = 7$ Hz, $f_3 = 13.5$ Hz $\delta = 0.14$).

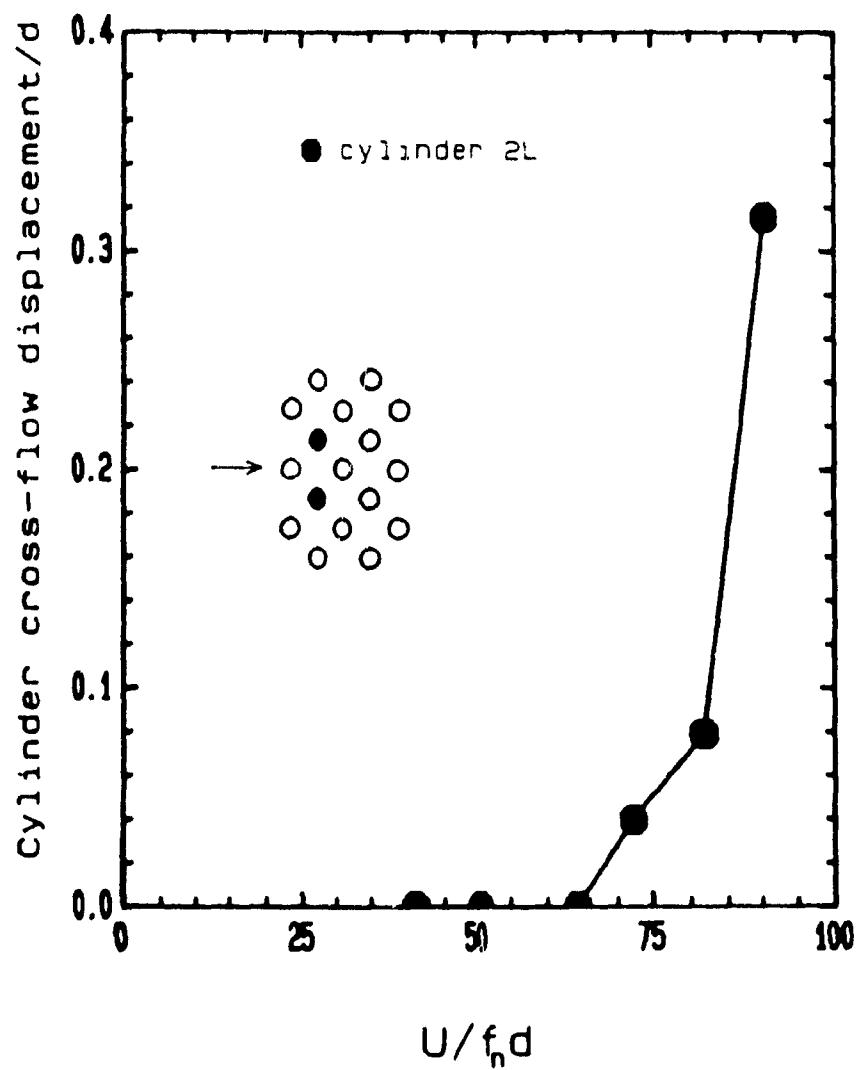


Figure 4.79: Variation of the cylinder cross-flow displacement with non-dimensional flow velocity (three-flexible cylinders - 2R, 2L and 3 -, $\bar{m} = 280$, $f_{2L} = f_{2R} = 7$ Hz, $f_3 = 13.5$ Hz and $\delta = 0.14$).

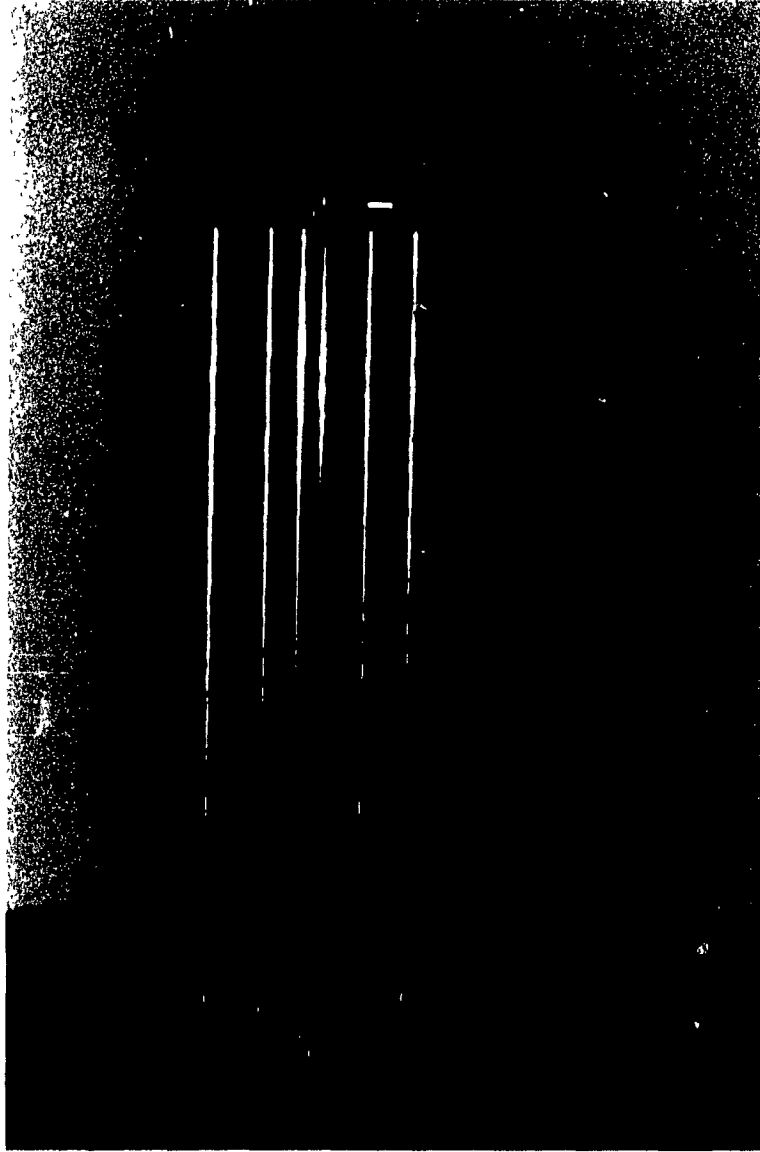


Figure 5.1: The force measurement insert.

PAGINATION ERROR.

ERREUR DE PAGINATION.

TEXT COMPLETE.

LE TEXTE EST COMPLET.

NATIONAL LIBRARY OF CANADA.

BIBLIOTHEQUE NATIONALE DU CANADA.

CANADIAN THESES SERVICE.

SERVICE DES THESES CANADIENNES.

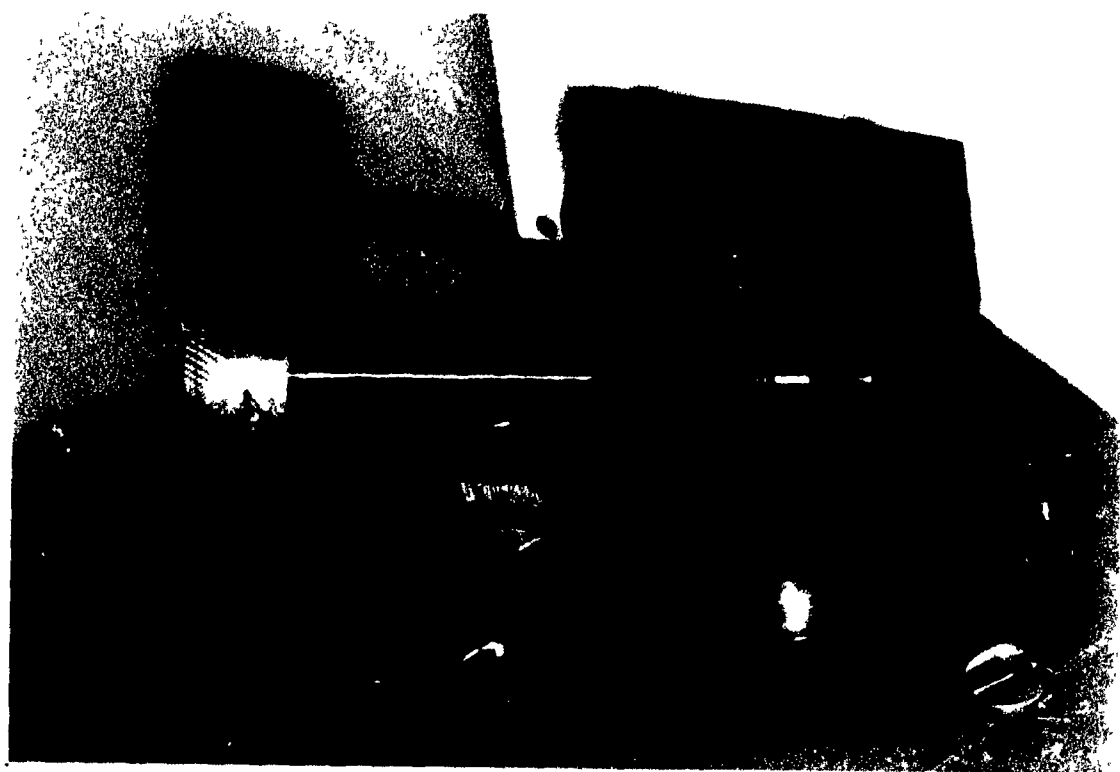


Figure 5.2: The gear arrangement.



Figure 5 3 The force balance and the instrumented cylinder

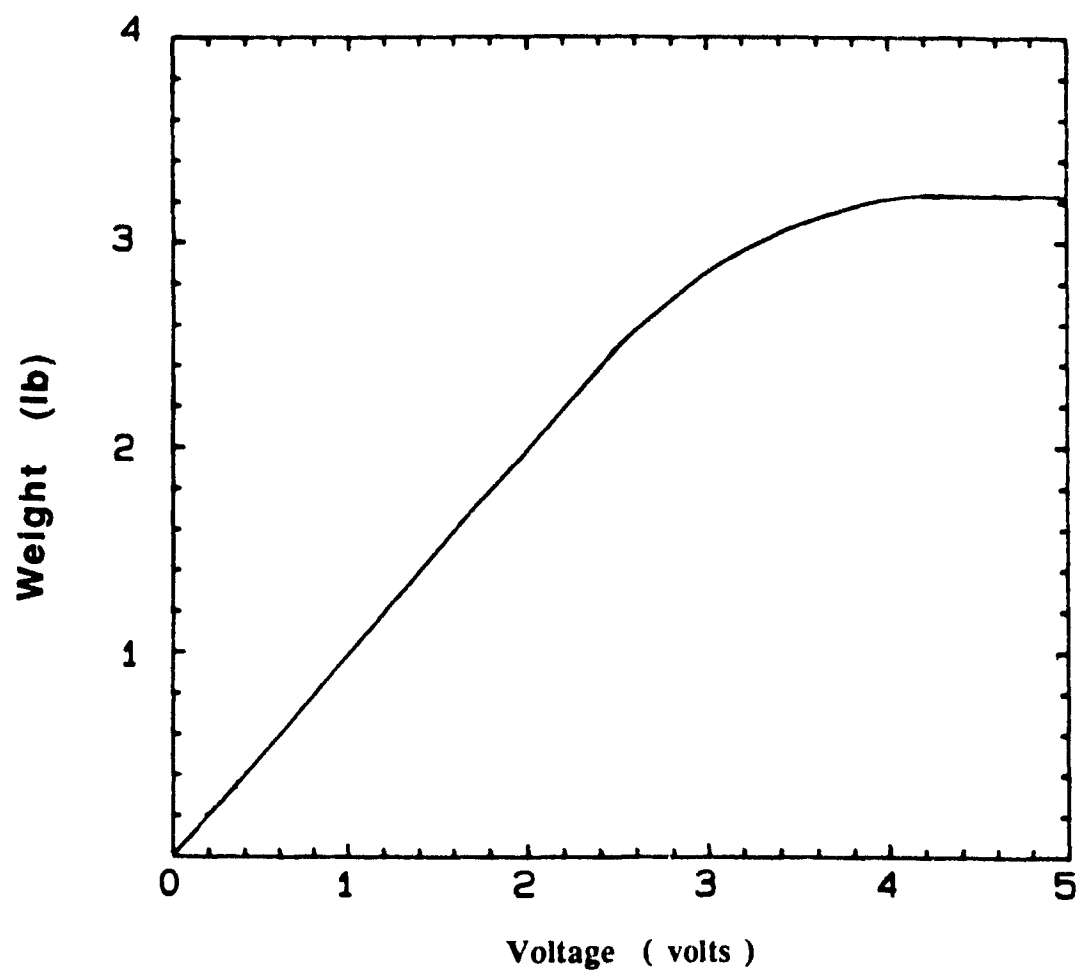


Figure 5 4 Calibration curve for the force transducers.

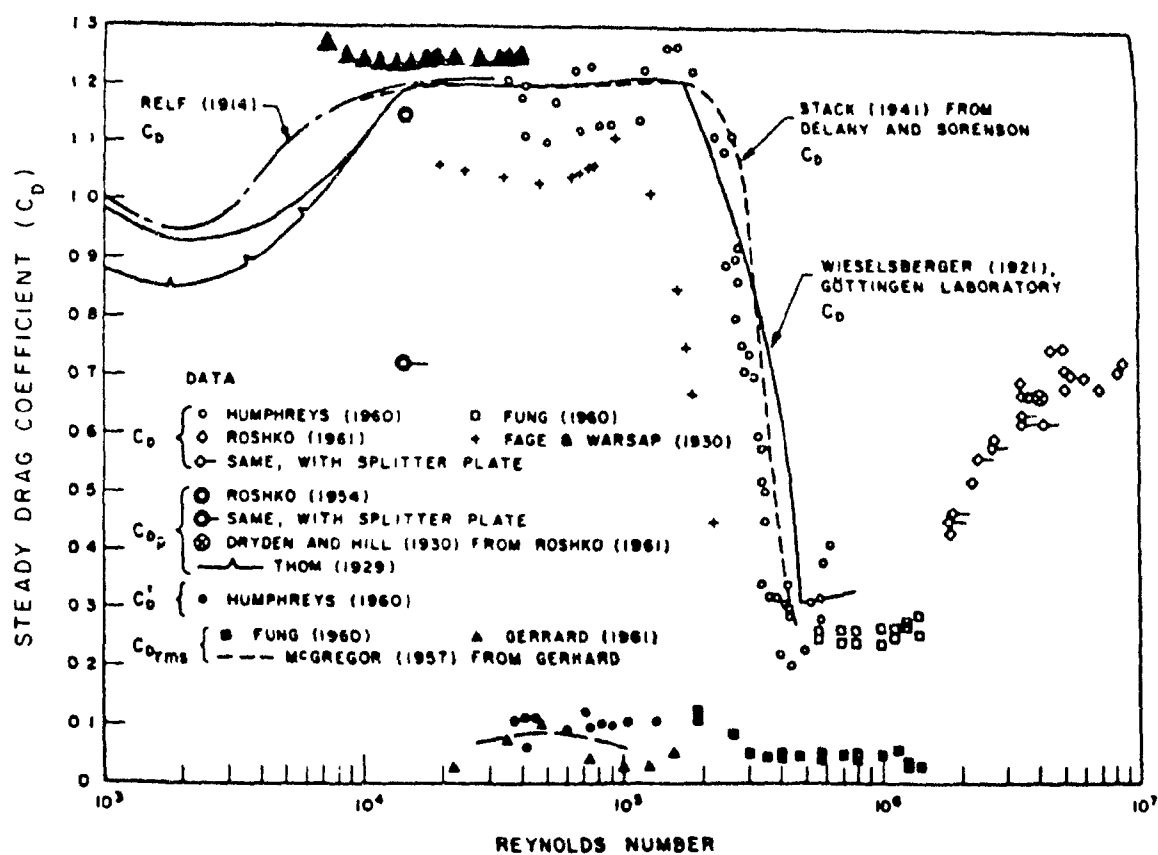


Figure 6.1: Variation of the steady drag coefficient of a single cylinder in cross-flow with Reynolds number. The original figure from reference 4. Note: drag coefficient values determined in this study are shown by full triangles.

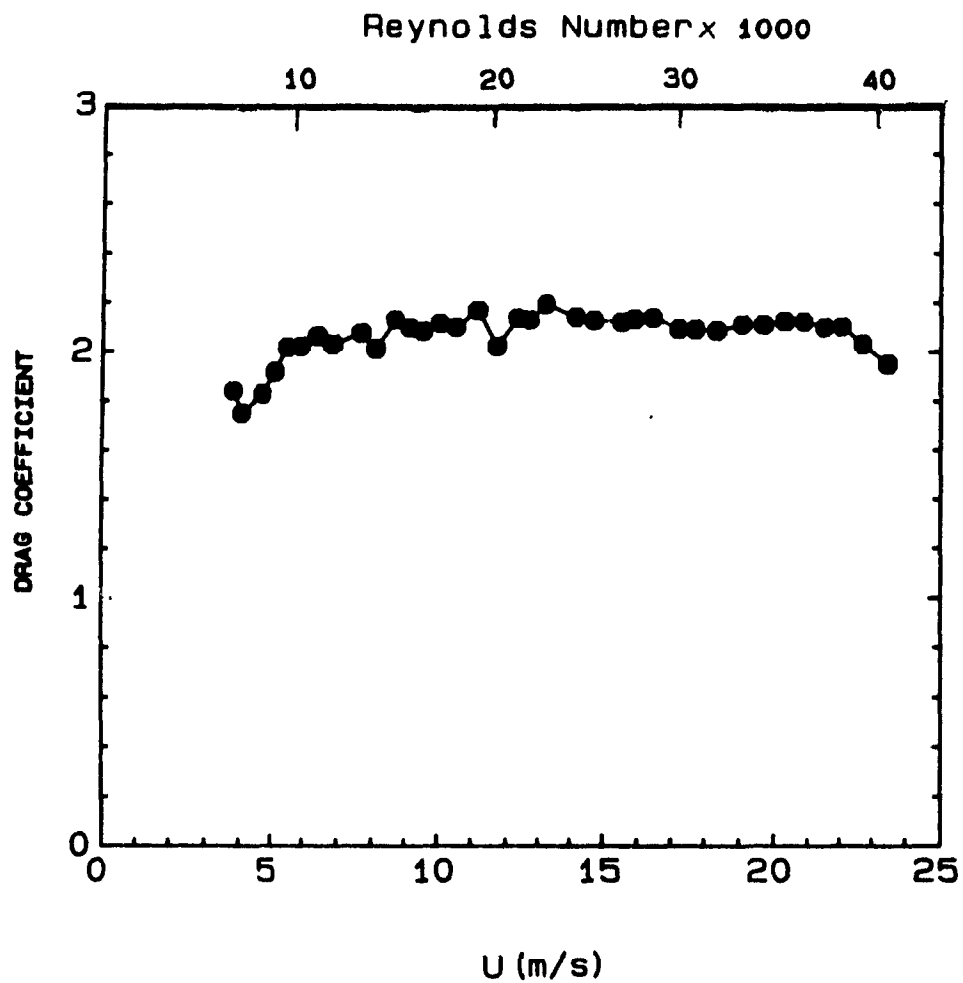


Figure 6.2: Variation of the drag coefficient with Reynolds number, for a cylinder in the first row of the array ($\bar{x} = 0, \bar{y} = 0$)

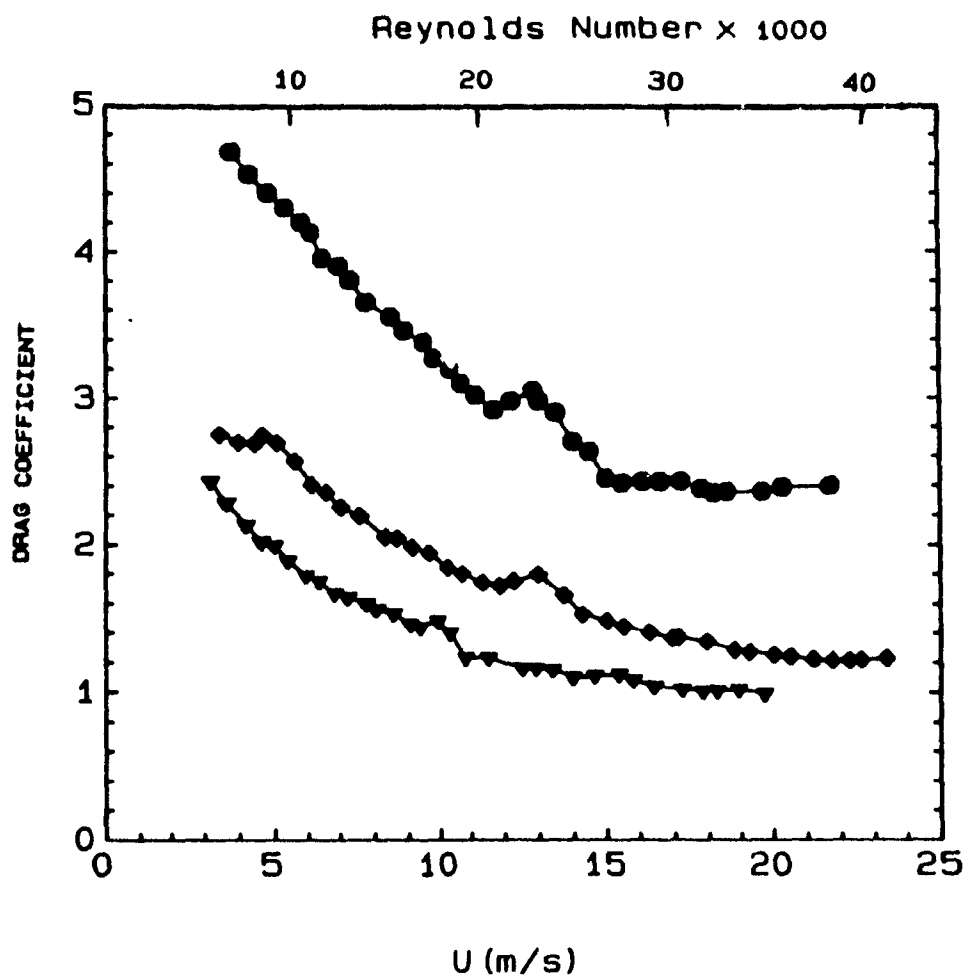


Figure 6.3: Variation of the drag coefficient with Reynolds number for cylinders in the second (●), third (◆) and fourth (▼) rows of the array ($\bar{x} = 0, \bar{y} = 0$).

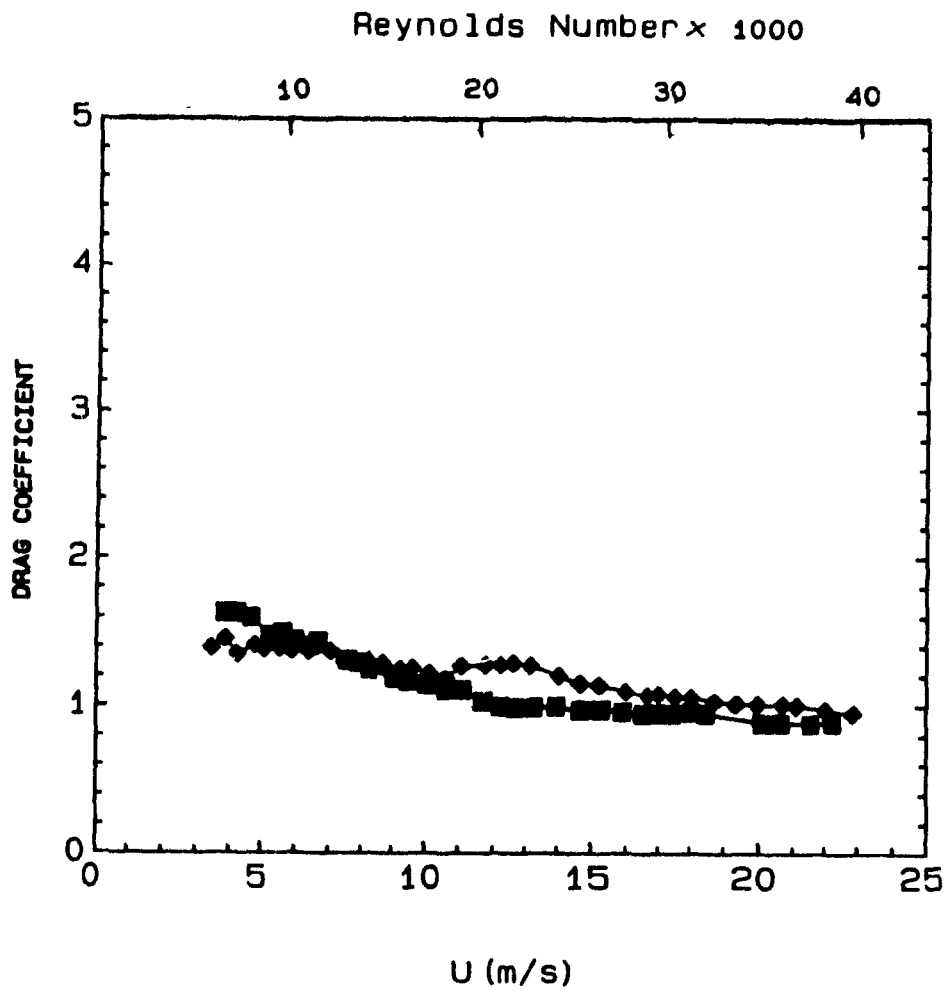


Figure 6.1. Variation of the drag coefficient with Reynolds number for cylinders in the fifth (\blacksquare) and seventh (\blacklozenge) rows of the array ($\bar{x} = 0, \bar{y} = 0$).

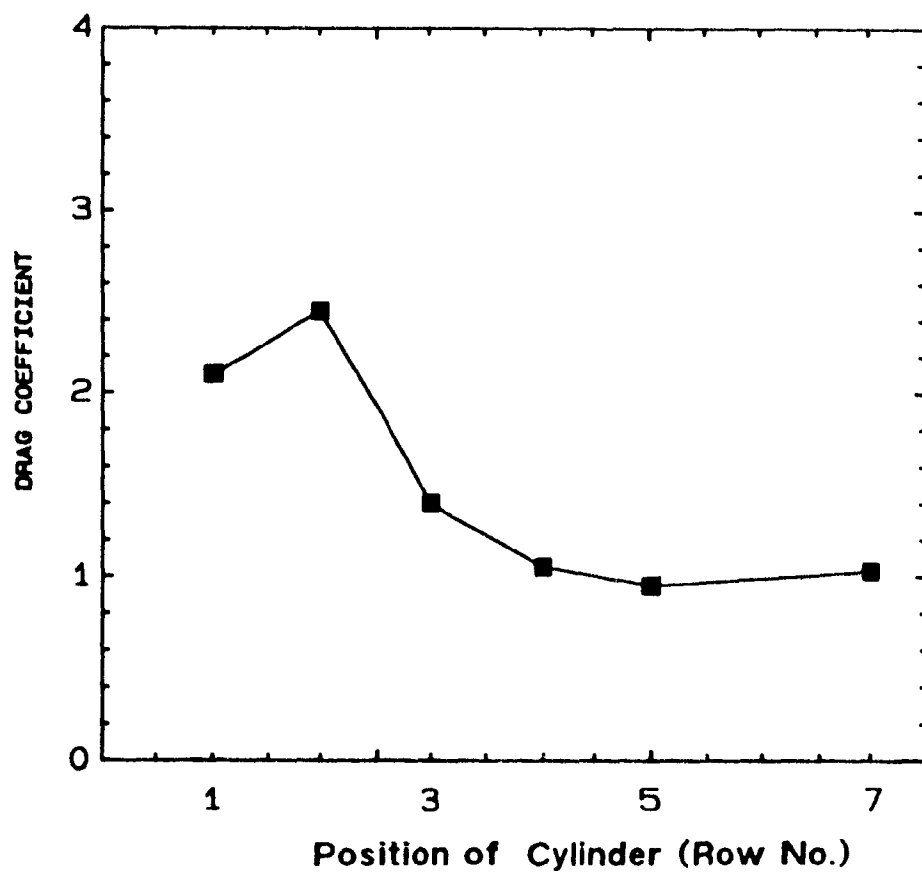


Figure 6.5 Variation of the drag coefficient with position in the array at a flow velocity of 16.6 m/s ($\bar{x} = 0, \bar{y} = 0$).

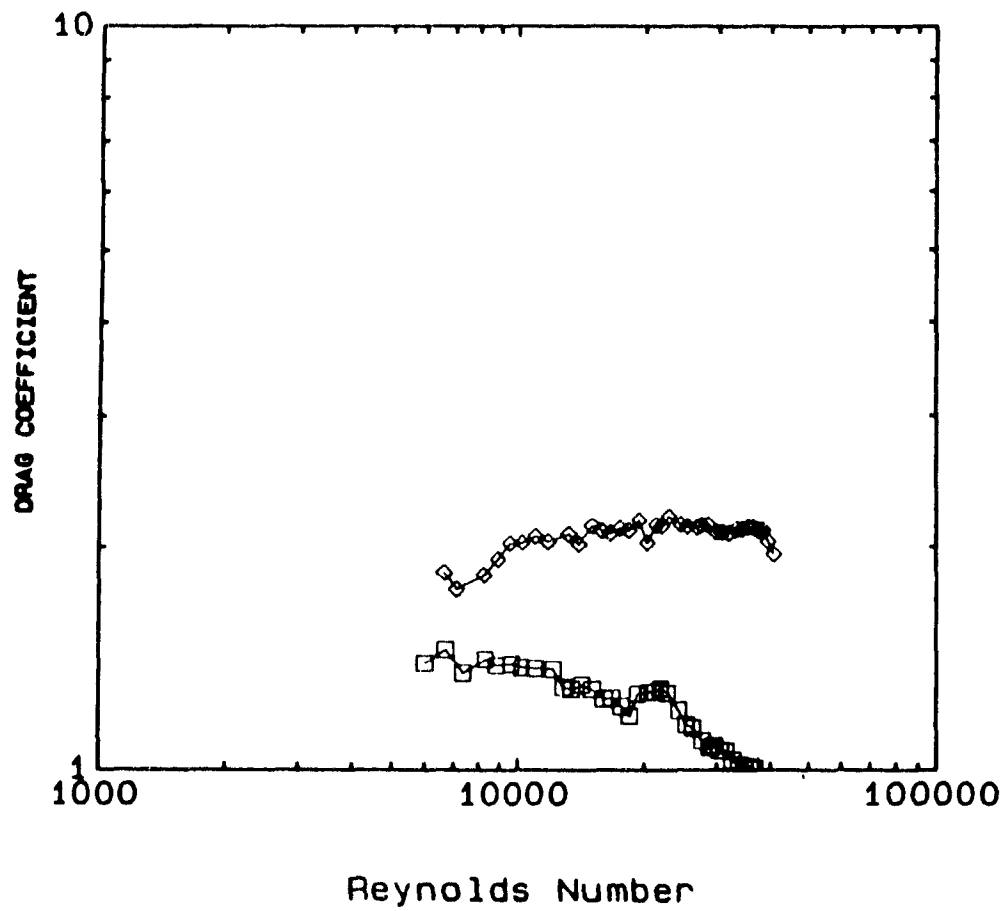


Figure 6.6 Variation of the drag coefficient with Reynolds number for cylinders in the first (\circ), seventh (\square) and 10th (\diamond) rows of the array ($\bar{x} = 0, \bar{y} = 0$).

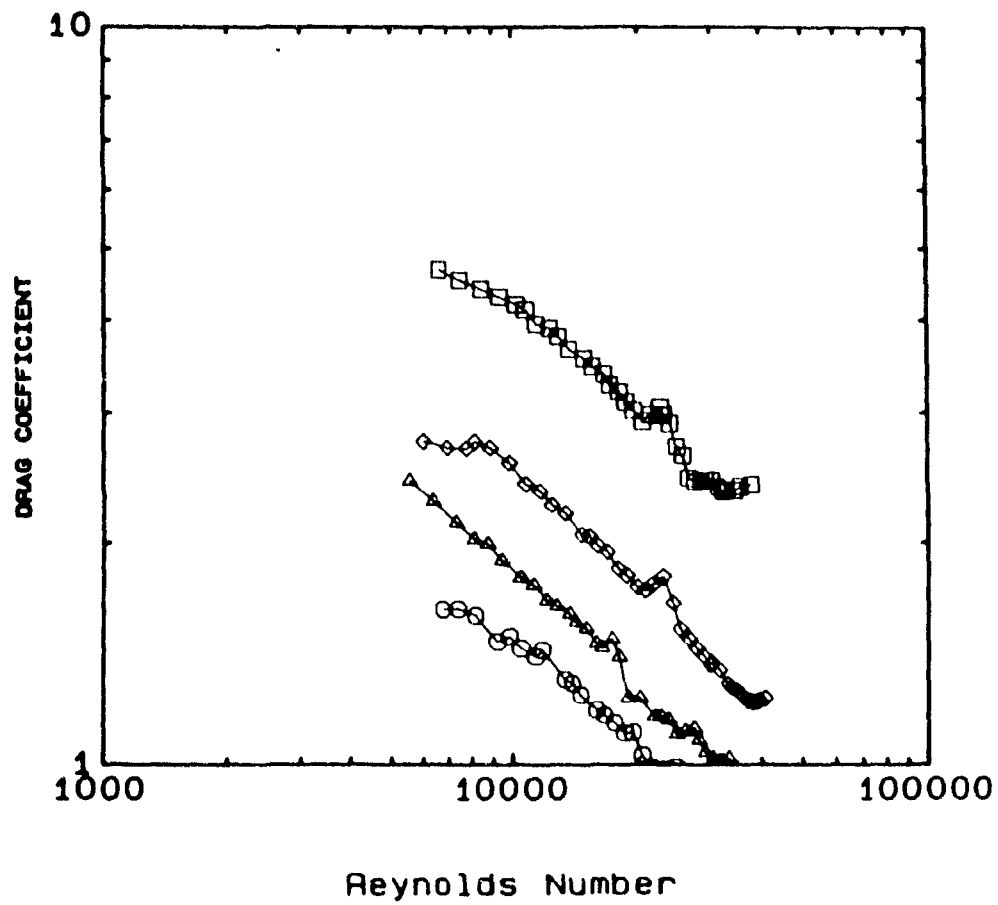


Figure 6.7: Variation of the drag coefficient with Reynolds number for cylinders in the second (\square), third (\diamond), fourth (\triangle) and fifth (\circ) rows of the array ($x = 0, y = 0$).

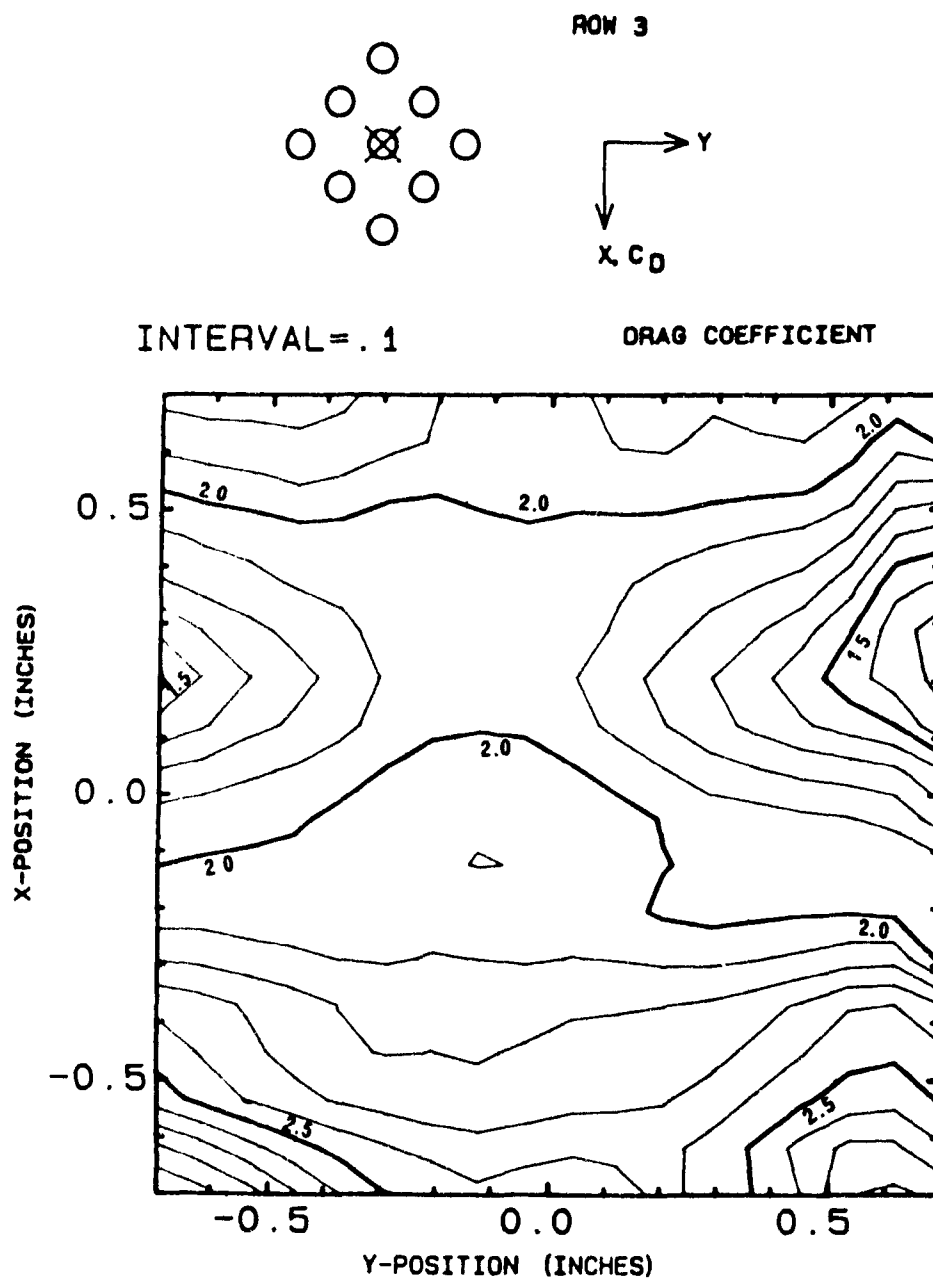


Figure 6.8. Variation of the drag coefficient with cylinder displacement (third row cylinder, $U_{\infty} = 8.3$ m/s).

1

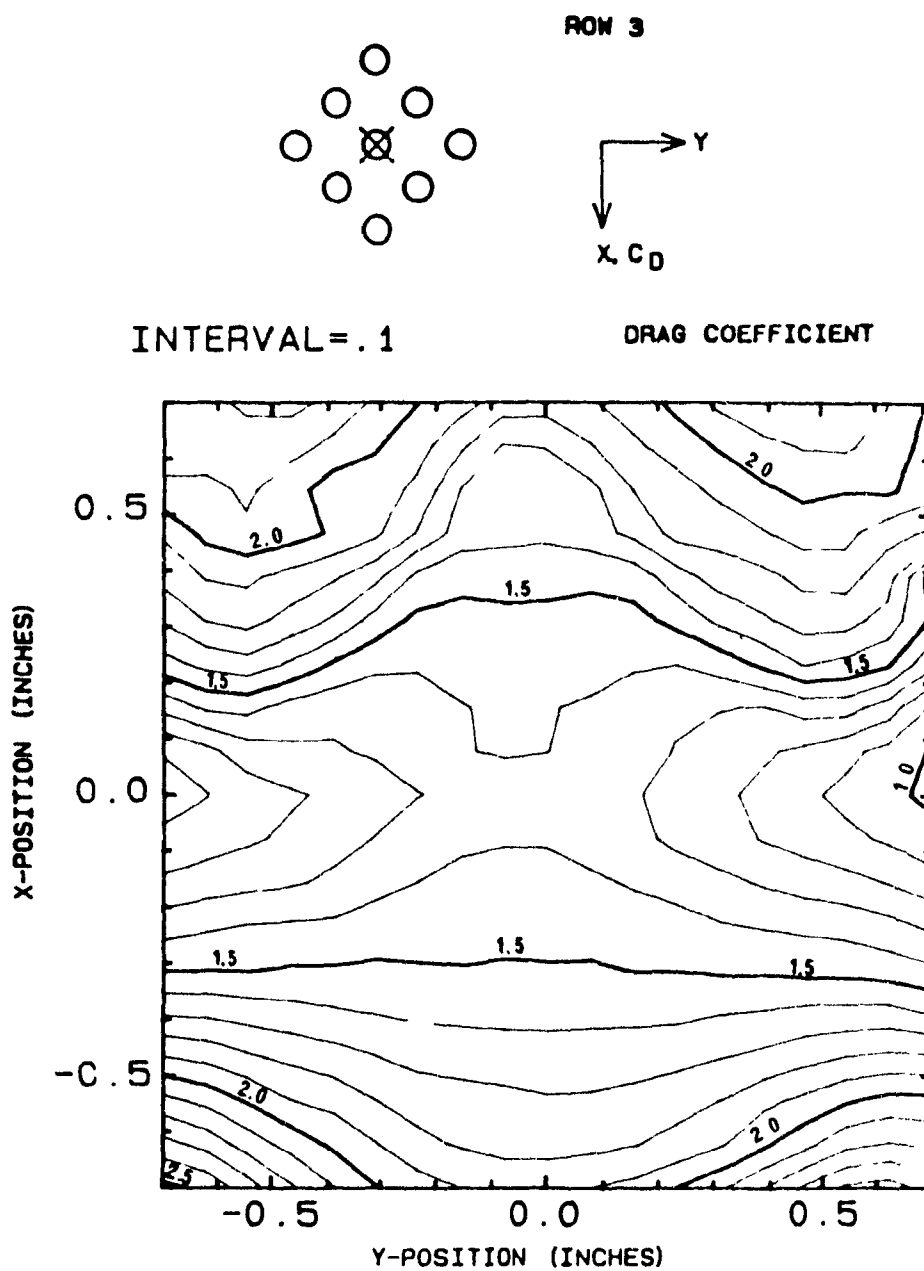
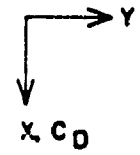
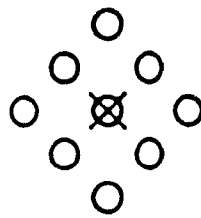


Figure 6.9: Variation of the drag coefficient with cylinder displacement (third row cylinder, $U_\infty = 16.6$ m/s).



INTERVAL = .1

DRAG COEFFICIENT

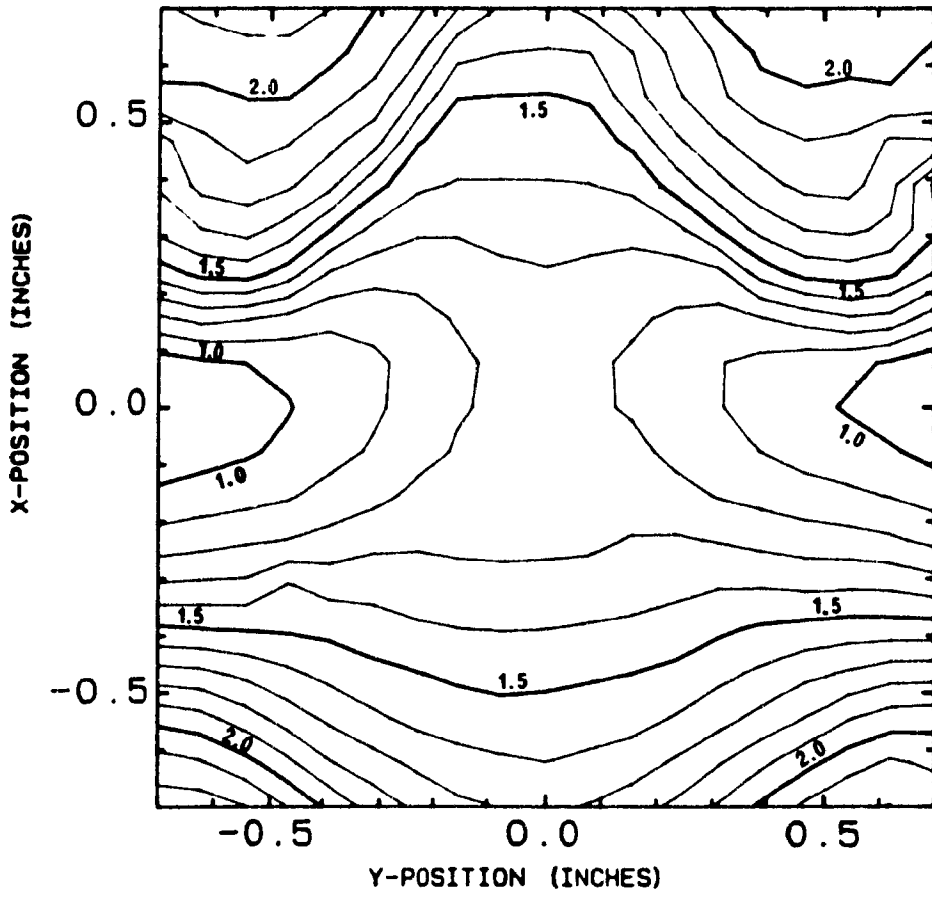
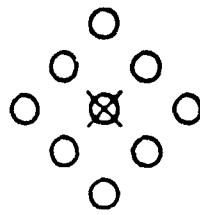


Figure 6 10. Variation of drag the coefficient with cylinder displacement (third row cylinder, $U_{\infty} = 21.4$ m/s).



INTERVAL = .1

LIFT COEFFICIENT

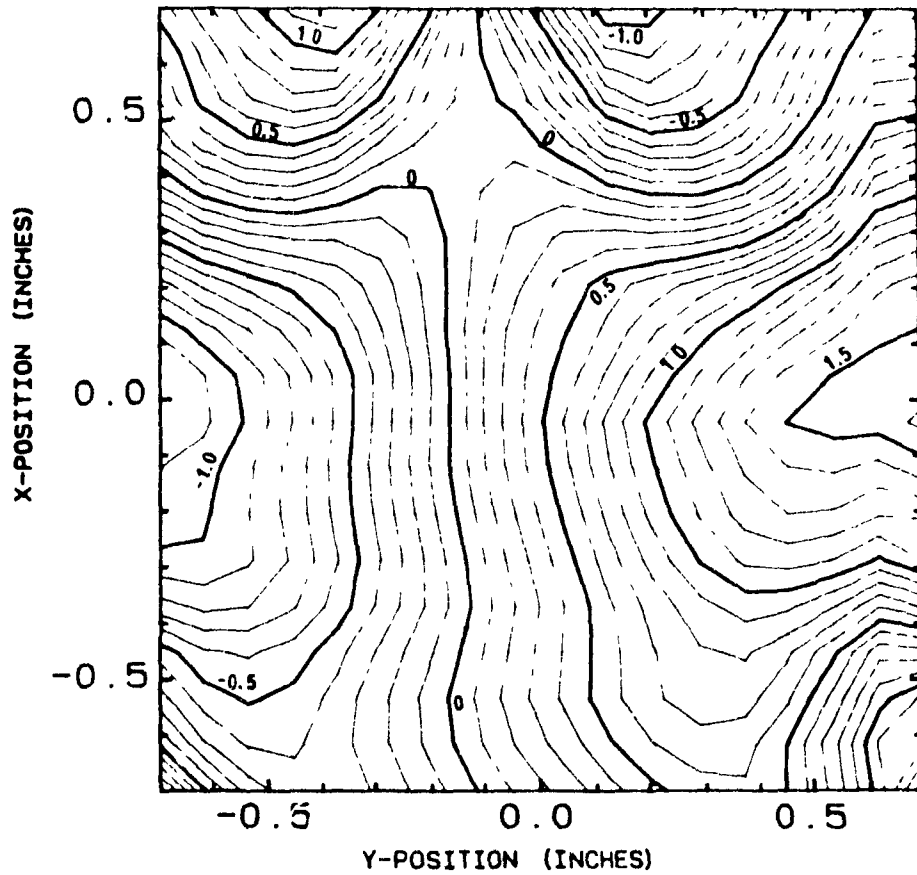


Figure 6.11: Variation of the lift coefficient with cylinder displacement (third row cylinder, $U_{\infty} = 8.3 \text{ m/s}$).

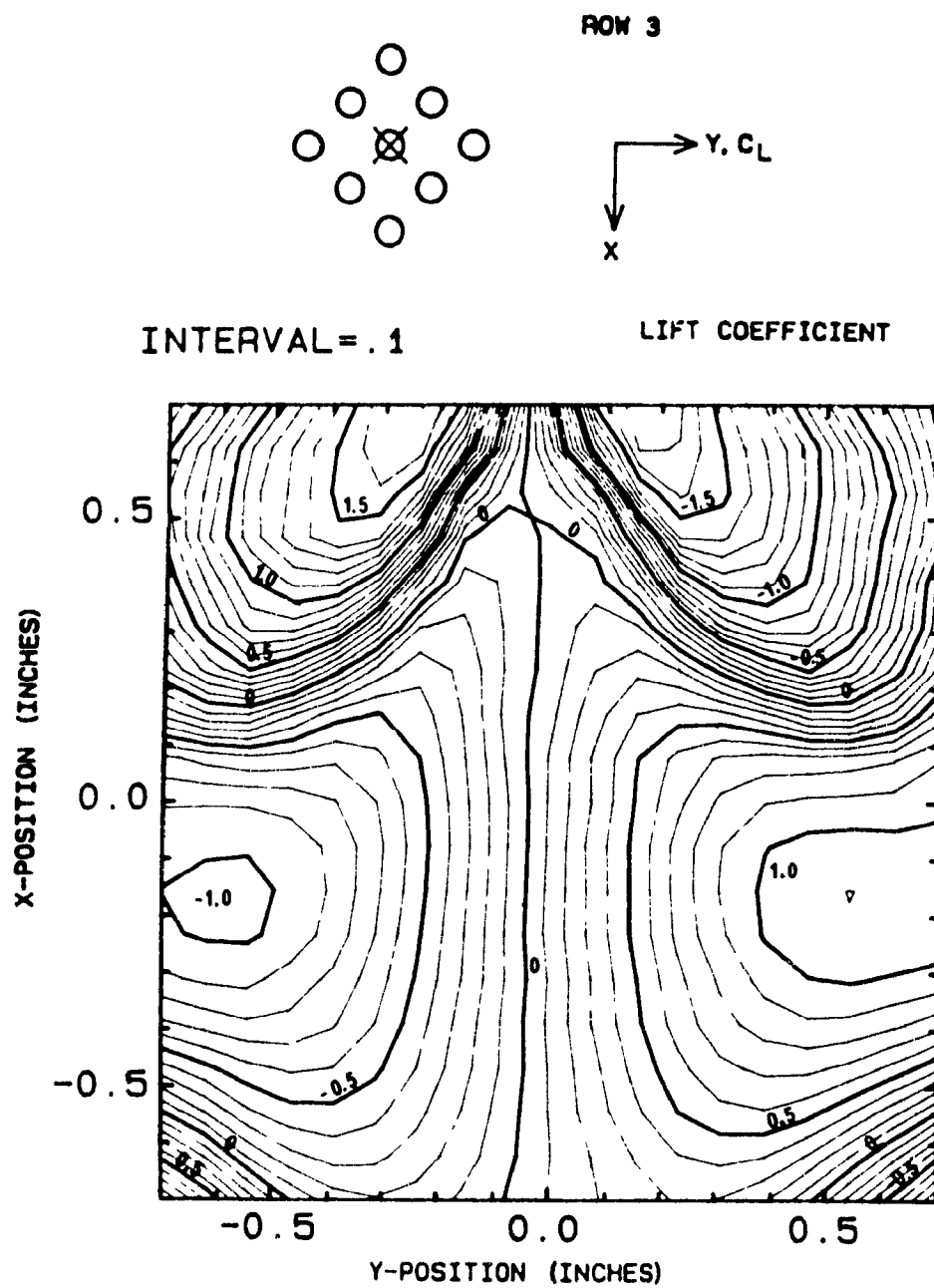


Figure 6 12: Variation of the lift coefficient with cylinder displacement (third row cylinder, $U_{\infty} = 16.6$ m/s).

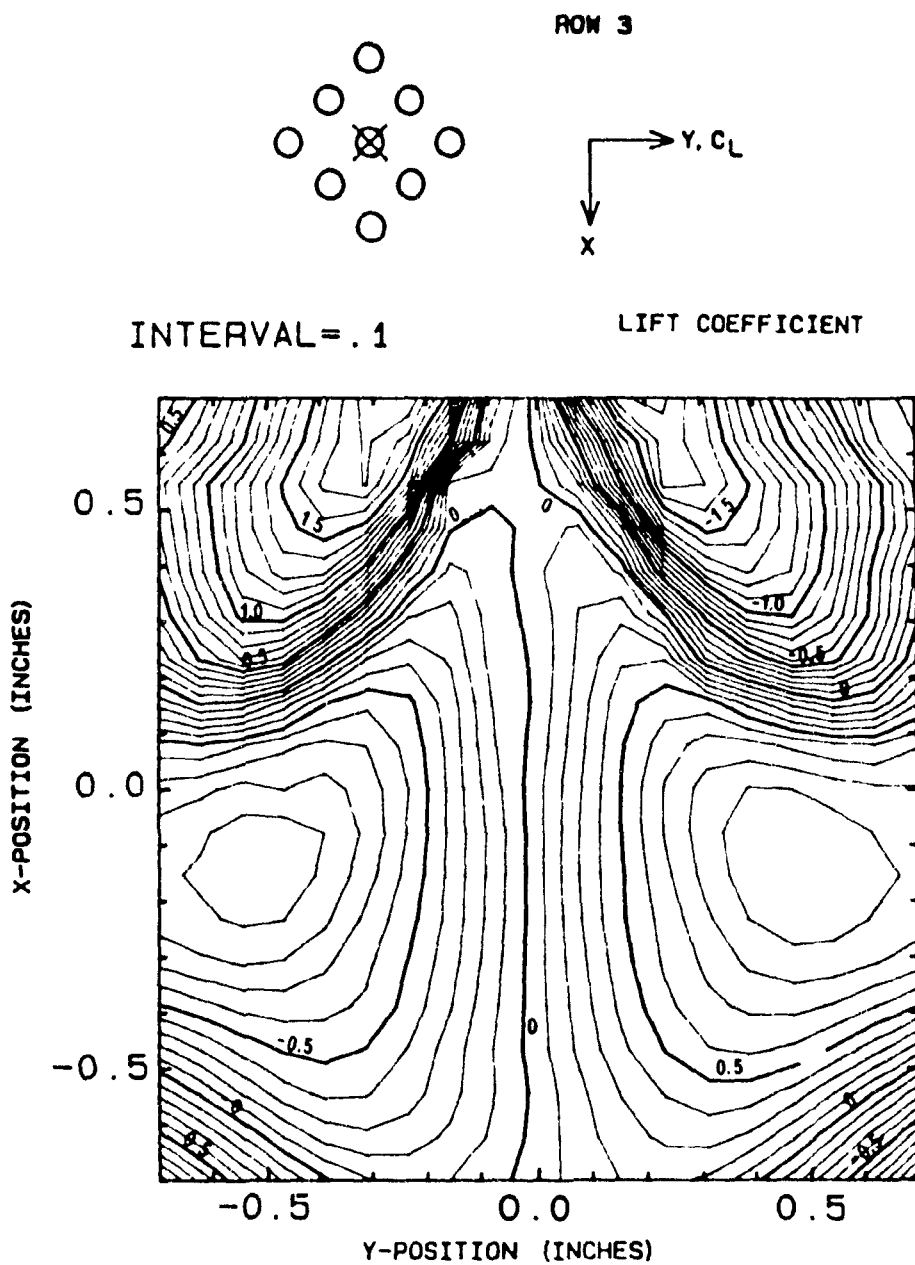


Figure 6.13: Variation of the lift coefficient with cylinder displacement (third row cylinder, $U_\infty = 21.4$ m/s).

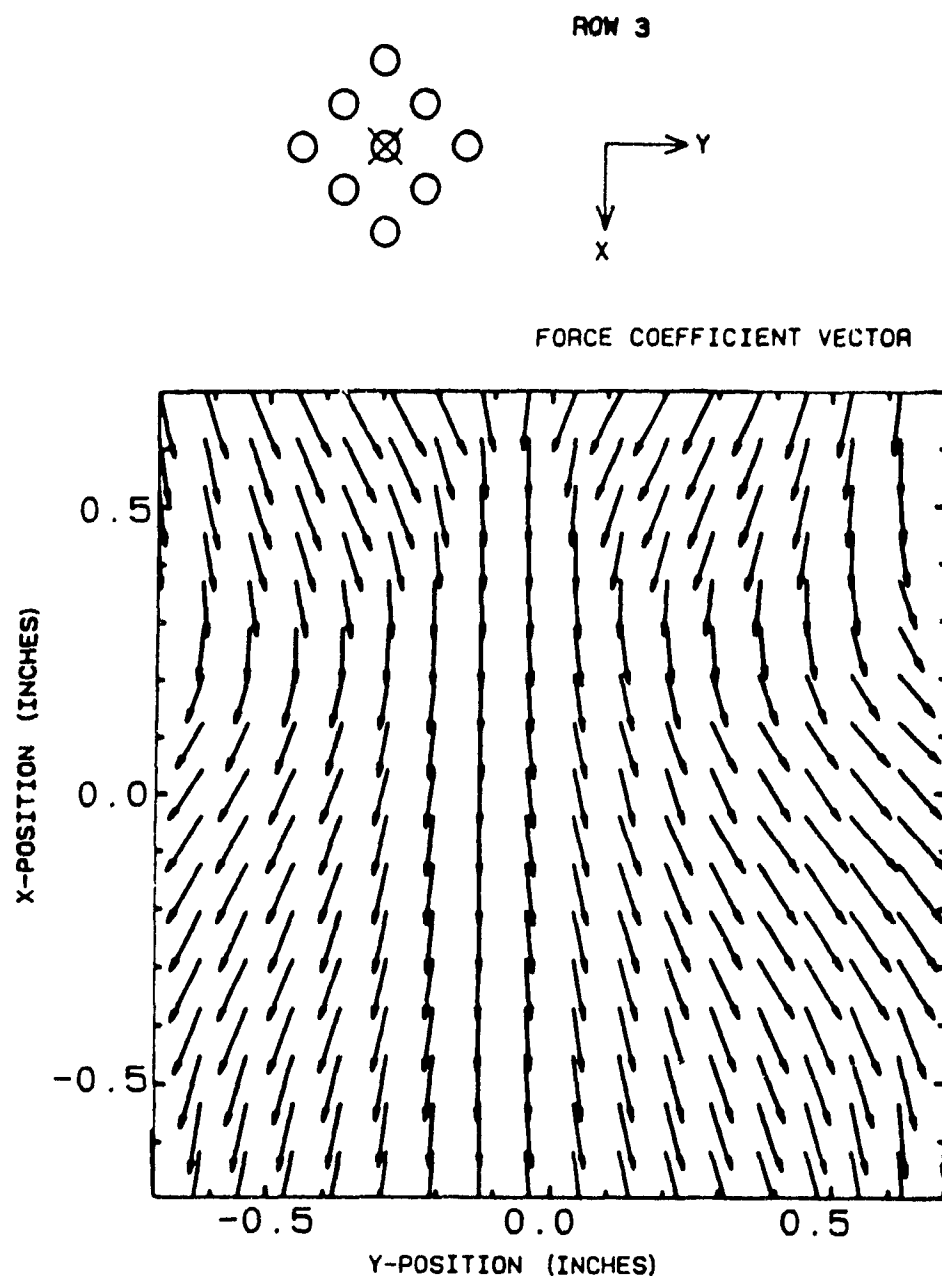


Figure 6 14: Variation of the force coefficient with cylinder displacement (third row cylinder, $U_{\infty} = 8.3$ m/s).

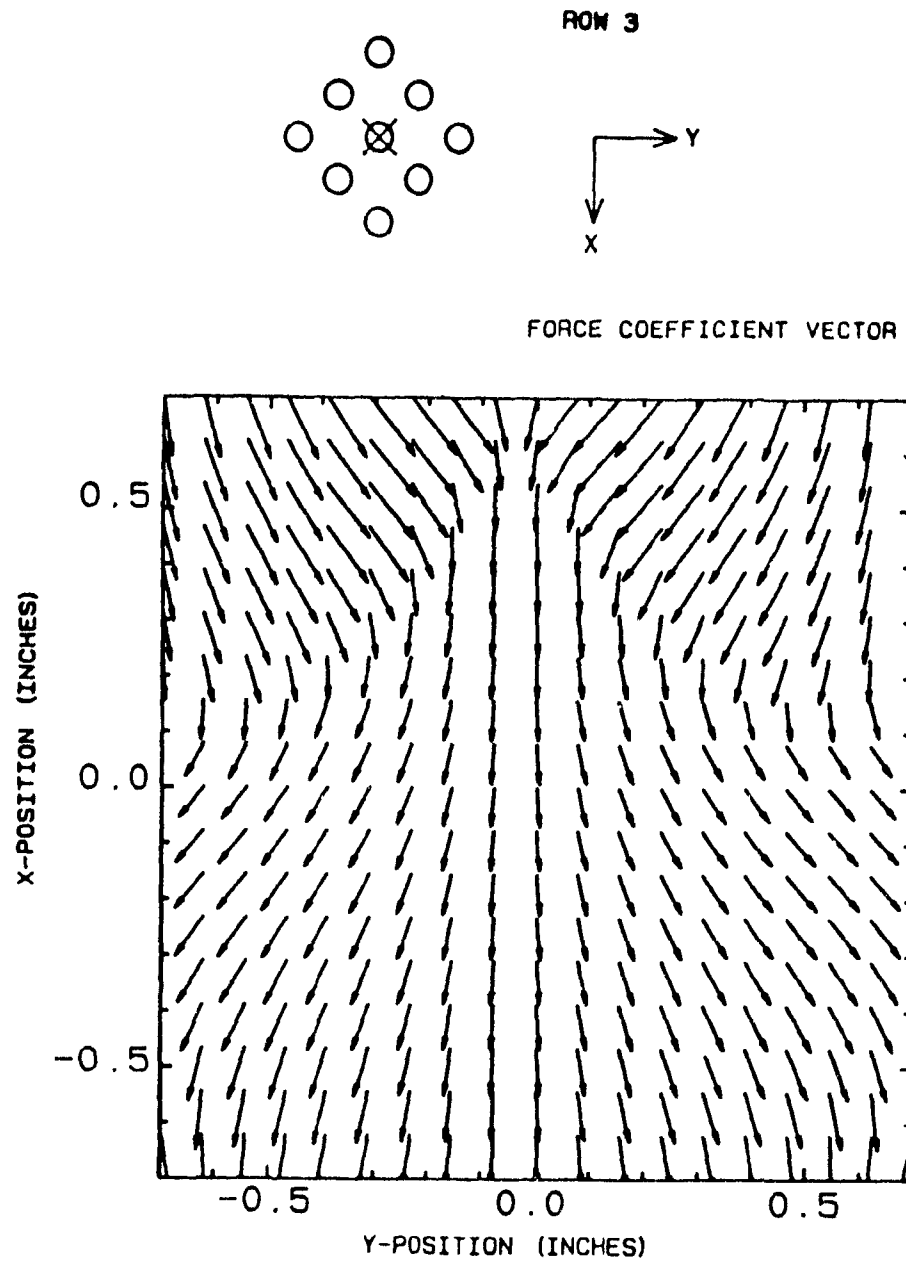


Figure 6.15. Variation of the force coefficient with cylinder displacement (third row cylinder, $U_{\infty} = 16.6 \text{ m/s}$).

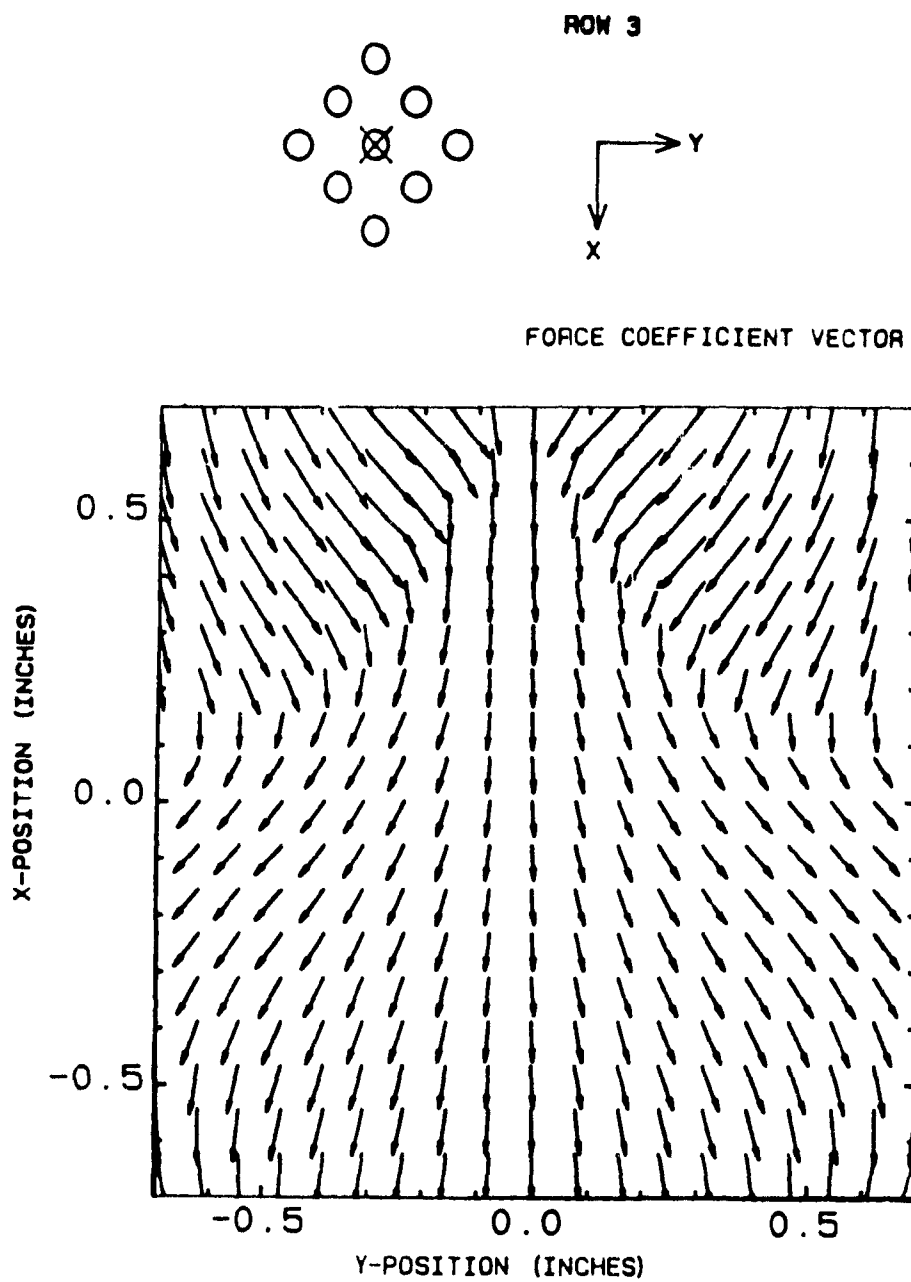


Figure 6 16. Variation of the force coefficient vector with cylinder displacement (third row cylinder, $U_{\infty} = 21.4$ m/s).

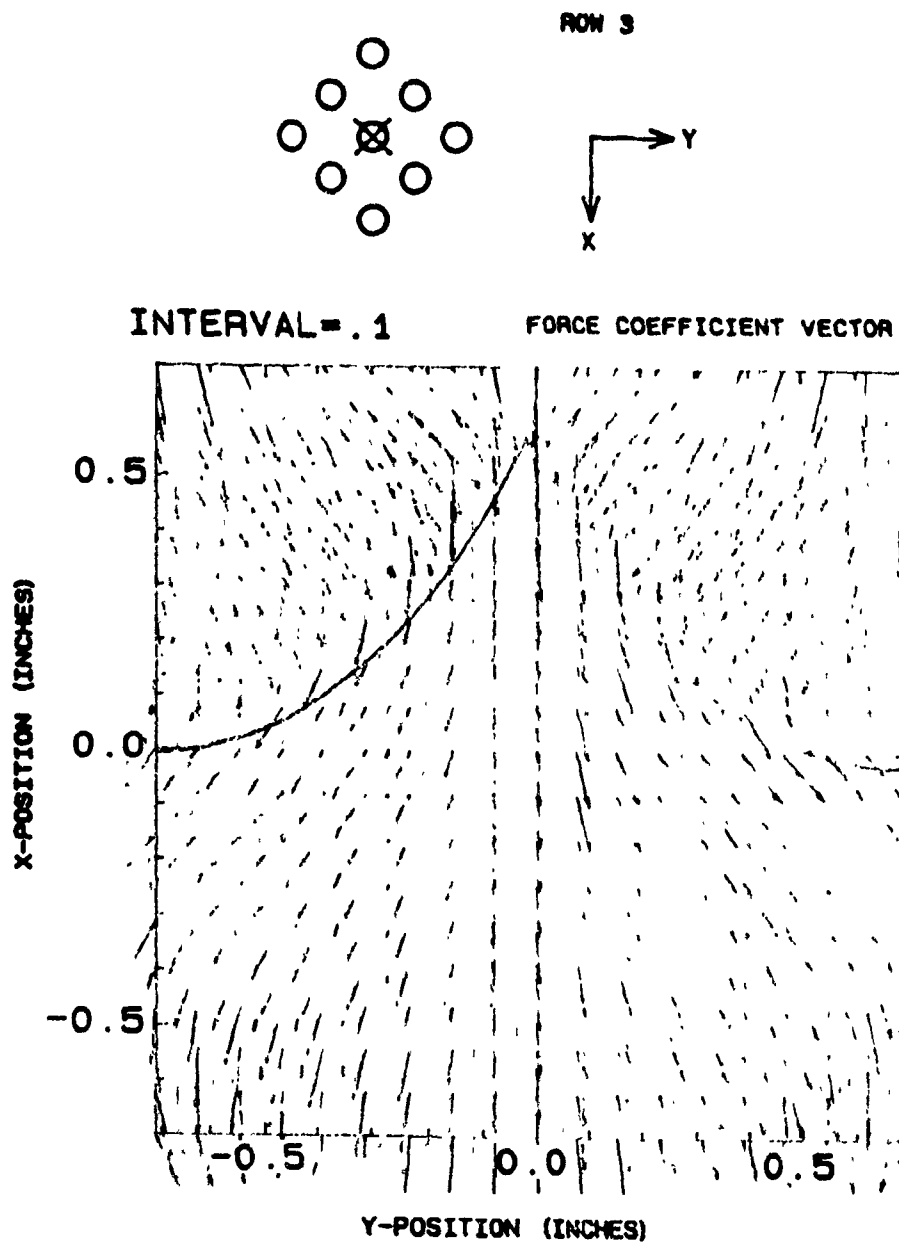


Figure 6.17: Comparison between the force coefficient vectors at $U_\infty = 8.3$ m/s (blue arrows) and the "normalised" force coefficient vectors at $U_\infty = 21.4$ m/s (red arrows)

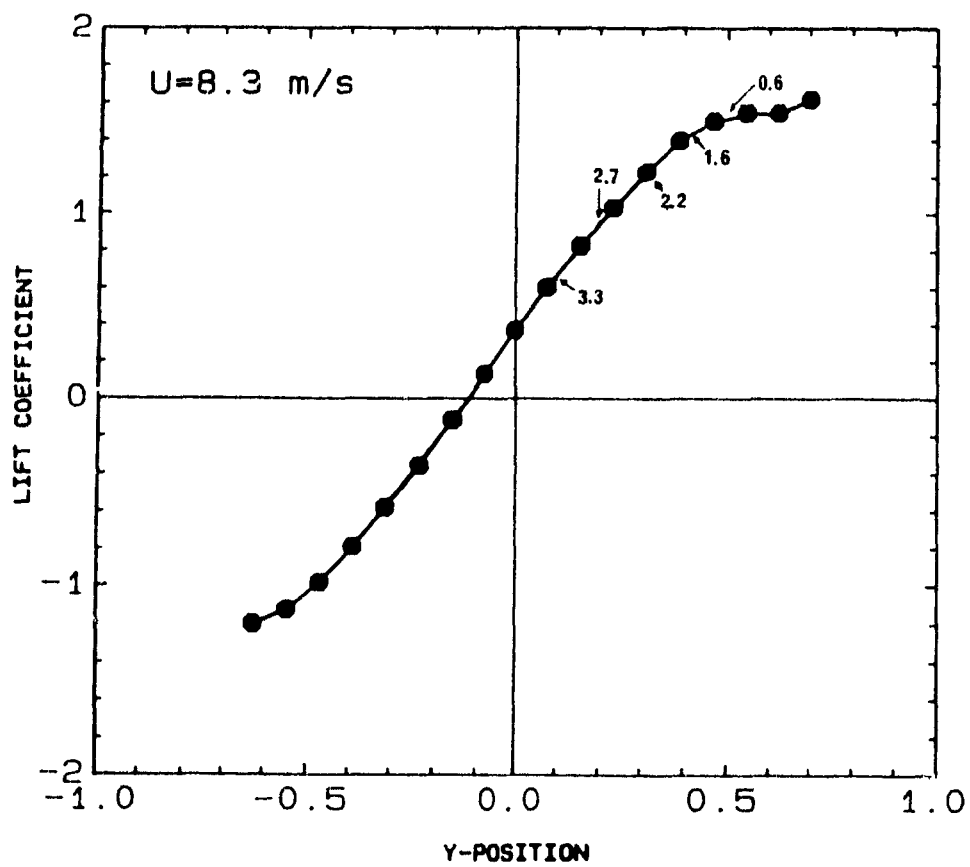


Figure 6.18: Variation of the lift coefficient with \bar{y} at $\bar{x} = 0$ (third row cylinder, $U = 8.3$ m/s)

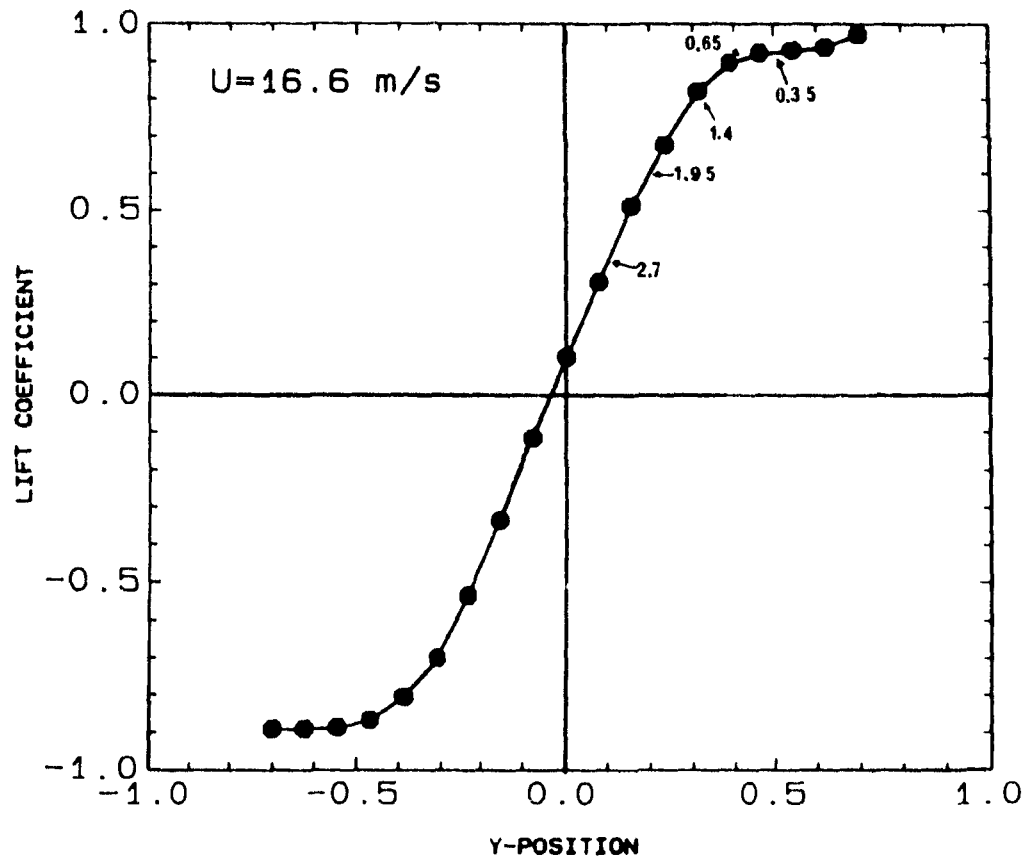


Figure 6 19: Variation of the lift coefficient with \bar{y} at $t = 0$ (third row cylinder, $U_{\infty} = 16.6 \text{ m/s}$)

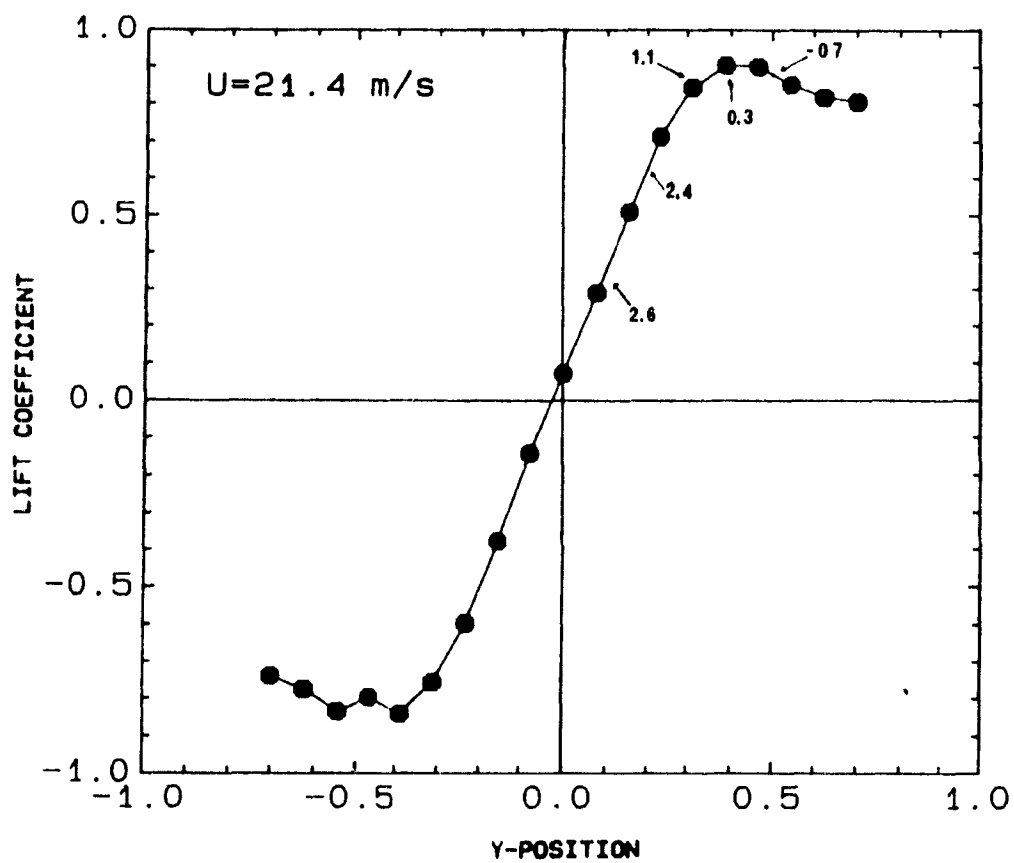


Figure 6 20. Variation of the lift coefficient with \bar{y} at $\bar{x} = 0$ (third row cylinder, $U_{\infty} = 21.4 \text{ m/s}$).

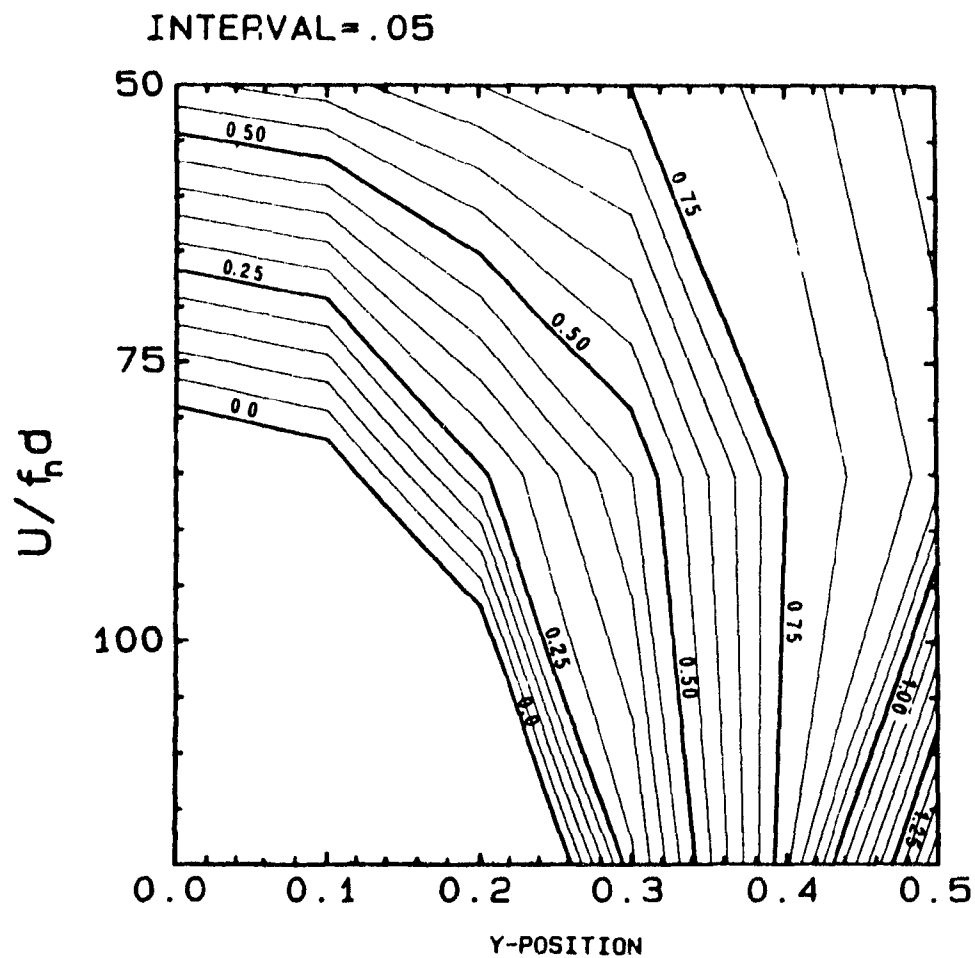


Figure 6.21: Variation of the frequency ratio, w^2/w_0^2 , with non-dimensional flow velocity and cross flow displacement (third row cylinder, $\bar{m} = 280$).

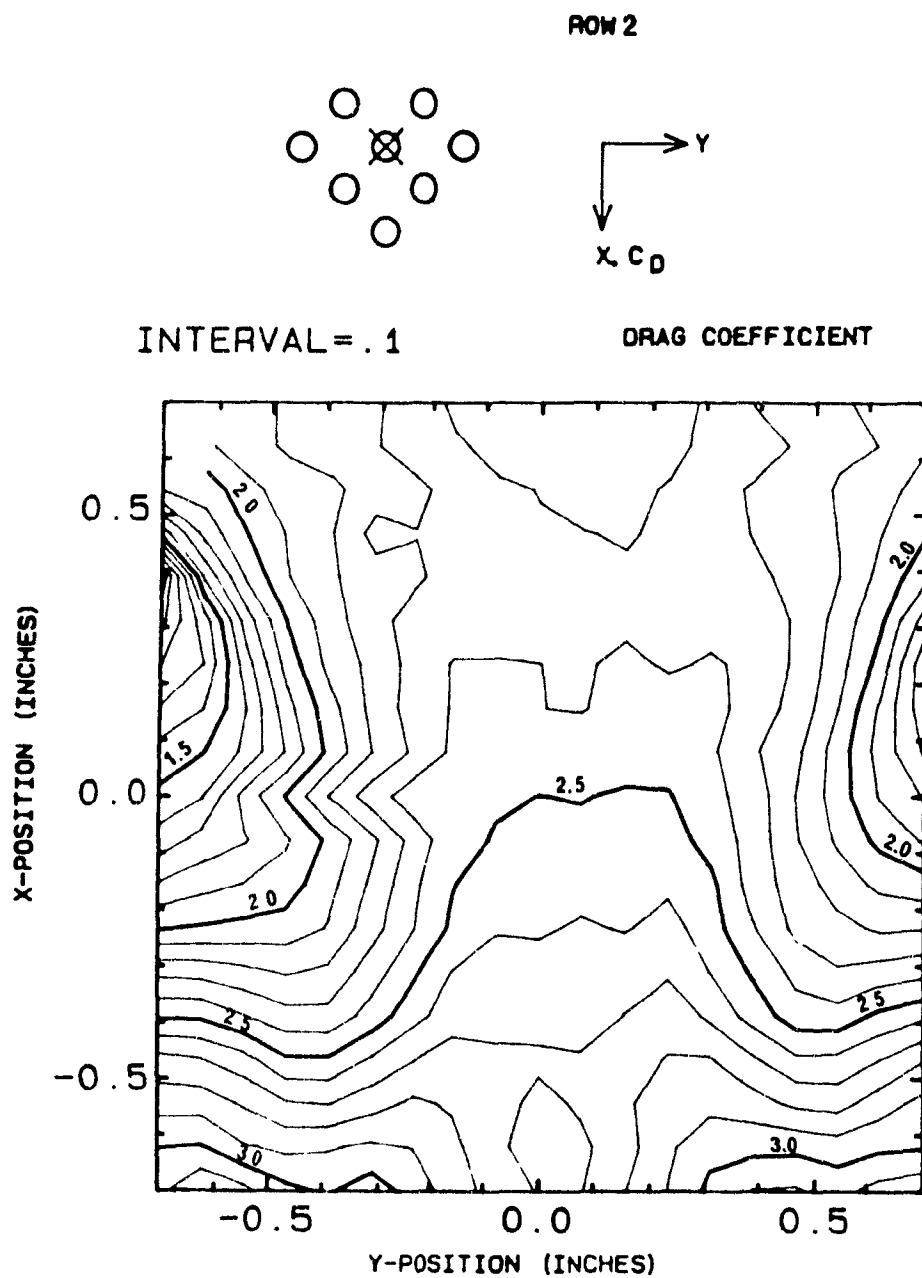


Figure 6-22 Variation of the drag coefficient with cylinder displacement (second row cylinder, $U_{\infty} = 16.6$ m/s).

ROW 2

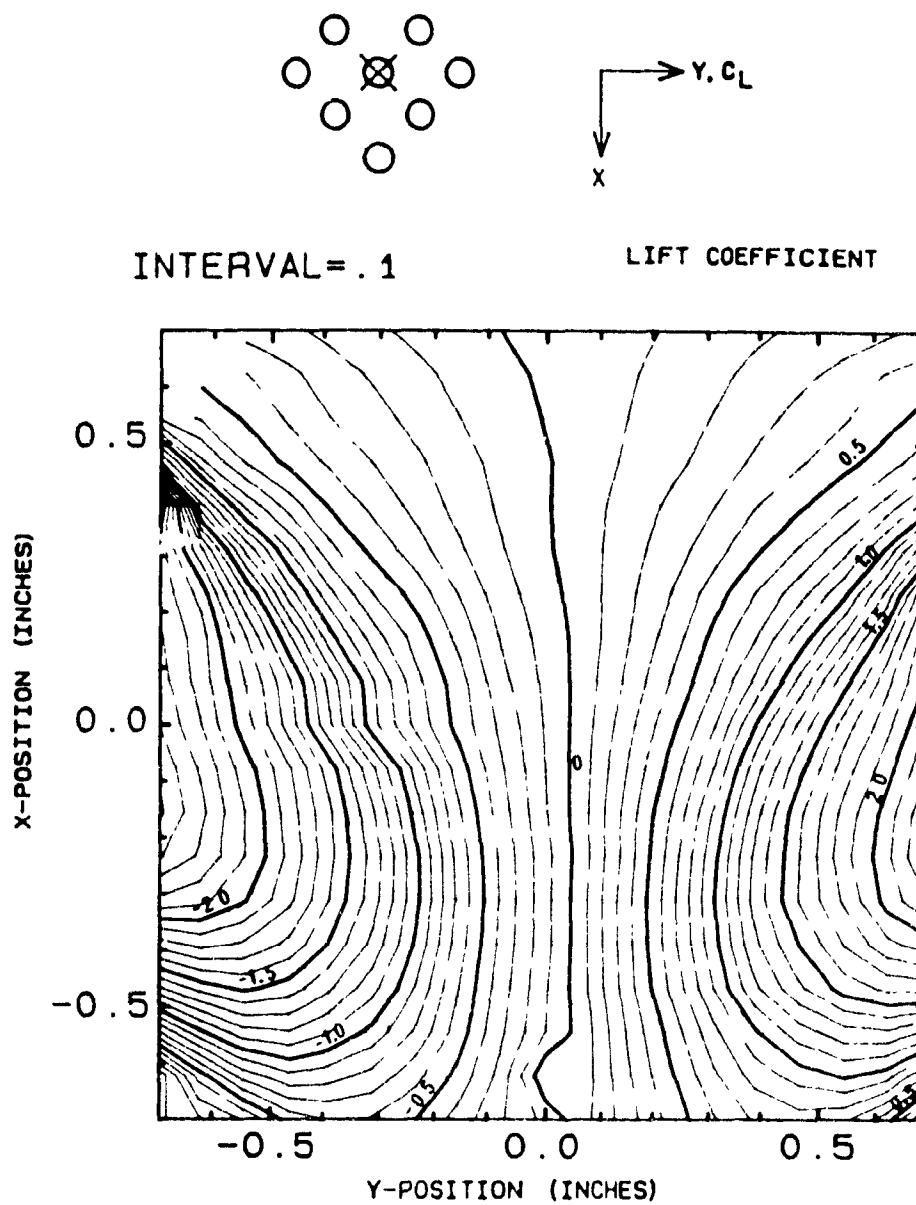
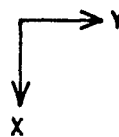
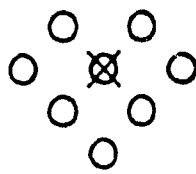


Figure 6.23: Variation of the lift coefficient with cylinder displacement (second row cylinder, $U_{\infty} = 16.6$ m/s).

ROW 2



FORCE COEFFICIENT VECTOR

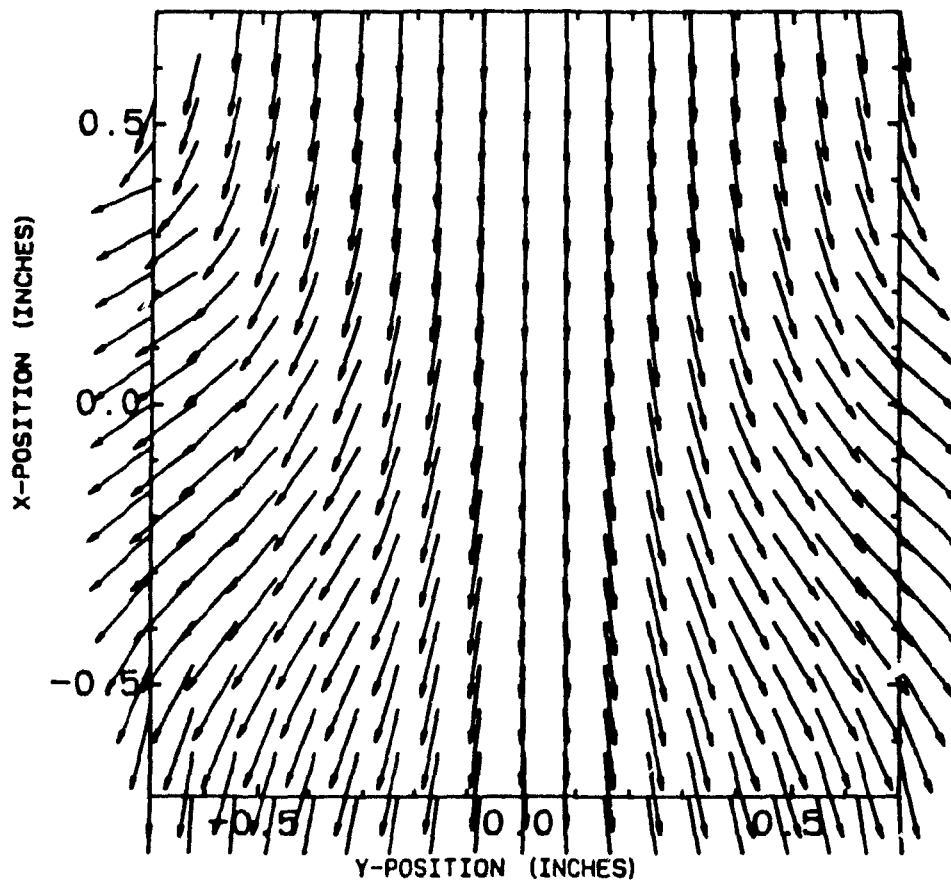


Figure 6.21. Variation of the force coefficient vector with cylinder displacement (second row cylinder, $U_\infty = 16.6$ m/s).

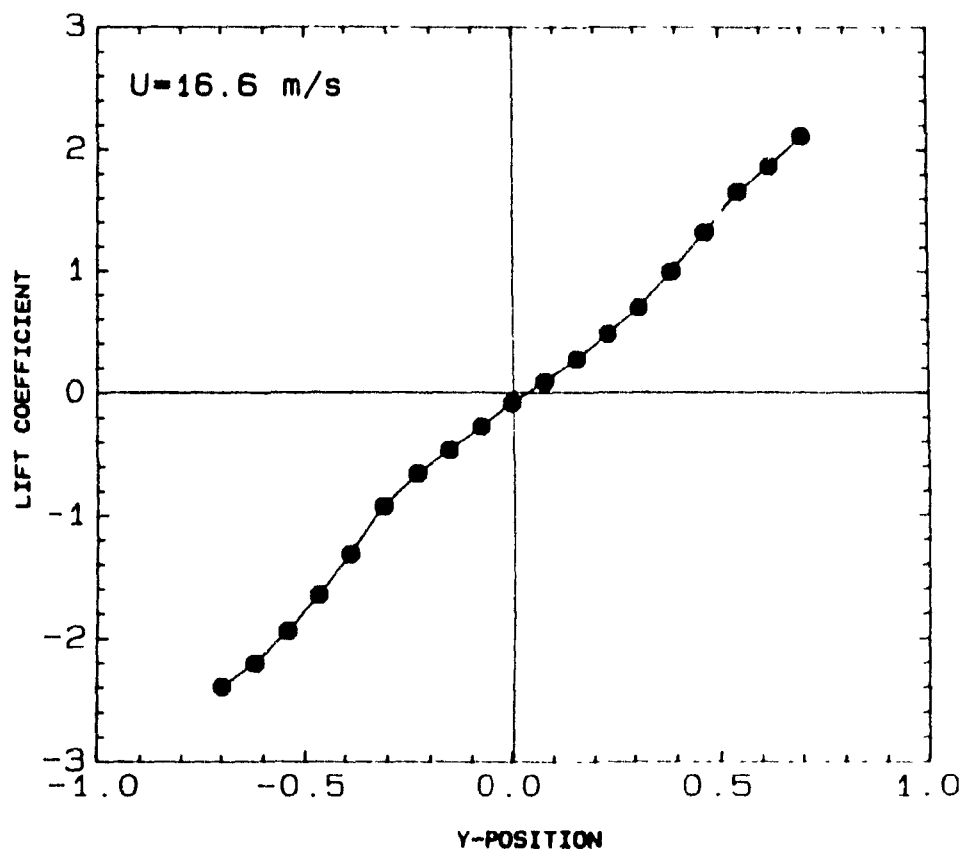


Figure 6 25: Variation of the lift coefficient with y at $x = 0$ (second row cylinder, $U_{\infty} = 16.6$ m/s).

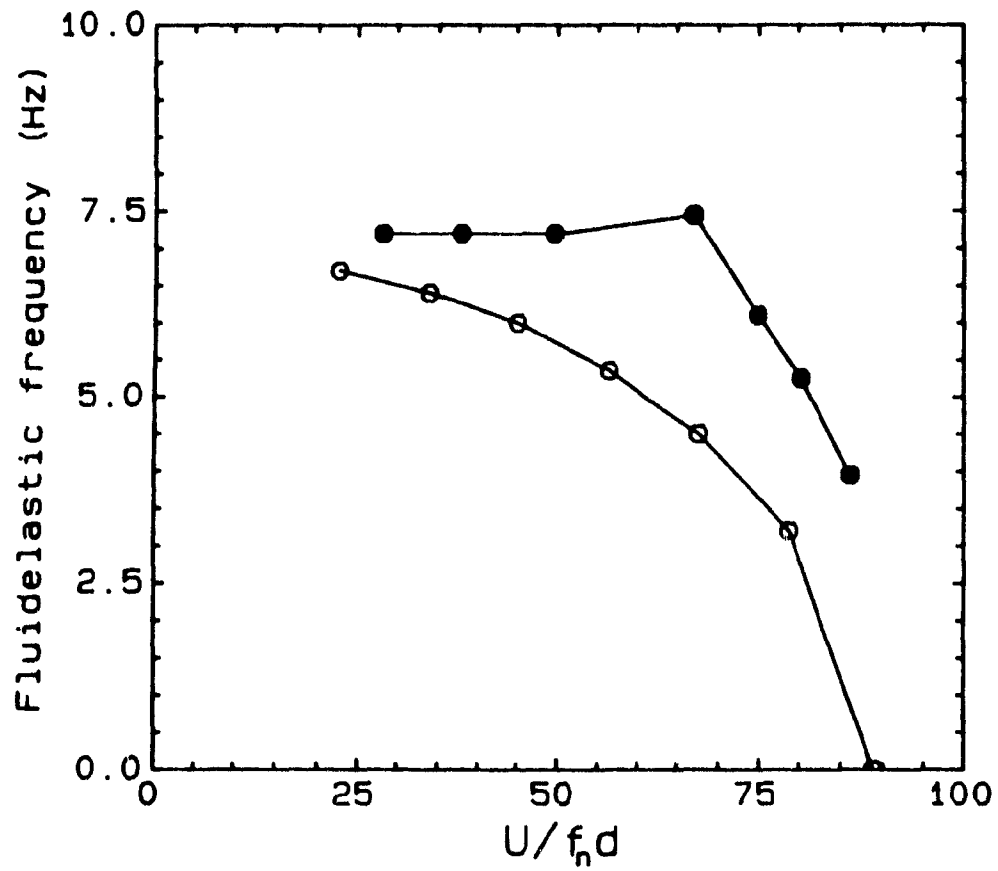


Figure 6.26: The experimental (●) and theoretical (○) variation of cross-flow fluidelastic frequency of a second row flexible cylinder with non-dimensional flow velocity ($m = 280$, $f_n = 7$ Hz and $\delta = 0.014$).

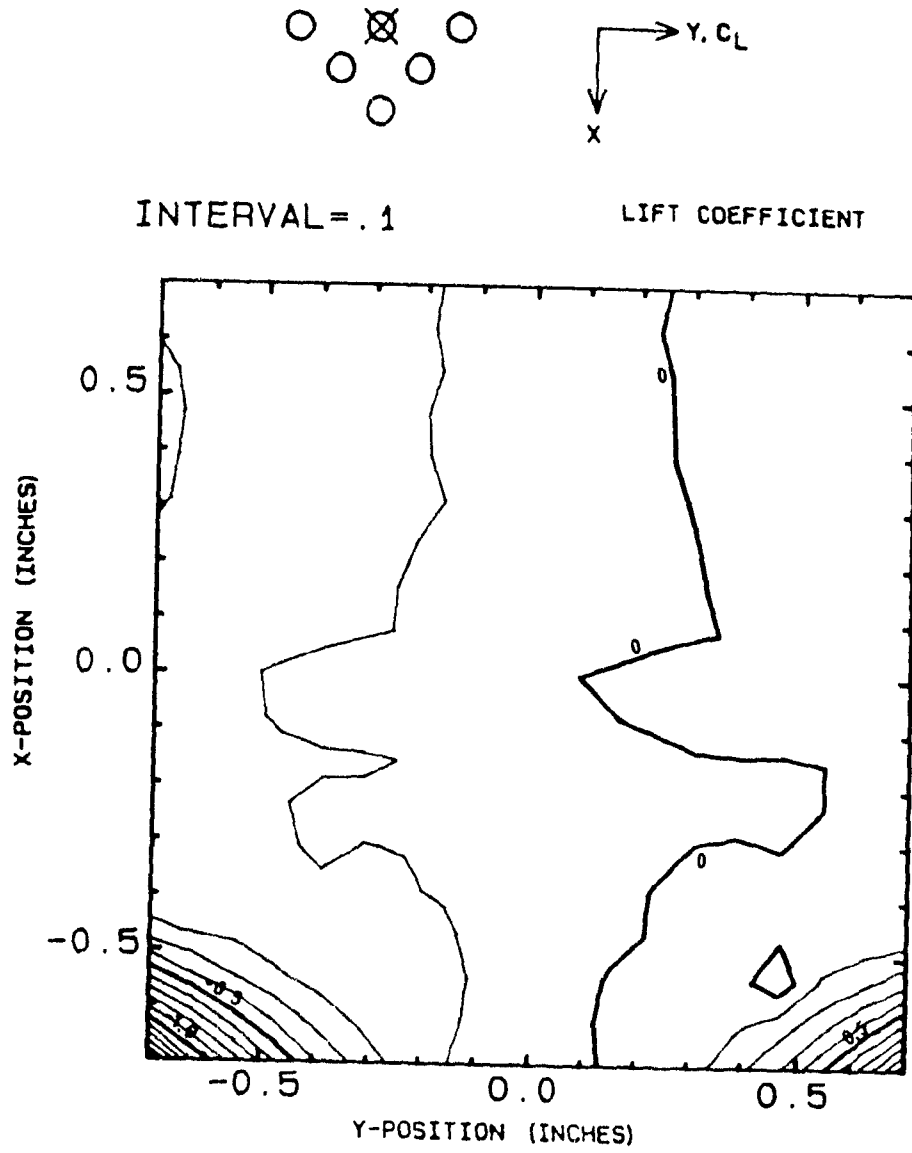
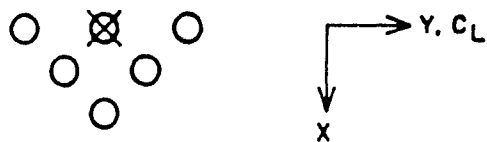


Figure 6.27. Variation of the lift coefficient with cylinder displacement (first row cylinder, $U_\infty = 16.6$ m/s).

ROW 1



INTERVAL = .1

DRAG COEFFICIENT

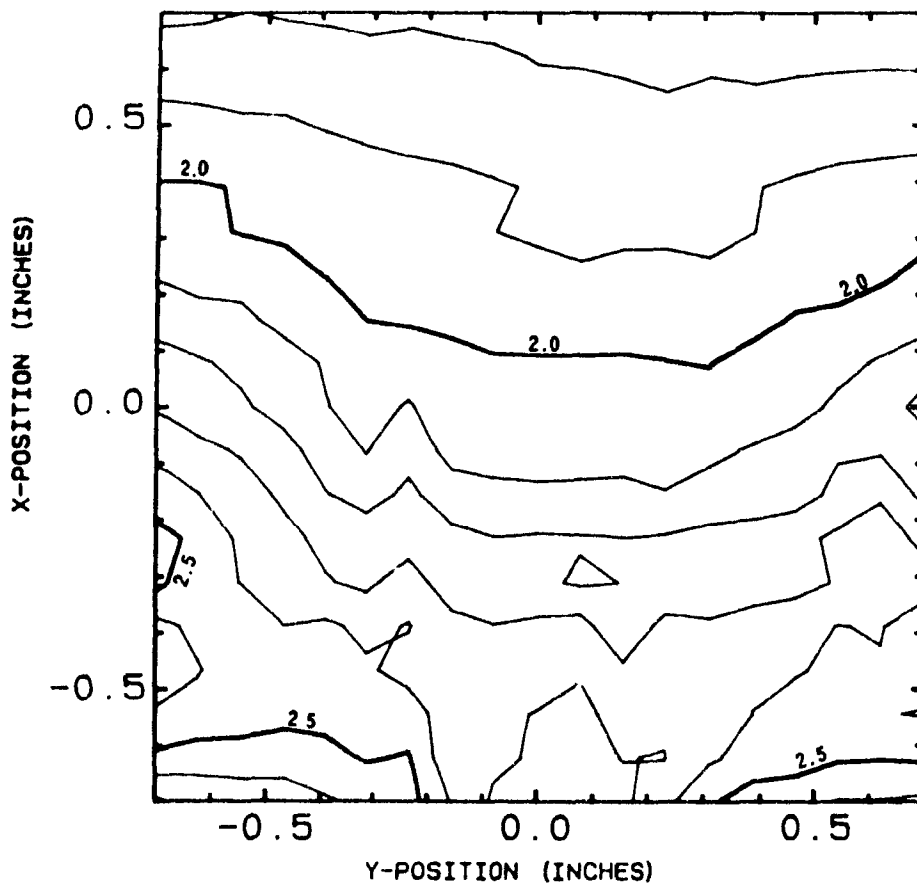
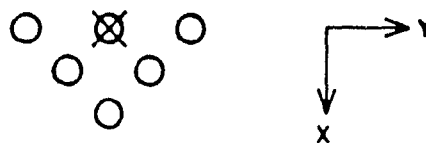


Figure 6.28. Variation of the drag coefficient with cylinder displacement (first row cylinder, $U_{\infty} = 16.6$ m/s).

ROW 1



FORCE COEFFICIENT VECTOR

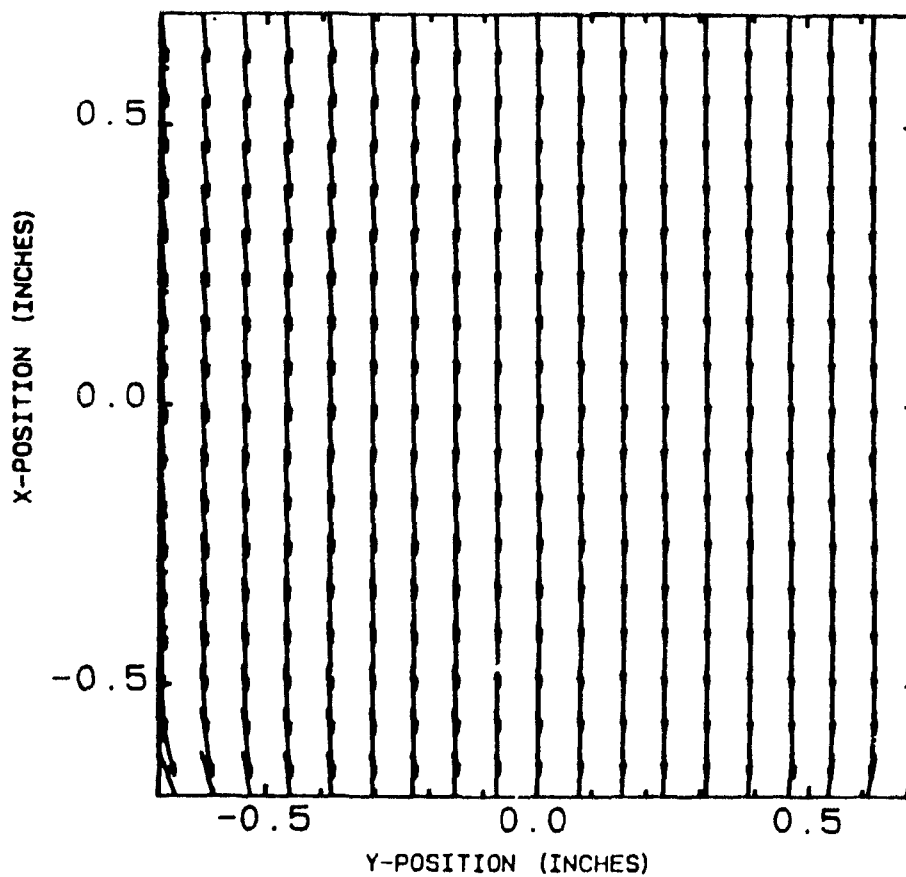


Figure 6 29. Variation of the force coefficient vector with cylinder displacement (first row cylinder, $U_{\infty} = 16.6$ m/s).

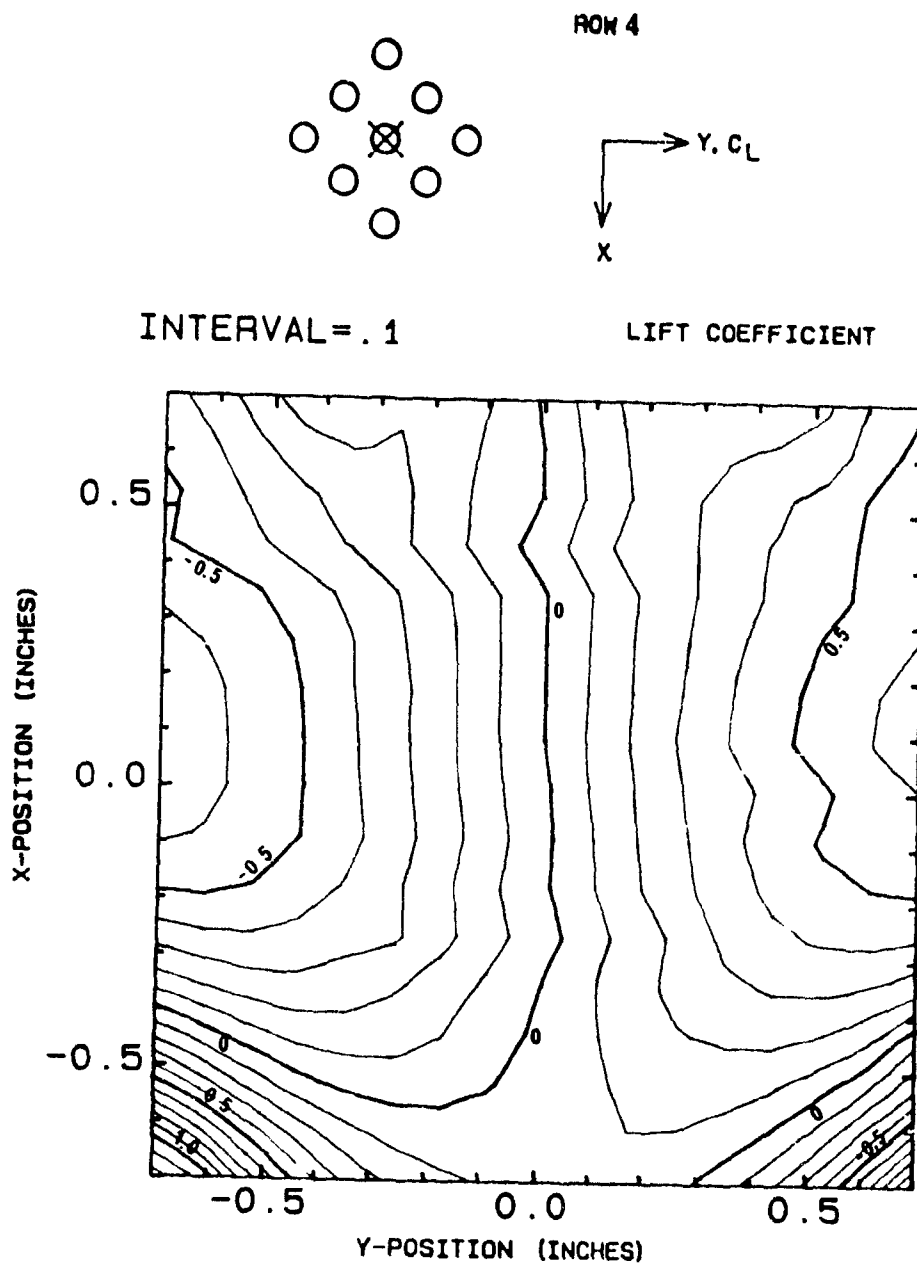


Figure 6.30: Variation of the lift coefficient with cylinder displacement (fourth row cylinder, $U_\infty = 16.6$ m/s).

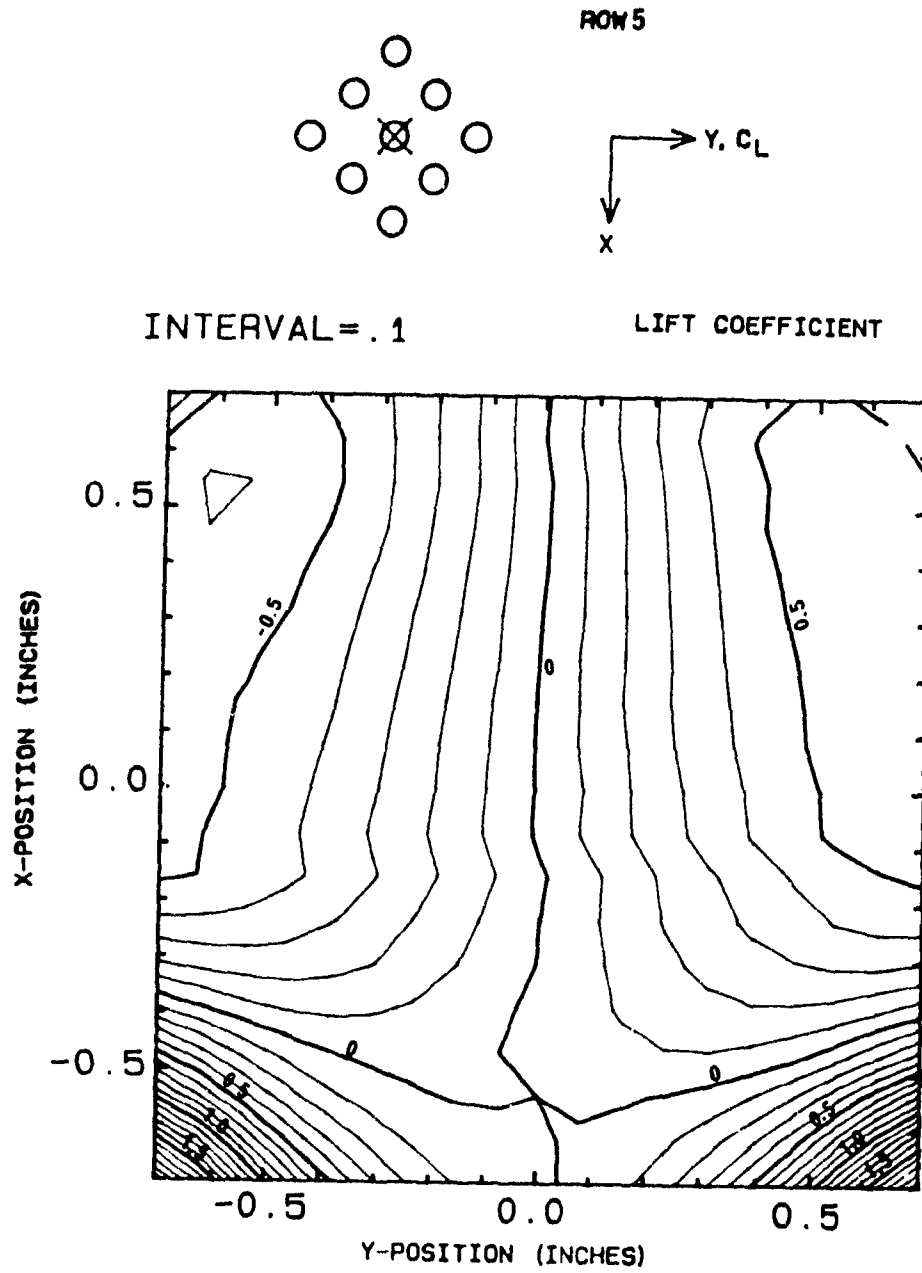


Figure 6.31: Variation of the lift coefficient with cylinder displacement (fifth row cylinder, $U_{\infty} = 16.6$ m/s).

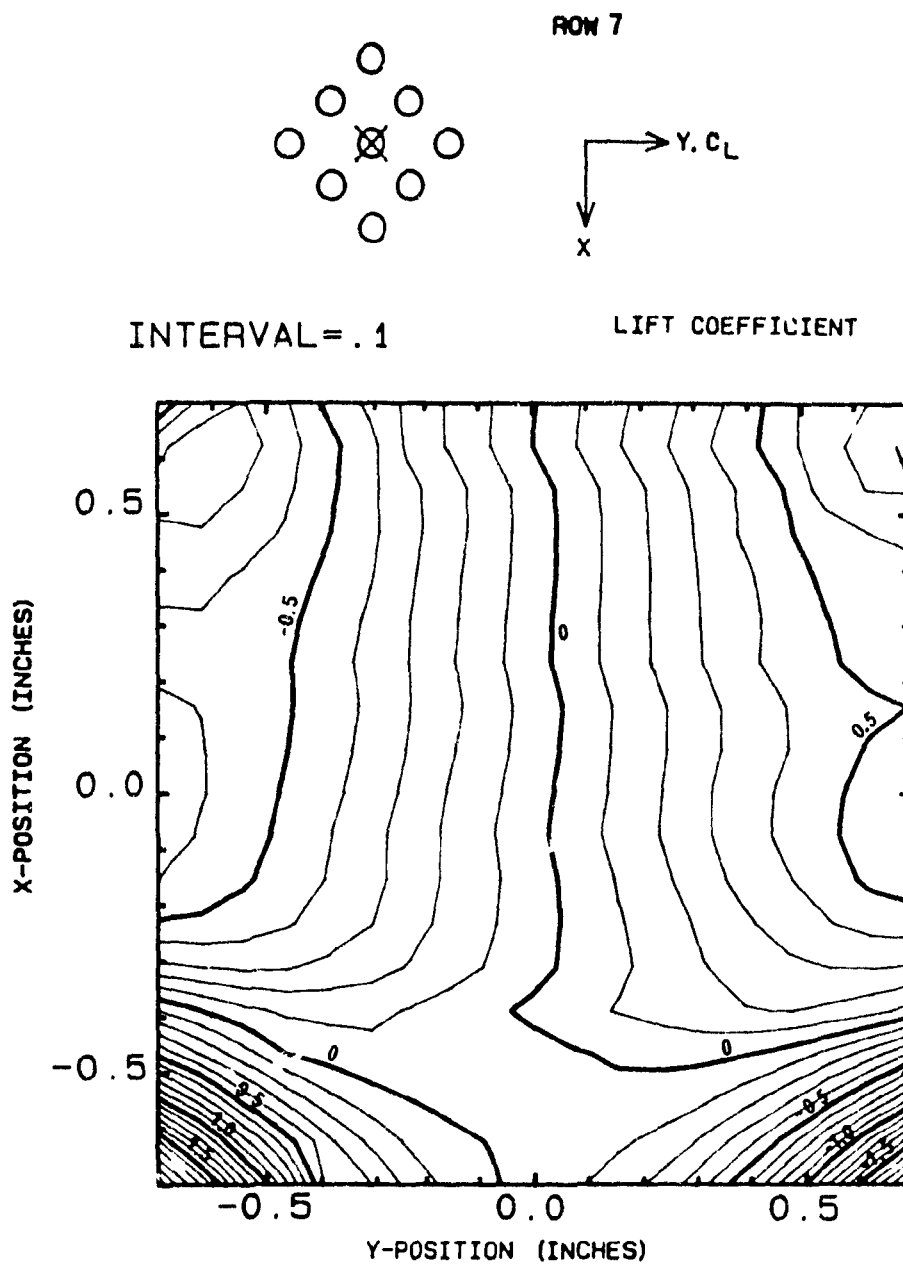


Figure 6.32: Variation of the lift coefficient with cylinder displacement (seventh row cylinder, $U_\infty = 16.6$ m/s).

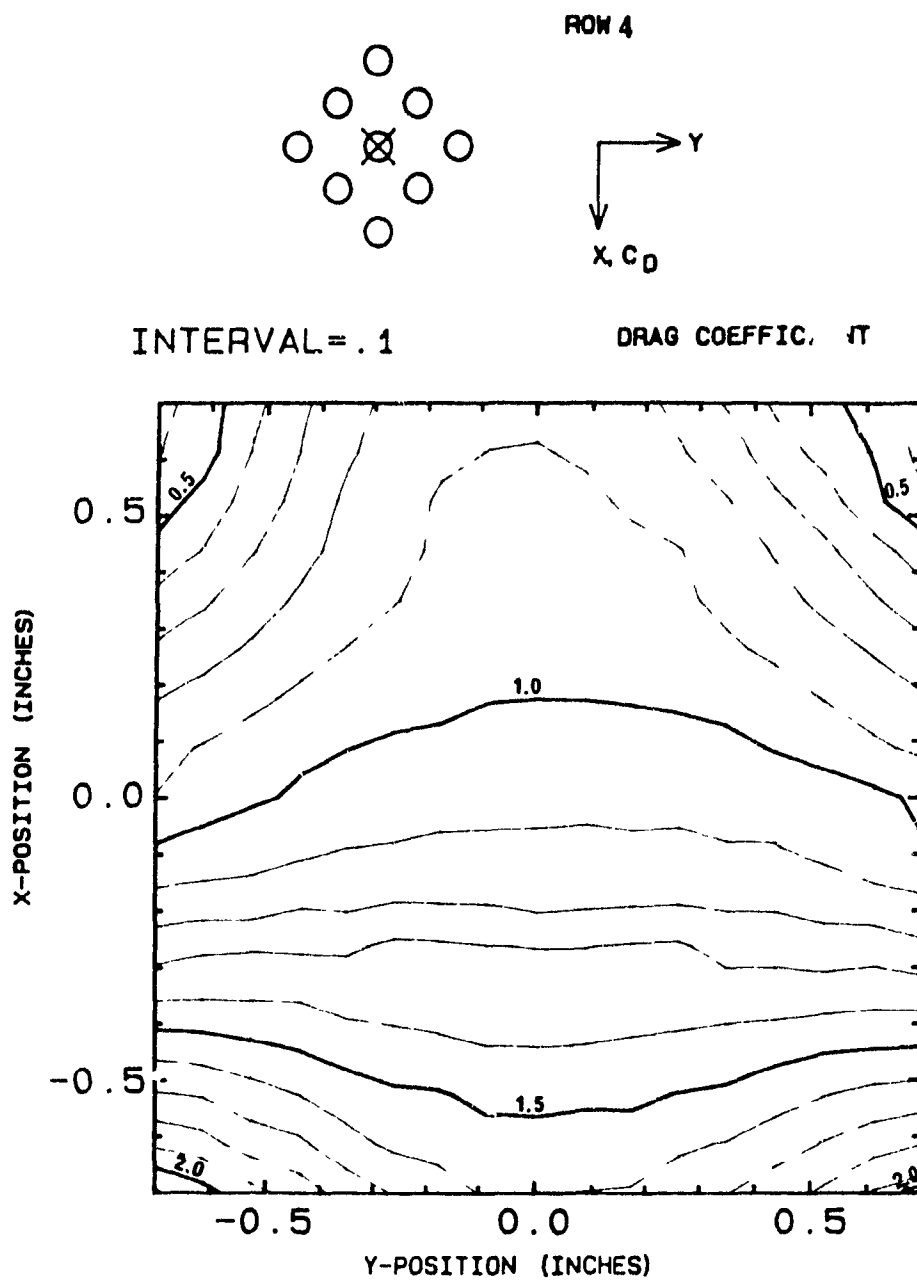


Figure 6.33: Variation of the drag coefficient with cylinder displacement (fourth row cylinder, $U_{\infty} = 16.6$ m/s).

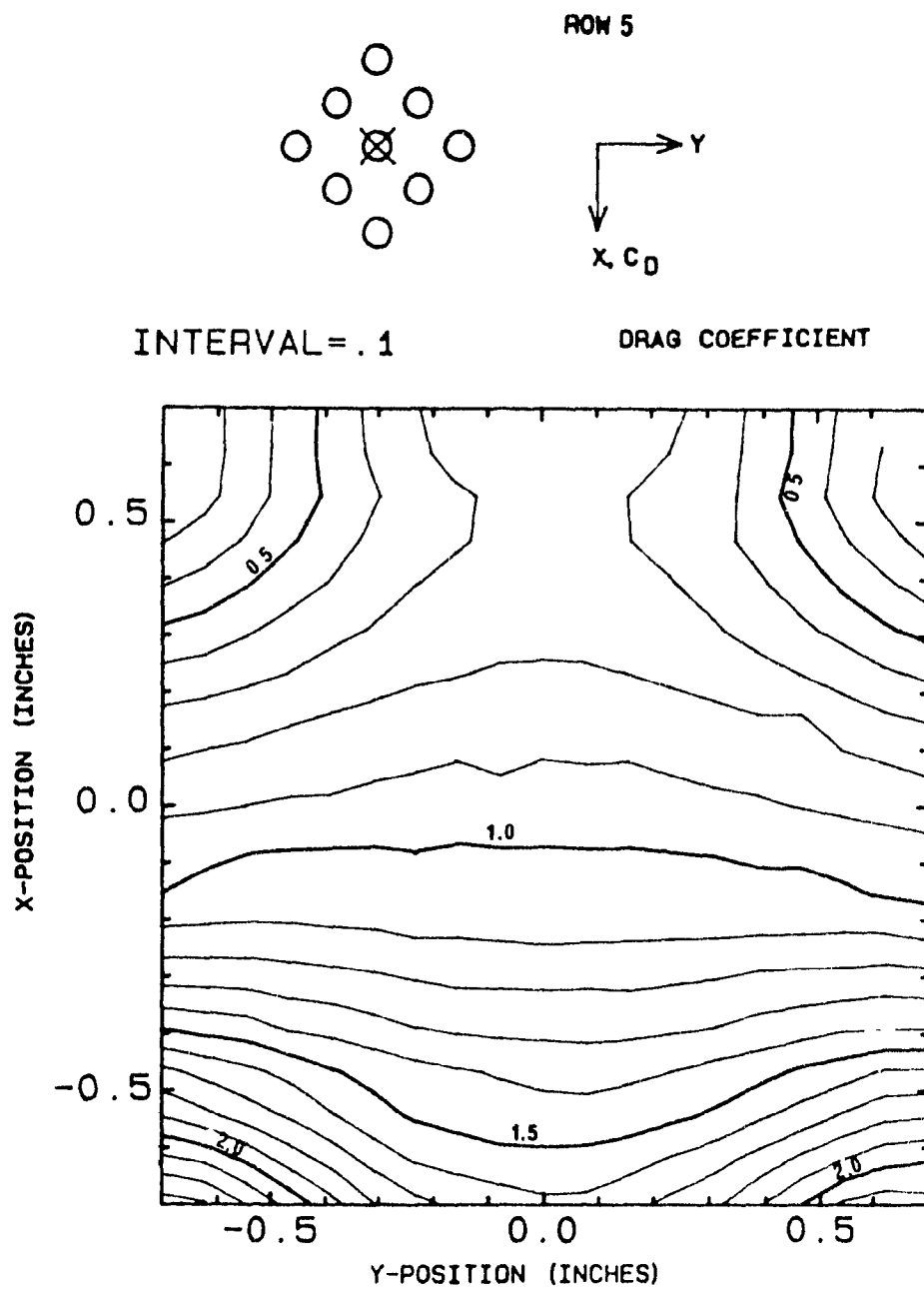


Figure 6.31: Variation of the drag coefficient with cylinder displacement (fifth row cylinder, $U_\infty = 16.6$ m/s).

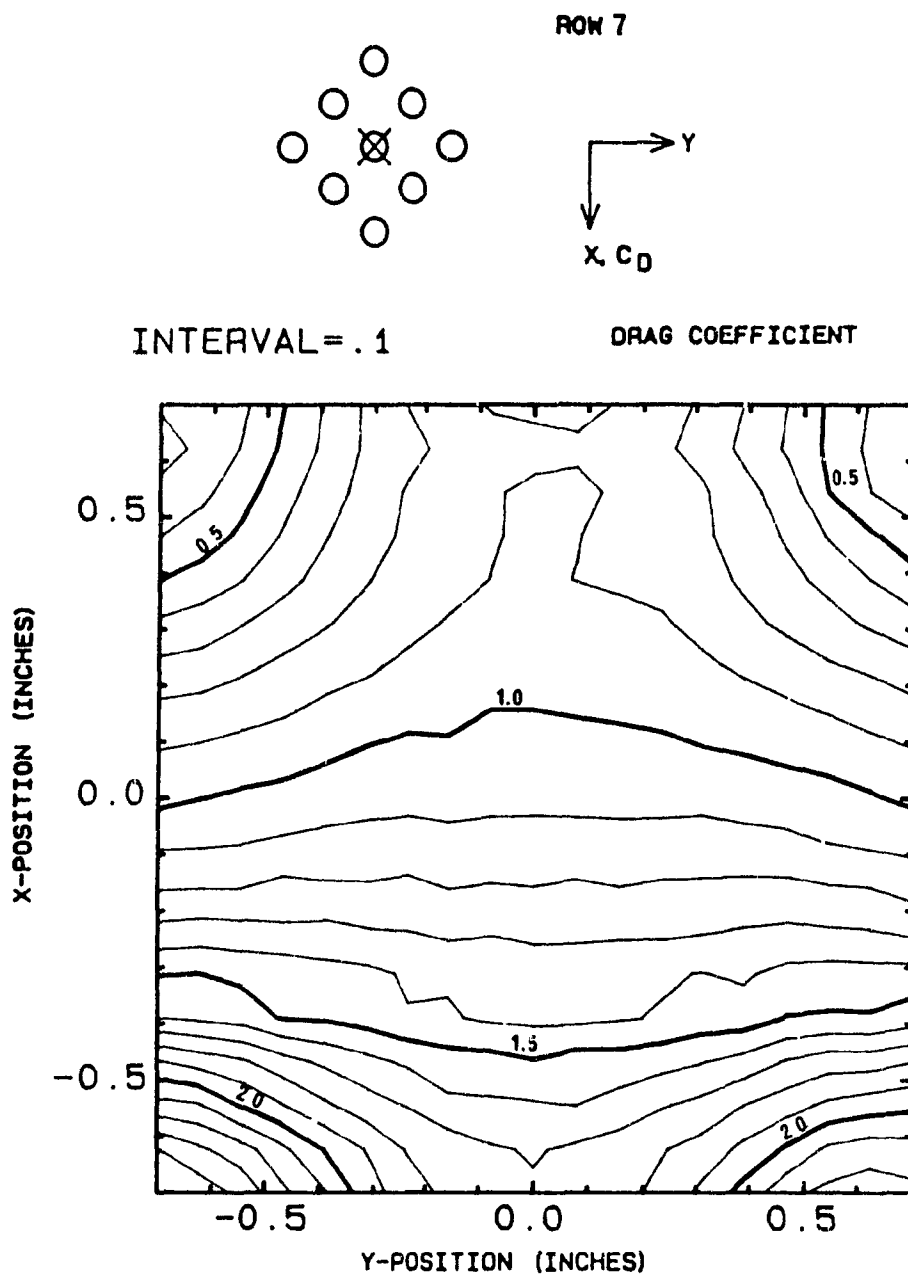


Figure 6.35: Variation of the drag coefficient with cylinder displacement (seventh row cylinder, $U_{\infty} = 16.6$ m/s).

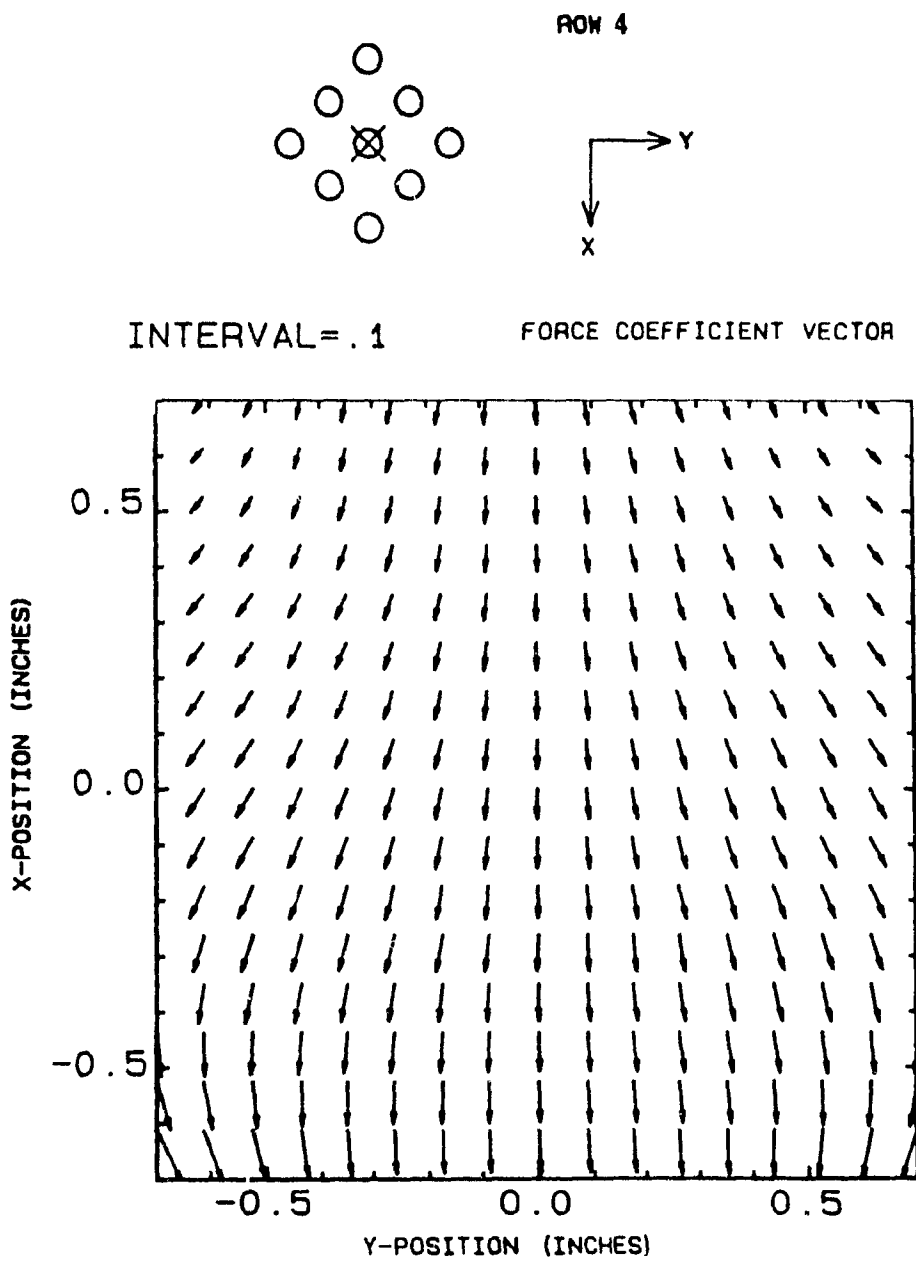


Figure 6.36: Variation of the force coefficient vector with cylinder displacement (fourth row cylinder, $U_\infty = 16.6$ m/s).

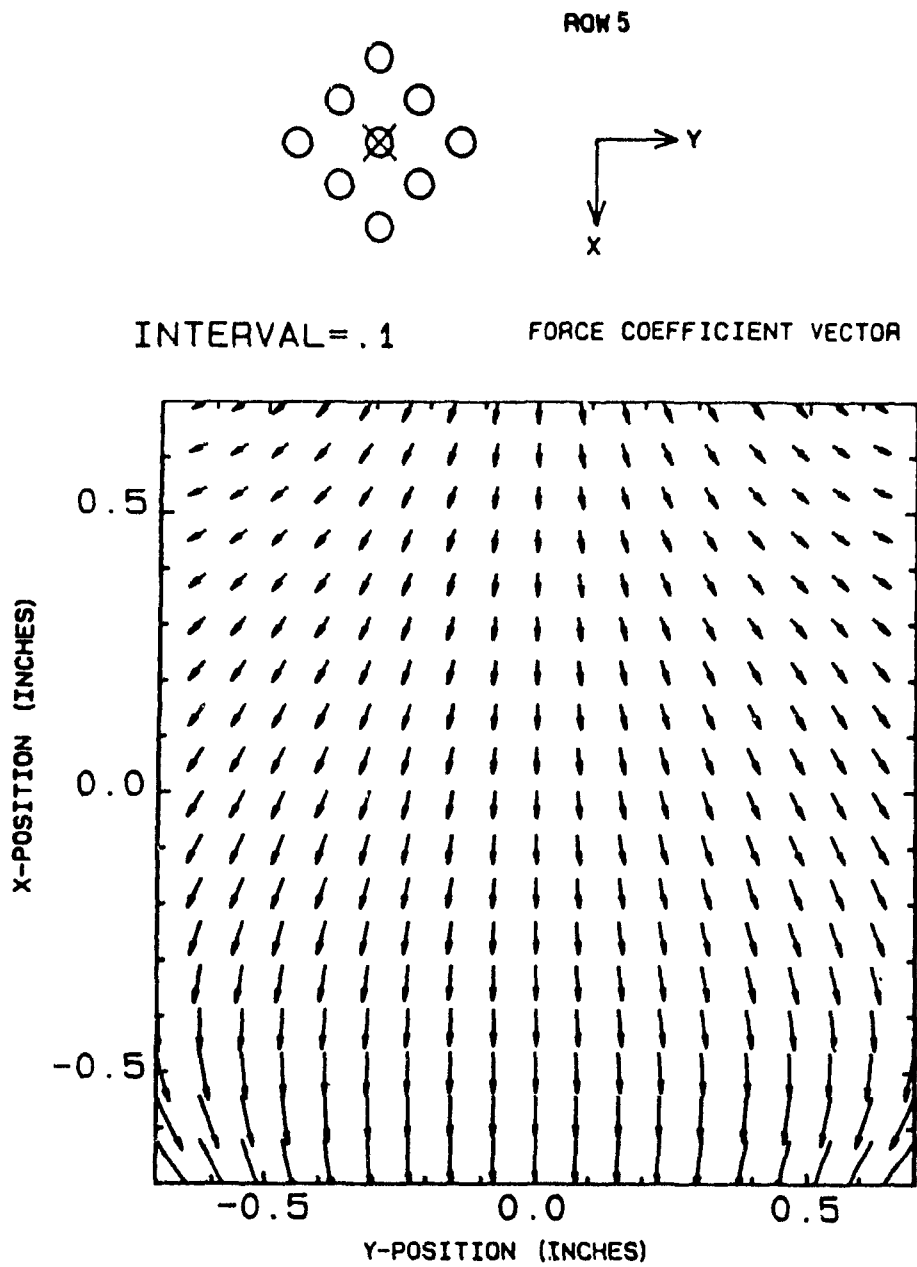


Figure 6.37: Variation of the force coefficient vector with cylinder displacement (fifth row cylinder, $U_\infty = 16.6$ m/s).

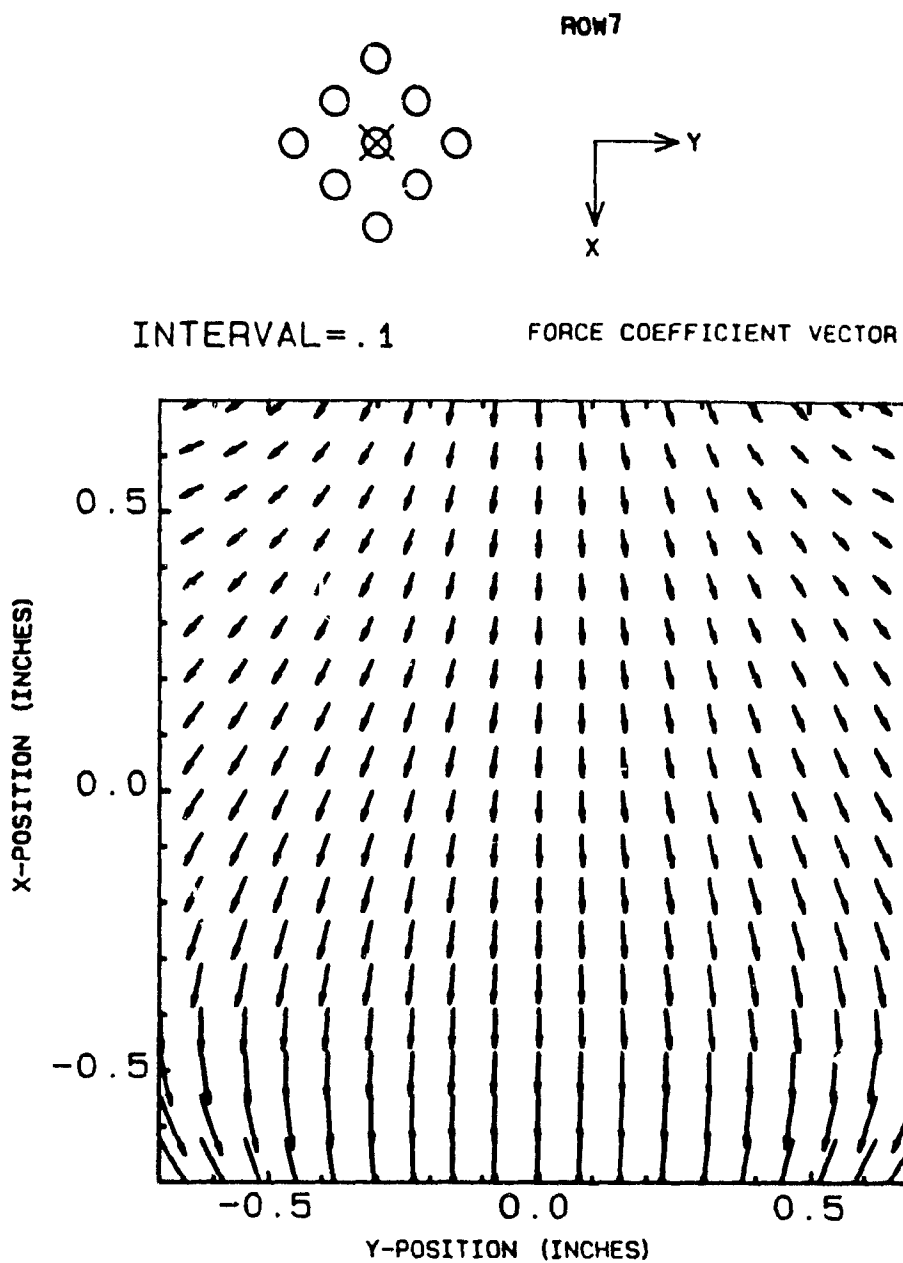


Figure 6.38: Variation of the force coefficient vector with cylinder displacement (seventh row cylinder, $U_\infty = 16.6$ m/s).

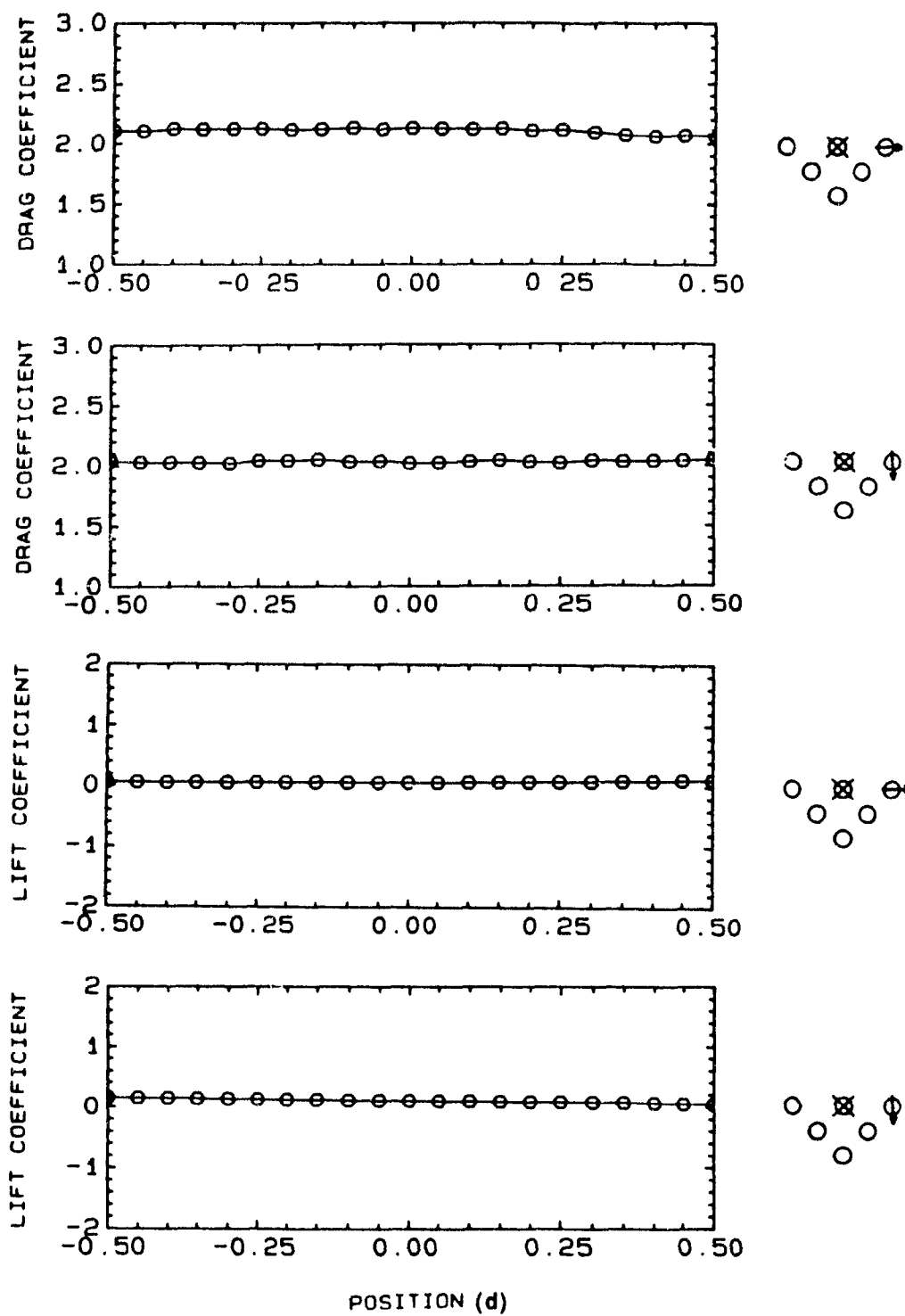


Figure 6.39: Changes in the fluid force coefficients of a first row cylinder due to the displacement of cylinder 1R.

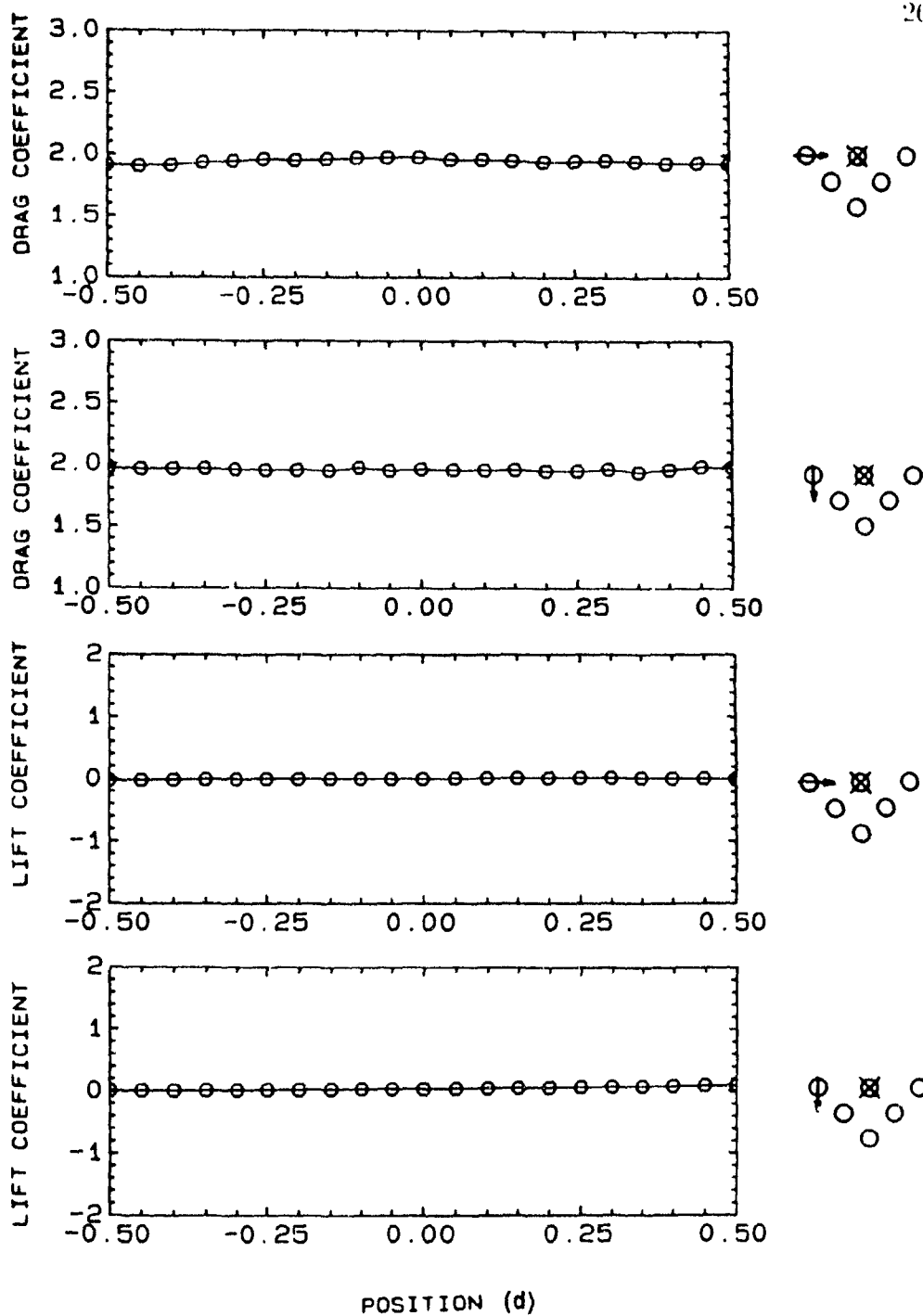


Figure 6.40: Changes in the fluid force coefficients of a first row cylinder due to the displacement of cylinder II.

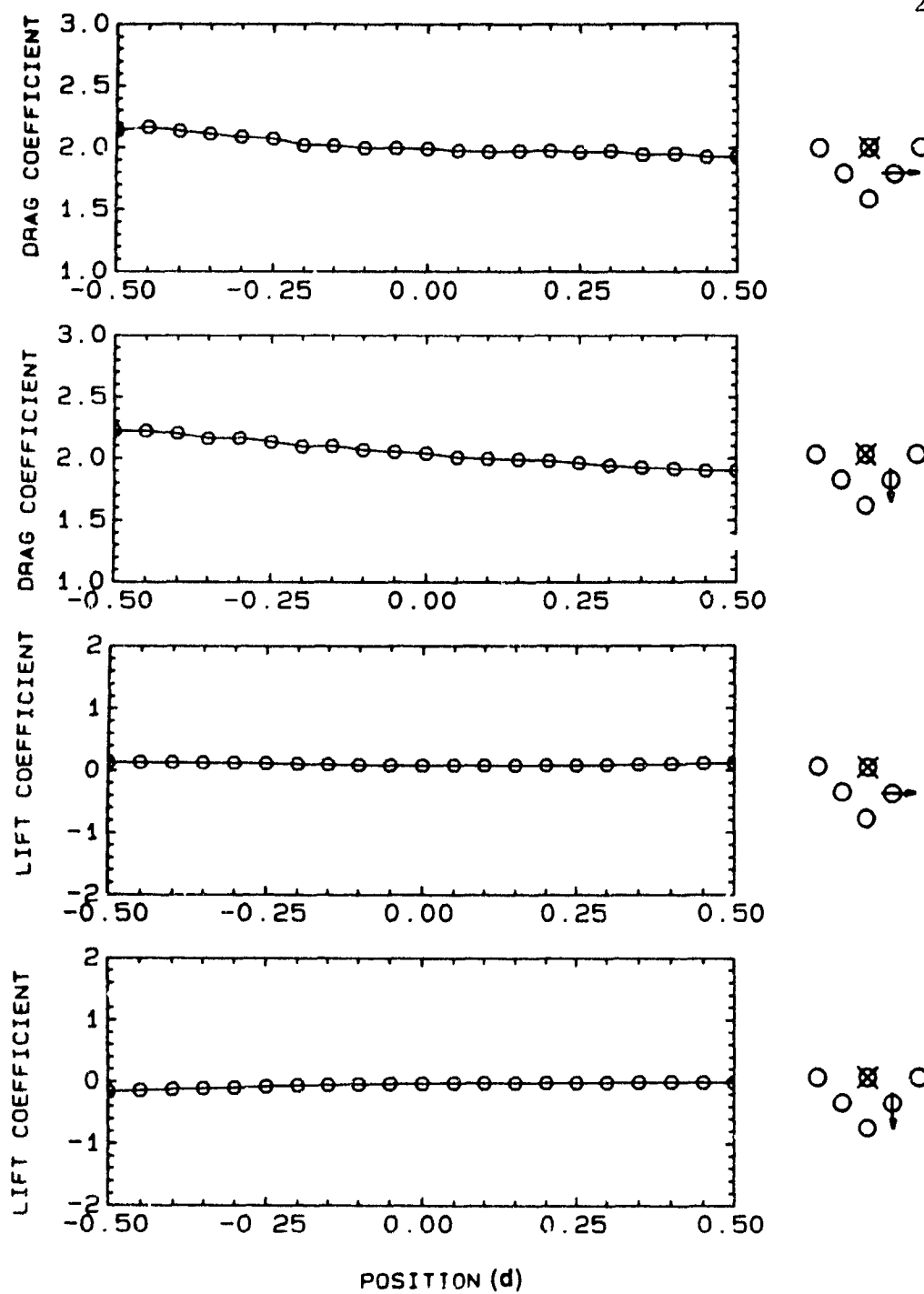


Figure 6.11. Changes in the fluid force coefficients of a first row cylinder due to the displacement of cylinder 2R.

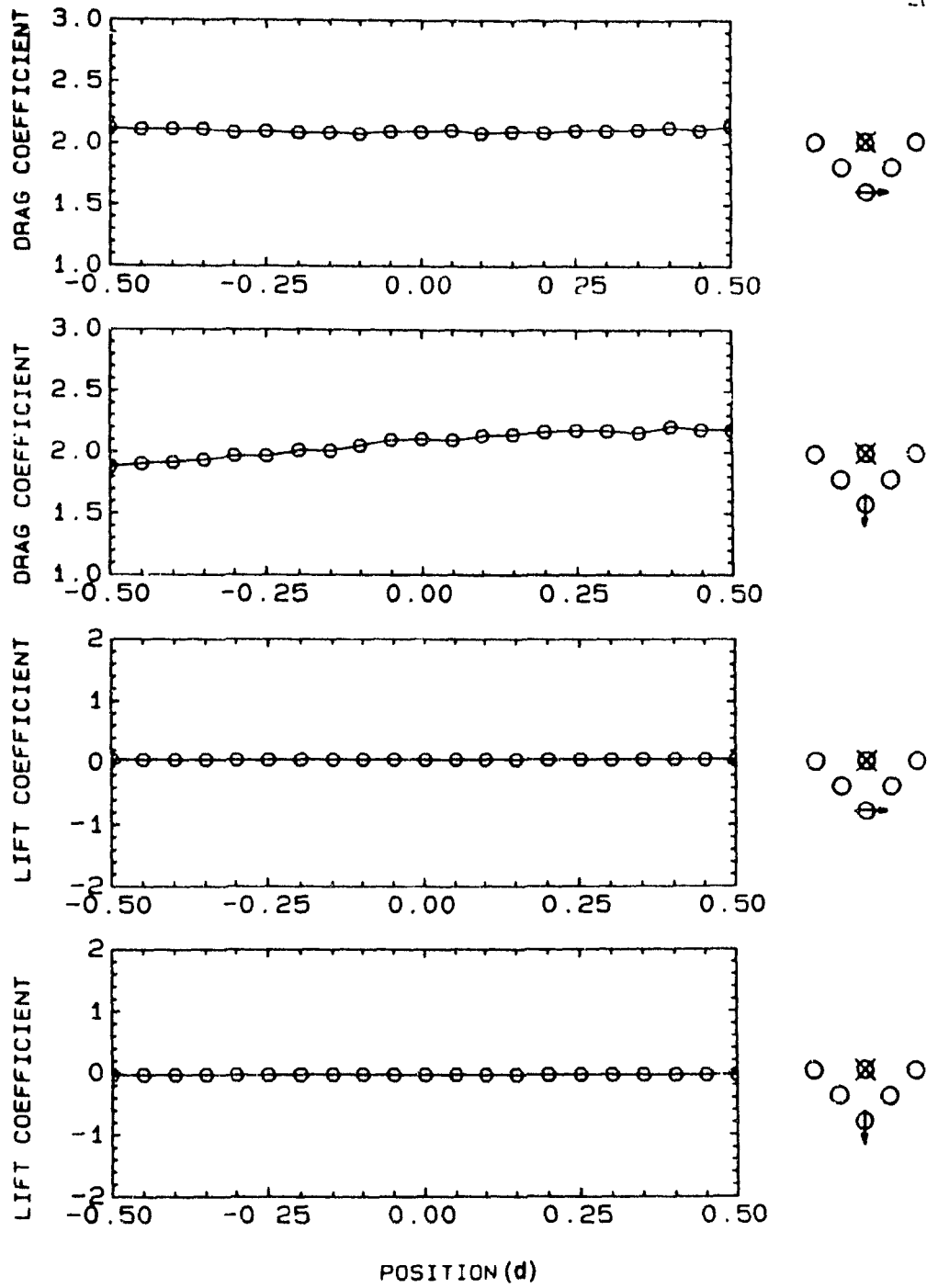


Figure 6.42: Changes in the fluid force coefficients of a first row cylinder due to the displacement of cylinder 3.

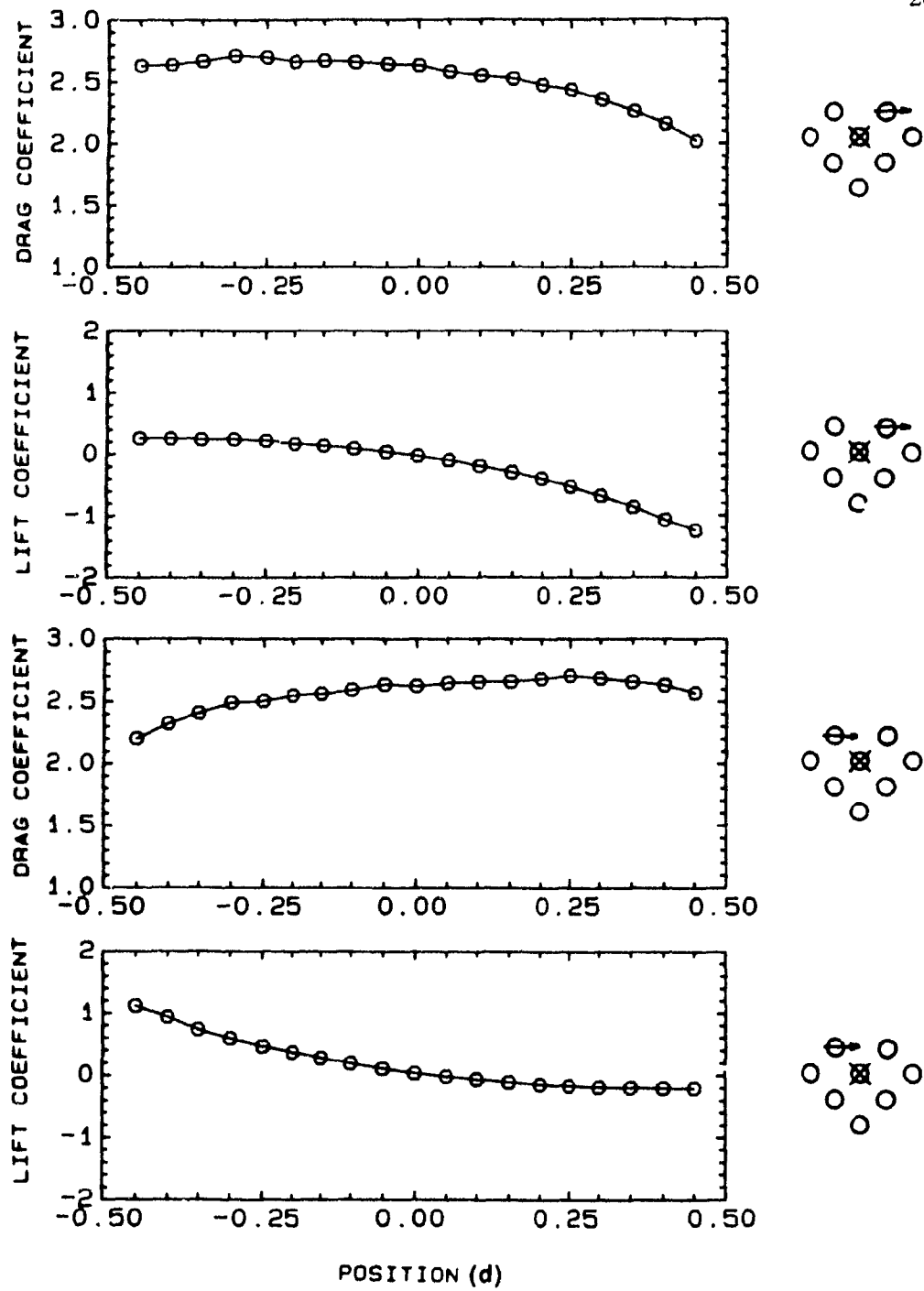


Figure 6.43: Changes in the fluid force coefficients of a second row cylinder due to the displacement of cylinder 1R and 1L.

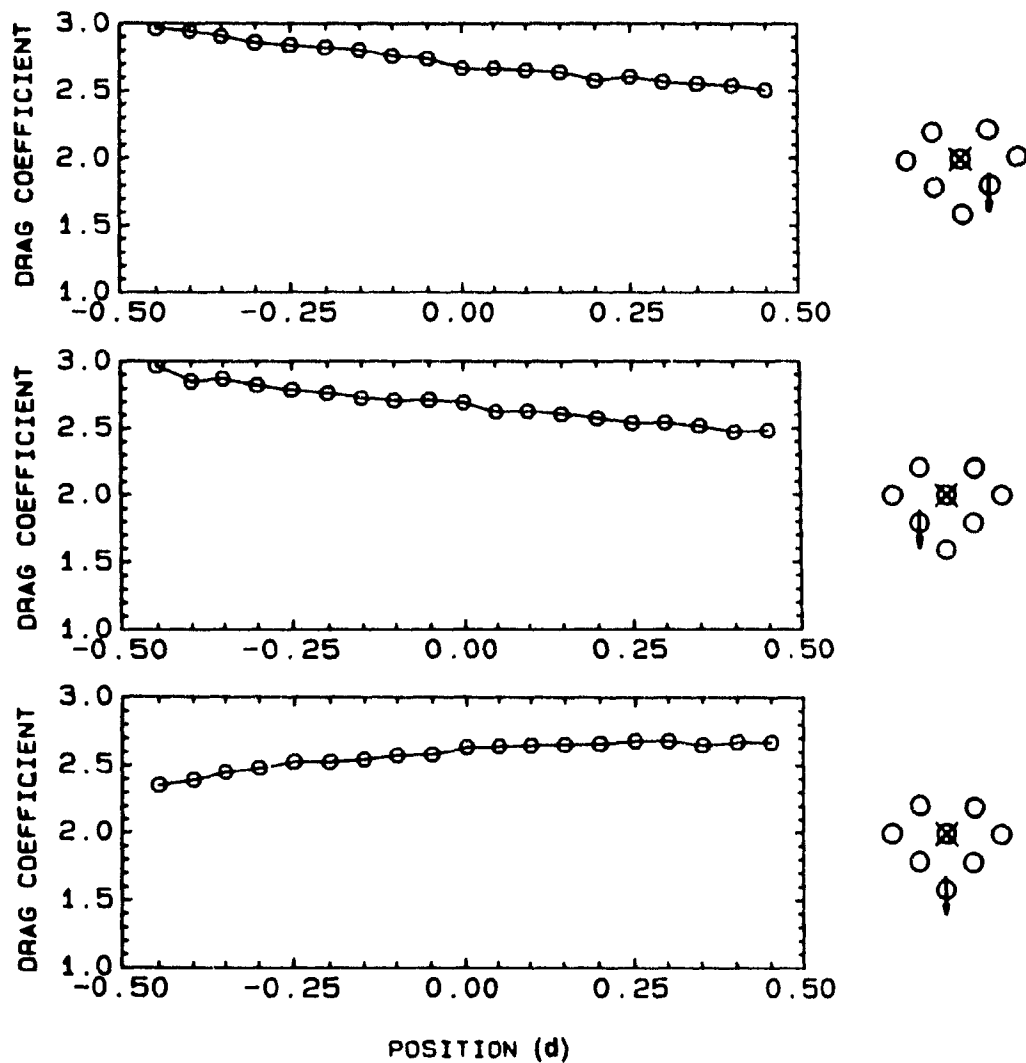


Figure 6.44: Changes in the fluid force coefficients of a second row cylinder due to the displacement of cylinders 3R, 3L and 4.

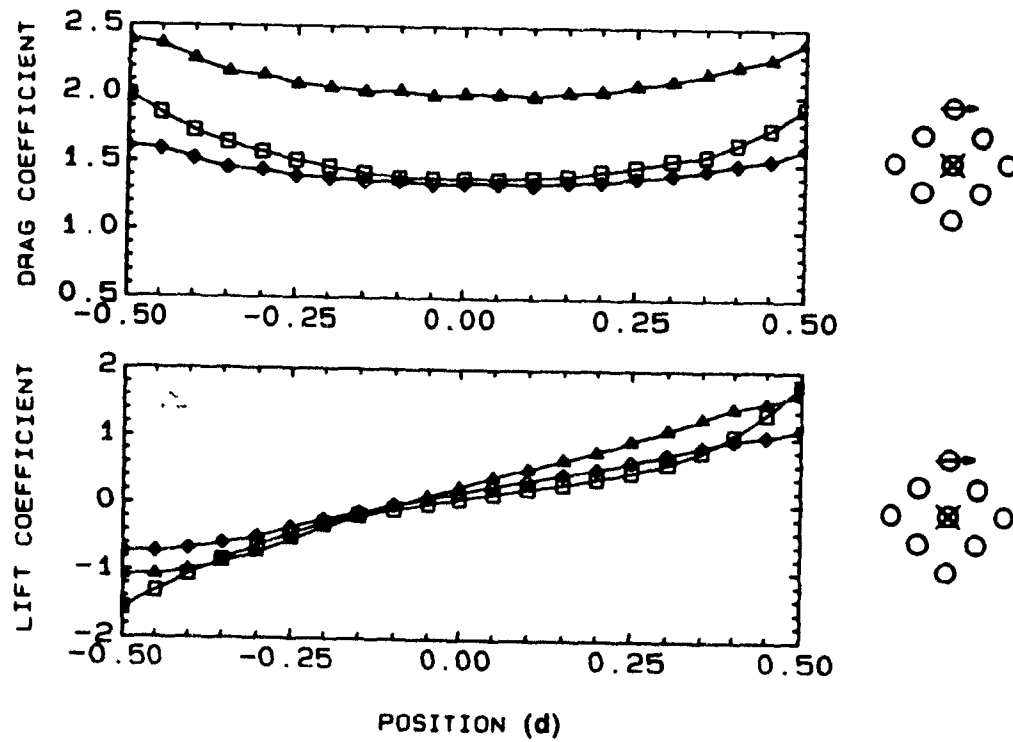


Figure 6.45: Changes in the fluid force coefficients of a third row cylinder due to the cross-flow displacement of cylinder 1 (Δ : $U_\infty = 8.3$ m/s, \square : $U_\infty = 16.6$ m/s and \diamond : $U_\infty = 8.3$ m/s normalised).

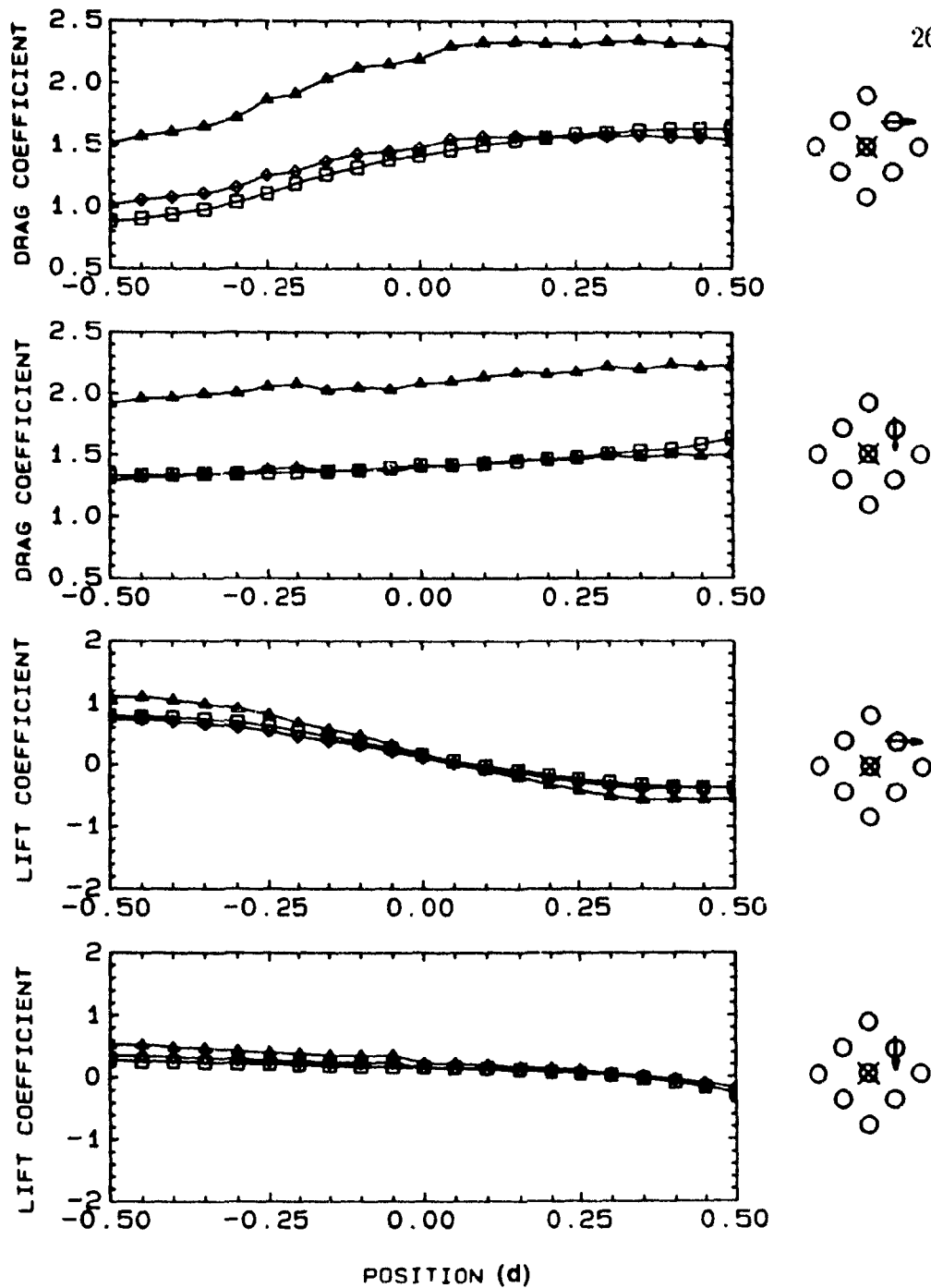


Figure 6.46: Changes in the fluid force coefficients of a third row cylinder due to the displacement of cylinder 2R (Δ : $U_\infty = 8.3$ m/s, \square : $U_\infty = 16.6$ m/s and \circ : $U_\infty = 8.3$ m/s normalised).

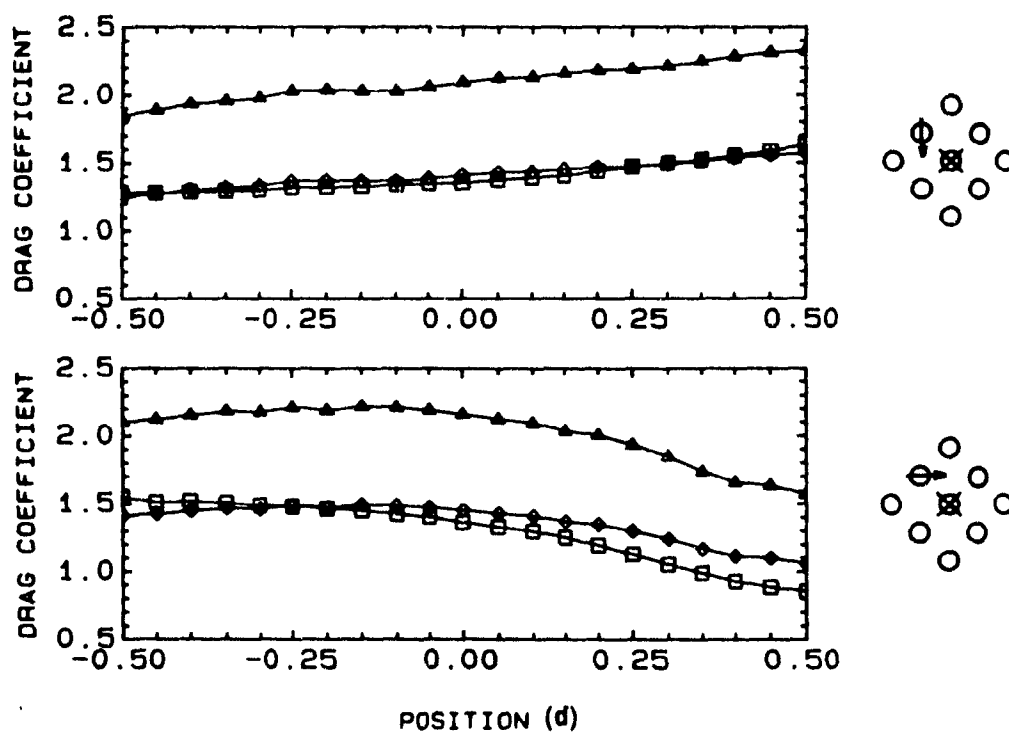


Figure 6.47: Changes in the fluid force coefficients of a third row cylinder due to the displacement of cylinder $2L$ (Δ : $U_\infty = 8.3$ m/s, \square : $U_\infty = 16.6$ m/s and \diamond : $U_\infty = 8.3$ m/s normalised).

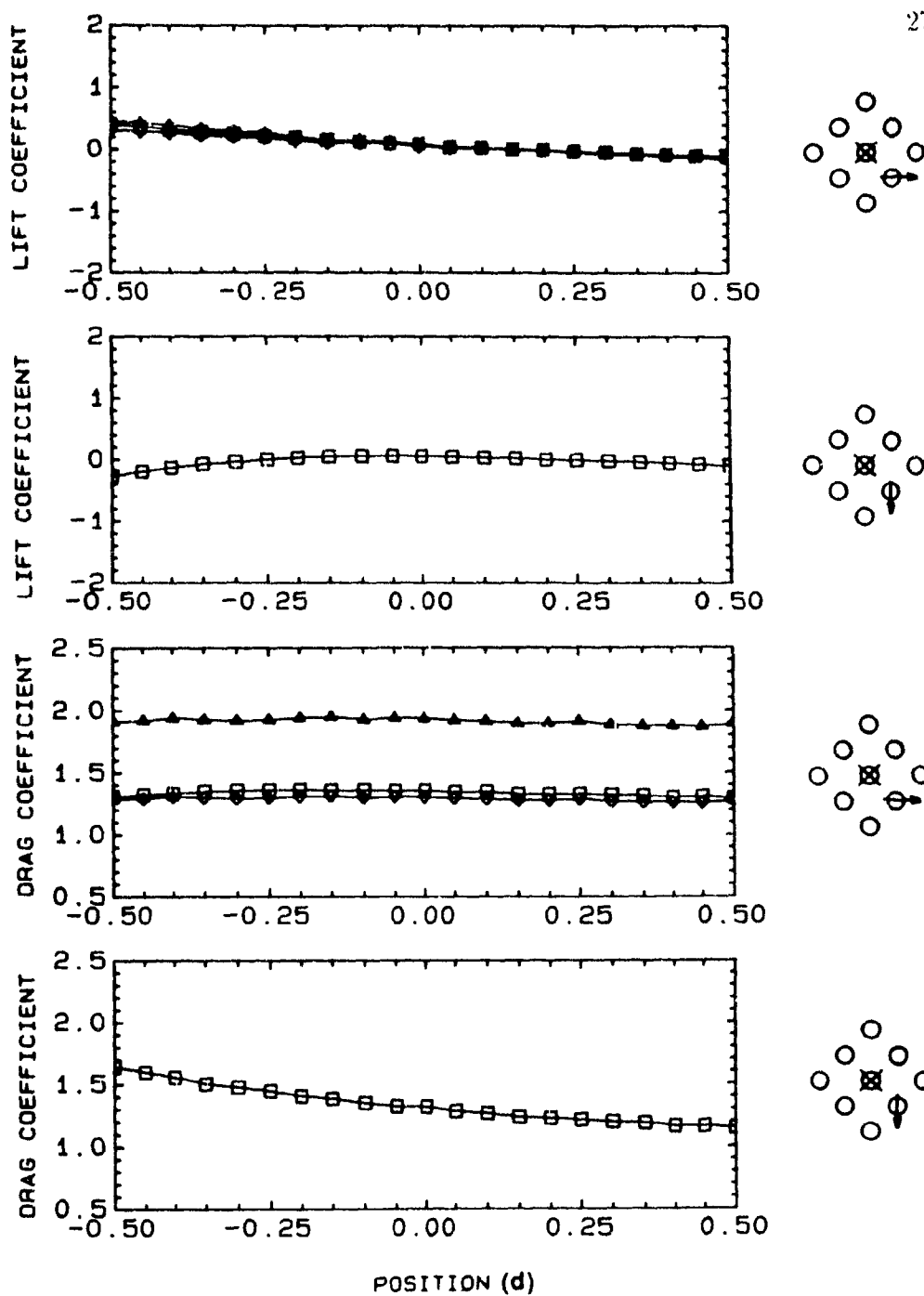


Figure 6.48: Changes in the fluid force coefficients of a third row cylinder due to the displacement of cylinder 4R (Δ : $U_\infty = 8.3$ m/s, \square : $U_\infty = 16.6$ m/s and \circ : $U_\infty = 8.3$ m/s normalised).

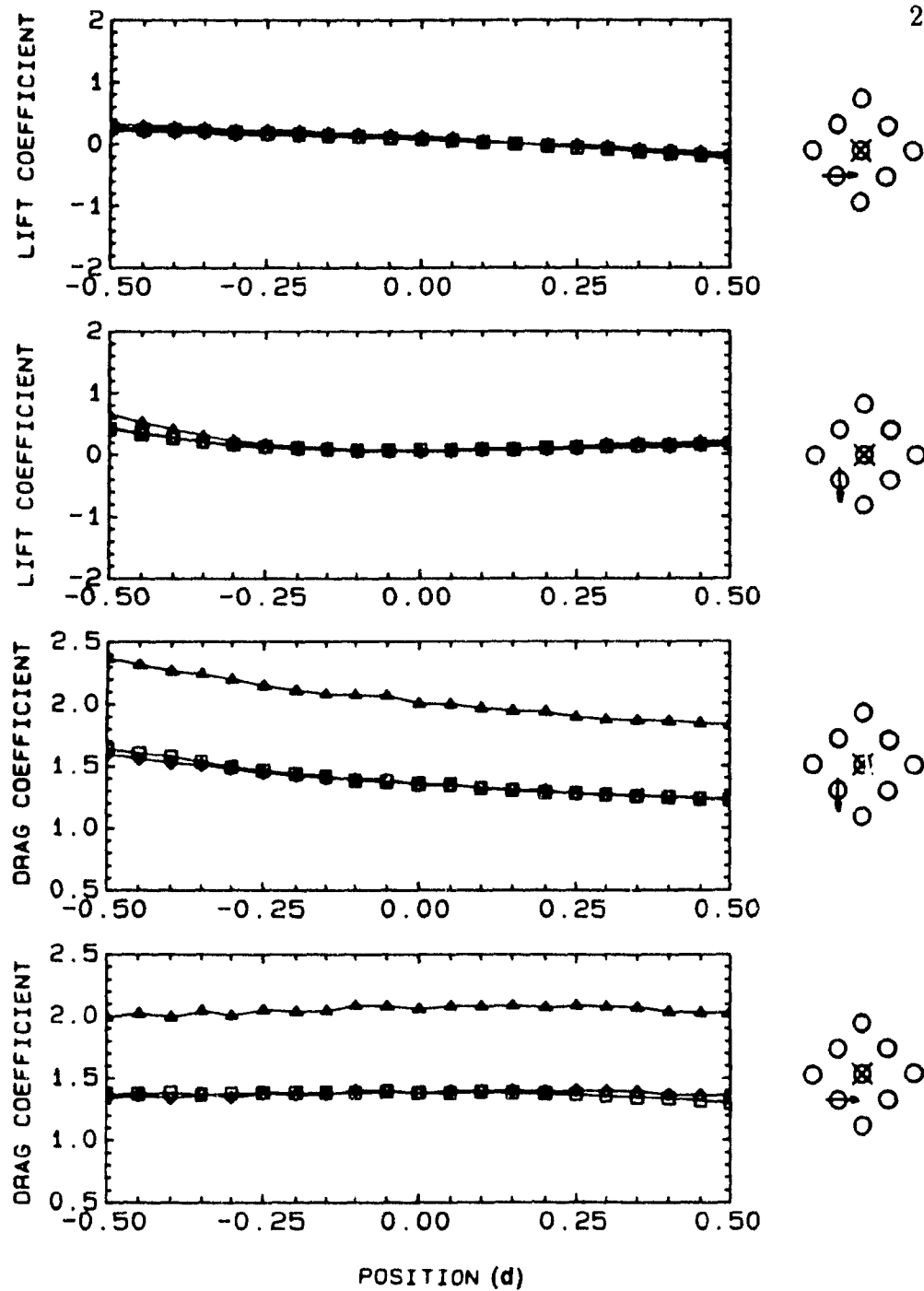


Figure 6.49: Changes in the fluid force coefficients of a third row cylinder due to the displacement of cylinder 4L (Δ : $U_\infty = 8.3$ m/s, \square : $U_\infty = 16.6$ m/s and \diamond : $U_\infty = 8.3$ m/s normalised).

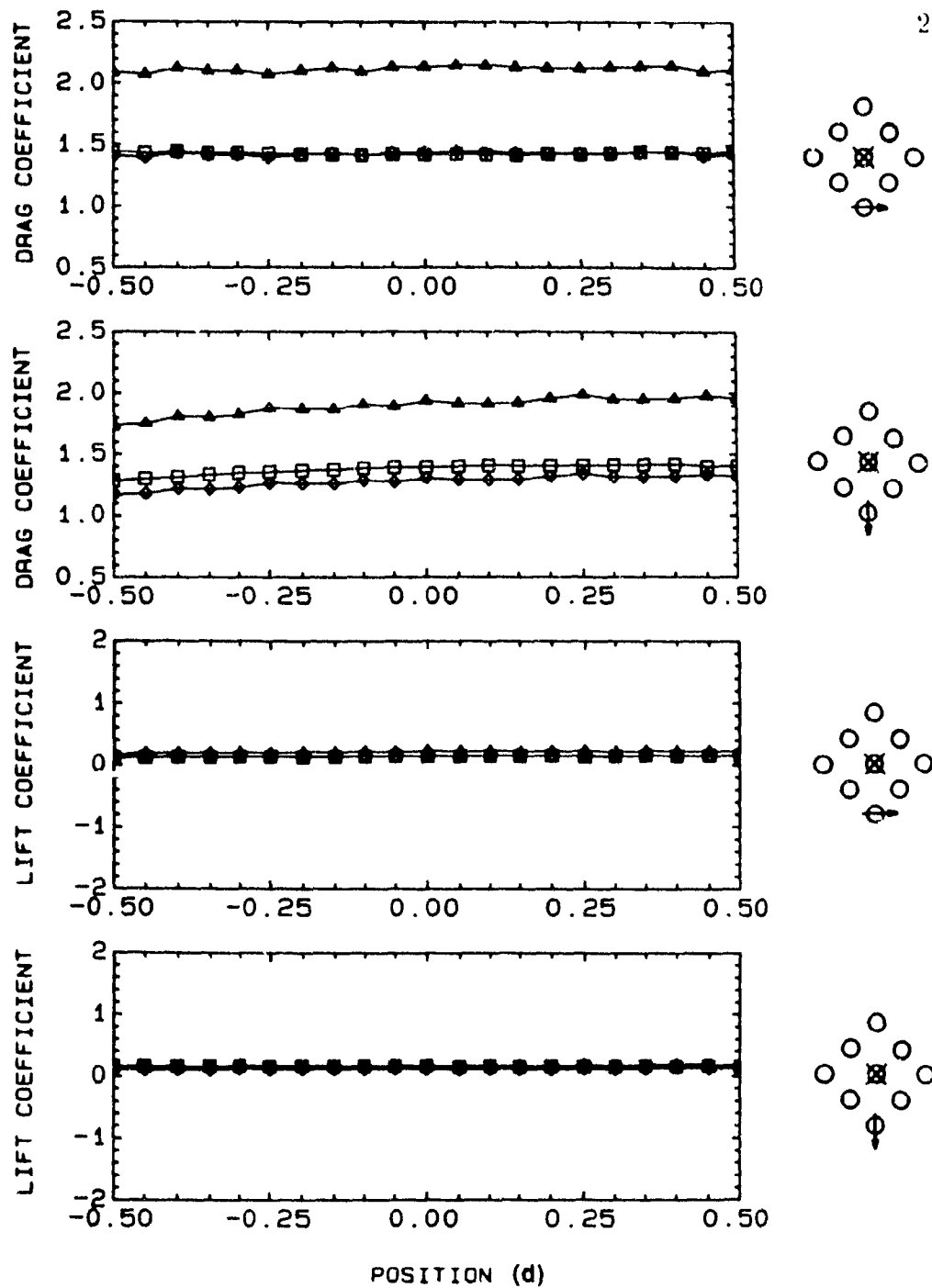


Figure 6.50: Changes in the fluid force coefficients of a third row cylinder due to the displacement of cylinder 5 (Δ : $U_\infty = 8.3$ m/s, \square : $U_\infty = 16.6$ m/s and \diamond : $U_\infty = 8.3$ m/s normalised).

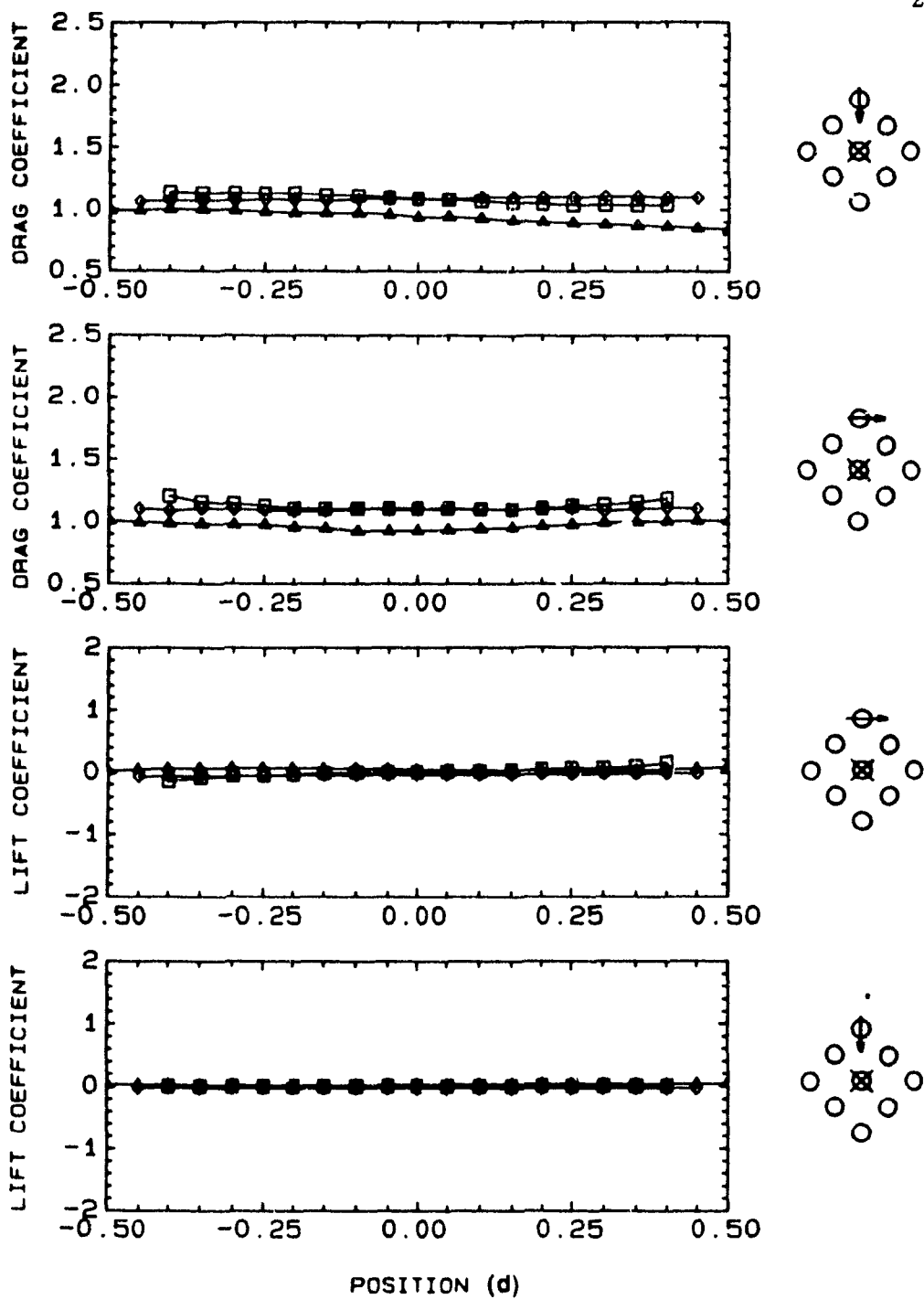


Figure 6.51: Changes in the fluid force coefficients of fourth (\square), fifth (\triangle) and seventh (\diamond) row cylinders due to the displacement of an upstream cylinder at $U_\infty = 16.6$ m/s.

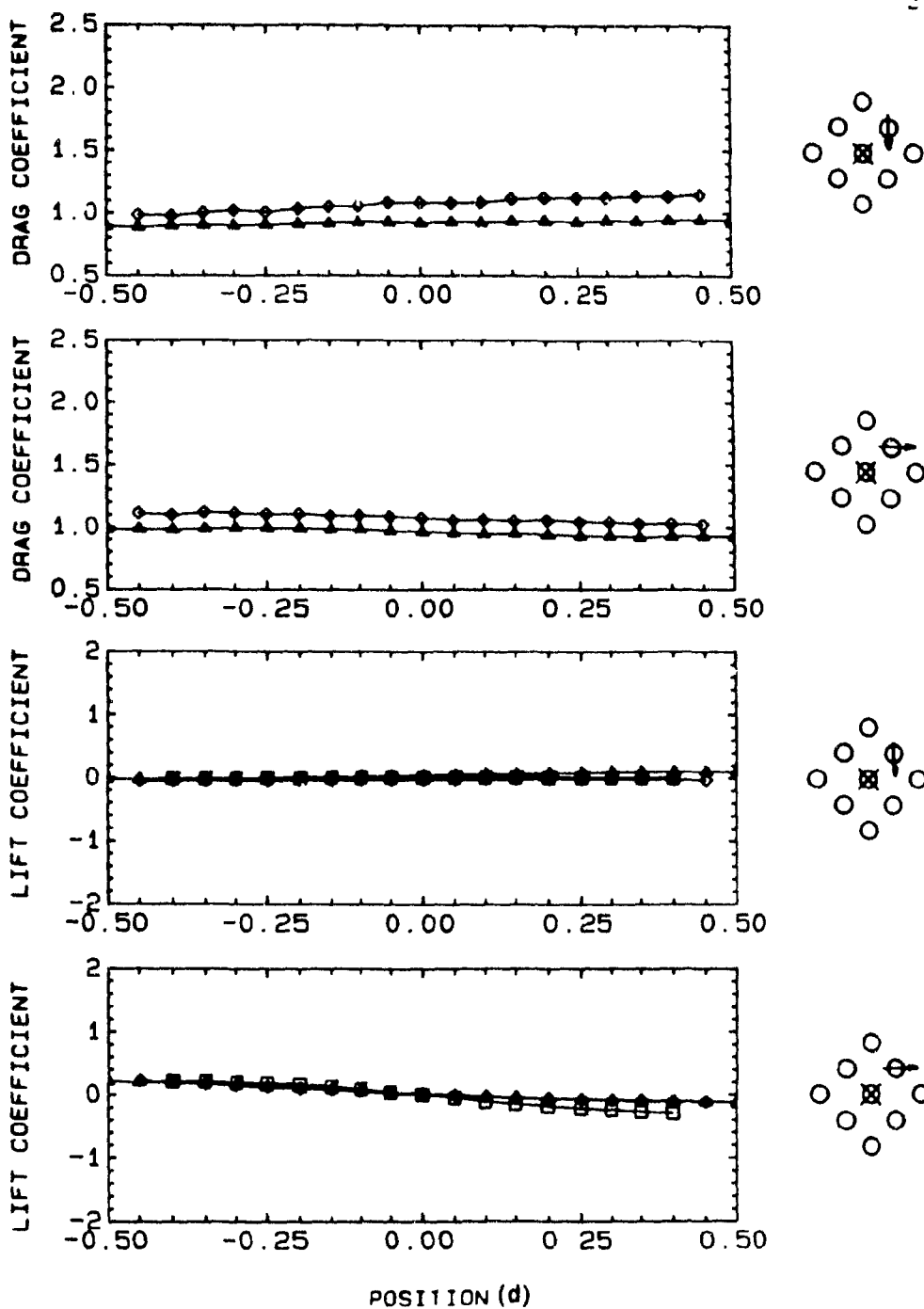


Figure 6.52: Changes in the fluid force coefficients of fourth (\square), fifth (\triangle) and seventh (\diamond) row cylinders due to the displacement of an upstream cylinder at $U_{\infty} = 16.6$ m/s.

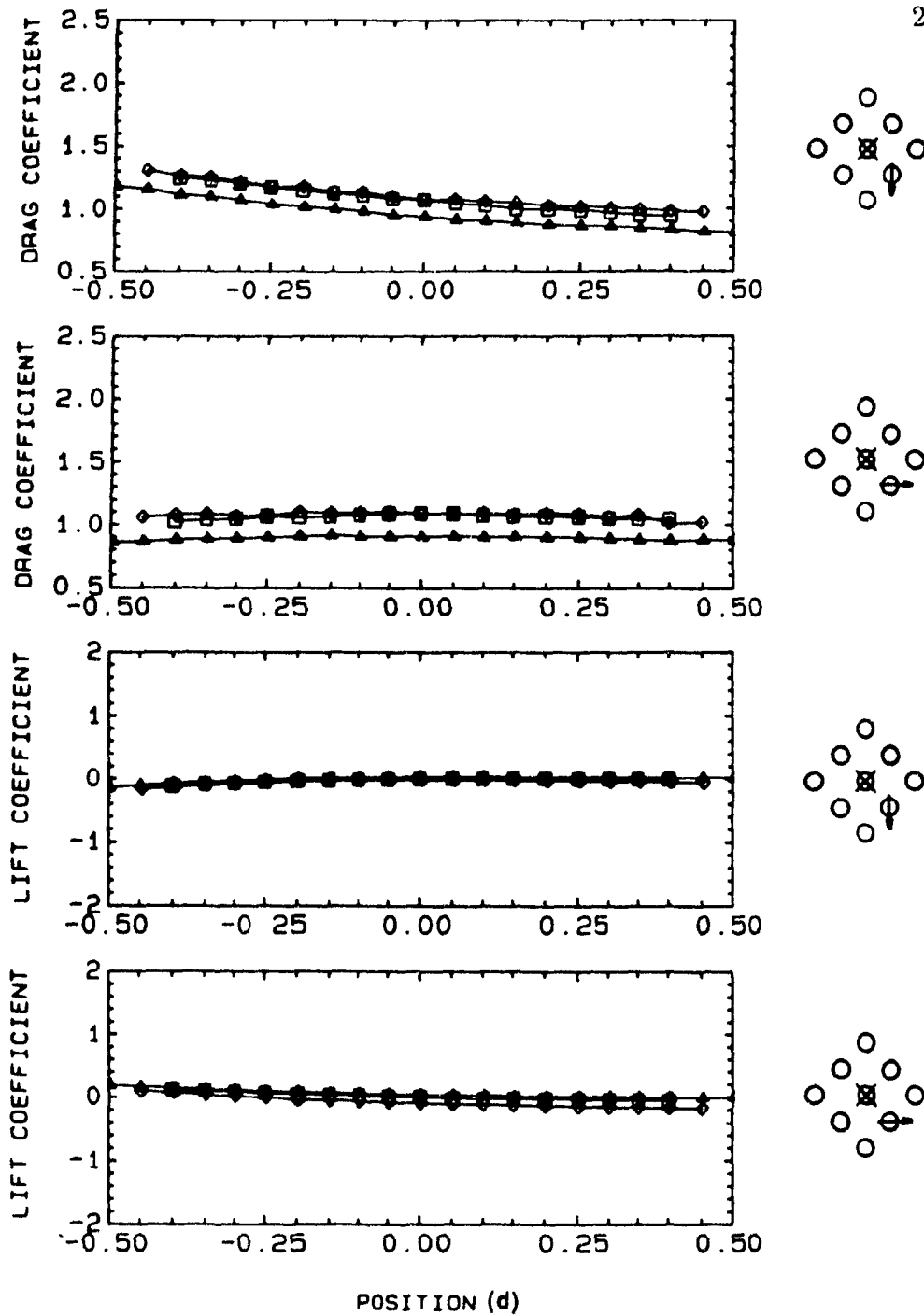


Figure 6.53: Changes in the fluid force coefficients of fourth (□), fifth (△) and seventh (◇) row cylinders due to the displacement of a downstream cylinder at $U_\infty = 16.6$ m/s

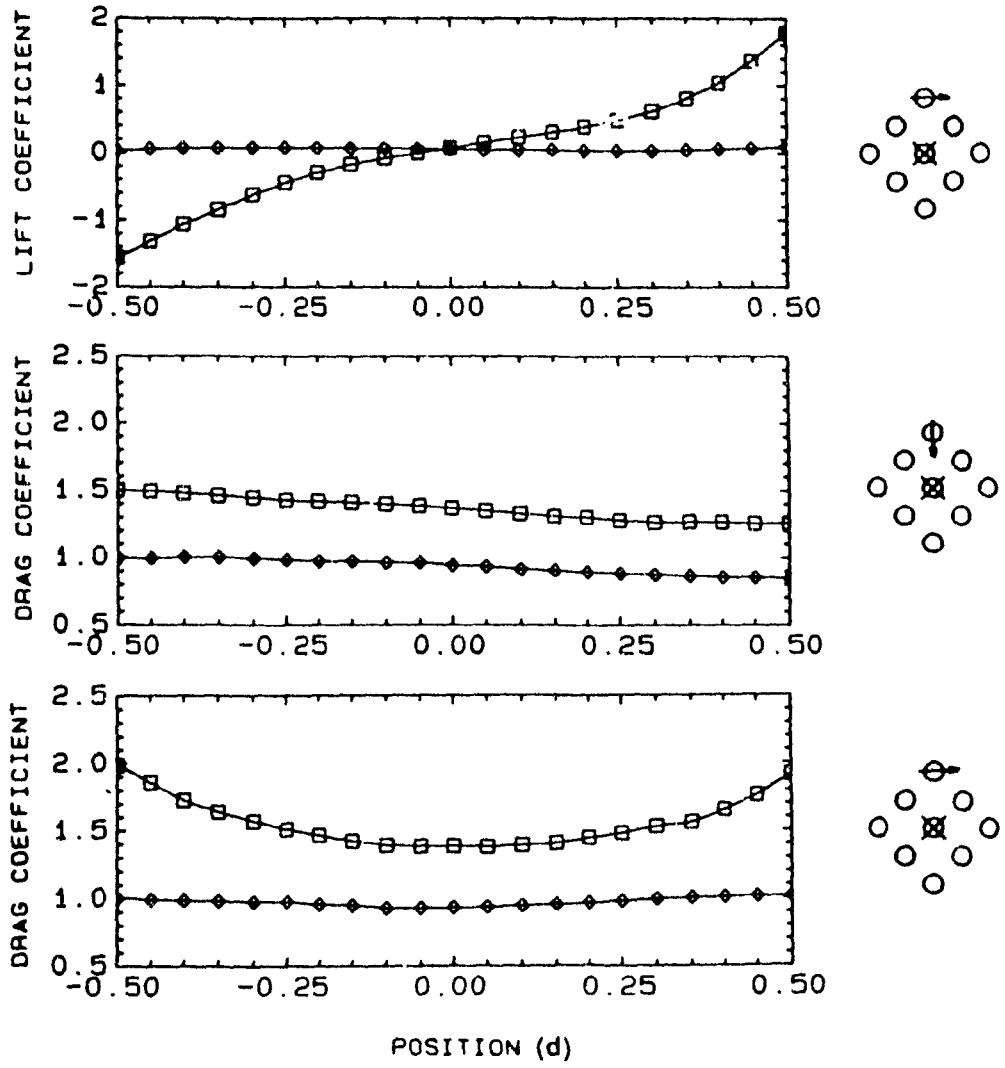


Figure 6.54. The effect induced by the displacement of surrounding cylinders upon the fluid force coefficients of a third (\square) and fifth (\diamond) row cylinder at $U_\infty = 16.6 \text{ m/s}$

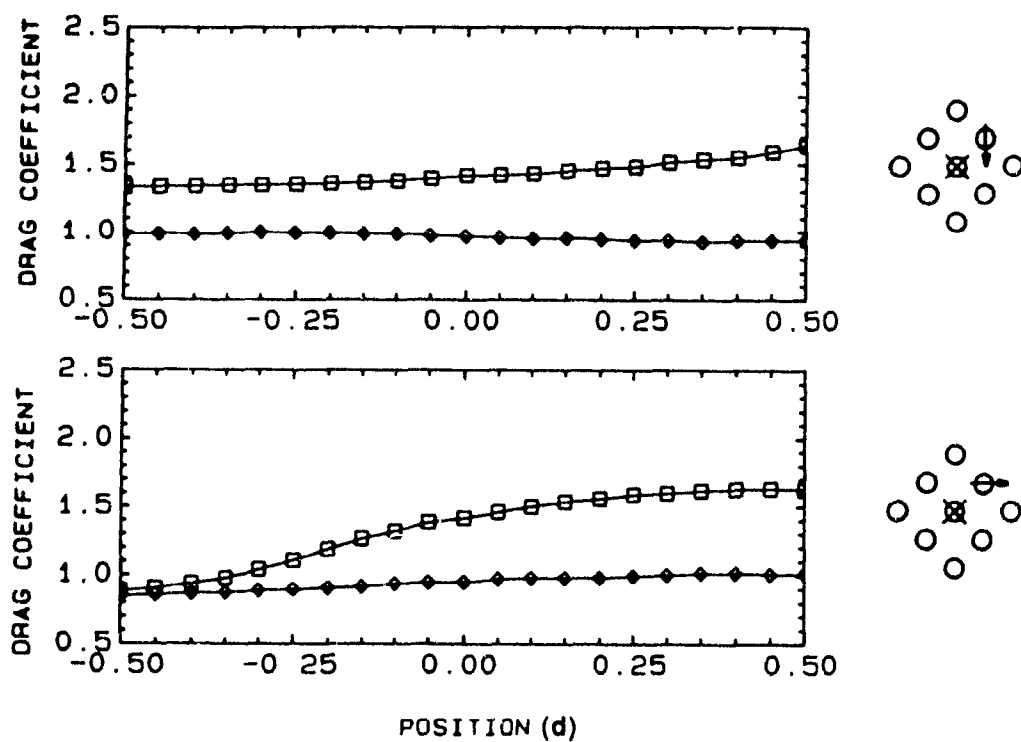


Figure 6.55 The effect induced by the displacement of surrounding cylinders upon the fluid force coefficients of a third (\square) and fifth (\diamond) row cylinder at $U_\infty = 16.6$ m/s.

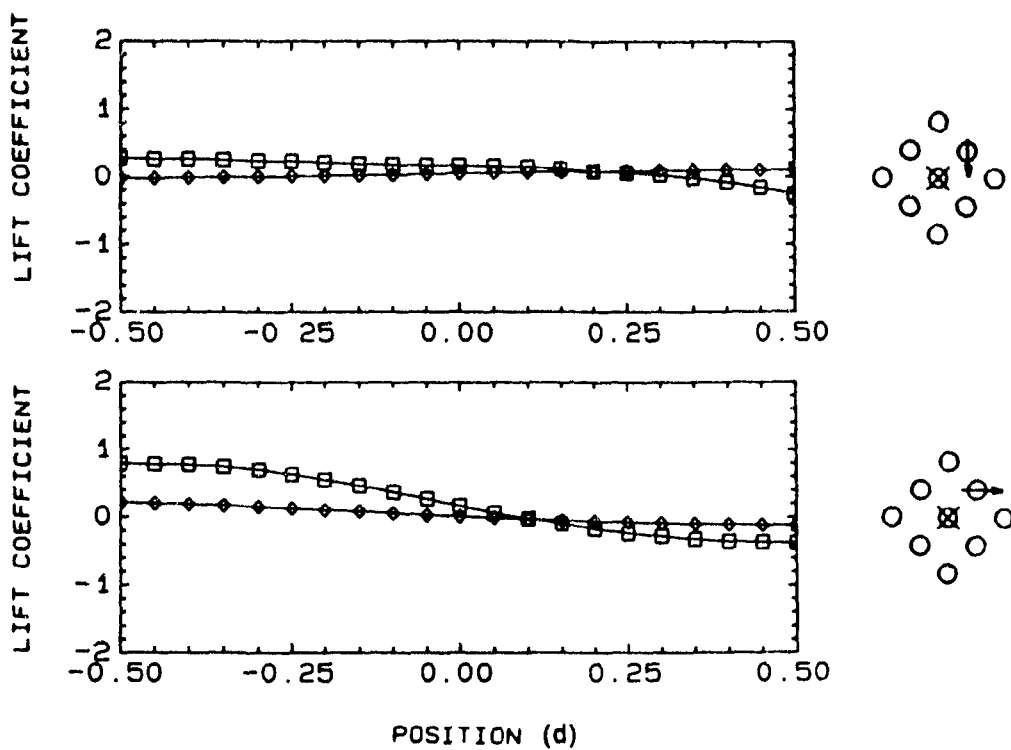


Figure 6.56: The effect induced by the displacement of surrounding cylinders upon the fluid force coefficients of a third (\square) and fifth (\diamond) row cylinder at $U_{\infty} = 16.6$ m/s.

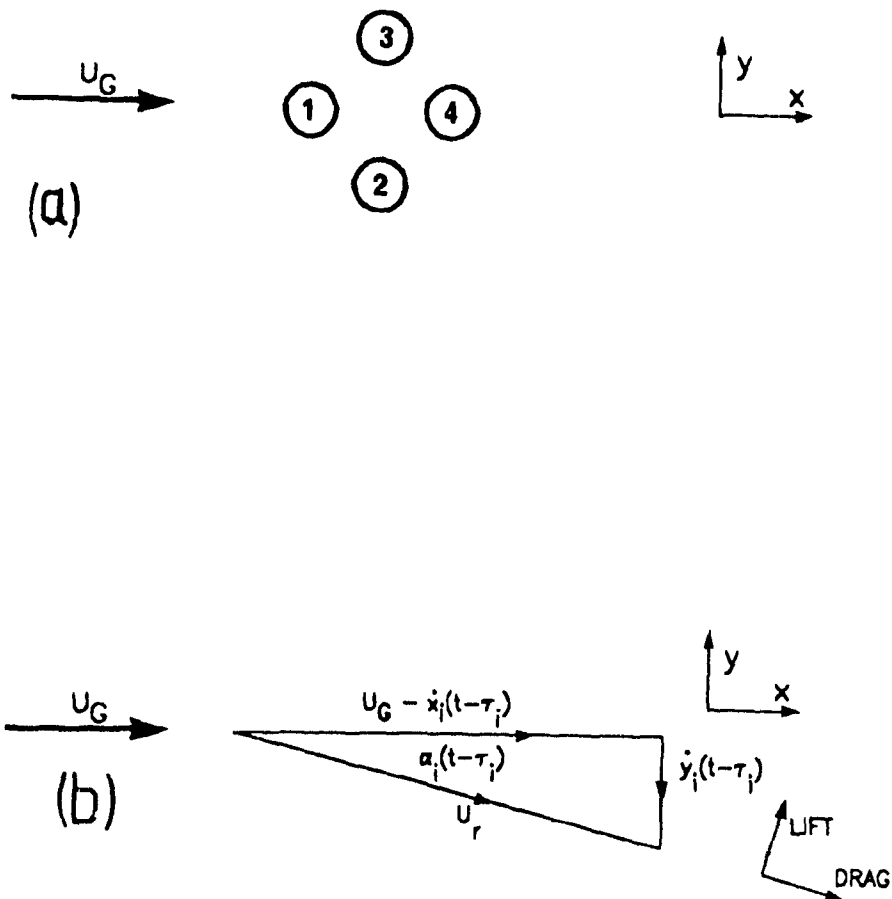


Figure 7.1: (a) Schematic of four flexible cylinders; (b) the resultant velocity vector for cylinder i

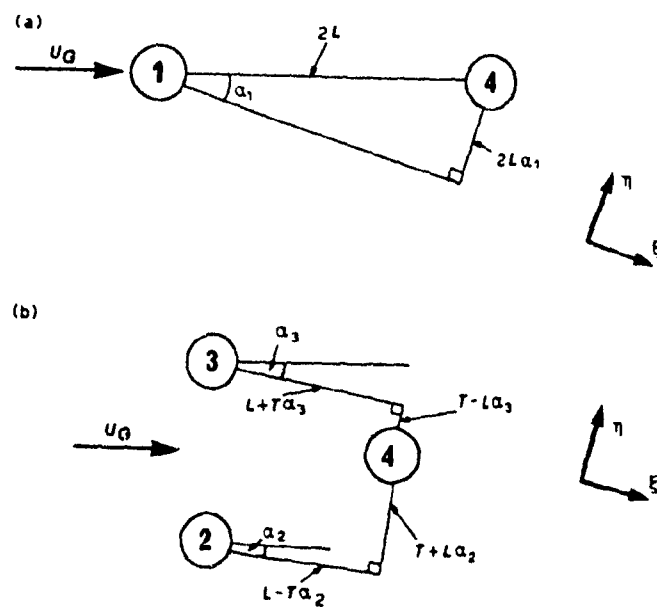


Figure 7.2: The apparent displacements (reproduced from ref. [80])

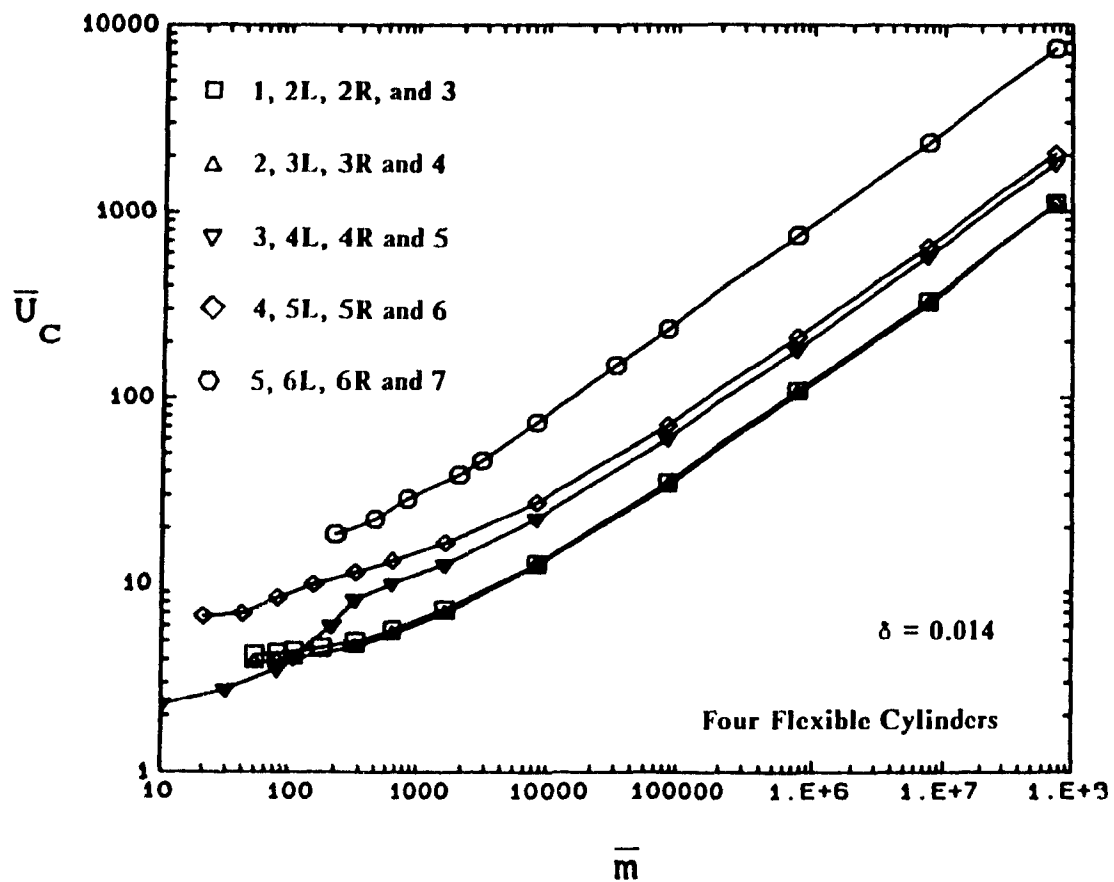


Figure 8.1: Variation of the non-dimensional critical flow velocity with dimensionless mass for a four-flexible cylinder configuration in different positions of the array.

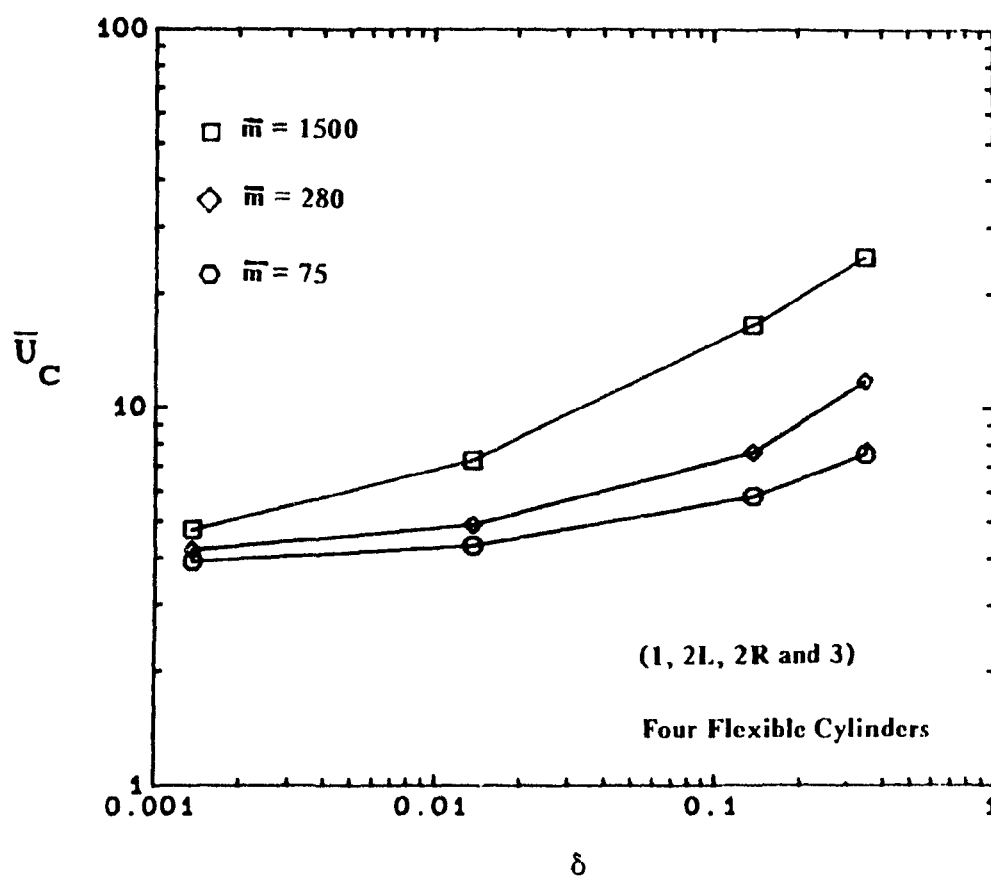


Figure 8.2: Variation of non-dimensional critical flow velocity with damping for a four-flexible cylinder configuration.

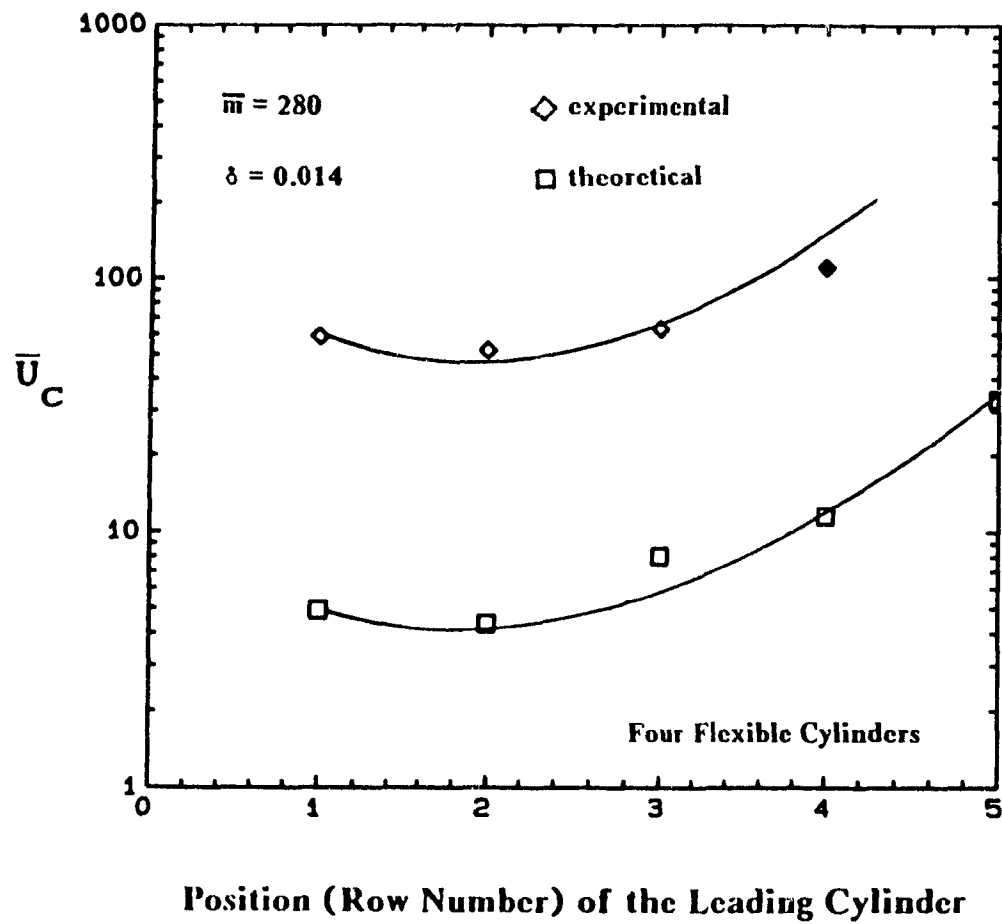


Figure 8.3: The experimental and theoretical variation of the non-dimensional critical velocity with position in the array.

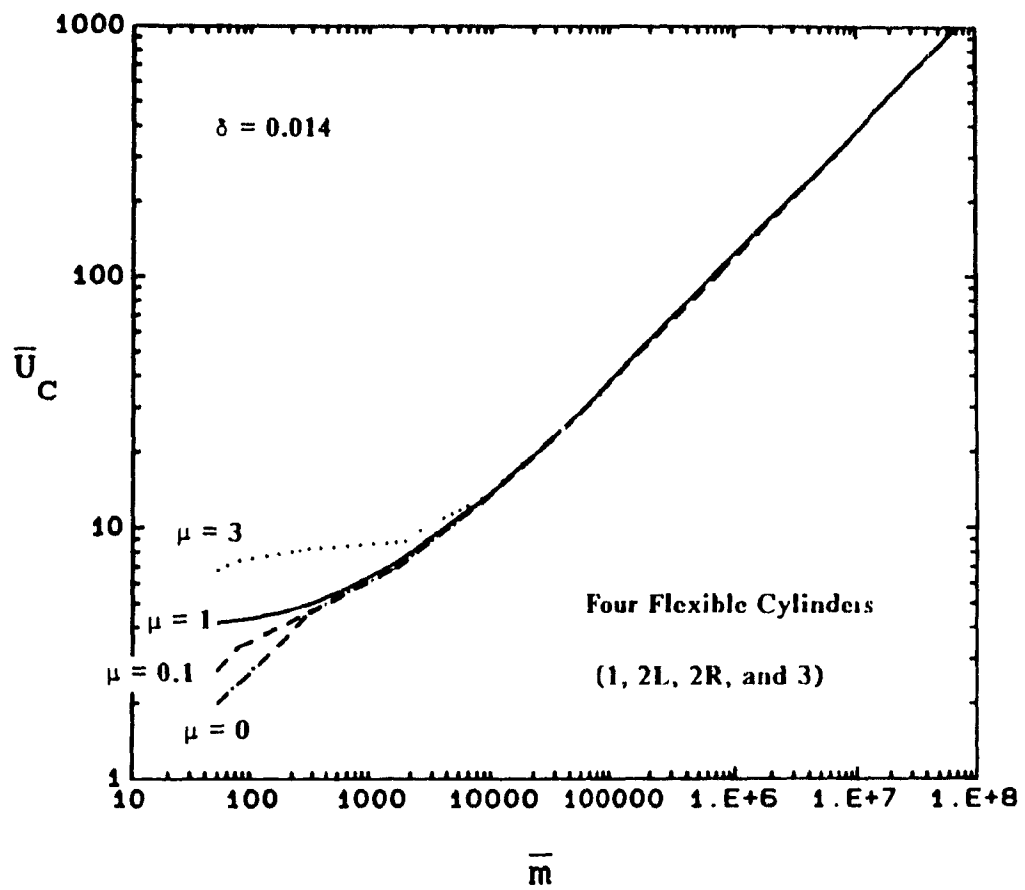


Figure 8.4: Effect of the time delay factor, μ , on the non-dimensional critical flow velocity

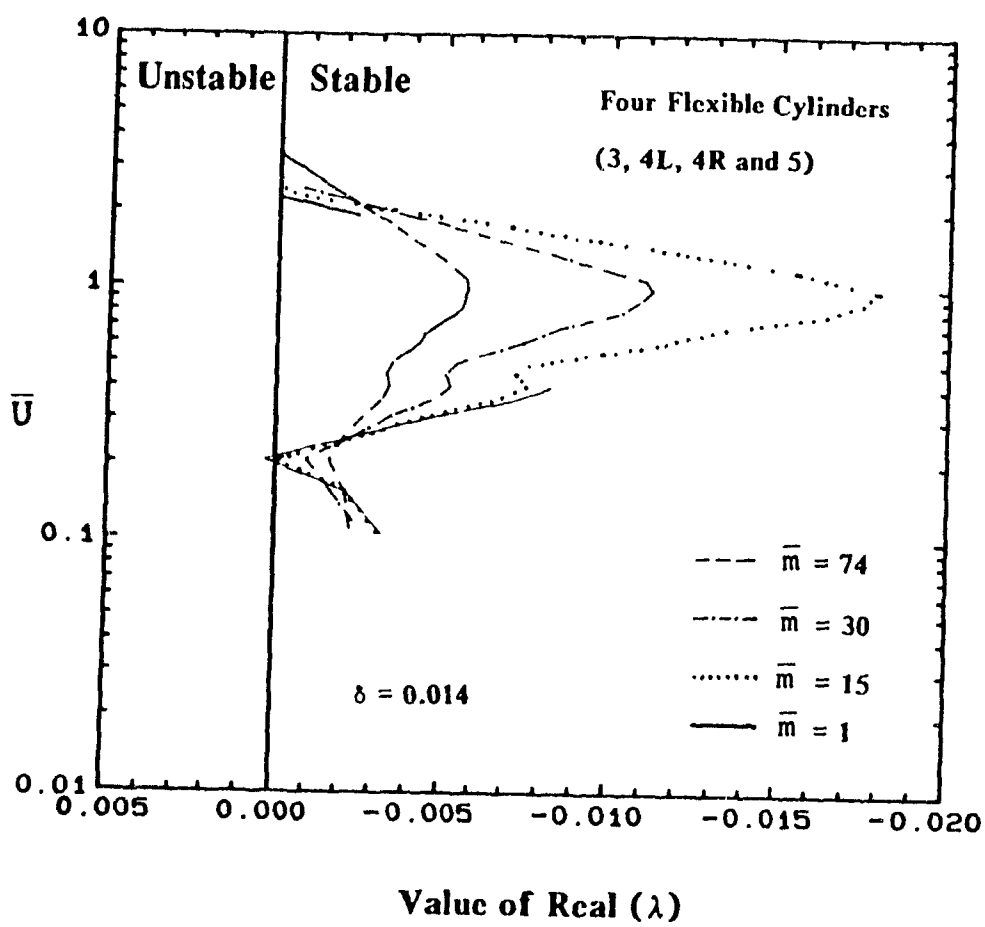


Figure 8.5: A "numerical search" for multiple instability bands.

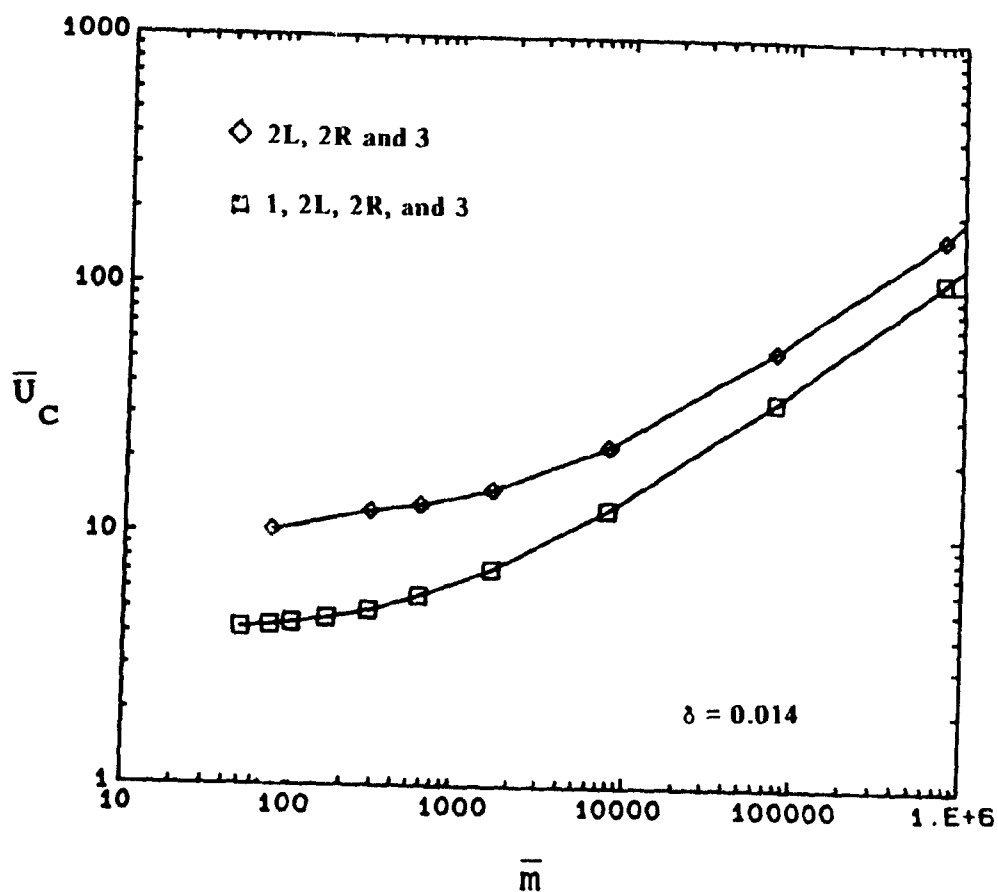


Figure 8.6: Comparison of the non-dimensional critical flow velocity for three and four-flexible cylinder configurations.

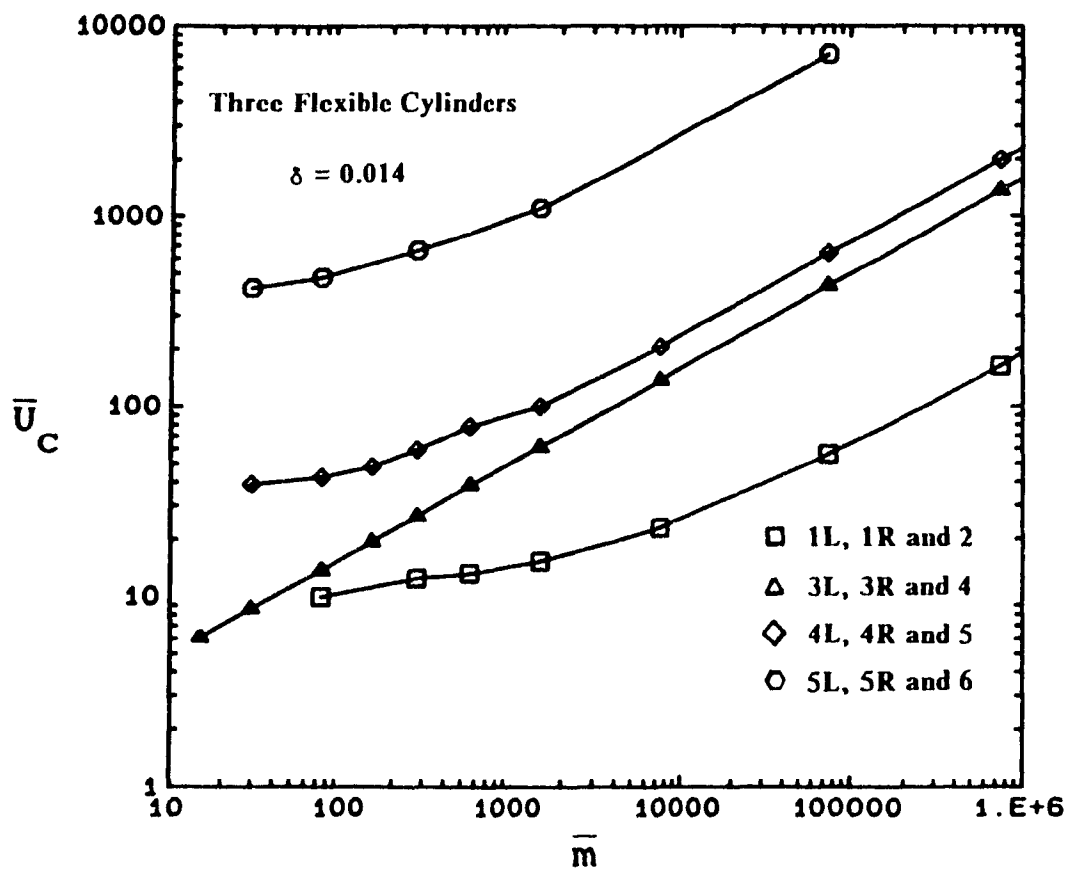


Figure 8.7: Variation of the non-dimensional critical flow velocity with dimensionless mass for a three flexible cylinder configuration in different positions of the array.

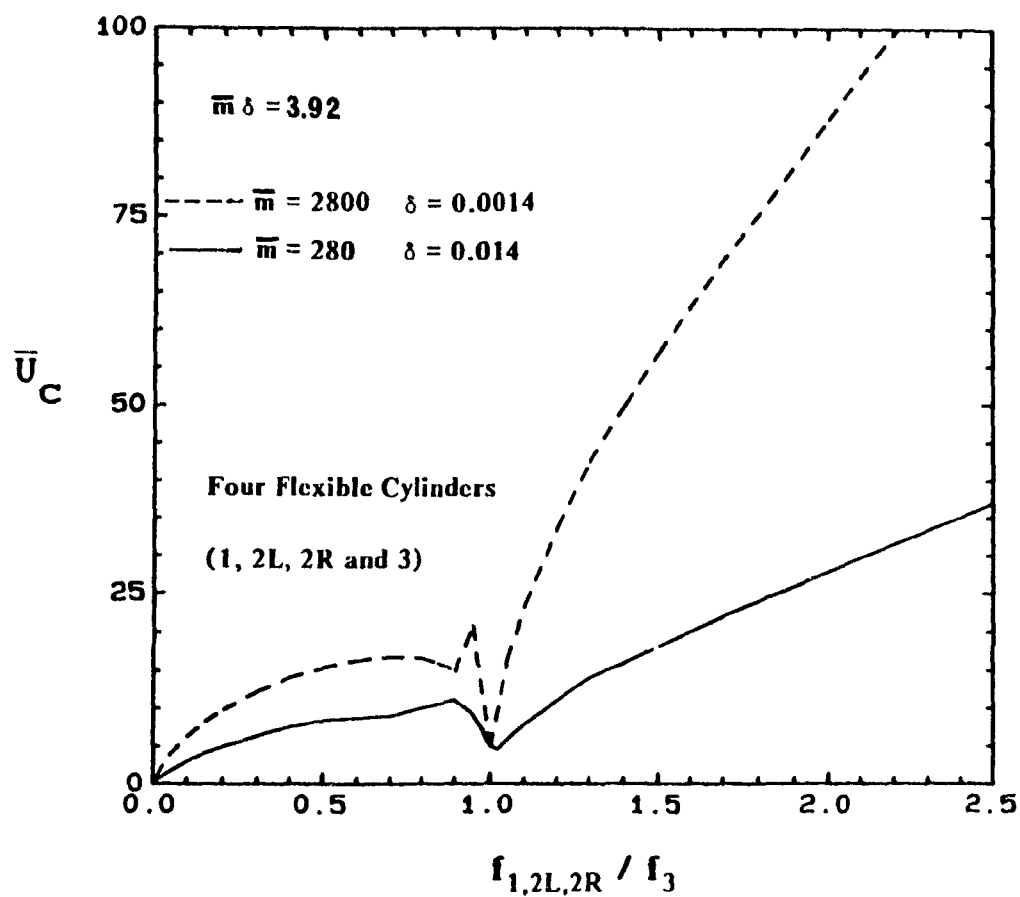


Figure 8.8: Effect of the mass-damping parameter upon the non-dimensional critical velocity of a detuned, four flexible cylinder configuration.

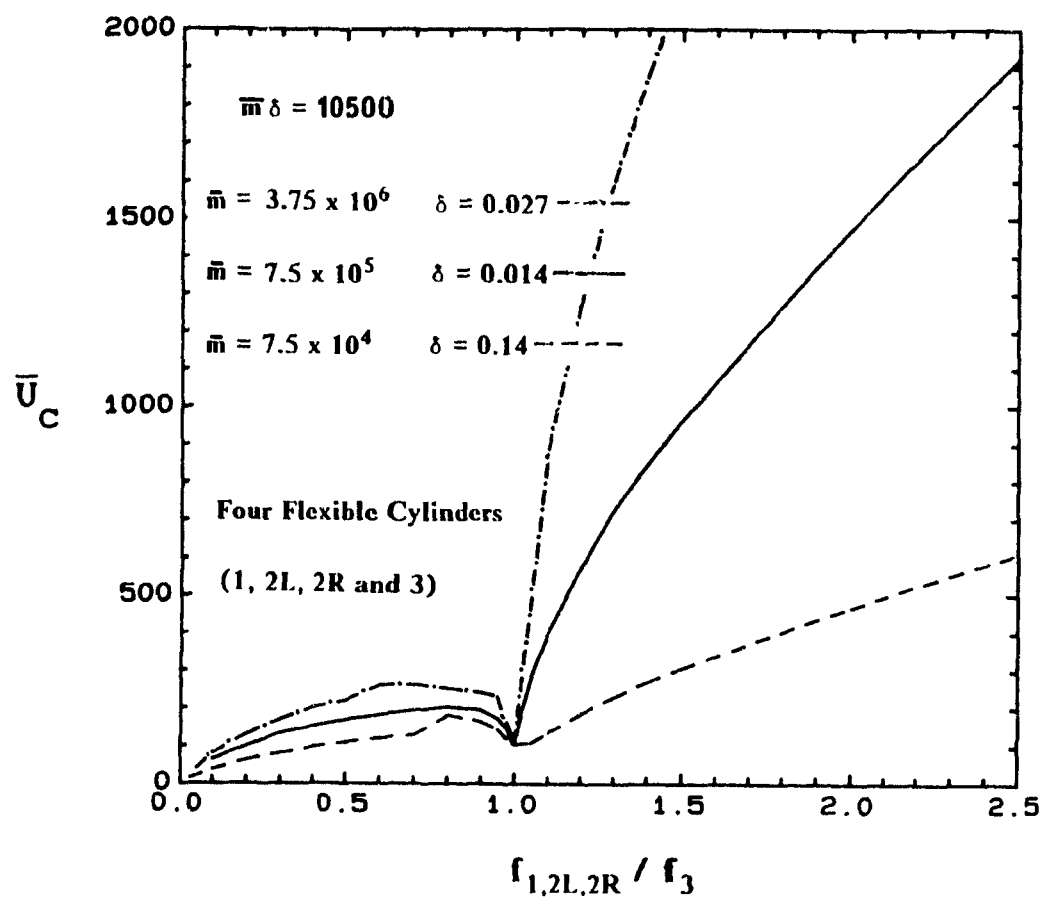


Figure 8.9: Effect of the mass-damping parameter upon the non-dimensional critical velocity of a detuned, four flexible cylinder configuration.

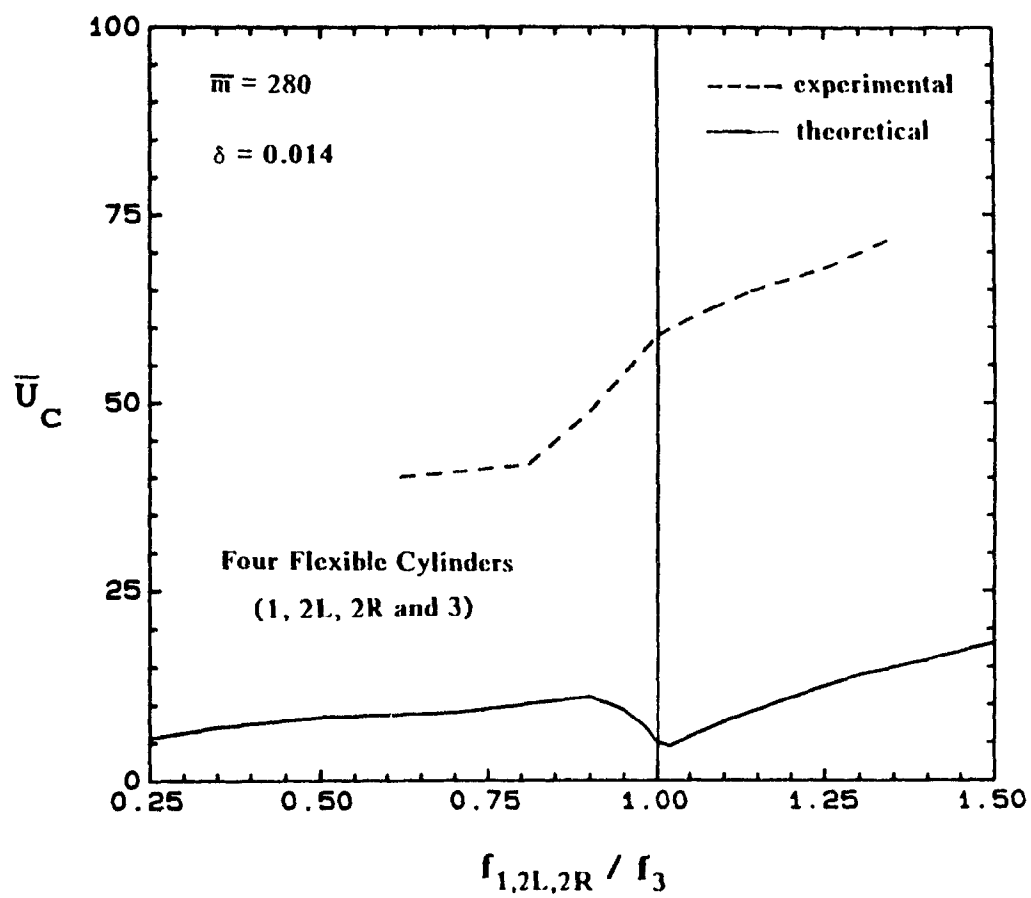


Figure 8.10: Comparison of experimental and theoretical detuning results

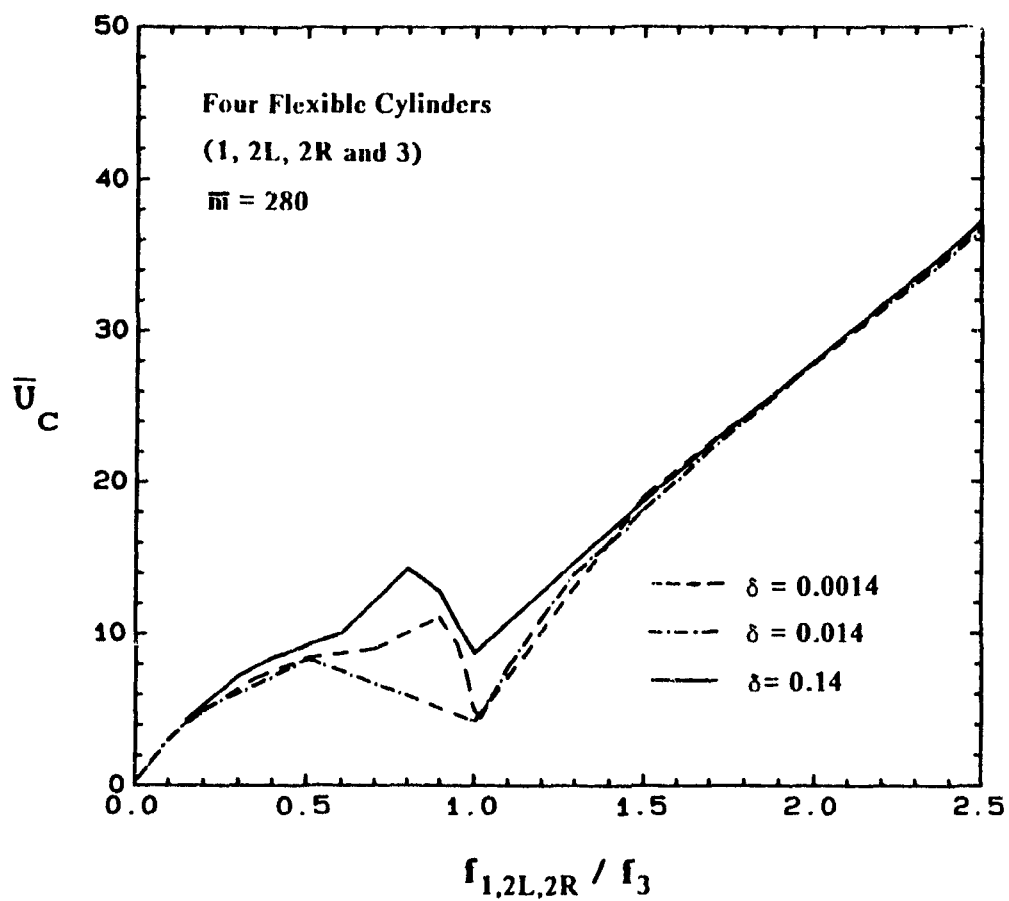


Figure 8.11: Effect of damping upon the non-dimensional critical velocity of a detuned, four flexible cylinder configuration.

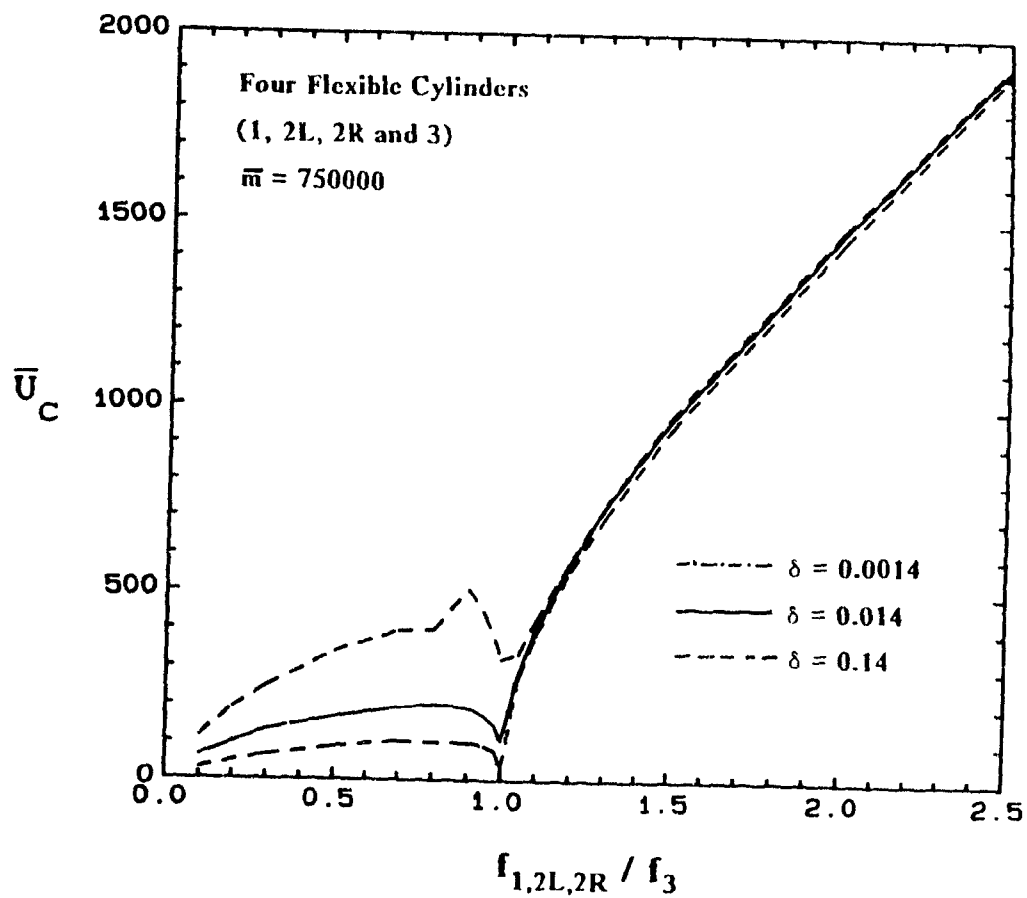


Figure 8.12: Effect of damping upon the non-dimensional critical velocity of a detuned, four flexible cylinder configuration

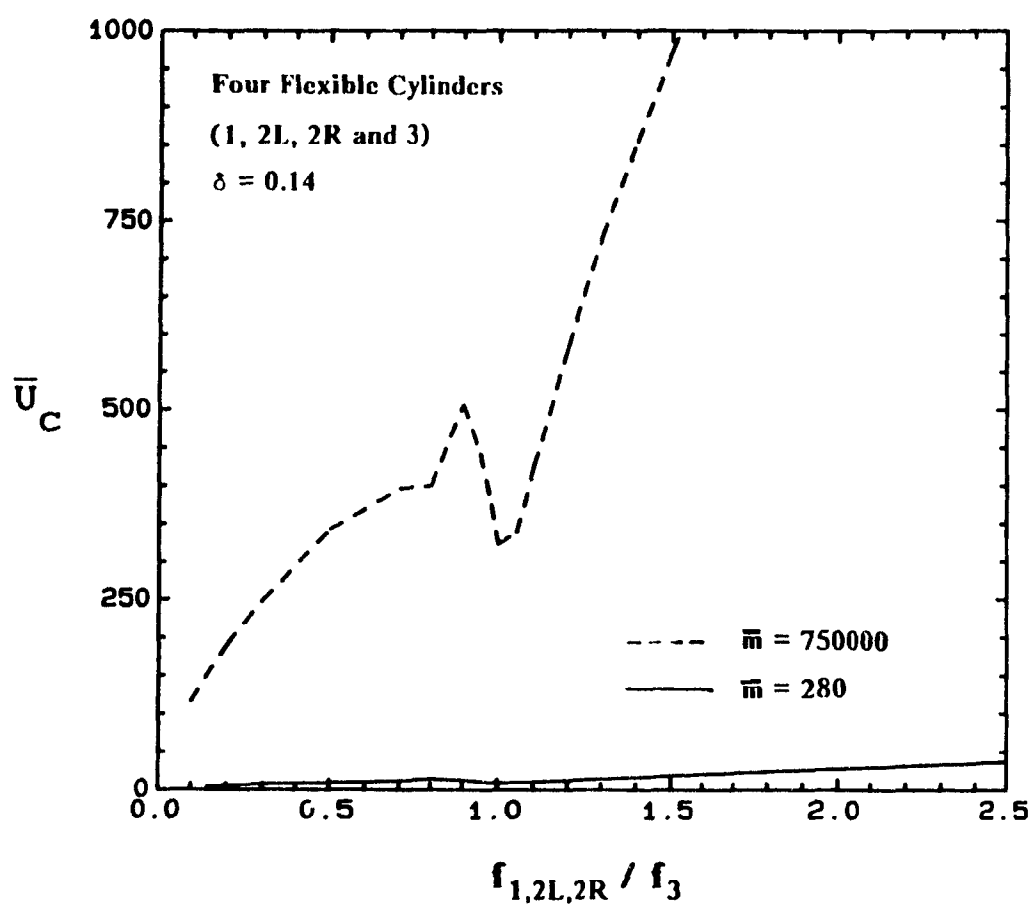


Figure 8.13: Effect of dimensionless mass upon the non-dimensional critical velocity of a detuned, four flexible cylinder configuration.

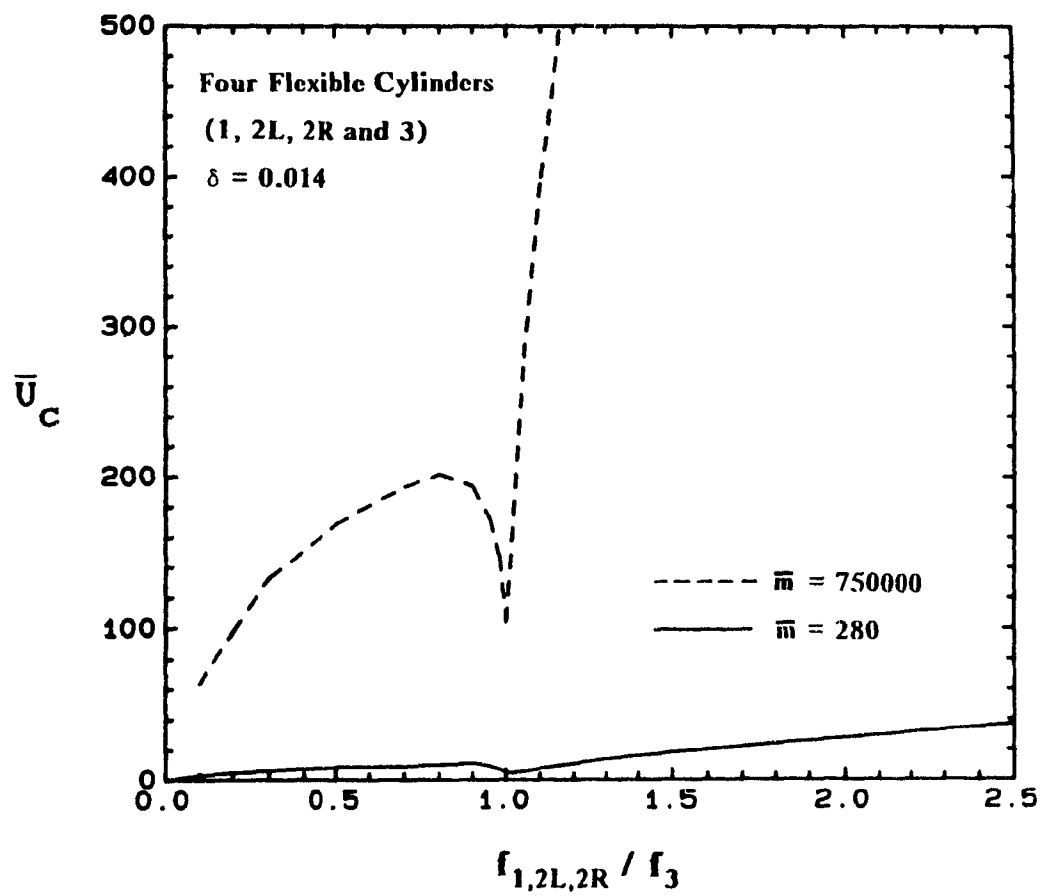


Figure 8.14: Effect of dimensionless mass upon the non-dimensional critical velocity of a detuned, four flexible cylinder configuration.

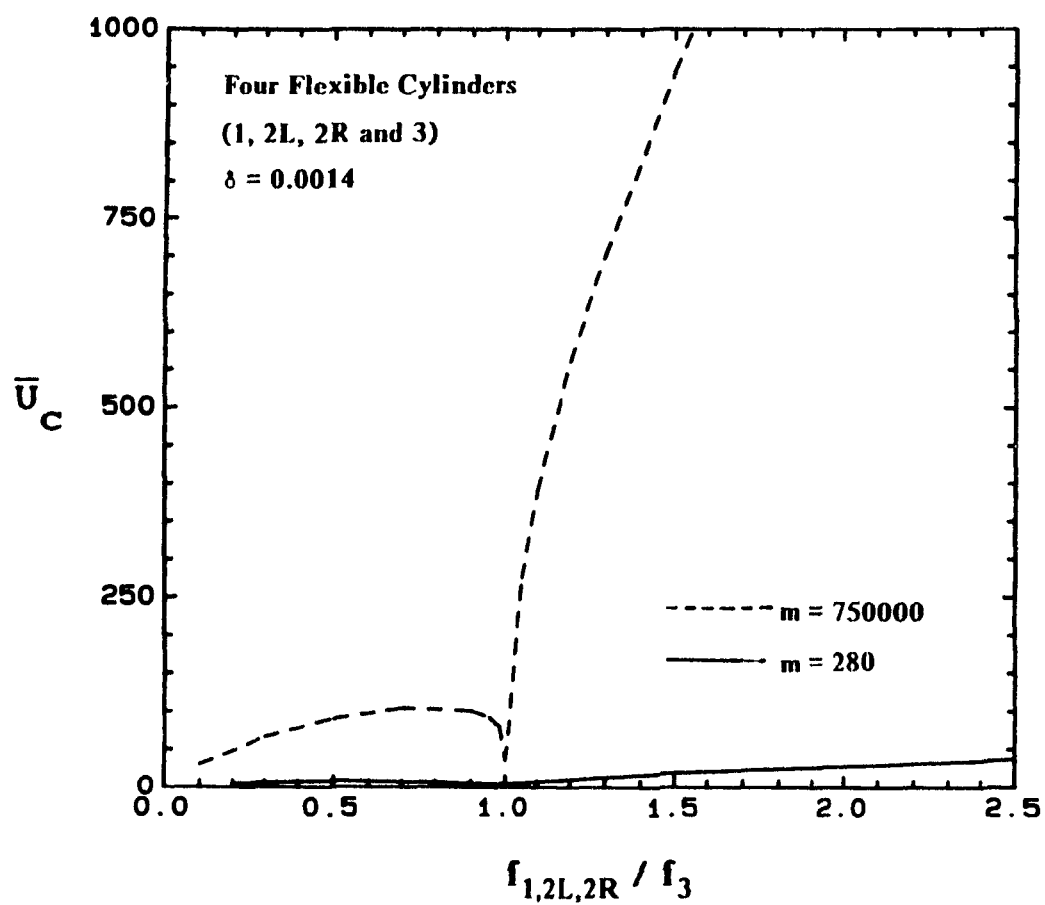


Figure 8 15: Effect of dimensionless-mass upon the non-dimensional critical velocity of a detuned, four flexible cylinder configuration.

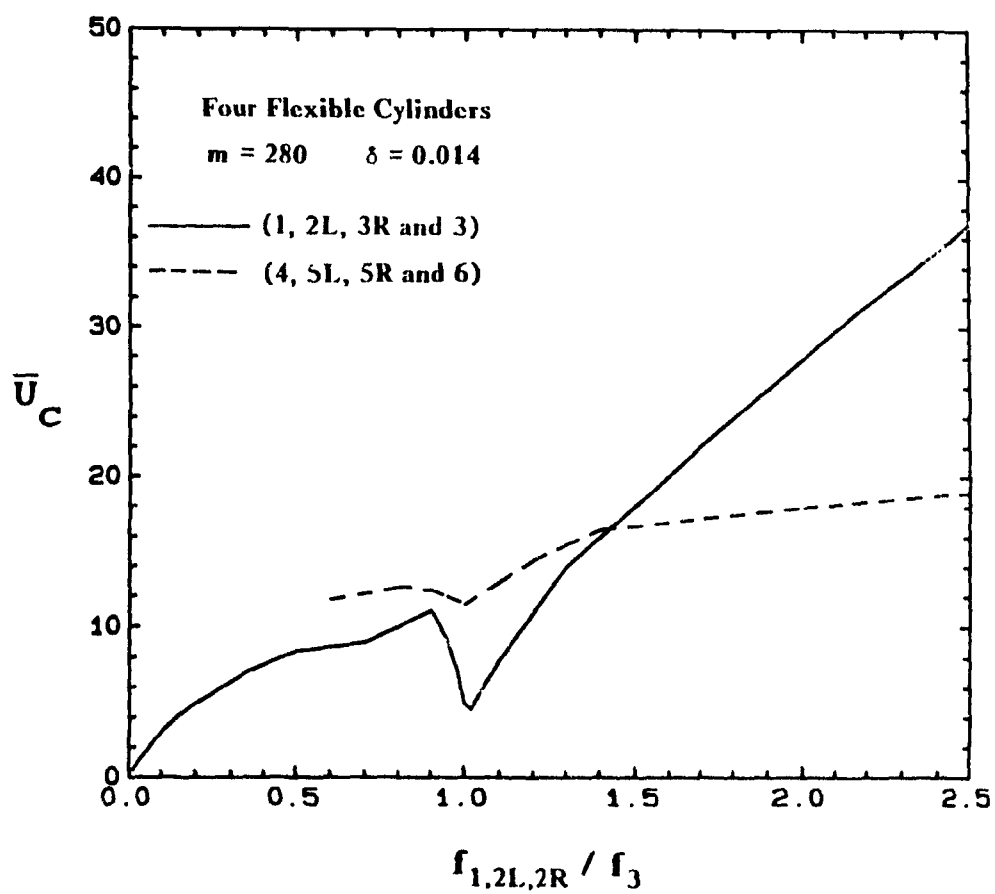


Figure 8.16: Effect of detuning at different locales in the array.

APPENDIX 1

**FLUID FORCE COEFFICIENTS AND THEIR VARIATION WITH
DISPLACEMENT**

For a four flexible cylinder configuration in positions 1, 2R, 2L and 3.

$$C_{D_1} = 1.95$$

$$\frac{\partial C_{D_1}}{\partial x_1} = 0.43 \quad \frac{\partial C_{D_1}}{\partial x_2} = -0.35 \quad \frac{\partial C_{D_1}}{\partial x_4} = 0.35 \quad \frac{\partial C_{D_1}}{\partial y_2} = -0.20$$

$$\frac{\partial C_{L_1}}{\partial x_2} = 0.10 \quad \frac{\partial C_{L_1}}{\partial y_1} = 0.00 \quad \frac{\partial C_{L_1}}{\partial y_2} = 0.00 \quad \frac{\partial C_{L_1}}{\partial y_4} = 0.00$$

$$C_{D_2} = 2.50$$

$$\frac{\partial C_{D_2}}{\partial x_1} = 0.00 \quad \frac{\partial C_{D_2}}{\partial x_2} = 0.40 \quad \frac{\partial C_{D_2}}{\partial x_4} = -0.50 \quad \frac{\partial C_{D_2}}{\partial y_1} = 0.30 \quad \frac{\partial C_{D_2}}{\partial y_2} = -0.30$$

$$\frac{\partial C_{L_2}}{\partial x_1} = -0.15 \quad \frac{\partial C_{L_2}}{\partial x_4} = 0.00 \quad \frac{\partial C_{L_2}}{\partial y_1} = -1.30 \quad \frac{\partial C_{L_2}}{\partial y_2} = 2.90 \quad \frac{\partial C_{L_2}}{\partial y_4} = -0.20$$

$$C_{D_3} = 2.50$$

$$\frac{\partial C_{D_3}}{\partial x_1} = 0.00 \quad \frac{\partial C_{D_3}}{\partial x_3} = 0.40 \quad \frac{\partial C_{D_3}}{\partial x_4} = -0.50 \quad \frac{\partial C_{D_3}}{\partial y_1} = -0.30 \quad \frac{\partial C_{D_3}}{\partial y_4} = 0.30$$

$$\frac{\partial C_{L_3}}{\partial x_1} = 0.15 \quad \frac{\partial C_{L_3}}{\partial x_4} = 0.00 \quad \frac{\partial C_{L_3}}{\partial y_1} = -1.30 \quad \frac{\partial C_{L_3}}{\partial y_3} = 2.90 \quad \frac{\partial C_{L_3}}{\partial y_4} = -0.20$$

$$C_{D_4} = 1.35$$

$$\frac{\partial C_{D_4}}{\partial x_1} = 0.35 \quad \frac{\partial C_{D_4}}{\partial x_2} = 0.30 \quad \frac{\partial C_{D_4}}{\partial x_4} = 0.00 \quad \frac{\partial C_{D_4}}{\partial y_3} = -0.60$$

$$\frac{\partial C_{L_4}}{\partial x_2} = -0.10 \quad \frac{\partial C_{L_4}}{\partial y_1} = 1.45 \quad \frac{\partial C_{L_4}}{\partial y_2} = -1.90 \quad \frac{\partial C_{L_4}}{\partial y_4} = 2.75$$

For a four-flexible cylinder configuration in positions 2, 3R, 3L, 4.

$$C_{D_1} = 2.50$$

$$\frac{\partial C_{D_1}}{\partial x_1} = 0.40 \quad \frac{\partial C_{D_1}}{\partial x_2} = -0.50 \quad \frac{\partial C_{D_1}}{\partial x_4} = 0.35 \quad \frac{\partial C_{D_1}}{\partial y_2} = -0.30$$

$$\frac{\partial C_{L_1}}{\partial x_2} = 0.00 \quad \frac{\partial C_{L_1}}{\partial y_1} = 2.90 \quad \frac{\partial C_{L_1}}{\partial y_2} = -0.20 \quad \frac{\partial C_{L_1}}{\partial y_4} = 0.00$$

$$C_{D_2} = 1.35$$

$$\frac{\partial C_{D_2}}{\partial x_1} = 0.30 \quad \frac{\partial C_{D_2}}{\partial x_2} = 0.00 \quad \frac{\partial C_{D_2}}{\partial x_4} = -0.45 \quad \frac{\partial C_{D_2}}{\partial y_1} = -0.60 \quad \frac{\partial C_{D_2}}{\partial y_2} = -0.10$$

$$\frac{\partial C_{L_2}}{\partial x_1} = 0.10 \quad \frac{\partial C_{L_2}}{\partial x_4} = 0.00 \quad \frac{\partial C_{L_2}}{\partial y_1} = -1.90 \quad \frac{\partial C_{L_2}}{\partial y_2} = 2.75 \quad \frac{\partial C_{L_2}}{\partial y_4} = -0.40$$

$$C_{D_3} = 1.35$$

$$\frac{\partial C_{D_3}}{\partial x_1} = 0.30 \quad \frac{\partial C_{D_3}}{\partial x_3} = 0.00 \quad \frac{\partial C_{D_3}}{\partial x_4} = -0.45 \quad \frac{\partial C_{D_3}}{\partial y_1} = 0.60 \quad \frac{\partial C_{D_3}}{\partial y_4} = -0.10$$

$$\frac{\partial C_{L_3}}{\partial x_1} = 0.10 \quad \frac{\partial C_{L_3}}{\partial x_4} = 0.00 \quad \frac{\partial C_{L_3}}{\partial y_1} = -1.90 \quad \frac{\partial C_{L_3}}{\partial y_3} = 2.75 \quad \frac{\partial C_{L_3}}{\partial y_4} = -0.10$$

$$C_{D_4} = 1.05$$

$$\frac{\partial C_{D_4}}{\partial x_1} = -0.20 \quad \frac{\partial C_{D_4}}{\partial x_2} = 0.10 \quad \frac{\partial C_{D_4}}{\partial x_4} = 0.50 \quad \frac{\partial C_{D_4}}{\partial y_2} = -0.50$$

$$\frac{\partial C_{L_4}}{\partial x_2} = 0.05 \quad \frac{\partial C_{L_4}}{\partial y_1} = 0.20 \quad \frac{\partial C_{L_4}}{\partial y_2} = -0.90 \quad \frac{\partial C_{L_4}}{\partial y_4} = 1.35$$

For a four-flexible cylinder configuration in positions 3, 4R, 4L and 5.

$$C_{D_1} = 1.35$$

$$\frac{\partial C_{D_1}}{\partial x_1} = 0.00 \quad \frac{\partial C_{D_1}}{\partial x_2} = -0.45 \quad \frac{\partial C_{D_1}}{\partial x_4} = 0.10 \quad \frac{\partial C_{D_1}}{\partial y_2} = 0.00$$

$$\frac{\partial C_{L_1}}{\partial x_2} = -0.20 \quad \frac{\partial C_{L_1}}{\partial y_1} = 2.75 \quad \frac{\partial C_{L_1}}{\partial y_2} = -0.60 \quad \frac{\partial C_{L_1}}{\partial y_4} = 0.10$$

$$C_{D_2} = 1.05$$

$$\frac{\partial C_{D_2}}{\partial x_1} = 0.00 \quad \frac{\partial C_{D_2}}{\partial x_2} = 0.50 \quad \frac{\partial C_{D_2}}{\partial x_4} = -0.40 \quad \frac{\partial C_{D_2}}{\partial y_1} = 0.50 \quad \frac{\partial C_{D_2}}{\partial y_2} = 0.00$$

$$\frac{\partial C_{L_2}}{\partial x_1} = 0.00 \quad \frac{\partial C_{L_2}}{\partial x_4} = 0.00 \quad \frac{\partial C_{L_2}}{\partial y_1} = -0.90 \quad \frac{\partial C_{L_2}}{\partial y_2} = 1.35 \quad \frac{\partial C_{L_2}}{\partial y_4} = -0.20$$

$$C_{D_3} = 1.05$$

$$\frac{\partial C_{D_3}}{\partial x_1} = 0.00 \quad \frac{\partial C_{D_3}}{\partial x_3} = 0.50 \quad \frac{\partial C_{D_3}}{\partial x_4} = -0.40 \quad \frac{\partial C_{D_3}}{\partial y_1} = -0.50 \quad \frac{\partial C_{D_3}}{\partial y_4} = 0.00$$

$$\frac{\partial C_{L_3}}{\partial x_1} = 0.00 \quad \frac{\partial C_{L_3}}{\partial x_4} = 0.00 \quad \frac{\partial C_{L_3}}{\partial y_1} = -0.90 \quad \frac{\partial C_{L_3}}{\partial y_3} = 1.35 \quad \frac{\partial C_{L_3}}{\partial y_4} = -0.20$$

$$C_{D_4} = 0.95$$

$$\frac{\partial C_{D_4}}{\partial x_1} = 0.15 \quad \frac{\partial C_{D_4}}{\partial x_2} = -0.20 \quad \frac{\partial C_{D_4}}{\partial x_4} = 0.69 \quad \frac{\partial C_{D_4}}{\partial y_2} = 0.25$$

$$\frac{\partial C_{L_4}}{\partial x_2} = 0.20 \quad \frac{\partial C_{L_4}}{\partial y_1} = -0.10 \quad \frac{\partial C_{L_4}}{\partial y_2} = -0.50 \quad \frac{\partial C_{L_4}}{\partial y_4} = 1.10$$

For a four-flexible cylinder configuration in positions 5₁ 6 R, 6 L and 7.

$$C_{D_1} = 0.95$$

$$\frac{\partial C_{D_1}}{\partial x_1} = 0.69 \quad \frac{\partial C_{D_1}}{\partial x_2} = -0.40 \quad \frac{\partial C_{D_1}}{\partial x_4} = 0.15 \quad \frac{\partial C_{D_1}}{\partial y_2} = 0.00$$

$$\frac{\partial C_{L_1}}{\partial x_2} = -0.10 \quad \frac{\partial C_{L_1}}{\partial y_1} = 1.10 \quad \frac{\partial C_{L_1}}{\partial y_2} = -0.10 \quad \frac{\partial C_{L_1}}{\partial y_4} = 0.10$$

$$C_{D_2} = 0.95$$

$$\frac{\partial C_{D_2}}{\partial x_1} = 0.15 \quad \frac{\partial C_{D_2}}{\partial x_2} = 0.69 \quad \frac{\partial C_{D_2}}{\partial x_4} = -0.40 \quad \frac{\partial C_{D_2}}{\partial y_1} = 0.20 \quad \frac{\partial C_{D_2}}{\partial y_2} = 0.00$$

$$\frac{\partial C_{L_2}}{\partial x_1} = 0.20 \quad \frac{\partial C_{L_2}}{\partial x_4} = 0.00 \quad \frac{\partial C_{L_2}}{\partial y_1} = -0.50 \quad \frac{\partial C_{L_2}}{\partial y_2} = 1.15 \quad \frac{\partial C_{L_2}}{\partial y_4} = -0.20$$

$$C_{D_3} = 0.95$$

$$\frac{\partial C_{D_3}}{\partial x_1} = -0.15 \quad \frac{\partial C_{D_3}}{\partial x_3} = 0.69 \quad \frac{\partial C_{D_3}}{\partial x_4} = -0.40 \quad \frac{\partial C_{D_3}}{\partial y_1} = -0.20 \quad \frac{\partial C_{D_3}}{\partial y_4} = 0.00$$

$$\frac{\partial C_{L_3}}{\partial x_1} = -0.20 \quad \frac{\partial C_{L_3}}{\partial x_4} = 0.00 \quad \frac{\partial C_{L_3}}{\partial y_1} = -0.50 \quad \frac{\partial C_{L_3}}{\partial y_3} = 1.15 \quad \frac{\partial C_{L_3}}{\partial y_4} = -0.20$$

$$C_{D_4} = 1.05$$

$$\frac{\partial C_{D_4}}{\partial x_1} = 0.05 \quad \frac{\partial C_{D_4}}{\partial x_2} = -0.15 \quad \frac{\partial C_{D_4}}{\partial x_4} = 0.40 \quad \frac{\partial C_{D_4}}{\partial y_2} = 0.20$$

$$\frac{\partial C_{L_4}}{\partial x_2} = 0.10 \quad \frac{\partial C_{L_4}}{\partial y_1} = 0.00 \quad \frac{\partial C_{L_4}}{\partial y_2} = -0.40 \quad \frac{\partial C_{L_4}}{\partial y_4} = 1.05$$

APPENDIX 2

STATIC INSTABILITY

For the problem at hand, the overall (in-flow) fluidelastic stiffness, k_T , of the system can be expressed as

$$k_T = k_s - k_f \quad (2.1)$$

where k_s = structural restoring stiffness and k_f = total fluid stiffness. Those stiffness terms can be expressed by

$$\begin{aligned} k_T &= w^2 m_T, \\ k_s &= w_o^2 m_T, \end{aligned} \quad (2.2)$$

and

$$k_f = \frac{1}{2} \rho U_\infty^2 d \ell \left(\frac{\partial C}{\partial z} \right),$$

where w_o = initial cyclical frequency of the cylinder, w = overall in-flow cyclical fluidelastic frequency of the cylinder, m_T = total mass of the cylinder, U_∞ = upstream flow velocity, d = diameter of the cylinder, ρ = density of the flow and $\partial C/\partial z$ = variation of fluid force coefficient with displacement. Substituting equation (2.2) into (2.1) and rearranging gives

$$\frac{w^2}{w_o^2} = 1 - \frac{\rho U_\infty^2 d \ell}{2 m_T w_o^2} \left(\frac{\partial C}{\partial z} \right). \quad (2.3)$$

By taking $\bar{U} = U_\infty/w_o d$, $\bar{z} = z/d$ and $\bar{m} = m_T/\rho d^2 \ell$ equation (2.3) can be simplified further as

$$\frac{w^2}{w_o^2} = 1 - \frac{\bar{U}^2}{2 \bar{m}} \left(\frac{\partial C}{\partial \bar{z}} \right). \quad (2.4)$$

At static instability, the overall in-flow cyclical frequency of the cylinder, w , will become zero. Therefore from equation (2.4), the critical non-dimensional flow velocity

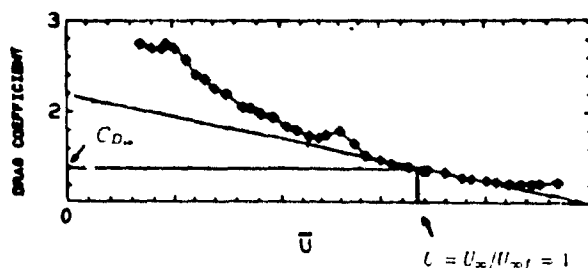
for static instability can be found to be

$$\bar{U}_{cr} = \left[\frac{2\bar{m}}{(\partial C / \partial \bar{z})} \right]^{\frac{1}{2}} . \quad (2.5)$$

APPENDIX 3

THE EFFECT OF REYNOLDS NUMBER UPON THE DRAG AND LIFT COEFFICIENTS

In section 6.2 the variation of the drag coefficient versus the Reynolds number for a non-displaced cylinder positioned in different rows of the array was presented. A typical result, for a cylinder positioned in the third row, is reproduced below. To obtain the variation of C_D with flow velocity in a dimensionless format the upstream velocity is non-dimensionalised with respect to a flow velocity of 16.6 m/s denoted by $U_{\infty f}$. It should be recalled that the major portion of the force measurements have been performed at this velocity. Therefore non-dimensionalisation with respect to this velocity is reasonable.



In a fairly broad range around $\bar{U} = U_{\infty}/U_{\infty f} = 1$, if the value of C_D at $U = 1$ is taken to be $C_{D,0}$, then an equation of the form

$$C_{D,0} + \Delta \bar{U} \frac{\partial C_{D,0}}{\partial \bar{U}}$$

can be used to represent the variation of the drag coefficient with flow velocity.

In section 7.2 it has been found that $U_r = U_{\infty} - \dot{x}$. Based on this an incremental change in velocity can be defined as

$$\Delta U = U_{\infty} - \dot{x} - U_{\infty f} .$$

Upon non-dimensionalisation this incremental velocity will be

$$\Delta \bar{U} = \frac{U_{\infty}}{U_{\infty f}} - 1 - \frac{\dot{x}}{U_{\infty f}} .$$

Therefore the Reynolds number dependent term of the drag coefficient becomes,

$$\Delta \bar{U} \frac{\partial C_{D,0}}{\partial \bar{U}} = \left[\frac{U_{\infty}}{U_{\infty f}} - 1 - \frac{\dot{x}}{U_{\infty f}} \right] \frac{\partial C_{D,0}}{\partial \bar{U}} .$$

APPENDIX 4

LINEARISED FLUID FORCE COEFFICIENTS

The linearised lift and drag coefficients of a four flexible cylinder configuration are

$$\begin{aligned}
 C_{L_1} = & \left[g_G g_2 (1 + \lambda \tau_2) \frac{\partial C_{L_1}}{\partial \xi_2} \right] x_2 - \left[g_G g_2 (1 + \lambda \tau_2) \frac{\partial C_{L_1}}{\partial \xi_2} \right] x_3 \\
 & + \left[g_\infty \frac{\partial C_{L_1}}{\partial \eta_1} + \left(\frac{2T\lambda}{U_G} \right) \frac{\partial C_{L_1}}{\partial \xi_2} + \frac{2L\lambda}{U_\infty} \left(\frac{\partial C_{L_1}}{\partial \eta_2} + \frac{\partial C_{L_1}}{\partial \eta_1} \right) \right] y_1 \\
 & + \left[g_G g_2 \frac{\partial C_{L_1}}{\partial \eta_2} \right] y_2 + \left[g_G g_2 \frac{\partial C_{L_1}}{\partial \eta_2} \right] y_3 + \left[g_G g_4 \frac{\partial C_{L_1}}{\partial \eta_4} \right] y_4
 \end{aligned}$$

$$\begin{aligned}
 C_{D_1} = & C_{D_{01}} + \left[\frac{U_\infty}{U_{\infty f}} - 1 - \frac{\dot{x}d}{U_{\infty f}} \right] \frac{\partial C_{D_{01}}}{\partial \bar{U}} + \left[g_\infty \frac{\partial C_{D_1}}{\partial \xi_1} \right] x_1 \\
 & + \left[g_G g_2 (1 + \tau_2 \lambda) \frac{\partial C_{D_1}}{\partial \xi_2} \right] x_2 + \left[g_G g_2 (1 + \tau_2 \lambda) \frac{\partial C_{D_1}}{\partial \xi_2} \right] x_3 \\
 & + \left[g_G g_4 (1 + \tau_4 \lambda) \frac{\partial C_{D_1}}{\partial \xi_4} \right] x_4 + \left[g_G g_2 \frac{\partial C_{D_1}}{\partial \eta_2} \right] y_2 - \left[g_G g_2 \frac{\partial C_{D_1}}{\partial \eta_2} \right] y_3
 \end{aligned}$$

$$\begin{aligned}
 C_{L_2} = & - \left[g_\infty g_1 (1 + \lambda \tau_1) \frac{\partial C_{L_2}}{\partial \xi_1} \right] x_1 - \left[g_G g_4 (1 + \lambda \tau_4) \frac{\partial C_{L_2}}{\partial \xi_4} \right] x_4 \\
 & + \left[g_\infty g_1 \left(\frac{T\lambda}{U_\infty} \right) \frac{\partial C_{L_2}}{\partial \xi_1} + g_\infty g_1 \left(1 - \frac{L\lambda}{U_\infty} \right) \frac{\partial C_{L_2}}{\partial \eta_1} \right] y_1 \\
 & + \left[g_G \frac{\partial C_{L_2}}{\partial \eta_2} + g_G \left(\frac{L\lambda}{U_G} \right) \frac{\partial C_{L_2}}{\partial \eta_4} + g_G \left(\frac{T\lambda}{U_G} \right) \frac{\partial C_{L_2}}{\partial \xi_4} \right] y_2 + \left[g_G g_4 \frac{\partial C_{L_2}}{\partial \eta_4} \right] y_3
 \end{aligned}$$

$$\begin{aligned}
 C_{D_2} = & C_{D_{02}} + \left[\frac{U_\infty}{U_{\infty f}} - 1 - \frac{\dot{x}d}{U_{\infty f}} \right] \frac{\partial C_{D_{02}}}{\partial \bar{U}} + \left[g_\infty g_1 (1 + \lambda \tau_1) \frac{\partial C_{D_2}}{\partial \xi_1} \right] x_1 + \left[g_G \frac{\partial C_{D_2}}{\partial \xi_2} \right] x_2 \\
 & + \left[g_G g_4 (1 + \lambda \tau_4) \frac{\partial C_{D_2}}{\partial \xi_4} \right] x_4 - \left[g_\infty g_1 \left(\frac{T\lambda}{U_\infty} \right) \frac{\partial C_{D_2}}{\partial \xi_1} + g_\infty g_1 \left(1 - \frac{L\lambda}{U_\infty} \right) \frac{\partial C_{D_2}}{\partial \eta_1} \right] y_1
 \end{aligned}$$

$$- \left[g_G \left(\frac{T\lambda}{U_G} \right) \frac{\partial C_{D_2}}{\partial \xi_4} + g_G \left(\frac{L\lambda}{U_G} \right) \frac{\partial C_{D_2}}{\partial \eta_4} \right] y_2 - \left[g_G g_4 \frac{C_{D_2}}{\partial \eta_4} \right] y_4$$

$$\begin{aligned} C_{L_3} = & \left[g_\infty g_1 (1 + \lambda \tau_1) \frac{\partial C_{L_3}}{\partial \xi_1} \right] x_1 + \left[g_G g_4 (1 + \lambda \tau_4) \frac{\partial C_{L_3}}{\partial \xi_4} \right] x_4 \\ & + \left[g_\infty g_1 \left(1 - \frac{L\lambda}{U_\infty} \right) \frac{\partial C_{L_3}}{\partial \eta_1} + g_\infty g_1 \left(\frac{T\lambda}{U_G} \right) \frac{\partial C_{L_3}}{\partial \xi_1} \right] y_1 \\ & + \left[g_G \left(\frac{\partial C_{L_3}}{\partial \eta_3} + \frac{L\lambda}{U_G} \frac{\partial C_{L_3}}{\partial \eta_4} + \frac{T\lambda}{U_G} \frac{\partial C_{L_3}}{\partial \xi_4} \right) \right] y_3 + \left[g_G g_4 \frac{\partial C_{L_3}}{\partial \eta_4} \right] y_4 \end{aligned}$$

$$\begin{aligned} C_{D_3} = & C_{D_{30}} + \left[\frac{U_\infty}{U_{\infty f}} - 1 - \frac{\sharp d}{U_{\infty f}} \right] \frac{\partial C_{D_{30}}}{\partial U} + \left[g_\infty g_1 (1 + \lambda \tau_1) \frac{\partial C_{D_3}}{\partial \xi_1} \right] x_1 + \left[g_G \frac{\partial C_{D_3}}{\partial \xi_3} \right] x_3 \\ & + \left[g_G g_4 (1 + \lambda \tau_4) \frac{\partial C_{D_3}}{\partial \xi_4} \right] x_4 + \left[g_\infty g_1 \left(1 - \frac{L\lambda}{U_\infty} \right) \frac{\partial C_{D_3}}{\partial \eta_1} + g_\infty g_1 \left(\frac{T\lambda}{U_\infty} \right) \frac{\partial C_{D_3}}{\partial \xi_1} \right] y_1 \\ & + \left[g_G \frac{T\lambda}{U_G} \frac{\partial C_{D_3}}{\partial \xi_4} + g_G \frac{L\lambda}{U_G} \frac{\partial C_{D_3}}{\partial \eta_4} \right] y_3 + \left[g_G g_4 \frac{\partial C_{D_3}}{\partial \eta_4} \right] y_4 \end{aligned}$$

$$\begin{aligned} C_{L_4} = & \left[g_G g_2 (1 + \lambda \tau_2) \frac{\partial C_{L_4}}{\partial \xi_2} \right] x_2 - \left[g_G g_2 (1 + \lambda \tau_2) \frac{\partial C_{L_4}}{\partial \xi_2} \right] x_3 \\ & + \left[g_\infty g_1 \left(1 - \frac{2L\lambda}{U_G} \right) \frac{\partial C_{L_4}}{\partial \eta_1} \right] y_1 + \left[g_G g_2 \left(1 - \frac{\lambda L}{U_G} \right) \frac{\partial C_{L_4}}{\partial \eta_2} + g_G g_2 \left(\frac{T\lambda}{U_G} \right) \frac{\partial C_{L_4}}{\partial \xi_2} \right] y_2 \\ & + \left[g_G g_2 \left(1 - \frac{\lambda L}{U_G} \right) \frac{\partial C_{L_4}}{\partial \eta_2} + g_G g_2 \left(\frac{T\lambda}{U_G} \right) \frac{\partial C_{L_4}}{\partial \xi_2} \right] y_3 + \left[g_G \frac{\partial C_{L_4}}{\partial \eta_4} \right] y_4 \end{aligned}$$

$$\begin{aligned} C_{D_4} = & C_{D_{40}} + \left[\frac{U_\infty}{U_{\infty f}} - 1 - \frac{\sharp d}{U_{\infty f}} \right] \frac{\partial C_{D_{40}}}{\partial U} + \left[g_\infty g_1 (1 + \tau_1 \lambda) \frac{\partial C_{D_4}}{\partial \xi_1} \right] x_1 \\ & + \left[g_G g_2 (1 + \tau_2 \lambda) \frac{\partial C_{D_4}}{\partial \xi_2} \right] x_2 + \left[g_G g_2 \left(1 + \lambda \tau_2 \right) \frac{\partial C_{D_4}}{\partial \xi_2} \right] x_3 + \left[g_G \frac{\partial C_{D_4}}{\partial \xi_4} \right] x_4 \\ & + \left[g_G g_2 \left(1 - \frac{L\lambda}{U_G} \right) \frac{\partial C_{D_4}}{\partial \eta_2} + g_G g_2 \left(\frac{T\lambda}{U_G} \right) \frac{\partial C_{D_4}}{\partial \xi_2} \right] y_2 \end{aligned}$$

$$- \left[g_G g_2 \left(1 - \frac{L\lambda}{U_G} \right) \frac{\partial C_{D_1}}{\partial \eta_2} + g_G g_2 \left(\frac{T\lambda}{U_G} \right) \frac{\partial C_{D_1}}{\partial \xi_2} \right] y_3$$

APPENDIX 5

FLUID STIFFNESS MATRICES

The elements of the fluid stiffness matrix of a four flexible cylinder configuration are

$$K_{11} = g_{\infty} \frac{\partial C_{D1}}{\partial \xi_1}$$

$$K_{12} = 0$$

$$K_{13} = g_G g_2 (1 + \tau_2 \lambda) \frac{\partial C_{D1}}{\partial \xi_2}$$

$$K_{14} = g_G g_2 \frac{\partial C_{D1}}{\partial \eta_2}$$

$$K_{15} = g_G g_2 (1 + \tau_2 \lambda) \frac{\partial C_{D1}}{\partial \xi_2}$$

$$K_{16} = -g_G g_2 \frac{\partial C_{D1}}{\partial \eta_2}$$

$$K_{17} = g_G g_1 (1 + \tau_1 \lambda) \frac{\partial C_{D1}}{\partial \xi_4}$$

$$K_{18} = 0$$

$$K_{21} = 0$$

$$K_{22} = g_{\infty} \frac{\partial C_{L1}}{\partial \eta_1} + \frac{2T\lambda}{U_{\infty}} \left(\frac{\partial C_{L1}}{\partial \xi_2} \right) + \frac{2L\lambda}{U_{\infty}} \left(\frac{\partial C_{L1}}{\partial \eta_2} + \frac{\partial C_{L1}}{\partial \eta_4} \right)$$

$$K_{23} = g_G g_2 (1 + \lambda \tau_2) \frac{\partial C_{L1}}{\partial \xi_2}$$

$$K_{24} = g_G g_2 \frac{\partial C_{L1}}{\partial \eta_2}$$

$$K_{25} = -g_G g_2 (1 + \lambda \tau_2) \frac{\partial C_{L1}}{\partial \xi_2}$$

$$K_{26} = g_G g_2 \frac{\partial C_{L1}}{\partial \eta_2}$$

$$K_{27} = 0$$

$$K_{28} = g_G g_1 \frac{\partial C_{L1}}{\partial \eta_2}$$

$$K_{32} = -g_{\infty} g_2 \left(\frac{T\lambda}{U_{\infty}} \right) \frac{\partial C_{D2}}{\partial \xi_1} - g_{\infty} g_2 \left(1 - \frac{L\lambda}{U_{\infty}} \right) \frac{\partial C_{D2}}{\partial \eta_1}$$

$$K_{33} = g_G \frac{\partial C_{D2}}{\partial \xi_2}$$

$$K_{34} = -g_G \left(\frac{T\lambda}{U_G} \right) \frac{\partial C_{D_2}}{\partial \xi_4} - g_G \left(\frac{L\lambda}{U_G} \right) \frac{\partial C_{D_2}}{\partial \eta_4}$$

$$K_{35} = 0$$

$$K_{36} = 0$$

$$K_{37} = g_G g_2 (1 + \lambda \tau_2) \frac{\partial C_{D_2}}{\partial \xi_4}$$

$$K_{38} = -g_G g_2 \frac{\partial C_{D_2}}{\partial \eta_4}$$

$$K_{41} = -g_\infty g_2 (1 + \lambda \tau_2) \frac{\partial C_{L_2}}{\partial \xi_1}$$

$$K_{42} = g_\infty g_2 \left(\frac{T\lambda}{U_\infty} \right) \frac{\partial C_{L_2}}{\partial \xi_1} + g_\infty g_2 \left(1 - \frac{L\lambda}{U_\infty} \right) \frac{\partial C_{L_2}}{\partial \eta_1}$$

$$K_{43} = 0$$

$$K_{44} = g_G \frac{\partial C_{L_2}}{\partial \eta_2} + g_G \left(\frac{L\lambda}{U_G} \right) \frac{\partial C_{L_2}}{\partial \eta_4} + g_G \left(\frac{T\lambda}{U_G} \right) \frac{\partial C_{L_2}}{\partial \xi_4}$$

$$K_{45} = 0$$

$$K_{47} = -g_G g_2 (1 + \lambda \tau_2) \frac{\partial C_{L_2}}{\partial \xi_4}$$

$$K_{48} = g_G g_2 \frac{\partial C_{L_2}}{\partial \eta_2}$$

$$K_{51} = g_\infty g_2 (1 + \lambda \tau_1) \frac{\partial C_{D_3}}{\partial \xi_1}$$

$$K_{52} = g_\infty g_2 \left(1 - \frac{L\lambda}{U_\infty} \right) \frac{\partial C_{D_3}}{\partial \eta_1} + g_\infty g_2 \left(\frac{T\lambda}{U_\infty} \right) \frac{\partial C_{D_3}}{\partial \xi_1}$$

$$K_{53} = 0$$

$$K_{54} = 0$$

$$K_{55} = g_G \frac{\partial C_{D_3}}{\partial \xi_3}$$

$$K_{56} = g_G \left(\frac{L\lambda}{U_G} \right) \frac{\partial C_{D_3}}{\partial \eta_4} + g_G \left(\frac{T\lambda}{U_G} \right) \frac{\partial C_{D_3}}{\partial \xi_4}$$

$$K_{57} = g_G g_2 (1 + \lambda \tau_2) \frac{\partial C_{D_3}}{\partial \xi_4}$$

$$K_{58} = g_G g_2 \frac{\partial C_{D_3}}{\partial \eta_4}$$

$$K_{61} = g_\infty g_2 (1 + \lambda \tau_2) \frac{\partial C_{L_3}}{\partial \xi_1}$$

$$K_{62} = g_\infty g_2 \left(1 - \frac{L\lambda}{U_\infty} \right) \frac{\partial C_{L_3}}{\partial \eta_1} + g_\infty g_2 \left(\frac{T\lambda}{U_\infty} \right) \frac{\partial C_{L_3}}{\partial \xi_1}$$

$$K_{63} = 0$$

$$K_{64} = 0$$

$$K_{65} = 0$$

$$K_{66} = g_G \frac{\partial C_{L_3}}{\partial \eta_3} + g_G \left(\frac{L\lambda}{U_G} \right) \frac{\partial C_{L_3}}{\partial \eta_4} + g_G \left(\frac{T\lambda}{U_G} \right) \frac{\partial C_{L_3}}{\partial \xi_4}$$

$$K_{67} = g_G g_2 (1 + \lambda \tau_2) \frac{\partial C_{D_3}}{\partial \xi_4}$$

$$K_{68} = g_G g_2 \frac{\partial C_{L_3}}{\partial \eta_4}$$

$$K_{71} = g_{\infty} g_1 (1 + \tau_2 \lambda) \frac{\partial C_{D_4}}{\partial \xi_1}$$

$$K_{72} = 0$$

$$K_{73} = g_G g_2 (1 + \tau_2 \lambda) \frac{\partial C_{D_4}}{\partial \xi_2}$$

$$K_{74} = g_G g_2 \left(1 - \frac{L\lambda}{U_G} \right) \frac{\partial C_{D_4}}{\partial \eta_2} + g_G g_2 \left(\frac{T\lambda}{U_G} \right) \frac{\partial C_{D_4}}{\partial \xi_2}$$

$$K_{75} = g_G g_2 (1 + \tau_2 \lambda) \frac{\partial C_{D_4}}{\partial \xi_2}$$

$$K_{76} = -g_G g_2 \left(1 - \frac{L\lambda}{U_G} \right) \frac{\partial C_{D_4}}{\partial \eta_2} - g_G g_2 \left(\frac{T\lambda}{U_G} \right) \frac{\partial C_{D_4}}{\partial \xi_2}$$

$$K_{77} = g_G \frac{\partial C_{D_4}}{\partial \xi_4}$$

$$K_{78} = 0$$

$$K_{81} = 0$$

$$K_{82} = g_G g_1 \left(1 - \frac{2L\lambda}{U_G} \right) \frac{\partial C_{L_4}}{\partial \eta_1}$$

$$K_{83} = g_G g_2 (1 + \tau_2 \lambda) \frac{\partial C_{L_4}}{\partial \xi_2}$$

$$K_{84} = g_G g_2 \left(1 - \frac{\lambda L}{U_G} \right) \frac{\partial C_{L_4}}{\partial \eta_2} - g_G g_2 \left(\frac{T\lambda}{U_G} \right) \frac{\partial C_{L_4}}{\partial \xi_2}$$

$$K_{85} = -g_G g_2 (1 + \lambda \tau_2) \frac{\partial C_{L_4}}{\partial \xi_2}$$

$$K_{86} = g_G g_2 \left(1 - \frac{\lambda L}{U_G} \right) \frac{\partial C_{L_4}}{\partial \eta_2} - g_G g_2 \left(\frac{T\lambda}{U_G} \right) \frac{\partial C_{L_4}}{\partial \xi_2}$$

$$K_{87} = 0$$

$$K_{88} = g_G \frac{\partial C_{L_4}}{\partial \eta_4}$$

APPENDIX 6

FLUID DAMPING MATRICES

The elements of the fluid damping matrix of a four flexible cylinder configuration are

$$\begin{aligned}
 B_{11} &= \left(-\frac{2}{U_\infty}\right) \left[C_{D_{10}} + \left(\frac{U_\infty}{U_{\infty f}} - 1\right) \frac{\partial C_{D_{10}}}{\partial \bar{U}} \right] - \left(\frac{1}{U_{\infty f}}\right) \frac{\partial C_{D_{10}}}{\partial U} \\
 B_{22} &= \left(-\frac{1}{U_\infty}\right) \left[C_{D_{10}} + \left(\frac{U_\infty}{U_{\infty f}} - 1\right) \frac{\partial C_{D_{10}}}{\partial \bar{U}} \right] \\
 B_{33} &= \left(-\frac{2}{U_\infty a}\right) \left[C_{D_{20}} + \left(\frac{U_\infty}{U_{\infty f}} - 1\right) \frac{\partial C_{D_{20}}}{\partial \bar{U}} \right] - \left(\frac{1}{U_{\infty f}}\right) \frac{\partial C_{D_{20}}}{\partial U} \\
 B_{44} &= \left(-\frac{2}{U_\infty}\right) \left[C_{D_{20}} + \left(\frac{U_\infty}{U_{\infty f}} - 1\right) \frac{\partial C_{D_{20}}}{\partial \bar{U}} \right] \\
 B_{55} &= \left(-\frac{2}{U_\infty a}\right) \left[C_{D_{30}} + \left(\frac{U_\infty}{U_{\infty f}} - 1\right) \frac{\partial C_{D_{30}}}{\partial \bar{U}} \right] - \left(\frac{1}{U_{\infty f}}\right) \frac{\partial C_{D_{30}}}{\partial U} \\
 B_{66} &= \left(-\frac{1}{U_\infty a}\right) \left[C_{D_{30}} + \left(\frac{U_\infty}{U_{\infty f}} - 1\right) \frac{\partial C_{D_{30}}}{\partial \bar{U}} \right] \\
 B_{77} &= \left(-\frac{2}{U_\infty a}\right) \left[C_{D_{40}} + \left(\frac{U_\infty}{U_{\infty f}} - 1\right) \frac{\partial C_{D_{40}}}{\partial \bar{U}} \right] - \left(\frac{1}{U_{\infty f}}\right) \frac{\partial C_{D_{40}}}{\partial U} \\
 B_{88} &= \left(-\frac{1}{U_\infty a}\right) \left[C_{D_{40}} + \left(\frac{U_\infty}{U_{\infty f}} - 1\right) \frac{\partial C_{D_{40}}}{\partial \bar{U}} \right]
 \end{aligned}$$

all other terms for $i \neq j$

$$B_{ij} = 0$$

Initial numerical solutions revealed that considering the variation of the drag coefficient with flow velocity, $\partial C_D / \partial \bar{U}$, has little or no impact upon the critical velocity in this array. So for most results presented in Chapter 8 the $\partial C_D / \partial U$ terms are neglected. Therefore the elements of the fluid-damping matrix are expressed, in a

simplified and non-dimensional form, as

$$B_{11} = -2C_{D10} \quad B_{55} = -2C_{D30}$$

$$B_{22} = -C_{D10} \quad B_{66} = -C_{D30}$$

$$B_{33} = -2C_{D20} \quad B_{77} = -2C_{D30}$$

$$B_{44} = -C_{D20} \quad B_{88} = -C_{D40}$$